Study of τ lepton decays involving K^0_S at Belle

Ryu, Soo

Under the supervision of
Professor Kim, Sun Kee

A dissertation submitted to
the Graduate Faculty of Seoul National University
in partial fulfillment of the requirement
for the Degree of Doctor of Philosophy

Department of Physics and Astronomy
The Graduate School of Natural Sciences
Seoul National University
Seoul, KOREA

August, 2012

Abstract

The τ lepton is the only known lepton massive enough to decay into hadrons via a weak vector current, and this provides a sensitive probe of the standard model parameters, $|V_{us}|$, α_s and m_s. However, because of the limited numbers of $\tau^+\tau^-$ events, the hadronic decays involving kaons in τ lepton which is directly related to $|V_{us}|$ determination has not been well studied for the decades. The Belle experiment provides the best environments for studying τ leptons because of the high luminosity of e^+e^- collisions result in the production of large numbers of $\tau^+\tau^-$ events. We report measurements of branching fractions for inclusive/exclusive τ decays involving $K^0_S \to \pi^-\pi^+$ with 669 fb^{-1} accumulated data at Belle detector at the asymmetric energy KEKB e^+e^- collider. The branching fraction measured for the inclusive decay is $\mathcal{B}(\tau^- \to K^0_S\, X^-\nu_\tau) = (0.910\pm0.001\pm0.046)\%$, where X^- can be anything; for exclusive decays we report:

$$\begin{aligned}
\mathcal{B}(\tau^- \to \pi^- K^0_S\nu_\tau) &= (4.10 \pm 0.01 \pm 0.21) \times 10^{-3} \\
\mathcal{B}(\tau^- \to K^- K^0_S\nu_\tau) &= (7.09 \pm 0.06 \pm 0.41) \times 10^{-4} \\
\mathcal{B}(\tau^- \to \pi^- K^0_S\pi^0\nu_\tau) &= (1.95 \pm 0.02 \pm 0.11) \times 10^{-3} \\
\mathcal{B}(\tau^- \to K^- K^0_S\pi^0\nu_\tau) &= (7.31 \pm 0.12 \pm 0.49) \times 10^{-4}
\end{aligned}$$

We also studied decays involving two K^0_S:

$$\begin{aligned}
\mathcal{B}(\tau^- \to \pi^- K^0_S K^0_S\nu_\tau) &= (2.41 \pm 0.04 \pm 0.26) \times 10^{-4} \\
\mathcal{B}(\tau^- \to \pi^- K^0_S K^0_S\pi^0\nu_\tau) &= (2.06 \pm 0.23 \pm 0.24) \times 10^{-5}
\end{aligned}$$

where $\mathcal{B}(\tau^- \to \pi^- K^0_S K^0_S\pi^0\nu_\tau)$ is the first measurement. We also report the first observation of the channel $\tau^- \to \pi^- f_1(1285)\nu_\tau$ in $\pi^- K^0_S K^0_S\pi^0$ decay with

its total branching fraction of $(1.07 \pm 0.23 \pm 0.16) \times 10^{-5}$. With these results, we expect the most precise value of $|V_{us}|$ can be achieved.

Keywords: tau lepton, hadronic decays, Vus, Belle

Student Number: **2007-30779**

Contents

List of Figures

List of Tables

Chapter 1

Introduction

τ is the third kind of elementary particle in our world which is the only lepton heavy enough to decay into hadrons in final state, not like as other two leptons, muon(μ) and electron(e). This point makes τ lepton attractive for studying the mixing parameter between u quark and s quark($|V_{us}|$) of Kobayashi-Maskawa model, the strange quark mass and the strong coupling constant α_s in QCD, which are important parameters to describe the Standard Model of today. The hadronic decays of τ lepton provides very a clean environment to test the Chiral perturbation theory(ChPT) and Lattice Quantum ChromoDynamics(LQCD) on the limit of the chiral symmetry region. Furthermore, τ decays can provide a sensitive probe for the discovery of so to speak "beyond-the-Stardard-Model" pheonmena. In this chapter, the general features of τ lepton and their decay properties in the standard model are discussed in the section 1.1. In the section 1.2, we explain the hadronic τ decays and the relations among the standard model parameters: m_s, α_s and $|V_{us}|$. The applications to the $|V_{us}|$ determination using hadronic τ decays are explained in the section 1.3. In the last section, the outline of this thesis is presented.

1.1 The τ lepton

The τ lepton is the one of building block of the standard model. The standard model explains the properties of six quarks and six leptons and their interplays with massive/massless vector bosons(g, γ, $W^{\pm}, Z$) which take responsible for three of four fundamental forces in our world. The properties of leptons and quarks are summarized in Table 1.2. Among the leptons, τ is the heaviest one and its mass is bigger than 3 quarks: u,d and s , so that it can decay not only into leptons but also hadrons in the limit of phase space and allowed symmetries. The τ lepton always decay with ν_τ via charged massive vector boson, $W^{\pm}$, and the mass and momentum can not be reconstructed by kinematic constraints. This is critical weakness of τ physics study, in other word it could provide a challenging field to develope different analysis techniques. In addition, the τ hadronic decays provide a clean environment for extensive study of QCD models. The leptonic/hadronic τ decays can be expressed by vector-axial vector(V-A) current formalism. The hadronization is thought to be very weak or completely independent to the coupling to the massive vector boson so that it make easy to build the perturbative QCD theories.

1.1.1 τ pair production

The τ pair event can be produced from e^+e^- collision where the center of mass energy is larger than twice the mass of τ lepton. Not only for the τ lepton pair but also other fermion pairs, and sometimes two electrons and another lepton or quark pairs, called as $\gamma\gamma$(two-photon) process, can be produced by e^+e^- collision. Figure 1.1 shows the feynman diagrams for the production of lepton and quark pairs in e^+e^- collision. The s-channel process(top left) can produce the τ pair event while the t-channel process(top right) can produce electron pair event exclusively. Other possible τ pair generation can be found in $\gamma\gamma$ process as depicted in Fig. 1.2. Since many vertexes in the diagram,

however, the production rate is less than the tree level diagram, so the most of τ pair production can be found in s-channel process in e^+e^- collision. [I]

The differential decay rate of s-chnanel process, $e^+e^- \to \gamma^* \to f\bar{f}$, at c.m. energy squred s is given by [38],

$$\frac{d\sigma}{d\Omega} = N_C \frac{\alpha^2}{4s}\beta\left[1+\cos^2\theta+(1-\beta^2)\sin^2\theta\right]Q_f^2, \tag{1.1}$$

where β is v/c for the produced fermions in the c.m., θ is the c.m. scattering angle, and Q_f is the charge of the fermion. The factor N_c is 1 for charged leptons and 3 for quarks. In the high energy limit(ultrarelativistic limit), $\beta \to 1$,

$$\sigma = N_c Q_f^2 \frac{4\pi\alpha^2}{3s} = N_c Q_f^2 \frac{86.8\text{nb}}{s(\text{GeV}^2)}. \tag{1.2}$$

Hence, in the high energy limit the cross sections for lepton(quark) pair production in e^+e^- anihilation are only dependent on the $s = E^2_{\text{c.m.}}$. On the other hands, near τ mass threshold the total cross section is :

$$\sigma = \frac{4\pi\alpha^2}{3s}\beta\left(\frac{3-\beta^2}{2}\right). \tag{1.3}$$

There is an extensive study for the $\sigma(e^+e^- \to \tau^+\tau^-)$ at the BABAR Collaboration [89] with $\Upsilon(4S)$ energy region concerning of final state radiation, coulomb correction, vacuum polarization, initial state radiation and beam energy spread correction. The present value of the cross section is $\sigma(e^+e^- \to \tau^+\tau^-) = 0.919$ nb at $E_{cm} = 10.58$ GeV/c^2 This value is comparable to the cross section of B meson production : 1.02 nb so that B-factory experiment can be called as τ factory, too.

1.1.2 Branching fraction

The τ can decay into lepton or hadrons accompanying one or two neutrinos. The branching fractions for leptonic decays take about 35% of total

[I] The $\gamma\gamma$, $e^+e^- \to q\bar{q}$, $e^+e^- \to \mu\mu$ and $e^+e^- \to e^+e^-$ are the major background for τ physics analysis

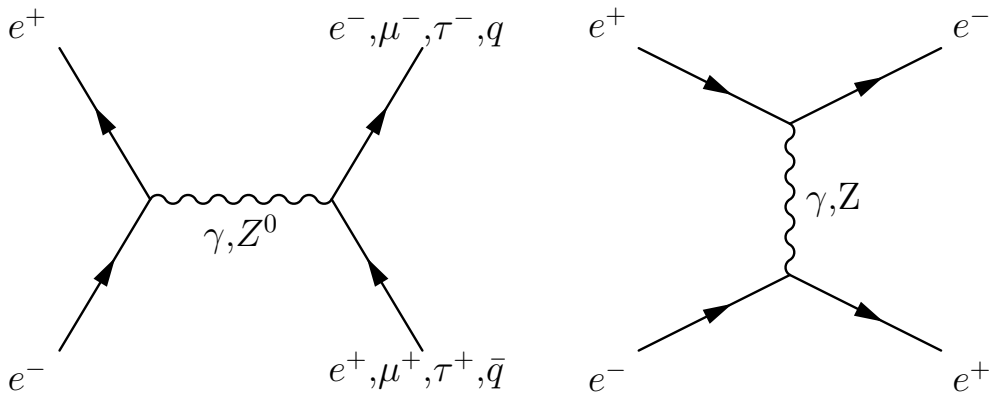

Figure 1.1: Feynman diagrams for the production of lepton and quark pairs in e^+e^- collisions. s channel on the left, t channel on the right

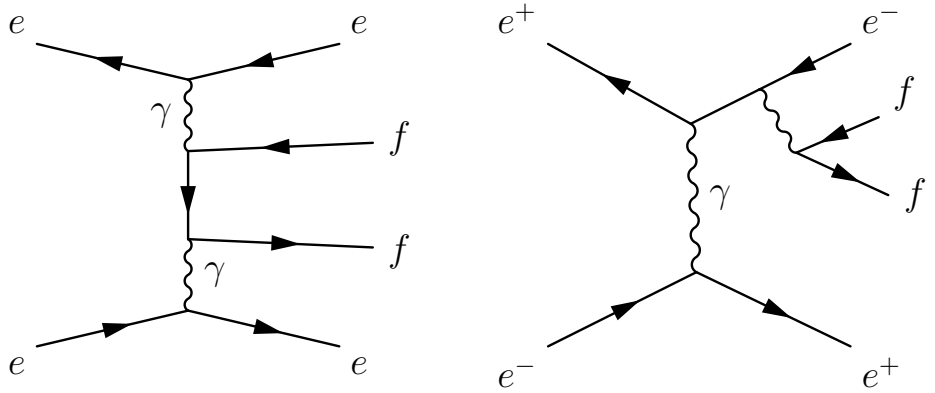

Figure 1.2: Feynman diagrams of two photon process in e^+e^- collisions.

Symbol	Mass(MeV/c^2)	Spin(J)	Q(e)	L_e	L_μ	L_τ
e^-/e^+	0.511	1/2	-1/+1	+1/-1	0	0
$\nu_e/\bar{\nu}_e$	unknown	1/2	0	+1/-1	0	0
μ^-/μ^+	105.6	1/2	-1/+1	0	+1/-1	0
$\nu_\mu/\bar{\nu}_\mu$	unknown	1/2	0	0	+1/-1	0
τ^-/τ^+	1776.8	1/2	-1/+1	0	0	+1/-1
$\nu_\tau/\bar{\nu}_\tau$	unknown	1/2	0	0	0	+1/-1

Table 1.1: The properties of leptons. L_i represents the lepton number.

Symbol	Mass(MeV/c^2)	Spin(J)	Q(e)	B	I_3	C	S	T	B'
$u/\bar{u}$	$1.5 \sim 3.3$	1/2	+2/3,-2/3	+1/3	+1/2,-1/2	0	0	0	0
$d/\bar{d}$	$2.5 \sim 6.0$	1/2	-1/3,+1/3	+1/3	-1/2,+1/2	0	0	0	0
$c/\bar{c}$	~ 1270	1/2	+2/3,-2/3	+1/3	0	+1,-1	0	0	0
$s/\bar{s}$	$80 \sim 120$	1/2	-1/3,+1/3	+1/3	0	0	-1,+1	0	0
$t/\bar{t}$	$\sim 172{,}900$	1/2	+2/3,-2/3	+1/3	0	0	0	+1,-1	0
$b/\bar{b}$	~ 4200	1/2	-1/3,+1/3	+1/3	0	0	0	0	-1,+1

Table 1.2: The properties of quarks. B stands for the baryon number.

and for hadronic decays takes the other, about 65% [39]. In early stage of τ physics analysis, τ decays are classified by their event topology, which is calls as "prong" that is the number of tracks in final state. In view of event topology, 1 prong modes account for 80% of the decays and 3 prong modes account for the remaining 20%. Since the limited phase-space in τ mass, 5-prong and others modes exist but their contributions are small, less than 1%.

For the details in τ decays, it is necessary to include/reconstruct netural mesons with particle identification. With powerful particle identification technique, several collaborations, L3, ALEPH, DELPHI and CLEO, determined the τ decay branching fractions with large number of τ pairs. The most complete analysis had been done by ALEPH [12] who introduced 13 classes of τ decay modes to obtain the branching fractions using global method, where the 13 classes are : $h^-\nu_\tau$, $h^-\pi^0\nu_\tau$, $h^-2\pi^0\nu_\tau$, $h^-3\pi^0\nu_\tau$, $h^-4\pi^0\nu_\tau$, $2h^-h^+\nu_\tau$, $2h^-h^+\pi^0\nu_\tau$, $2h^-h^+2\pi^0\nu_\tau$, $2h^-h^+3\pi^0\nu_\tau$, $3h^-2h^+\nu_\tau$, $3h^-2h^+\pi^0\nu_\tau$, where h stands for a pion or kaon. However, the number of event for some decay modes involving kaon are too small to determine the branching fractions for these collaborations. On the other hands, B-factories had accumulated large number of τ events with hundred millions which is at least 100 times larger than that accumlated at non B-factory experiments. With their large $\tau^+\tau^-$ data samples, some branching fractions are determined with better precision or updated with better upper limits.

In addition to the ALEPH's classification, the Particle Data Group(PDG) [39] included additional decay modes that was/is measured precisely at later experiments and provided the fit results for the τ decay branching fractions using 31 decay modes from all official experimental results. Figure 1.3 shows the composition of the τ decays from PDG. In this figure the six decay modes account for 90% of decays and the other modes account for the remainings. The hadronic decays which account for 65% of decays can be categorized into their strangeness; Cabibbo-allowed and Cabbibo-suppressed. The Cabibbo-

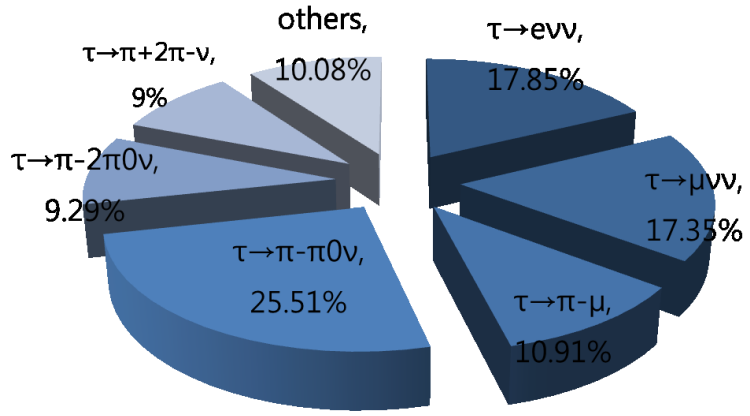

Figure 1.3: The composition of τ decays. the six decay modes account for 90% of decays.

suppressed decays account for 3% of total decays while the Cabibbo-allowed account for 62% of it. The details can be found in the latter subsections.

Leptonic branching fraction

The τ can decay into two other leptons, electron and muon, and their branching ratio is very important in term of the test of lepton universality and CKM unitarity which will be introduced later section. In addition, the hadronic spectral functions(See Sec. 1.2.2) which provide enomous information for many standard model parameters are obtained by the normalization to the leptonic decay width. The theoretical expectation for leptonic branching fractions including radiative correction and safely neglecting neutrino masses is:

$$\Gamma(\tau \to l\bar{\nu}_l\nu_\tau) = \frac{G_\tau G_l m_\tau^5}{192\pi^3} f\left(\frac{m_l^5}{m_\tau^2}\right) \delta_W^\tau \delta_\gamma^\tau \tag{1.4}$$

where

$$
\begin{aligned}
G_l &= \frac{g_l^2}{4\sqrt{2}M_W^2}, \\
\delta_W^\tau &= 1 + \frac{3}{5}\frac{m_L^2}{M_W^2}, \\
\delta_\gamma^\tau &= 1 + \frac{\alpha(m_L)}{2\pi}\left(\frac{25}{4} - \pi^2\right), \\
f(x) &= 1 - 8x + 8x^3 - x^4 - 12x^2 \ln x. \qquad (1.5)
\end{aligned}
$$

And the radiative and W propagator corrections are small;

$$
\begin{aligned}
\delta_W^\tau &= 1 + 2.9 \times 10^{-4}, \quad \delta_\gamma^\tau = 1 - 43.2 \times 10^4, \\
\delta_W^\mu &= 1 + 1.0 \times 10^{-6}, \quad \delta_\gamma^\mu = 1 - 42.4 \times 10^4.
\end{aligned}
$$

One arrives at the following predictions:

$$
\mathcal{B}_e = (17.772 \pm 0.075)\%, \quad \mathcal{B}_\mu = (17.282 \pm 0.073)\%
$$

where $\mathcal{B}_e = \mathcal{B}(\tau^- \to e^- \bar{\nu}_e \nu_\tau)$ and $\mathcal{B}_\mu = \mathcal{B}(\tau^- \to e^- \bar{\nu}_\mu \nu_\tau)$. The errors are dominated by the uncertainty in the lifetime of the τ.

The measurements for $\mathcal{B}_e$ and $\mathcal{B}_\mu$ has been done by several experiments : [7, 8, 9, 10, 11, 12].

The averaged results are

$$
\mathcal{B}_e = (17.82 \pm 0.052)\%, \quad \mathcal{B}_\mu = (17.332 \pm 0.049)\% \qquad (1.6)
$$

with 0.3 % precision. These two branching fractions are used to check the lepton universality by using their ratio,

$$
\frac{\mathcal{B}_\mu}{\mathcal{B}_e} = 0.9726 \pm 0.0041. \qquad (1.7)
$$

This is consistent with the predicted value

$$
f\left(\frac{m_\mu^2}{m_\tau^2}\right) / f\left(\frac{m_e^2}{m_\tau^2}\right) = 0.972565 \pm 0.000009 \qquad (1.8)
$$

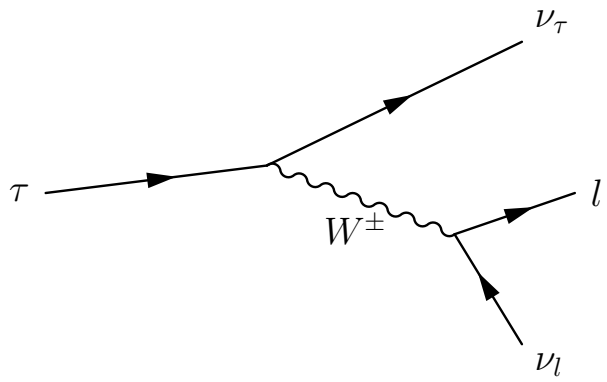

Figure 1.4: Feynman diagram of leptonic τ decay

which uses lepton masses from the Particle Data Group(PDG)[39]. The electronic branching fraction $\mathcal{B}_e$ can be written by the τ and μ masses and lifetimes, $\tau_{\tau,\mu}$, under the assumption of $\tau - \mu$ universality :

$$\mathcal{B}_e = \frac{\tau_\tau}{\tau_\mu}\left(\frac{m_\tau}{m_\mu}\right)^5 \frac{f(m_e^2/m_\tau^2}{f(m_e^2/m_\mu^2} = \frac{\tau_\tau}{(1631.9 \pm 1.4)\text{fs}}. \tag{1.9}$$

Using the τ lifetime, $\tau_\tau = (290.6 \pm 1.1)$fs, one obtains $\mathcal{B}_e = (17.807 \pm 0.067)\%$ which is consistent with the direct measurement.

Using $\mathcal{B}_e$ and $\mathcal{B}_\mu$, we can obtain the hadronic branching fraction in τ and $\mathcal{B}(\tau^- \to \text{hadrons}^-\nu_\tau) = 1 - \mathcal{B}_e - \mathcal{B}_\mu = (64.85 \pm 0.06)\%$.

Hadronic branching fraction

As mentioned in previous section, the hadronic decay width obtained by subtracting the leptonic branching fraction to unity is equal to $(64.85 \pm 0.06)\%$. But this is not the whole story of the hadronic branching fraction.

In general, hadronic branching fractions for τ decays are classified by their strangeness, which is related to the number of kaons in final state. Among the τ decay modes involving kaon, the decay modes of net strangeness is 1, odd number of kaons in final state, attain special attention these days, because the Cabbibo-suppressed hadronic decay width leads to the interesting physics

application: $|V_{us}|$ and CP violation. The decay modes of net strangeness 0, even number of kaons in final state, can be a good playground for studying strong couplings and QCD dynamics at $\sqrt{s} = 2$ GeV region.

In early stage of tau analysis, the most complete analysis of τ decays involving kaon has been done by ALEPH Collaboration[13, 14, 15, 16, 17, 18, 19]. Recently, B-factories has accumulated the enomous number of τ pair events and improved the accuracy of the branching fractions. Heavy Flaver Averaging Group(HFAG) provides the fit results for the branching fractions by using all latest results [37].(See Table 1.3) And they also provides the results separated by the experiments.

After inclusion of B-factory results, the precisions are much better than before so that it is sufficient for various significant tests: $\tau - \mu$ lepton universality, resonance production, QCD analysis, and the measurement of the Cabibbo angle.

The hadronic τ decay branching fractions were expected by using several assumptions on the hadronic currents. According to the extensive studies from ALEPH, OPAL and DELPHI, the hadronic τ decays are known to be strongly dominated by some resonances, vector or axial-vector currents, but their specific informations are not revealed precisely, yet. Some theoretical expectations for hadronic branching fractions were reported by using the simplest assumptions on QCD models and parameters according to the results from the $e^+e^- \to q\bar{q}$ processes[22, 24, 25]. The simple case for comparing the experimental result to the theoretical prediction is to use the fit result for $\mathcal{B}(\tau^- \to K^-\nu_\tau) = (0.696 \pm 0.010)$ by assuming $\tau - \mu$ universality and using τ life times, masses, $K^- \to \mu^-\bar{\nu}_\mu$ branching fraction, and a small radiative correction $\delta_{\tau/K} = 1.0090 \pm 0.0022$,

$$\begin{aligned}\mathcal{B}(\tau^- \to K^-\nu_\tau) &= \frac{\tau_\tau \mathcal{B}(K \to \mu\nu)}{\tau_K} \frac{m_\tau^3}{2m_K m_\mu^2} \left(\frac{1 - m_K^2/m_\tau^2}{1 - m_\mu^2/m_K^2}\right)^2 \delta_{\tau/K} \\ &= \frac{\tau_\tau}{(40636 \pm 162)\text{fs}} = (0.715 \pm 0.003)\% \end{aligned} \tag{1.10}$$

This expectation is agreed with the experimental results.

Base modes from τ^- decay	No B-Factory Data	With B-Factory Data
$K^-\nu_\tau$	0.686 ± 0.022	0.696 ± 0.010
$K^-\pi^0\nu_\tau$	0.453 ± 0.027	0.431 ± 0.015
$K^-2\pi^0\nu_\tau$ (ex. K^0)	0.057 ± 0.023	0.061 ± 0.022
$K^-3\pi^0\nu_\tau$ (ex. K^0, η)	0.037 ± 0.022	0.040 ± 0.022
$\bar{K}^0\pi^-\nu_\tau$	0.884 ± 0.038	0.826 ± 0.018
$\bar{K}^0\pi^-\pi^0\nu_\tau$	0.355 ± 0.036	0.347 ± 0.015
$\bar{K}^0\pi^-2\pi^0\nu_\tau$	0.026 ± 0.023	0.028 ± 0.023
$\bar{K}^0h^-h^-h^+\nu_\tau$	0.022 ± 0.020	0.022 ± 0.020
$K^-\pi^-\pi^+\nu_\tau$ (ex. K^0, ω)	0.334 ± 0.023	0.292 ± 0.007
$K^-\pi^-\pi^+\pi^0\nu_\tau$ (ex. K^0, ω, η)	0.039 ± 0.014	0.041 ± 0.014
$K^-\phi\nu_\tau$ ($\phi \to K\bar{K}$)		0.004 ± 0.001
$K^-\eta\nu_\tau$	0.027 ± 0.006	0.015 ± 0.001
$K^-\pi^0\eta\nu_\tau$	0.018 ± 0.009	0.005 ± 0.001
$\bar{K}^0\pi^-\eta\nu_\tau$	0.022 ± 0.007	0.009 ± 0.001
$K^-\omega\nu_\tau$	0.041 ± 0.009	0.041 ± 0.009
Sum of strange modes	3.0002 ± 0.0764	2.8604 ± 0.0515

Table 1.3: Fit results for strange branching fractions (in %) from HFAG tau group. The result are unconstrained to the unity.

Base modes from τ^- decay	No B-Factory Data	With B-Factory Data
$\pi^-\nu_\tau$	10.898 ± 0.066	10.811 ± 0.053
$\pi^-\pi^0\nu_\tau$	25.489 ± 0.097	25.506 ± 0.092
$\pi^-2\pi^0\nu_\tau$ (ex. K^0)	9.227 ± 0.100	9.245 ± 0.100
$\pi^-3\pi^0\nu_\tau$ (ex. K^0)	1.029 ± 0.075	1.035 ± 0.075
$\pi^-4\pi^0\nu_\tau$ (ex. K^0, η)	0.098 ± 0.039	0.109 ± 0.039
$K^-\bar{K}^0\nu_\tau$	0.152 ± 0.016	0.157 ± 0.016
$K^-\pi^0\bar{K}^0\nu_\tau$	0.154 ± 0.020	0.158 ± 0.020
$\pi^-K^0_SK^0_S\nu_\tau$	0.024 ± 0.005	0.024 ± 0.005
$\pi^-K^0_SK^0_L\nu_\tau$	0.107 ± 0.025	0.111 ± 0.025
$\pi^-K^0_LK^0_L\nu_\tau$	0.022 ± 0.042	0.018 ± 0.042
$\pi^-\pi^0K^0\bar{K}^0\nu_\tau$	0.031 ± 0.023	0.031 ± 0.023
$\pi^-\pi^-\pi^+\nu_\tau$ (ex. K^0, ω)	8.948 ± 0.062	8.970 ± 0.051
$\pi^-\pi^-\pi^+\pi^0\nu_\tau$ (ex. K^0, ω)	2.752 ± 0.070	2.761 ± 0.069
$h^-h^-h^+2\pi^0\nu_\tau$ (ex. K^0, ω, η)	0.085 ± 0.037	0.098 ± 0.036
$h^-h^-h^+3\pi^0\nu_\tau$	0.025 ± 0.005	0.032 ± 0.003
$\pi^-K^-K^+\nu_\tau$	0.153 ± 0.007	0.143 ± 0.003
$\pi^-K^-K^+\pi^0\nu_\tau$	0.006 ± 0.002	0.006 ± 0.002
$3h^-2h^+\nu_\tau$ (ex. K^0)	0.081 ± 0.005	0.082 ± 0.003
$3h^-2h^+\pi^0\nu_\tau$ (ex. K^0)	0.019 ± 0.003	0.020 ± 0.002
$\pi^-\pi^0\eta\nu_\tau$	0.174 ± 0.024	0.139 ± 0.007
$\pi^-\omega\nu_\tau$	1.952 ± 0.064	1.954 ± 0.064
$h^-\pi^0\omega\nu_\tau$	0.404 ± 0.042	0.406 ± 0.042
$a_1^-(\to \pi\gamma)\nu_\tau$	0.040 ± 0.020	0.040 ± 0.020

Table 1.4: Fit results for non-strange branching fractions (in %) from HFAG tau group. The result are unconstrained to the unity.

Nonstrange hadronic branching fractions account for the largest part of τ decays and the physics goals require the achievement of small systematic uncertainties. The fit results from HFAG are shown in Table 1.4. In the table, the branching fraction $\mathcal{B}(\tau^- \to \pi^- \nu_\tau) = 10.811$ agrees well with theoretical prediction depending only on the assumption of $\tau - \mu$ universality and using τ, π life times, masses, $\pi^- \to \mu^- \bar{\nu}_\mu$ branching fraction, and a small radiative correction $\delta_{\tau/\pi} = 1.0016 \pm 0.0014$,

$$\begin{aligned} \mathcal{B}(\tau^- \to \pi^- \nu_\tau) &= \frac{\tau_\tau \mathcal{B}(\pi \to \mu\nu)}{\tau_\pi} \frac{m_\tau^3}{2 m_\pi m_\mu^2} \left(\frac{1 - m_\pi^2/m_\tau^2}{1 - m_\mu^2/m_\pi^2} \right)^2 \delta_{\tau/\pi} \\ &= \frac{\tau_\tau}{(2663.7 \pm 4.0)\text{fs}} = (10.910 \pm 0.044)\% \end{aligned} \tag{1.11}$$

For the two and more mesons we need to introduce the structure functions which will be explained in the next section.

1.2 Hadronic τ decay

The decay of the τ lepton into hadrons was calculate by Paul Tsai [20], even before the discovery of the τ. In analogy to purely leptonic decays, the invariant amplitude for hadronic decays can be written in the form of a factorized current-current interaction,

$$\mathcal{M}(\tau^- \to \text{hadrons}^- \nu_\tau) = \frac{G_F}{\sqrt{2}} |V_{CKM}| l_\mu h^\mu \tag{1.12}$$

with the corresponding nonstrange or strange CKM matrix element $|V_{CKM}|$, and where l_μ describes the leptonic $V - A$ current

$$l_\mu = \bar{\nu}_\tau \gamma_\mu (1 - \gamma_5) \tau \tag{1.13}$$

of the weak interaction. (assuming $g_V = g_A = 1$) The hadronic transition current h_μ can be expressed by

$$h_\mu = \langle \text{hadrons} | V_\mu(0) - A_\mu(0) | 0 \rangle \tag{1.14}$$

where $V_\mu(0)$ and $A_\mu(0)$ are the vector and axial-vector quark currents, respectively. These currents can be changed by the number of pseudoscalars in final state. Then the differential τ hadronic width can be expressed as follows:

$$d\Gamma(\tau^- \to \text{hadrons}^- \nu_\tau) = \frac{G_F^2}{4M_\tau} |V_{CKM}| L_{\mu\nu} H^{\mu\nu} d\text{PS} \tag{1.15}$$

with the leptonic(hadronic) tensor $L_{\mu\nu}(H_{\mu\nu})$ and the Lorentz invariant phase-space element dPS.

1.2.1 Hadronic decays and their structures

Most of the hadronic decays of the τ lepton are dominated by intermediate vector or axial-vector mesons, eventually decaying into pseudoscalars. This feature had been called as Vector Meson Dominance(VMD) and when theorists formulate such features in their interpretation, the Vector Dominance

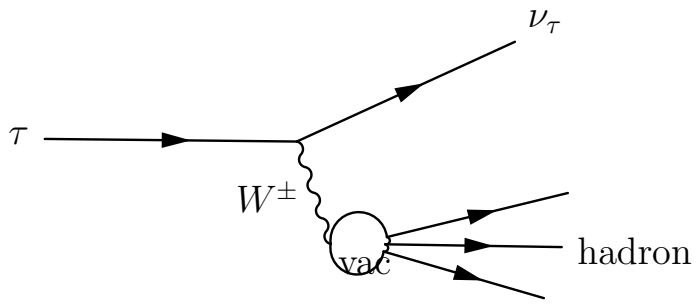

Figure 1.5: A diagram of hadronic τ decay

Model(VDM) is the main guidline. However, none of resonances can be predicted from current theory but simply parametrized with Briet-Wigner form factors with the mass and width as free parameters. The various and detailed studies for two and three meson decays have been done by Kuhn, Mirkes and their collagues.[23, 24, 25]

The single meson decay modes

For the compeleteness we bring the similar but full expression of the branching fractions for the channel when τ decays into the single meson final state. As mentioned before, there are two decay modes: $\tau^- \to \pi^-\nu_\tau$ and $\tau^- \to K^-\nu_\tau$. The decay width for $\tau^- \to \pi^-\nu_\tau$ and $\tau^- \to K^-\nu_\tau$ can be calculated by using the decay constant $f_{\pi/K}$ which determine the strength of the coupling of the pion to the charged current, masses of pion/kaon and tau and the Cabibbo angles. The decay width for $\tau^- \to \pi^-\nu_\tau$ can be calculated by,

$$\mathcal{B}(\tau^- \to \pi^-\nu_\tau) = \frac{G_F^2 f_\pi^2 |V_{ud}|^2}{16\pi} m_\tau^2 \left(1 - \frac{m_\pi^2}{m_\tau^2}\right) S_{EW} \tag{1.16}$$

where S_{EW} is the electroweak correction. The decay width for $\tau^- \to K^-\nu_\tau$ can be easily obtained by changing from f_π to f_K and from $|V_{ud}|$ to $|V_{us}|$.

The decay width for single meson final state in Eq. 1.16 actually has no finite width but expressed as a δ function.

The two meson decay modes

The two meson final state in τ decay can be described by the vector currents and possible scalar currents. The matrix element for the semileptonic decay into two mesons h_1 and h_2,

$$\tau(l,s) \to \nu(l,s) + h_1(q_1, m_1) + h_2(q_2, m_2), \tag{1.17}$$

can be expressed in terms of a leptonic(L_μ) and a hadronic vector current(H^μ) just like as in Eq. 1.12,

$$\mathcal{M} = \frac{G_F}{\sqrt{2}} \begin{pmatrix} \cos\theta_c \\ \sin\theta_c \end{pmatrix} L_\mu H^\mu \tag{1.18}$$

where the leptonic current is given in Eq. 1.13 and the hadronic currents given in Eq. 1.14 is expressed as

$$H^\mu = \langle h_1(q_1) h_2(q_2) | V^\mu(0) | 0 \rangle \tag{1.19}$$

The two-pion decay channel is dominated by the ρ resonance,

$$\langle \pi(q_1)\pi(q_2) | V^\mu(0) | 0 \rangle = \sqrt{2} T_\rho^{(1)}(Q^2)(q_1 - q_2)_\nu T^{\mu\nu} \tag{1.20}$$

where $T_\rho^{(1)}(Q^2)$ denotes the combination of Breit-Winger functions that models ρ resonance(shown latter), $Q = q_1 + q_2$ and $T^{\mu\nu}$ is the transverse projector, defined by

$$T^{\mu\nu} = g^{\mu\nu} - \frac{Q^\mu Q^\nu}{Q^2} \tag{1.21}$$

On the other hand, the Cabbibo suppressed decay modes $K^-\pi^0\nu_\tau$, $\bar{K}^0\pi^-\nu_\tau$ are dominated by the K^* resonance $T_{K^*}^{(1)}(Q^2)$, whereas the one for the Cabibbo

allowed mode K^0K^- is dominated by the high energy tail of the ρ. These can be written by

$$\begin{aligned}\langle K^-(q_1)\pi^0(q_2)|V^\mu(0)|0\rangle &= \frac{1}{\sqrt{2}}\langle K^-(q_1)\pi^0(q_2)|V^\mu(0)|0\rangle \\ &= \frac{1}{\sqrt{2}}T^{(1)}_{K^*}(Q^2)(q_1-q_2)_\nu T^{\mu\nu} \\ \langle K^0(q_1)K^-(q_2)|V^\mu(0)|0\rangle &= T^{(1)}_{\rho}(Q^2)(q_1-q_2)_\nu T^{\mu\nu} \end{aligned} \tag{1.22}$$

The two mesons decay from a vector meson so that the two particle Breit-Wigner propagator is now introduced with an energy dependent width $\Gamma_X(s)$

$$\mathrm{BW}_X(s) = \frac{M_X^2}{M_X^2 - s - i\sqrt{s}\Gamma_X(s)}, \tag{1.23}$$

where X stands for the various resonances of the two meson channels. The energy dependent width in which $1 \to 2$ process is

$$\begin{aligned}\Gamma_X(s) &= \Gamma_X \frac{M_X^2}{s}\left(\frac{p}{p_X}\right)^{2n+1}, \\ p &= \frac{1}{2\sqrt{s}}\sqrt{(s-(M_1+M_2)^2)(s-(M_1-M_2)^2)}, \\ p_X &= \frac{1}{2M_X}\sqrt{(M_X^2-(M_1+M_2)^2)(M_X^2-(M_1-M_2)^2)},\end{aligned}$$

where n is the power of $|p|$ in the matrix element, *i.e.* $n = 1$ for the two body decay.

The parametrization for the ρ resonance is :

$$T^{(1)}_{\rho}(s) = \frac{1}{1+\beta_\rho}[BW_\rho(s) + \beta_\rho BW_{\rho'}(s)], \tag{1.24}$$

where $\beta_\rho = -0.145$, $m_\rho = 0.773$ GeV, $\Gamma_\rho = 0.145$ GeV, $m_{\rho'} = 1.370$ GeV, $\Gamma_{\rho'} = 0.510$ GeV. These parameters are determined from the $e^+e^- \to \pi^+\pi^-$ in Ref. [23] assuming Conserved Vector Current(CVC) [21]. For the vector resonances with strange quark, two K^* is considered: $K^*(892)$ and $K^*(1410)$. In analogy to 1.24, the Briet-Wigner propagator for the vector resonance is :

$$T^{(1)}_{K^*}(s) = \frac{1}{1+\beta_{K^*}}[BW_{K^*}(s) + \beta_{K^*} BW_{K^{*\prime}}(s)], \tag{1.25}$$

where $\beta_{K^*} = -0.145$, $m_{K^*} = 0.892$ GeV, $\Gamma_{K^*} = 0.050$ GeV, $m_{K^{*\prime}} = 1.412$ GeV, $\Gamma_{K^{*\prime}} = 0.227$ GeV

The numerical results for the decay rates are very sensitive to the parameter β_X in Eq. 1.24 and Eq. 1.25. The expected and measured branching fractions for two meson final state are given in Table 1.5

The three meson decay modes

The three meson final state in hadronic τ decay is described by the axial-vector current with small contribution from the vector current. The matrix element for the semi-leptonic decay into three mesons h_1, h_2 and h_3,

$$\tau(l,s) \to \nu(l,s) + h_1(q_1,m_1) + h_2(q_2,m_2) + h_3(q_3,m_3), \tag{1.26}$$

can be expressed in terms of a leptonic(L_μ) and a hadronic vector current(H^μ) just like as in Eq. 1.12,

$$\mathcal{M} = \frac{G_F}{\sqrt{2}} \begin{pmatrix} \cos\theta_c \\ \sin\theta_c \end{pmatrix} L_\mu H^\mu \tag{1.27}$$

where the leptonic current is given in Eq. 1.13 and the hadronic currents given in Eq. 1.14 is expressed as

$$H^\mu = \langle h_1(q_1) h_2(q_2) h_3(q_3) | V^\mu(0) - A^\mu(0) | 0 \rangle \tag{1.28}$$

The most general ansatz for the hadronic current(H^μ) is characterized by four form factors

$$H^\mu(q_1,q_2,q_3) = V_1^\mu F_1 + V_2^\mu F_2 + i V_3^\mu F_3 + V_4^\mu F_4 \tag{1.29}$$

where,

$$\begin{aligned} V_1^\mu &= (q_1 - q_3)_\nu T^{\mu\nu}, \\ V_2^\mu &= (q_2 - q_3)_\nu T^{\mu\nu}, \\ V_3^\mu &= \epsilon^{\mu\alpha\beta\gamma} q_{1\alpha} q_{2\beta} q_{3\gamma}, \\ V_4^\mu &= q_1^\mu + q_2^\mu + q_3^\mu = Q^\mu. \end{aligned} \tag{1.30}$$

Decay modes	theory[27],[25]	experiment [39]
nonstrange modes		
$\pi^-\nu_\tau$	10.9	10.81 ± 0.053
$\pi^-\pi^0\nu_\tau$	24.5	25.51 ± 0.092
$\pi^-3\pi^0\nu_\tau$	1.07	1.035 ± 0.075
$\pi^-\pi^0\eta\nu_\tau$	0.13	0.174 ± 0.024
$\pi^-\omega\nu_\tau$	2.2	1.952 ± 0.064
$K^-\bar{K}^0\nu_\tau$	0.11	0.157 ± 0.016
$K^-\pi^0\bar{K}^0\nu_\tau$	0.16	0.158 ± 0.020
$\pi^-K^-K^+\nu_\tau$	0.20	0.143 ± 0.003
$K^0\pi^-\bar{K}^0\nu_\tau$	0.20	0.153 ± 0.045
strange modes		
$K^-\nu_\tau$	0.71	0.696 ± 0.010
$K^-\pi^0\nu_\tau$	0.56	0.431 ± 0.015
$K^-2\pi^0\nu_\tau$	0.09	0.061 ± 0.022
$\bar{K}^0\pi^-\nu_\tau$	0.80	0.826 ± 0.018
$\bar{K}^0\pi^-\pi^0\nu_\tau$	0.41	0.347 ± 0.015
$K^-\pi^-\pi^+\nu_\tau$	0.40	0.292 ± 0.007

Table 1.5: The expected/measured branching fractions for hadronic τ decays.

Since the strong interaction conserves parity, the axial-vector current induces the form factors F_1, F_2 and F_4 while the vector current induces F_3. In high energy limit where the quark masses vanishes, the weak axial-vector current is conserved and the scalar form factor F_4 vanishes. Even if the massive pseudoscalar give a contribution to F_4, the effect is very small and it can be neglected($F_4 = 0$). The vector current, F_3, arise from the Wess-Zumino Lagrangian for the axial anomaly[28, 29, 30, 31].

In general, the form factors F_i are the functions of Q^2, $s_1 = (q_2 + q_3)^2$, $s_2 = (q_1 + q_3)^2$ and , $s_3 = (q_1 + q_2)^2$. The hadronic axial-vector current is expressed as follow:

$$\begin{aligned}\langle h_a h_b h_c|A^\mu(0)|0\rangle &= V_1^\mu F_1 + V_2^\mu F_2 \\ &= \frac{2\sqrt{2}A^{(abc)}}{3f_\pi}\{G_1^{(abc)}(q_1 - q_2)_\nu + G_2^{(abc)}(q_2 - q_3)_\nu\}T^{\mu\nu},\end{aligned} \tag{1.31}$$

For the hadronic vector current, the expression is :

$$\begin{aligned}\langle h_a h_b h_c|V^\mu(0)|0\rangle &= iV_3^\mu F_3 \\ &= \frac{i}{2\sqrt{2}\pi^2 f_\pi^3}A^{(abc)}\epsilon^{\mu\alpha\beta\gamma}q_{1\alpha}q_{2\beta}q_{3\gamma}G_3^{(abc)}.\end{aligned} \tag{1.32}$$

where the $A^{(abc)}$ is the coefficients consist of Cabibbo angle and the coefficients from ChPT expansion, the $G^{(abc)}$ is the combination of Breit-Wigner functions corresponding to the relevant vector/axial-vector resonances. More detailed informations for two variables can be found in Table 1,2 of Ref. [25].

The graphical explanation for hadronic current in τ can be found in Fig. 1.6. The diagrams in left column represent the axial-vector-vector-pseudoscalr vertex and the diagrams in the other column represent the vector-vector-pseudoscalar current(Wess-Zumino current). Usually, in $3\pi\nu$ decays, a dominant intermediate resonance is found to be a_1 which decays into $\rho^0\pi^-$. The two K_1 axial-vector resonances are give a dominant contribution to $K\pi\pi\nu$ and $K\bar{K}\pi$ decays according to the studies of CLEO [51]. On the other hand,

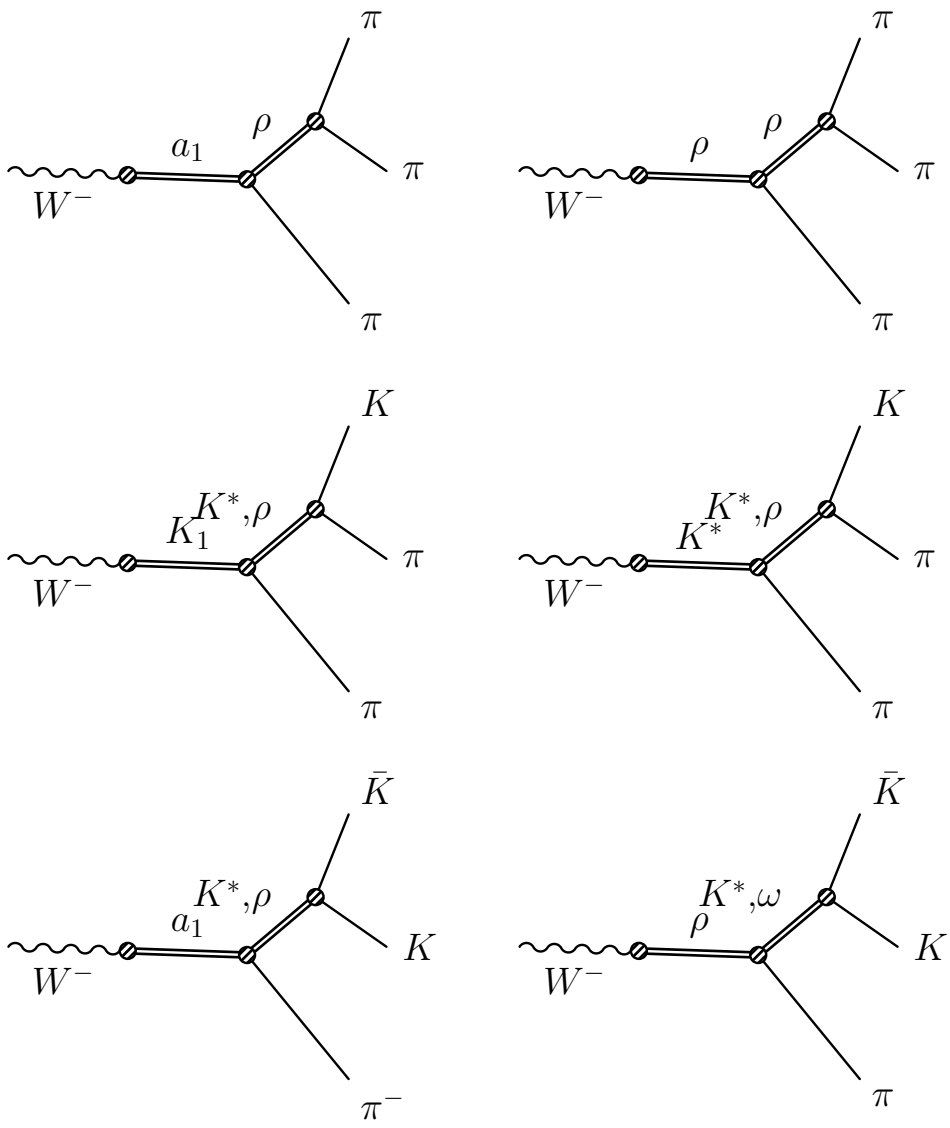

Figure 1.6: Decay diagrams for τ decays into three pseudoscalars. The diagrams in the left column include a axial-vector-pseudoscalar vertex(F_1, F_2), and the diagrams in the right column include a vector-vector-pseudoscalar vertex, which is generated in ChPT by Wess-Zumino anomaly(F_3)

it is also expected to found Wess-Zumino current among 3 mesons [50]. The axial anomaly is expected to be more enhanced at $\tau \to K\bar{K}\pi\nu$ decays otherwise the $\tau \to 3\pi\nu$ decay is not due to the isospin symmetry. The possible vector currents in $K\pi\pi\nu(K\bar{K}\pi)$ decay is the $K^*(\rho^*)$ current.

In this parametrization, one expects the branching fractions for $K\pi\pi\nu$ and $K\bar{K}\pi\nu$ channels and the predictions are given in Table 1.5. Not like as the single meson final state, their theoretical predictions show rather different from the experimental measurements, because the magnitude of the hadronic currents and their interferences are still unknown.

More than three meson decay modes

The hadronic τ decays into more than three mesons are not estabilished, but using the isospin symmetries in pions and CVC hyphothesis, it is possible to make rough estimation for the branching fractions for the decays into four pions. [II] Under the CVC hyphothesis the weak charge is not altered by quantum corrections and the coupling constant becomes a process-independent quantity dependent only on Q^2. Quantitatively, the relation is

$$\Gamma(\tau \to \mathrm{had}\nu_\tau) = \frac{\cos^2\theta_C G_\mathrm{F}^2 m_\tau^3}{32\pi^2} \times 2\int_0^{m_\tau^2} ds \left(1-\frac{s}{m_\tau^2}\right)^2 \left(1+2\frac{s}{m_\tau^2}\right) \frac{s}{8\pi^2\alpha^2}\ \sigma^{I=1}_{e^+e^-\to\mathrm{had}}(s) \tag{1.33}$$

Using this relation, several authors have predicted as given in Table 1.5.

1.2.2 Spectral function

The spectral function is the one of observables that describe the interaction of the quarks, which can be used for giving additional constraints on the strong coupling constant, $\alpha_S(m_\tau^2)$. Even we don't know much about the specific

[II] It should be noticed that CVC only give a constraint to the decays into nonstrange vector final states and the proper charge combinations of the hadrons.

current of hadronic decays, it is possible to extract the quark's properties inclusively. The derivation of the spectral function start from the differential τ hadronic width which can be reexpressed by the imaginary part of the forward scattering amplitude using the optical theorem.

$$d\Gamma_{\text{hadron}} = \frac{G_F}{2\sqrt{2}m_\tau}\left(|V_{ud}|^2 + |V_{us}|^2\right) L^{\mu\nu} 2\text{Im}\langle 0|J_\mu(q)J_\nu^\dagger(q)|0\rangle d\text{PS}_{\nu_\tau}^{(4)} \quad (1.34)$$

where q is the 4-momentum hadronic system ($q^2 = s$). The dynamics of the amplitude in Eq. 1.34 can be made explicit by two point correlation functions,

$$\langle 0|J_\mu(q)J_\nu^\dagger(q)|0\rangle = (q_\mu q_\nu - g_{\mu\nu}q^2)\Pi^{(1)}(q^2) + q_\mu q_\nu \Pi^{(0)}(q^2) \quad (1.35)$$

where the equation describe the creation of hadronic states with total angluar momentum J from the vacuum by means of QCD. Conventionally the coupling of the quark current to the $W^\pm$ are not included in Π^J. The integration over the phase space of the neutrino can be performed and we can get,

$$\Gamma_{\text{hadron}}(m_\tau^2) = \frac{G_F^2 m_\tau^5}{16\pi^2}\int_0^{m_\tau^2}\frac{ds}{m_\tau^2}\left(1-\frac{s}{m_\tau^2}\right)^2\left[\left(1+\frac{2s}{m_\tau^2}\right)\text{Im}\Pi^{(1+0)}(s) - 2\frac{s}{m_\tau^2}\text{Im}\Pi^{(0)}(s)\right] \quad (1.36)$$

The correlators $\Pi^{(J)}(s)$ can be decomposed according to the quantum numbers of the states involved,

$$\Pi^{(J)}(s) = |V_{ud}|^2\left(\Pi_{ud,V}^{(J)}(s) + \Pi_{ud,A}^{(J)}(s)\right) + |V_{us}|^2\left(\Pi_{us,V}^{(J)}(s) + \Pi_{us,A}^{(J)}(s)\right) \quad (1.37)$$

where the lower indices on $\Pi^{(J)}$ indicate the quark flavors and type of current(vector or axial-vector). The imaginary part of the correlator $\Pi^J(s)$ can

be redefined as the spectral functions,$v_J(a_J)$, by

$$\begin{aligned} 2\pi \mathrm{Im}\Pi^{(J)}_{ud,V}(s) = v_J(s), \quad 2\pi \mathrm{Im}\Pi^{(J)}_{ud,A}(s) = a_J(s) \\ 2\pi \mathrm{Im}\Pi^{(J)}_{us,V}(s) = v^s_J(s), \quad 2\pi \mathrm{Im}\Pi^{(J)}_{us,A}(s) = a^s_J(s) \end{aligned} \tag{1.38}$$

where the superscript s in $v_J(a_J)$ represents the strangeness 1. Then the hadronic decay width becomes,

$$\begin{aligned} \Gamma_{\mathrm{hadron}} = \frac{G_F^2 m_\tau^5}{16\pi^2} \int_0^{m_\tau^2} \frac{ds}{m_\tau^2} \left(1 - \frac{s}{m_\tau^2}\right)^2 \left\{ \cos^2\theta \left[\left(1 + \frac{2s}{m_\tau^2}\right) (v_1(s) + a_1(s)) + a_0(s) \right] \right. \\ \left. + \sin^2\theta \left[\left(1 + \frac{2s}{m_\tau^2}\right) (v^s_1(s) + a^s_1(s)) + v^s_0(s) + a^s_0(s) \right] \right\} \end{aligned} \tag{1.39}$$

where the nonstrange scalar current owing to conserved vector current(CVC) has been obmitted. This expression indicates that the hadronic decay width can be decomposed into non-strange and strange spectral function as well as vector and axial-vector spectral function.

$$\Gamma_{\mathrm{hadron}} = \Gamma_{\tau,V} + \Gamma_{\tau,A} + \Gamma_{\tau,S}. \tag{1.40}$$

Like as the total hadronic cross-sections in e^+e^- collision, $R = \sigma(e^+e^- \to q\bar{q})/\sigma(e^+e^- \to \mu^+\mu^-)$, one can define the ratio of branching fractions, R_τ :

$$R_\tau \equiv \frac{\Gamma(\tau^- \to \mathrm{hadron}^-\nu_\tau)}{\Gamma(\tau^- \to e^-\bar{\nu_e}\nu_\tau)} = \frac{\Gamma_{\mathrm{hadron}}}{\Gamma_e}. \tag{1.41}$$

This is called as electronic decay width or electronic branching fractions. Then, the Eq. 1.40 can be expressed as :

$$R_\tau = \frac{\Gamma_{\mathrm{hadron}}}{\Gamma_e} = R_{\tau,V} + R_{\tau,A} + R_{\tau,S} \tag{1.42}$$

The spectral function can be obtained from the experiment. One can

rewrite Eq. 1.39 as :

$$
\begin{aligned}
v_1(s) &= \frac{m_\tau^2}{6|V_{CKM}|^2 \mathrm{S_{EW}}} \frac{dR_{\tau,V}}{ds} \left[\left(1 - \frac{s}{m_\tau^2}\right)^2 \left(1 + \frac{2s}{m_\tau^2}\right) \right]^{-1}, \\
a_1(s) &= \frac{m_\tau^2}{6|V_{CKM}|^2 \mathrm{S_{EW}}} \frac{dR_{\tau,A}}{ds} \frac{dN_A}{N_A ds} \left[\left(1 - \frac{s}{m_\tau^2}\right)^2 \left(1 + \frac{2s}{m_\tau^2}\right) \right]^{-1}, \\
a_0(s) &= \frac{m_\tau^2}{6|V_{CKM}|^2 \mathrm{S_{EW}}} \frac{dR_{\tau,A}}{ds} \frac{dN_A}{N_A ds} \left(1 - \frac{s}{m_\tau^2}\right)^2,
\end{aligned} \tag{1.43}
$$

where $\mathrm{S_{EW}}$ indicates the electroweak radiative corrections and,

$$
\frac{dR_{\tau,V}}{ds} = \frac{\mathcal{B}(\tau^- \to V^- \nu_\tau)}{\mathcal{B}(\tau^- \to e^- \bar{\nu}_e \nu_\tau)} \times \frac{dN_V}{N_V ds}, \tag{1.44}
$$

$$
\frac{dR_{\tau,A}}{ds} = \frac{\mathcal{B}(\tau^- \to A^- \nu_\tau)}{\mathcal{B}(\tau^- \to e^- \bar{\nu}_e \nu_\tau)} \times \frac{dN_A}{N_A ds}, \tag{1.45}
$$

$dN_{V/A}/N_{V/A}ds$ is the mass spectra normalized by the total number of events, which can be extracted from the data.

The τ spectral moments at $s_0 = m_\tau^2$ are defined by,

$$
R_\tau^{kl} = \int_0^{m_\tau^2} ds \left(1 - \frac{s}{m_\tau^2}\right)^k \left(\frac{s}{m_\tau^2}\right)^l \frac{dR_\tau}{ds} \tag{1.46}
$$

where $R_\tau^{00} = R_\tau$. This spectral moments can give additional constraints on α_s using the nonstrange τ decay width and can be used for determining V_{us}, m_s and even α_s.

1.2.3 $|V_{us}|$ and m_s

As describe in previous section, the inclusive hadronic τ decay ratio can be expressed by normalizing leptonic decay ratio using the framwork of the operator product expansion(OPE) [3]

$$
R_\tau = R_{\tau,V} + R_{\tau,A} + R_{\tau,S} \tag{1.47}
$$

One can separate the decay ratio by the quark contents of interest: $R_{\tau,V/A}$

is the decay ratio of vector or axial-vector contribution in non-strangeness decay and $R_{\tau,S}$ is for the strange decay. From Eq. 1.36 , R_τ [5] is given by,

$$R_\tau(m_\tau^2) = 12\pi \mathrm{S_{EW}} \int_0^{m_\tau^2} \frac{ds}{m_\tau^2}\left(1-\frac{s}{m_\tau^2}\right)\left[\left(1+\frac{2s}{m_\tau^2}\right)\right. \\ \left. \times \mathrm{Im}\ \Pi^{(1+0)}(s+i\epsilon) - 2\frac{s}{m_\tau^2}\mathrm{Im}\ \Pi^{(0)}(s+i\epsilon)\right] \tag{1.48}$$

This expression contains not only strange part $R_{\tau,S}$ but also non-strange part $R_{\tau,NS}$.For the strange part Eq. 1.48 can be decomposed as:

$$R_{\tau,S} = 3|V_{us}|^2 \mathrm{S_{EW}}(1+\delta^{(0)}+\delta'_{\mathrm{EW}}+\delta_S^{(2,m_q)}+\delta^{(X)}) \tag{1.49}$$

The first term in the correction part in Eq. 1.49, $\delta^{(0)}$, is the massless perturbative contribution which is expanded with $\alpha_s(m_\tau^2)/\pi$, the strong coupling constant. The sencond term represents the residual nonlogarithmic electroweak correction $\delta_{\mathrm{EW}} = 0.0010$ [4]. The $\delta_S^{(2,m_q)}$ term have direct relation to the strange quark mass contribution. One can find the taylor expansion of this term in the framwork of Fixed-order perturbative theory [6],

$$\delta_s^{(2,m_s)} = -8\frac{m_s^2(m_\tau^2)}{m_\tau^2}\left[1+\frac{16}{3}\alpha_s + 46.00\alpha_s^2 + \right. \\ \left. \left(283.6+\frac{3}{4}x_3^{(1+0)}\right)\alpha_s^3\cdots\right] \tag{1.50}$$

And other papers give perturbative expansion formula using different approaches. For example, using the spectral moments defined in previous section(Eq.**??**) the strange quark mass can be obtained from

$$m_S^2(m_\tau^2) \backsimeq \frac{M_\tau^2}{18(1-\epsilon_d^2)\Delta^{L+T}(a_\tau)}\left\{\frac{\delta R^{kl}}{\mathrm{S_{EW}}} - \delta R^{kl,L}_{\tau,\mathrm{phen}}\right\} \tag{1.51}$$

It is quite interesting since the inclusive $S=-1$ branching ratio in τ decay is directly related to not only the $|V_{us}|$ but also the strong coupling constant and the mass of strange quark.

1.3 $|V_{us}|$ and τ decays

1.3.1 Cabbibo Kobayashi Maskawa(CKM) matrix

The Standard Model(SM) is the most successful theory to describe the interactions between the fundamental particles ever discovered. The fundamental particles sorted by the generation according to their mass hierarchy. τ lepton belongs to the third generation, the most heaviest ones are placed. However, these fundamental particles does not keep their state forever. They decay into more lighter ones spontaneously under the law of nature, the symmetry. The symmetry to describe the Standard Model is a combination of $\mathrm{SU}(3)_C \times \mathrm{SU}(2)_L \times \mathrm{U}(1)$ continuous gauge symmetries, where the first one describes the strong force, the interaction between quarks, and the others describes the electroweak force as a unified one of electromagnetic and weak force, called Glashow-Salam-Weinberg model[32]. The standard model contains another dynamic sector for the origin of mass, a single SU(2) doublet of Higgs field which is originated by the Yukawa interactions of the quarks.

$$\begin{aligned} L_{Yukawa} = &- \sum_{i,j} (G_U)_{ij} (\bar{U}_{i,L}, \bar{D}_{i,L}) \begin{pmatrix} \phi^0 \\ -\phi^- \end{pmatrix} U_{j,R} \\ &- \sum_{i,j} (G_D)_{ij} (\bar{U}_{i,L}, \bar{D}_{i,L}) \begin{pmatrix} \phi^+ \\ \phi^0 \end{pmatrix} D_{j,R} \end{aligned} \tag{1.52}$$

where the indices i and j run over 1 to n, the number of families. Once the neutral Higgs field acquires a vacuum expactation value, $\langle \phi^0 \rangle = v$, fermion masses arise. The mass matrices for the up-type(U) and down-type(D) quarks are then proportional to the corresponding Yukawa couplings with the scale set by v:

$$M_U = vG_U \quad M_D = vG_D \tag{1.53}$$

By diagonalizing the up and down quark mass matrices by four unitary matrices, $V_{L,R}^{U,D}$, the physical states are obtained for the charged currents. As

a result, the charged current $W^{\pm}$ interaction couple to the physical up and down-type quarks with coupling given by

$$\mathbf{V} \equiv V_L^U V_R^{D\dagger} = \begin{pmatrix} V_{ud} & V_{us} & V_{ub} \\ V_{cd} & V_{cs} & V_{cb} \\ V_{td} & V_{ts} & V_{tb} \end{pmatrix} \tag{1.54}$$

This matrix is called the Cabbibo-Kobayashi-Maskawa(CKM) matrix[33, 34]. Note that $\mathbf{V}$ is unitary, which reflects weak universality, expressed by

$$\sum_j \mathbf{V}_{ij} \mathbf{V}_{ik}^* = \delta_{jk} \tag{1.55}$$

which means the sum of magnitude of elements in any row(colum) should be equal to 1; in the other word, this is called "CKM unitarity" condition.

1.3.2 Measurements of CKM matrix elements

The magnitudes of CKM elemtent has been observed in various ways and almost complete their measurements.

$|V_{ud}|$

$|V_{ud}|$ has been determined from the study of superallowed $0^+ \to 0^+$ nuclear beta decays. The combined result from 20 most precise determinations[36] yields

$$|V_{ud}| = 0.97425 \pm 0.00022 \tag{1.56}$$

The error is dominated by theoretical uncertainties. The other method to determine $|V_{ud}|$ is to measure the neutron lifetime. Even though small theoretical uncertainties, the determination is limited by the knowledge of the ratio of vector and axial-vector couplings, $g_A = G_A/G_V$. [40] The measurement of branching fraction for $\pi^+ \to \pi^0 e^+ \nu$ also provides $|V_{ud}|$ with good precision. They find $|V_{ud}| = 0.97425 \pm 0.00022$ in good agreement with the result above.

$|V_{us}|$

Traditionally, the product of V_{us} and the form factor at $q^2 = 0$, $|V_{us}|$ has been extracted from the $K_L^0 \to \pi e\nu$ decays. With the prescription [41] for the systematic uncertainties depending on the experiments, one obtained the averages of 5 channels: $K_L^0 \to \pi e\nu$, $K_L^0 \to \pi\mu\nu$, $K^\pm \to \pi^0 e^\pm \nu$, $K^\pm \to \pi^0 \mu^\pm \nu$, and $K_S^0 \to \pi e\nu$. The average of 5 channels for $|V_{us}|f_+(0)$ and the form factor value $f_+(0) = 0.9644 \pm 0.0049$ obtained from lattice QCD calculation gives

$$|V_{us}| = 0.2255 \pm 0.0019. \tag{1.57}$$

This result is very agreed with the one obtain by the unitarity constraint on the first low of the CKM matrix : using $\sqrt{1 - |V_{ud}|^2}$ where $|V_{ud}| = 0.97418 \pm 0.00027$, one gets $|V_{us}| = 0.2255 \pm 0.0010$. (neglecting $|V_{ub}|$ is good approximation) The calculation of the ratio of the kaon and pion decay constants gives antoher way to extract $|V_{us}|$. From $K \to \mu\nu(\gamma)$ and $\pi \to \mu\nu(\gamma)$, the ratio of two branching fractions leads to $|V_{us}| = 0.2259 \pm 0.0014$. $|V_{us}|$ can also be extraced from hyperon decays[42]. By taking into account first order SU(3) breaking effect in the axial-vector contribution, they find $|V_{us}| = 0.2250 \pm 0.0027$. The other way to determine $|V_{us}|$ is to concern hadronic τ decays to strange particles. This will be explained in latter section(See section 1.3.3).

$|V_{ub}|$

$|V_{ub}|$ can be extracted from inclusive $B \to X_u l\bar{\nu}$ decay suffering from the large background from $B \to X_c l\bar{\nu}$. Regarding the leading order shape function and reconstructing four-momenta of both the leptonic and hadronic system, it gives an inclusive average as $|V_{ub}| = (4.27 \pm 0.38) \times 10^{-3}$. An exclusive channel can also provide a way to extract $|V_{ub}|$, but the form factors have to be known. With unquenched lattice QCD calcultions of $B \to \pi l\bar{\nu}$ form factor, a simultaneous fit to the experimental partial rates yields $|V_{ub} =$

$(3.38 \pm 0.36) \times 10^{-3}|$. A combination of the determinations is quoted by Ref.[43] as

$$|V_{ub}| = (3.89 \pm 0.44) \times 10^{-3} \tag{1.58}$$

$|V_{cd}|$

The magnitude of V_{cd} can be extracted from semileptonic charm decays with a knowledge of the form factors. Like as $|V_{ub}|$, with unquenched lattice QCD calculation of the form factor for $D \to \pi l\nu$ and $D \to Kl\nu$, the average of CLEO and Belle measurements is $|V_{cd} = 0.229 \pm 0.006 \pm 0.024|$.

$|V_{cs}|$

The direct measurement of $|V_{cs}|$ is possible from leptonic D_s or semileptonic D decays, using unquenched lattice QCD calculations of the semileptonic D form factor or the D_s decay constant. Belle, BABAR and CLEO measured these branching fractions for $D_s^+ \to \mu^+\nu$, $D_s^+ \to \tau^+\nu$ [44, 45, 46, 47]. Using the mass and lifetime of the D_s, the masses of the leptons, and $f_{D_s} = (242.8 \pm 3.2 \pm 5.3)$MeV, the average of $|V_{cs}|$ yields $|V_{cs}| = 1.030 \pm 0.038$. In semileptonic D decays, using the measurement for $\mathcal{B}(D \to Kl\nu)$, one obtains $|V_{cs}| = 0.98 \pm 0.010$. The average of $|V_{cs}|$ is

$$|V_{cs}| = 1.023 \pm 0.036. \tag{1.59}$$

$|V_{cb}|$

The exclusive and inclusive semileptonic B decays into charm are used for extracting $|V_{cb}|$. The inclusive determinations use the semileptonic decay rate, together with the leptonic energy and the hadronic invariant-mass spectra. Inclusive measurements have been performed using B mesons from Z^0 decays at LEP and from $\Upsilon(4S)$ at B factories. The average of the measurements are provided by Ref.[43]: $|V_{cb}| = (41.5 \pm 0.7) \times 10^{-3}$ Exclusive measurements use

the semileptonic B decays to D and D^*. Concerning all form factors given by Isgur-Wise function, $|V_{cb}|$ is obtained as $|V_{cb}| = (38.7 \pm 1.1) \times 10^{-3}$. The combined one is

$$|V_{cb}| = (40.6 \pm 1.3) \times 10^{-3} \tag{1.60}$$

$|V_{td}|$ and $|V_{ts}|$

Since $|V_{td}|$ and $|V_{ts}|$ cannot be extracted from tree-level decays of the top quark, one has to rely on determinations from $B - \bar{B}$ oscillations mediated by box diagrams with top quarks, or loop-mediated rare K and B decays. Theoretical uncertainties in hadronic effects limit the accuracy of the determinations. The constraint on $|V_{td}/V_{ts}|$ from $\delta m_d/\delta m_s$ give more reliable results :

$$|V_{td}/V_{ts}| = 0.211 \pm 0.001 \pm 0.005 \tag{1.61}$$

A complementary determination of $|V_{td}/V_{ts}|$ is possible from the ratio of $\mathcal{B}(B \to \rho\gamma)$ and $\mathcal{B}(B \to K^*\gamma)$. The ratio of the neutral modes is theoretically cleaner than that of the charged ones. Combining the experimental and theoretical errors, one obtains $|V_{td}/V_{ts}| = 0.21 \pm 0.04$

$|V_{tb}|$

The ratio of branching fractions $R = \mathcal{B}(t \to Wb)/\mathcal{B}(t \to Wq)$ gives $|V_{tb}|^2$. The CDF and D$\varnothing$ measurements for the single top-quark-production cross section provide the direct determination of $|V_{tb}|$. The average cross section measured by CDF[49] and D$\varnothing$ [48] yields

$$|V_{tb}| = 0.88 \pm 0.07 \tag{1.62}$$

1.3.3 $|V_{us}|$ determination in hadronic τ decays

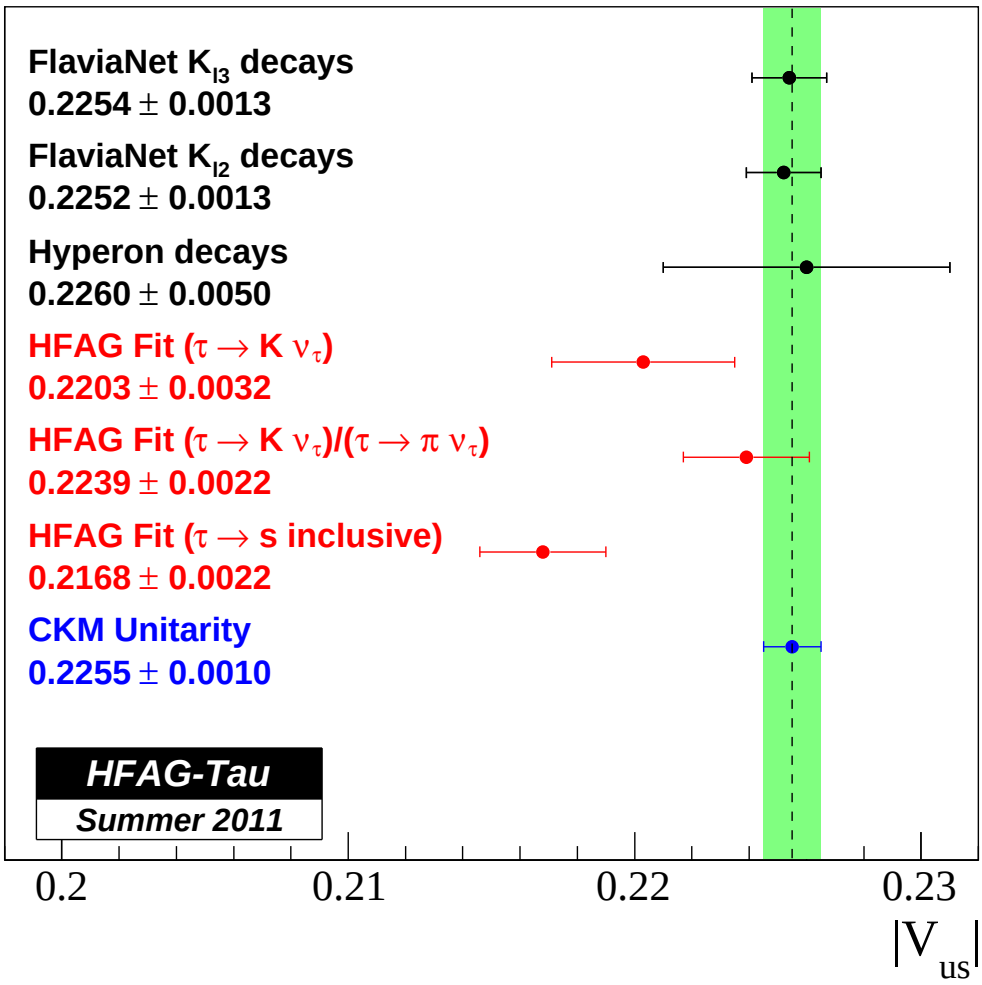

Figure 1.7: $|V_{us}|$ measurements from kaon, hyperon and tau decays. The $|V_{us}|$ from inclusive τ decays for Cabibbo suppressed shows 3σ deviation from the unitarity.

$|V_{us}|$ can be determined by using Cabibbo-suppressed($\Delta S = 1$) decay channels in τ lepton. There are three methods for extracting $|V_{us}|$ in τ decay, and the simplest way is to use the branching fraction for $\tau^- \to K^-\nu_\tau$. We bring here the theoretical expression for $\mathcal{B}(\tau^- \to K^-\nu_\tau)$ from Eq. 1.16,

$$\mathcal{B}(\tau^- \to K^-\nu_\tau) = \frac{G_F^2 f_K^2 |V_{ud}|^2}{16\pi} m_\tau^2 \left(1 - \frac{m_K^2}{m_\tau^2}\right) S_{EW}. \tag{1.63}$$

where the electroweak correction, $S_{EW} = 1.0201 \pm 0.003$ [1], the strength of the coupling of kaon, $f_K = 157 \pm 2$ MeV obtained from the Lattice QCD calculation [2]. Hence the $|V_{us}|$ is found to be 0.2203 ± 0.0032 which is consistent to the value from CKM unitarity.

The other way to extract $|V_{us}|$ is to use two single meson decays where one decays into $S = -1$ final state and the other decays into $S = 0$ final state; $\tau^- \to K^-\nu_\tau$ and $\tau^- \to \pi^-\nu_\tau$.

$$\frac{\mathcal{B}(\tau^- \to K^-\nu_\tau)}{\mathcal{B}(\tau^- \to \pi^-\nu_\tau)} = \frac{f_K^2 |V_{us}|^2 (1 - m_K^2/m_\tau^2)^2}{f_\pi^2 |V_{ud}|^2 (1 - m_K^2/m_\tau^2)^2} (1 + \delta_{LD}) \tag{1.64}$$

where δ_{LD} s the long-distance correction, 0.03 ± 0.44 and the ratio of decay constants$f_K/f_\pi = 1.189 \pm 0.007$ [2]. Using Eq. 1.64, the result is found to be $|V_{us}| = 0.2239 \pm 0.0022$, which is also consistent to the value deduced from CKM unitarity.

However, $|V_{us}|$ extracted from the inclusive τ decays into strange particles shows a little bit different result from the reference. The third way to determine the magnitude of V_{us} from strange τ lepton decay is to use the decay width of all Cabbibo allowed and suppressed decays [52]. In Eq. 1.42, the hadronic decay width of the τ lepton is

$$R_\tau = R_{\tau,NS} + R_{\tau,S}, \tag{1.65}$$

Here, we recall the spectral moments presented in Eq. 1.46.

$$R_\tau^{kl} = \int_0^{m_\tau^2} ds \left(1 - \frac{s}{m_\tau^2}\right)^k \left(\frac{s}{m_\tau^2}\right)^l \frac{dR_\tau}{ds} = R_{\tau,NS}^{kl} + R_{\tau,S}^{kl}, \tag{1.66}$$

Using the operator product expansion, R_τ^{kl} can be written as:

$$R_\tau^{kl} = 3S_{\rm EW}\{(|V_{ud}|^2 + |V_{us}|^2)(1 + \delta^{kl(0)}) + \sum_{D\geq 2}(|V_{ud}|^2\delta_{ud}^{kl(D)} + |V_{us}|^2\delta_{us}^{kl(D)})\}. \quad (1.67)$$

$\delta^{kl(0)}$ denotes the purely perturbative dimesion-zero contribution and $\delta_{ij}^{kl(D)}$ stand for higher dimensional correction in the OPE. The difference of R_{NS} and R_S can pin down the flavor SU(3)-breaking effect and vanishes in the SU(3) limit.

$$\delta R_\tau^{kl} = \frac{R_{\tau,NS}^{kl}}{|V_{ud}|^2} - \frac{R_{\tau,S}^{kl}}{|V_{us}|^2} = 3S_{\rm EW}\sum_{D\geq 2}(\delta_{ud}^{kl(D)} - \delta_{us}^{kl(D)}), \quad (1.68)$$

This difference can be used for determining $|V_{us}|$ with other input source, m_s(2GeV) which determined from QCD sum rules and lattice QCD. The sensitivity of δR_τ^{kl} to V_{us} is strongest for the (0,0) moment. Inserting the strange mass value into the theoretical expression for $\delta R_\tau^{(0,0)} = \delta R_\tau$, one finds ([53])

$$\delta R_\tau = 0.240 \pm 0.032 \quad (1.69)$$

Using the above result and the several inputs from the data, we then obtain

$$|V_{us}| = 0.2168 \pm 0.0022 \quad (1.70)$$

Figure 1.7 summarizes the $|V_{us}|$ measurements from kaon, hyperon and tau decay. One can cleary see 3 σ deviation from τ and the others. This implies a possibility that CKM matrix is not a unitary matrix, or the measurements from the τ decays with non-zero strangeness is incomplete. Therefore, the measurements of all strange decays of τ lepton are important to verify one of the main feature of Standard Model, CKM unitarity.

1.4 Outline of thesis

This thesis is dedicated to measure the branching fractions for the tau decays involving one and more K_S^0 in the final state. In chapter 1, we introduced the theoretical basis of τ decays : The leptonic and hadronic decays and thier decay width. In chapter 2, we start our discussion from the detector apparatus. We are focused on the goal, performance and persfectives of KEKB and Belle detector. The descriptions of tau Monte Carlo generator(TAUOLA) and the full detector simulation are included in the end of the chapter 2. In chapter 3, the selection of τ pair events and the reconstruction of signal event are described in a raw. In chapter 4, we concentrate our discussion on the studies of detector efficiency and corrections using data and MC samples. In the branching fraction measurements, the efficiencies and its systematic uncertainties are the most crucial part in our analysis. We also describe the backgrounds in τ decays. In chapter 5, the method of branching fractions calculation and their determination are explained. In chapter 6, we studied the systmeatic uncertainties from all possible sources. In the last chapter, we summarized the analysis and make a conclusion. In addition, we include the appendix which describes the important information for the π^0 efficiency studies using the $\tau^- \to \pi^-\pi^0\nu_\tau$ events.

Chapter 2

B-factory

More than 20 years ago, CP violation was one of the hot issues in the particle physics and many physicist focused on finding CP asymmetry in b quark sector. With the success of the CLEO experiment, the latecommer experimental group were motivated and boosted to build a facilities dedicated to the study of B mesons, so called B-fractory. There are several B-factory projects(Table.2.1). CESR, PEP-II and KEKB are electron-positron colliders whose collision energy is aimed at $\Upsilon(4S)$ resonance. Either of KEKB and PEP-II has two beam lines for electrons and positrons seperately in order to achieve an asymmetric beam energy for B mesons production with finite momentum, while CESR used single ring and provides symmetric colliding energy. Tevatron, HERA and LHC are hadron collider. The large production cross section, production of other higher state of B meson system and a big boost of B mesons are the merit of hadron collider. However, the enoumous background produced by the parton production is the critical demerit for the data analysis. The construction of KEKB accelerator started in 1994 utilizing the existing tunnel for TRISTAN. After 32 months of dismantling of TRISTAN, the construction of KEKB was completed in November 1998, and commissioning started in December 1998. With steady improvement for

Institute	Accelerator	Detector	Type	Operation
Cornel University	CESR	CLEO II,III	e^+e^- sym.	1995 - 2001
SLAC	PEP-II	BABAR	e^+e^- asym.	1999 - 2008
KEK	KEKB	Belle	e^+e^- asym.	1999 - 2010
DESY	HERA	HERA-B	fixed target	2000 - ?
FNAL	BTeV	Tevatron	$p\bar{p}$	2006(cancled)
CERN	LHC	LHCb	pp	2010 - current

Table 2.1: B-factory projects. Except for LHCb, All projects are closed or canceled.

over 10 years operations, KEKB accelerator achieved the world maximum luminosity, $2.0 \times 10^{34}\mathrm{cm}^{-2}\mathrm{s}^{-1}$ which is twice larger than orignial designed luminosity and ended the its operation in June 2010.

The Belle Collaboration was founded in 1994 with the submission of a proposal to construct a detection apparatus operating at an asymmetric-energy e^+e^- collider at a center of mass energy where the $\Upsilon(4S)$ resonance is produced. The main target of this experiment was the study of CP violation in B meson decays. However, not only B mesons but also τ lepton are produced with a large cross section in this energy region, thereby producing a huge number of $\tau^+\tau^-$ pairs. Thus, the Belle experiment provides an excellent environment for the study of τ physics. Since the start of operation in 1999, until the end of the operation in June,2010, the Belle experiment accumulated 1040 fb^{-1} of data, thanks to the remarkable performance of the KEKB asymmeteric collider. With the world-largest $\tau^+\tau^-$ data, Belle τ group reported the best results for lepton flavor violation and CP violation in τ sector[**?**, **?**, **?**, 56], and the Belle collaboration is one of the world leading group confront on the discovery of new physics.

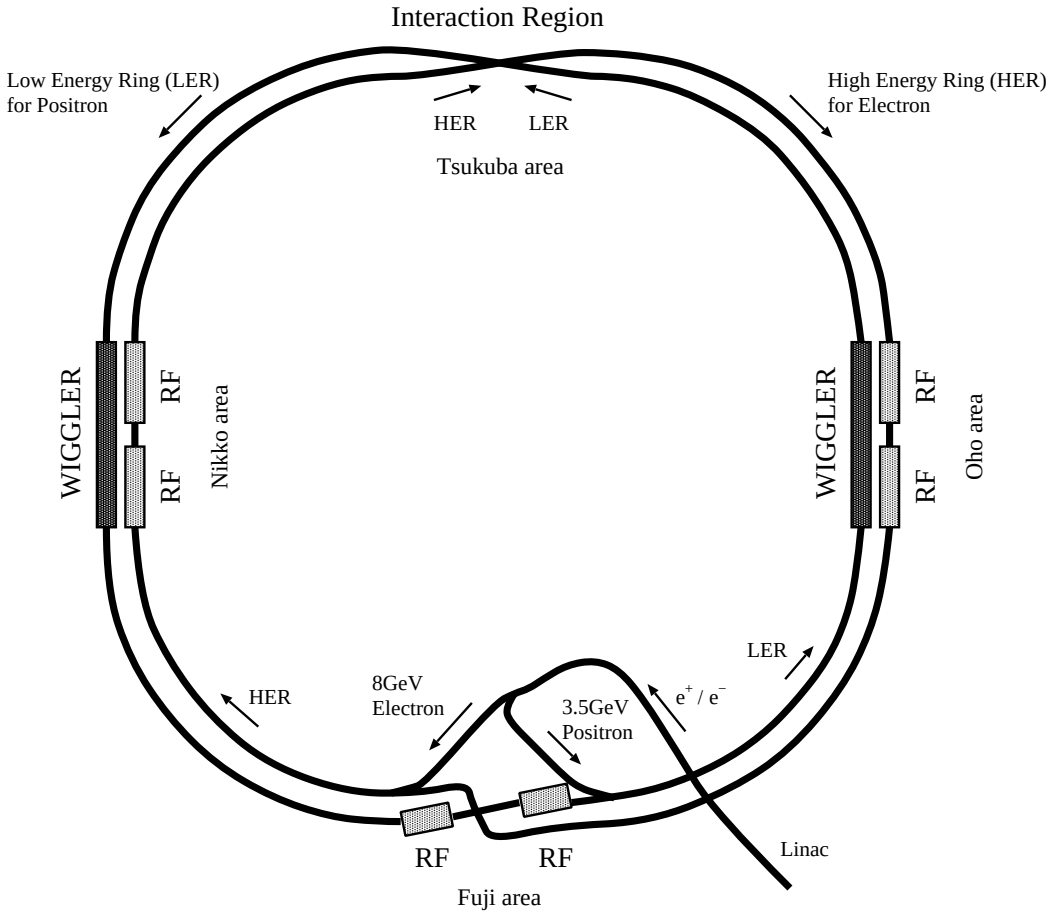

Figure 2.1: Layout of KEKB storage ring

2.1 KEKB storage ring

The main purpose of KEK B-factory project was to confirm the Kobayashi-Maskawa model and to study CP violation at the B meson decays. In order to achieve this purpose, it is required for KEKB acceleartor to fulfill several items : asymmetric energy collision, high luminosity, energy range covering Υ resonances and small beam energy spread. The designed luminosity is $1.0 \times 10^{34}\mathrm{cm}^{-2}\mathrm{sec}^{-1}$, which is more than one order of magnitude higher than the maximum luminosity ever achieved by electron-positron collider before the advent of B-factories. KEKB storage rings consist of two 3016 m long rings: An 8-GeV electron ring(HER) and a 3.5-GeV positron ring(LER) are installed side by side in a tunnel 11m below the ground level. The two rings cross at one point, called the interaction point(IP), where electrons and positrons collide, while at the opposite site the two rings does not cross over.

2.1.1 Physical requirements

Asymmetric Energy Collision The size of time dependent CP asymmetry which is one of the main target can be enhanced by boosting the time of flight of B mesons toward one direction in laboratory frame, as predicted by Carter, Bigi and Sanda [59, 60, 61]. One of the B meson decay mode, $B \to J/\psi K^0_S$, allows to measure the angle ϕ_1 which is one of the important quark mixing angle in CKM matrix. The time dependent asymmetry of $B \to J/\psi K^0_S$ can be expressed as

$$A(\Delta t) = \frac{\Gamma(B^0 \to J/\psi K^0_S; \Delta t) - \Gamma(\bar{B}^0 \to J/\psi K^0_S; \Delta t)}{\Gamma(B^0 \to J/\psi K^0_S; \Delta t) + \Gamma(\bar{B}^0 \to J/\psi K^0_S; \Delta t)} = \sin 2\phi_1 \sin(\Delta m \Delta t), \tag{2.1}$$

where Δm is the mass difference of two mass eigenstates of B^0 and $\bar{B}^0$ system, and Δt is the decay time difference between where B^0 and $\bar{B}^0$ decays. In case where B mesons produced in decays of $\Upsilon(4S)$ at rest, B mesons

will have only a small fixed momentum of $\sim$ 300 MeV/c in the laboratory frame, so that the situation does not suit for this purpose. On the other hand, the energy difference between the electron and positron beams gives a boost to the produced B meson pairs, which enhance the time difference in laboratory frame and results in better accuracy in their measurement. The energy asymmetry is characterized by the motion of the center-of-mass(CM) of the $B\bar{B}$ system in the laboratory frame. Its Lorentz boost parameter is written as

$$\beta\gamma = \frac{E_- - E_+}{\sqrt{s}} = 0.425 \tag{2.2}$$

where $E_-(E_+)$ is the energy of the electron(positron) beam. The $\sqrt{s}$ is the CM energy , $\sqrt{s} = \sqrt{4E_-E_+} = 10.58$GeV. This is equal to the invariant mass of $\Upsilon(4S)$ which decays into neutral B meson pair with more than 96% of branching fraction. With a larger energy asymmetry, time evolution measurements can be done with better accuracy. However, the effective acceptance of the detector is limited by a fixed geometry, so the optimum value of the energy asymmetry should be found by taking these two factors into account. It is seen that the asymmetry values between $\beta\gamma = 0.4$ and 0.8 result in a similar sensitivity for this measurement. On the other hand, there are a number of other important physics topics where time evolution study are not required, e.g. τ, 2-photon and some physics related to the Beyond the Standard Model(BSM). For these processes, a smaller asymmetry is preferred for a larger acceptance and for a better event reconstruction efficiency. In order to that purpose $\beta\gamma$ is decided to 0.425.

High Luminosity For time dependent CP analysis for B meson decays, e.g. $B \to J\psi K^0_S$, the required integrated luminosity is estimated to be between 30 $\sim$ 100 fb^{-1}. The uncertainty of this esitmate arises from quoted errors in the experimental data and their theoretical interpretations. Other channels to measure CP violation have been also studied and made a con-

clusion that at least 100 fb^{-1} of the integrated luminosity is required. From these considerations, it is concluded that the target luminosity for the first few years of the experiment should be 100 fb^{-1}. To achieve this in a timely manner, the target peak luminosity for KEKB should be $1.0 \times 10^3$4cm^{-2}s^{-1} or higher.

Small Beam Energy Spread In the experiment at KEKB, rare decay of B mesons is one of important topics and should be reconstructed, whereas the combinatorial background from continuum events is significant. In many of those decay modes, a reduction of this background is equivalent to an increase of the effective luminosity from the viewpoint of statistical significance. It has been shown by simulation studies that the signal-to-noise ratio S/N of the B decay reconstruction is approximately inversely proportional to the beam energy spread. By applying an adequate Lorentz boost according to the beam energy, the measured momentum vectors of B meson decay products can be brought into the rest frame of $\Upsilon(4S)$. The momentum of the B in this frame will have a fixed value of 300 MeV/c. This can be used as a powerful constraint for finding B. The effectiveness of this technique depends on the magnitude of the energy spread of the accelerator. For example, in the reconstruction of B_d decays into $\pi^+\pi^-$, the signal-to-noise ratio is expected to be approximately 1:1 with a beam energy spread of 7.8×10^{-4}. It will be worsened to 1:2, if the energy spread increases by a factor of two. This is equivalent to a factor of 1.7 reduction of the luminosity. The energy spread should, therefore, be chosen to be the smallest possible that is allowed by machine design considerations.

Energy Range Three resonances are known to exist below the $B\bar{B}$ threshold as shown in Fig. 2.2. while the first resonance above the $B\bar{B}$ threshold is $\Upsilon(4S)$ at 10.58 GeV. The $\Upsilon(4S)$ decays almost exclusively into $B\bar{B}$(either B_u or B_d), and it is at this resonance that the bulk of data should be col-

lected at KEKB. However, some data need to be collected at different CM energies for the following reasons. An energy scan is required to find the peak of $\Upsilon(4S)$. This is to ensure that the data taking is conducted at the most efficient energy. Since the mass and width of $\Upsilon(4S)$ is well known from measurements by CLEO, it also serves the purpose of cross-calibration of the machine configuration at KEKB. The width of the energy scan can be as small as 30 MeV, and the number of the data points will be at most 10.

Off-resonance data have to be collected to understand $q\bar{q}$ continuum events. This is important for some data analyses where the continuum background has to be statistically subtracted. An integrated luminosity of more than 10 % of the on-resonance data will be required for this purpose. The energy of the off-resonance run should be 10.50 GeV, where the cross section of the $B\bar{B}$ pair-production is negligible. At KEKB this determines the lowest CM energy for the required run.

It has been pointed out that studies of B_s should provide additional information on b-quark decays. For this purpose it is necessary to go to $\Upsilon(5S)$(10.87 GeV) to produce B_s mesons. However, its production rate is expected to be $\mathcal{O}(1/10)$ of the $B_{u,d}$ production rate at $\Upsilon(4S)$. The present perspective is that the measurement of B_s will be done only after a significant amount of data is collected for $B_{u,d}$ at $\Upsilon(4S)$. At KEKB this specifies the highest CM energy for the required run.

2.1.2 Accelerator Design

Based on the physical requirements discussed in previous section, the machine parameter for KEKB accelerator was decided. The main parameters for KEKB are summarized in Table **??**. The most important parameter for our goal is the luminosity. The luminosity can be expressed as following [63]:

$$L = 2.2 \times 10^{34} \xi \frac{EI}{\beta_y^*} \quad (\mathrm{cm}^{-1}\mathrm{s}^{-1}) \tag{2.3}$$

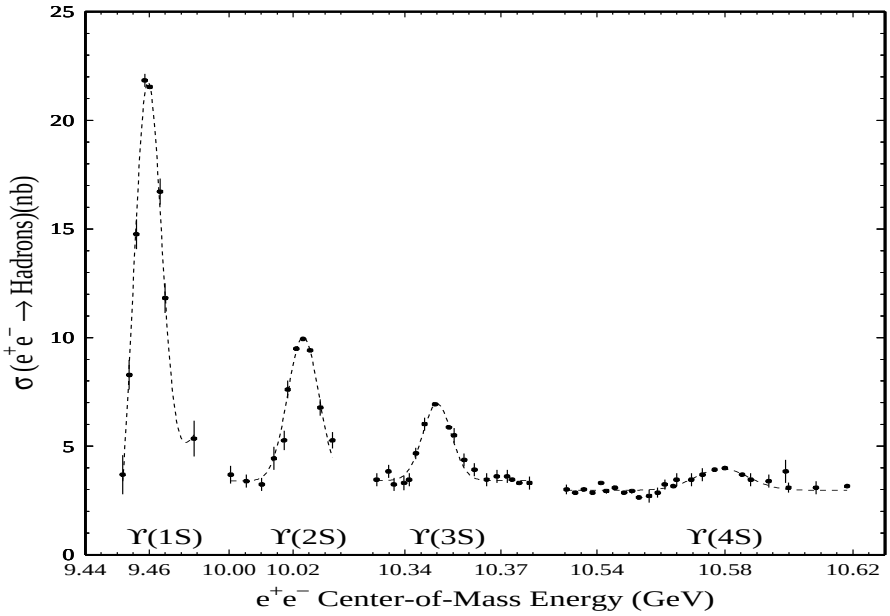

Figure 2.2: e^+e^- cross-section measured by CLEO and CUSB showing the masses of the Υ resonance[62]. There is an underlying continuum of $e^+e^- \to \gamma \to q\bar{q}$ events. Then there is a dramatic increase in the number of events observed when producing the ${}^3S_1$ states of $b\bar{b}$ bound state system. The observed resonances are the n = 1, 2, 3, and 4 radial excitations.

where ξ is the beam-beam tune shift, I is the beam current in ampere and β_y^* is the vertical beta function at the IP in unit of cm. In order to reach the target luminosity greater than $10^{34}\text{cm}^{-2}\text{sec}^{-1}$, KEKB strorage ring should contain 1.1[A] for the HER and 2.6 [A] for the LER with $\xi = 0.05$ and $\beta_y^* = 1\text{cm}$, which means the storage ring has to contain about 3000 bunches with keeping a certain level of stability. This is the most serious problem because containing large number of beam currents causes instabilities due to single-beam collective effects, impedance from various beamline elements, ion trapping, photoelectric effect, and beam-beam effect. These instabilities are suppresed by integrating a RF cavities with HOM damping, smoothing

the surface of accelerator elements and implementing feedback systems.

	LER	HER	unit
Circumference	3016		m
RF Frequency	508.88		MHz
Horizontal Emiitance	18	24	nm
Beam current	1637	1188	mA
Number of bunches	1584 + 1		
Bunch current	1.03	0.75	mA
Bunch spacing	1.84		m
Bunch trains	1		
Total RF voltage	8.0	13.0	MV
Synchrotron tune	-0.0246	-0.0209	
Betatron tune	45.506/43.561	44.511/41.585	
beta's at IP	120/0.59		cm
momentum compaction (a)	3.31×10^{-4}	3.43×10^{-4}	
Estimated vertical beam Size at IP from Luminosity σ_y^*	0.94		νm
beam-beam parameters	0.127/0.129	0.102/0.090	
Beam lifetime	133 @ 1637	200 @ 1188	min.@ mA
Luminosity	21.08×10^{33}		$cm^{-2}sec^{-1}$

Table 2.2: Machine Parameters of the KEKB (June 17, 2009)

In the KEKB design, a finite crossing angle scheme has been chosen, instead of the head-on collision scheme. The half crossing angle at KEKB is 11 mrad. This choice gain two merits for avoiding parasitic collision and for reducing the number of bending magnets for beam separation so that reduces the synchrotron radiation at IP significantly.

Many wiggler magnets are used to reduce the damping time of the positron beam. The LINAC was upgraded in energy from 2.5 GeV to 8.5 GeV to make it possible to inject electron and positron beam directly into the storage rings[**?**]. The beam optics of the storage rings remains unchanged both

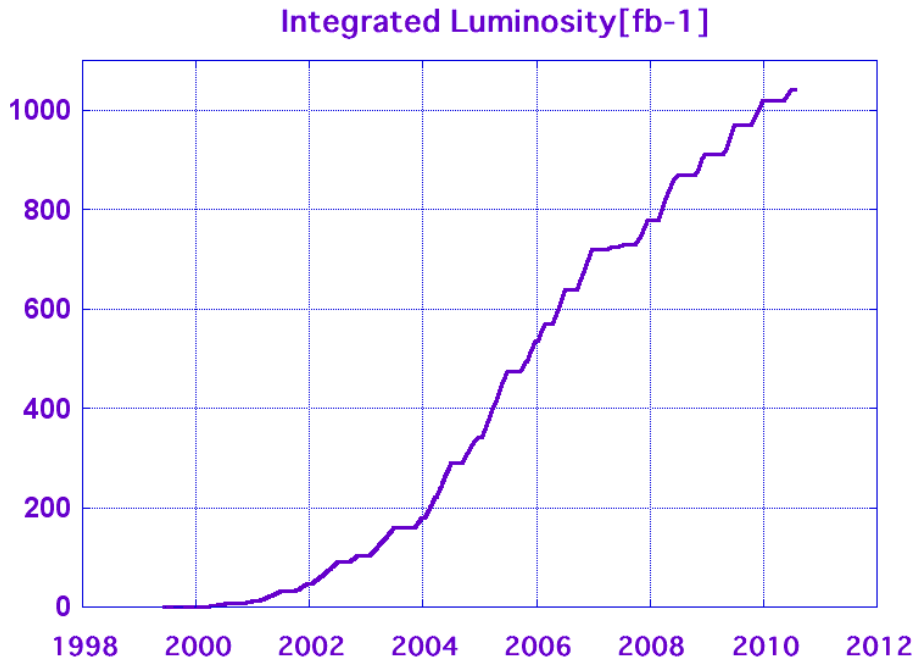

Figure 2.3: The history of integrated luminostiy of the KEKB

at the time of beam injection and beam storage. The two rings are equipped with more than 1000 beam position monitors to facilitate quick beam diagnostics.

2.1.3 Performance

The commissioning of the KEKB accelerator started in December, 1998. The first beam collision was observed in Februray, 1999 without the Belle detector. In May 31, 1999 the KEK machine operated with the Belle detector. The first collision was confirmed on June 1st, 1999 by observing hadronic events with the Belle detector. Since then, continuous efforts were paid to tune up the machine parameters and the luminosity had been improved gradually. The peak luminosity surpassed the target luminosity in May 2003. After this achievement, the luminosity had been growing due to the improvement of

the beam injection scheme, called as continuous injection [65]. The history of the luminosity are shown at Fig. 2.3. The total integrated luminosity is 1040 fb^{-1}. The highest peak luminosity $21.083 \times 10^{-33} cm^{-2} sec^{-1}$, was recored. The operation of KEKB accelerator was ended at June 2010 with the greate achievements.

2.2 The Belle Detector

The Belle detector is a large-solid-angle magnetic spectrometer that consists of a silicon vertex detector(SVD), a 50-layer central drift chamber(CDC), an array of aerogel threshold Chrenkov counters(ACC), a barrel-like arrangement of time-of-flight scintillation counters(TOF), and an electromagnetic calorimeter(ECL) comprised of CsI(Tl) crystals located inside a superconducting solenoid coil that provides a 1.5 T magnetic field. An iron flux-return located outside of the coil is instrumented to detect K_L^0 mesons and to identify muons(KLM). The detector is described in detail elsewhere [67]. The layout of Belle detector are shown at Fig. 2.4 and Fig. 2.5.

2.2.1 Extreme Forward Calorimeter(EFC)

The extreame forward calorimeter, EFC, is attached to the front faces of the cryostats of the compensation solenoid magnets, surrounding beam pipe. The purpose of EFC detector are 1) to monitor the beam luminosity, 2) to improve the polar coverage where ECL does not. EFC covers the angular range from 6.4° to 11.5° in the forward direction and 163.3° to 171.2° in the backward direction. EFC also functioned as a beam mask to reduce backgrounds for CDC and a trigger for some two-photon process.

Since EFC is placed in very high radiation-level area around the beam pipe, pure BGO(Bismuth Germanate, $Bi_4Ge_3O_{12}$ was chosen by its characteristics: 1) radiation hardness at megarad level, 2) excellent e/γ energy resolution of $(0.3-1)\%/\sqrt{E\mathrm{GeV}}$, 3) short radiation length 1.12 cm, 3) large refractive index of 2.15, 4) non-hygroscopic, and 5) suitable scintillating properties (the fast decay time of 300 ns and peak scintillation at 480 nm).

BGO crystals are used as an active medium of the electromagnetic showers. The resultant scintillation lights are collected by the photodiode detectors. The structure of EFC is shown in the Fig. 2.6. To check the performance of EFC, the correlation of the energy sum spectra for Bhabha events between

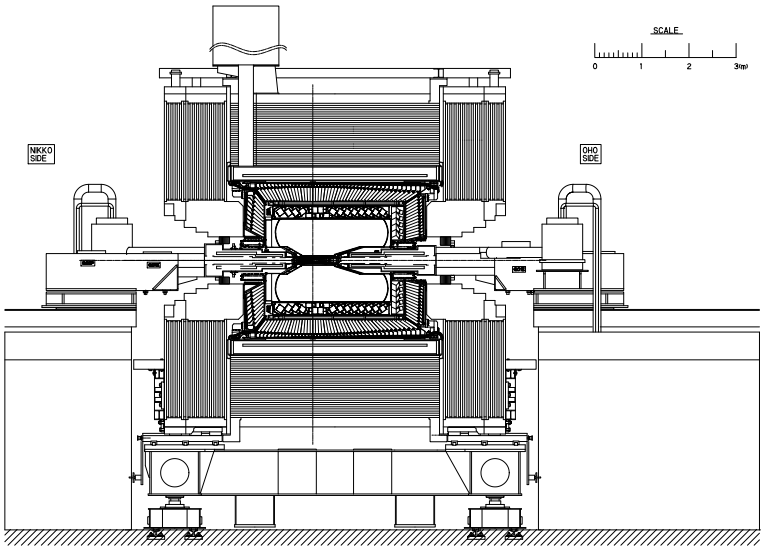

Figure 2.4: Belle detector side view

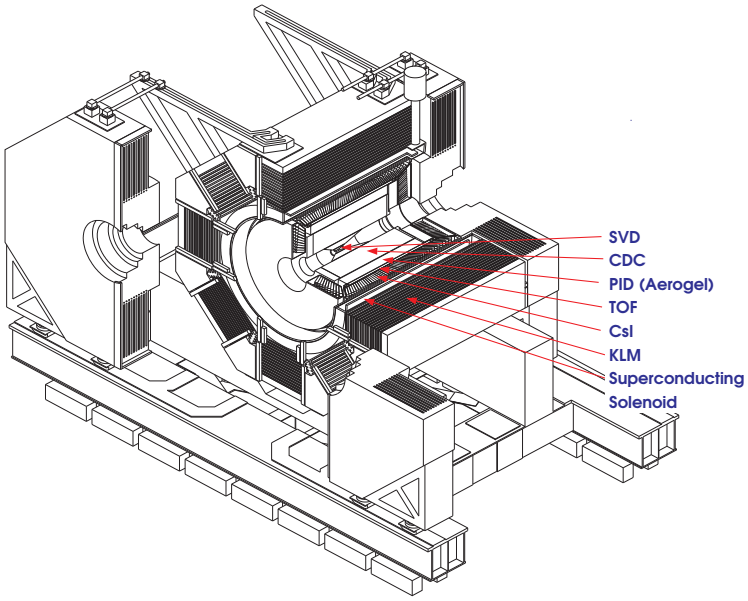

Figure 2.5: Belle detector isometric view

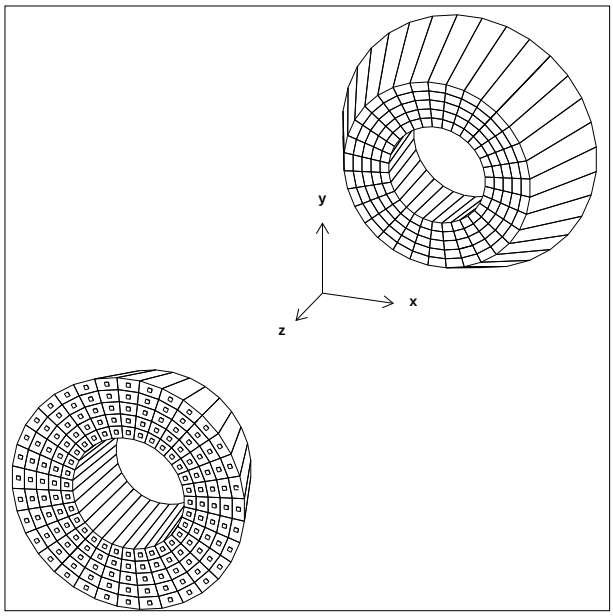

Figure 2.6: An isometric view of EFC detector

the forward and backward EFC detectors are used. A clear peak at 8 GeV is shown with an 7.3 % of RMS resolution on the forward EFC detector. On the other side, the backward EFC detector shows a clear 3.5 GeV energy peak with a 5.8 % of resolution in RMS. These results are compatible with the beam test results [82].

2.2.2 Silicon Vertex Detector(SVD)

The silicon vertex detector is designed for the measurement of the decay vertex of each B meson as precisly as possible to observe a time-dependent CP asymmetry of B meson decay. The required vertex resolution in the z-direction is $\sim 100\ \mu m$. The contraints or considerations for the SVD design are follows : (1) the momentum of the partilces of interest in Belle experiment are in a range where multiple-Coulomb scattering can prevent for acheivment of good resolution, (2) the need to approach as close as possible to the in-

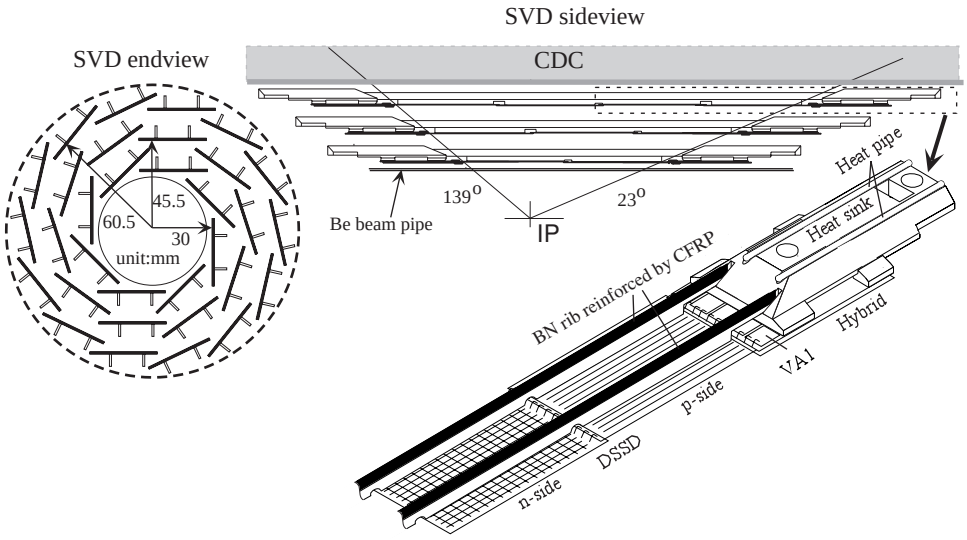

Figure 2.7: Configuration of SVD detector

teraction point, (3) the rigidity of the supporting structure and its low mass in order to reduce the materials near the interaction point while providing proper support, and (4) radiation hardness because of the high background radiation environment.

Figure. 2.7 shows the SVD configuration. The SVD was upgraded from its initial design(SVD1) to the final one(SVD2) in October, 2003 [70]. The main difference in the upgrade is the number of layers of double-sided silicon strip detectors(DSSD), 3 layers for SVD1 where supplemted one more layer by SVD2. This increased the particle track coverage from $23° < \theta < 139°$ for SVD1 to $17° < \theta < 150°$ for SVD2, where θ is the polar angle along the beam direction. The readout chain for the DSSD element is based on the VA1TA integrated circuit. The signal goes to flash analog-to-digital converter(FADC), digital signal processor(DSP), and field programmable gate array(FPGA). In addition for the VA1TA chips provides a fast trigger signal, that is to be used in signal shaping.

The core part of the SVD is the double-sided silicon detector element. [68, 69] The p+ and n+ type semiconductor strip are implemented orthognally on the opposite surfaces of n-type bulk semiconductor. A proper biasing on the strips generates the electric field inside the medium, which produce the electron-hole pairs when a particle traverses it. The electron-hole pairs are collected by the strips thereby providing the 2-dimensional information about the penetration position of the particle changed. In Belle SVD, each DSSD consists of 1280 sense strips and 640 readout pads on opposite sides. The z-strip and ϕ strip pitches are 42 μm and 25 μm, respectively. The size of the active region is 53.5 $\times$ 32.0 mm^2 on the z-side and 54.5 $\times$ 32.0 mm^2 on the ϕ-side. In total, 102 cells of DSSDs are used, the size of each cell is 53.5 $\times$ 32.0 mm^2.

The performance of the SVD is confirmed by measuring the efficiency, impact parameter resolution and radiation hardness. The track-matching efficiency is defined as the probability that a CDC track within the SVD acceptance has associated SVD hits in at least two layers, and in at least one layer with both the $r-\phi$ and $r-z$ information. Inefficiency can be caused by dead SVD channels, fake SVD clusters, and some inperfection in the SVD cluster finding software. The average matching efficiency is found to be larger than $\sim$ 97 % for both SVD1, and SVD2. The hit efficiency is measured by the cosmic ray data taking with back-to-back trigger is 95 $\sim$ 99%, where the inefficiencies come from the failure of a read-out chip or mis-wiring.

The momentum and angular dependence of the impact parameter resolution are shown in Fig. 2.8(for SVD1) and well represented by the formulae : $\sigma_{xy} = 19.2 \oplus 54.0/(p\beta\sin^{3/2}\theta), \mu$m and $\sigma_z = 42.2 \oplus 44.3/(p\beta\sin^{5/2}\theta), \mu$m. In addition the estimation of impact parameter resolution using the MC data showed good agreements with data.

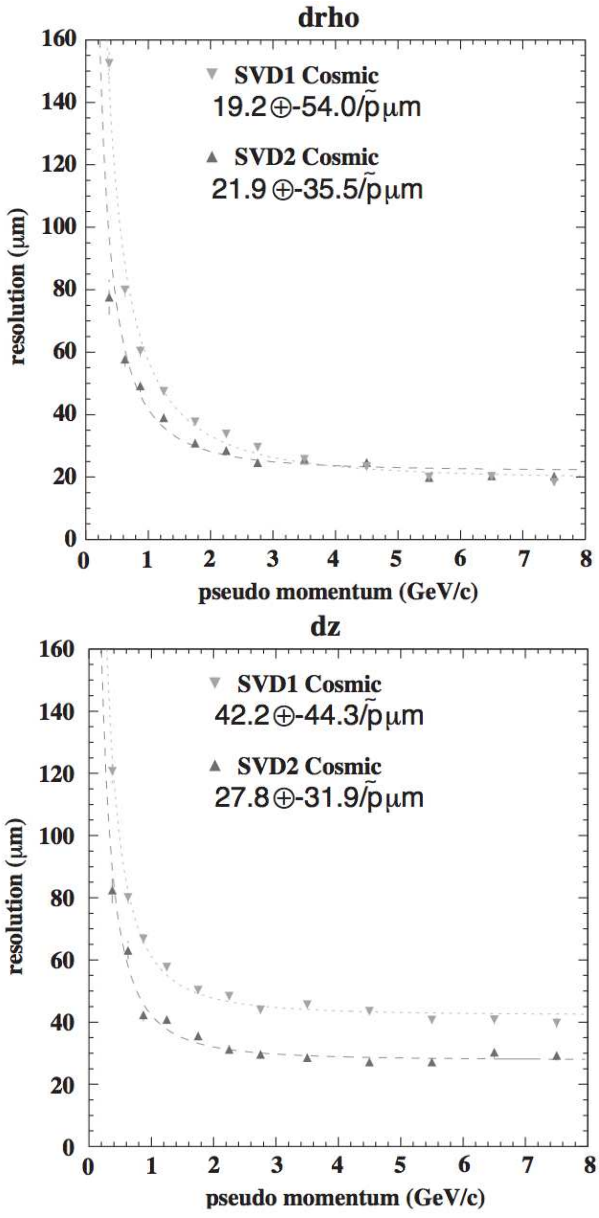

Figure 2.8: Performance of SVD detector : impact parameter resolution r,z

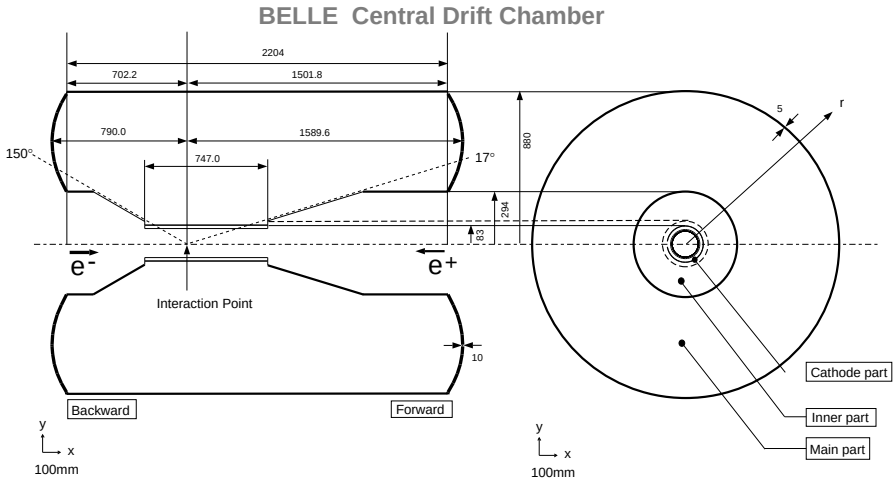

Figure 2.9: CDC structure

2.2.3 Central Drift Chamber(CDC)

The Belle central drift chamber is the essential part of the efficient reconstruction of charged particle tracks and precise determination of their momenta.[71, 72] Specifically, the physics goal requires a momentum resolution of $\sigma_{p_t}/p_t \sim 0.5\%\sqrt{1+p_t^2}$ (p_t in GeV/c) for all charged particles with $p_t > 100$MeV/c in the polar angle region of $17° < \theta < 150°$. In addition, the charged particle tracking system is expected to provide important information for the trigger system and particle identification information in the form of precise dE/dx measurements for charged particles. The structure of CDC is shown in Fig. 2.9. It is a cylindrical wire drift chamber that contains 50 layers of anode wires and three cathods strip layers. When a charged particle penetrates the gaseous material, it loses its energy near the trajectory of the incident particle are collected in the sense wires, where the ions follow the electric field generated by the field wires.

Since the momentum of the majority of the decay particles of a B meson are less than 1 GeV/c, the minization of multiple scattering is important for improving the momentum resolution, which results the use of a low-Z

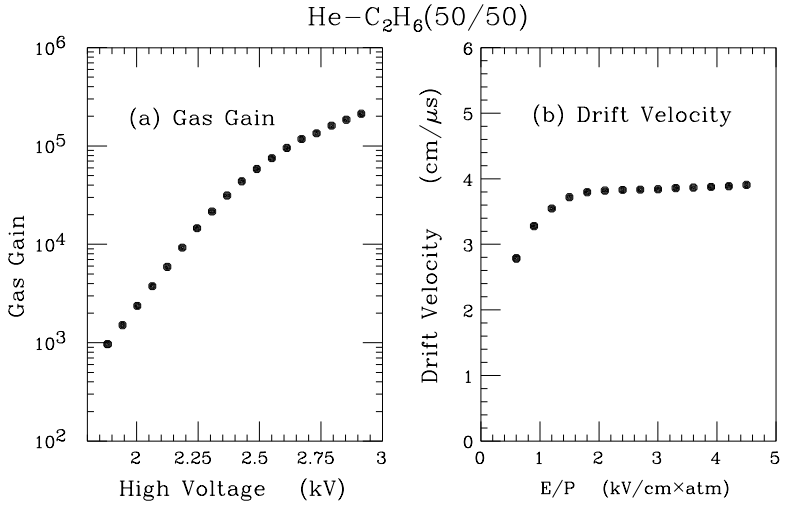

Figure 2.10: (a) The measured gas gain and (b) drift velocity for 50% He and 50% C_2H_6 gas mixture

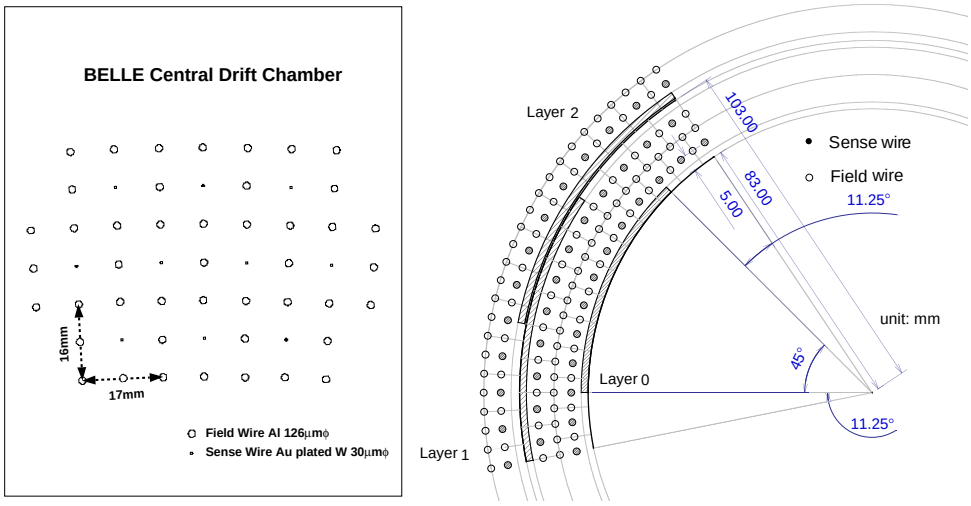

Figure 2.11: CDC wire structure

gas is desirable. Also low-Z gases have a smaller photoelectric cross-section than argon-based gases, which provides additional advantages of reduced background from synchrotron radiation. A 50% helium - 50% ethane gas was employed. The radiation length of this mixture is long as 640 m, which results small energy loss. The electric field strength where the drift velocity saturates at 4 cm/μs is relatively low, which is favored when there is a large field non-uniformities. In Fig. 2.10 (a) and (b) show measured gas gain and drift velocity for the 50% helium - 50% ethane gas mixture.

The wire structure for a few inter super layer of wires are shown in Fig. 2.11. The CDC is composed of 14 cylindrical superlayers of wire, where each layer is categorized into one of the cathods, axial, and stereo wires. The wires in a axial layer are parallel to the z direction, which gives the ϕ information of a track. Each layer contains 64 to 288 signal channels, when each signal channel corresponds to a sense wire. The cathode layer consist 7.4 mm wide strips along ϕ direction with 8.2 mm pitch in the z direction, where each strips are divided into eight segments along ϕ direction. There three cathode layer at the inner-most radii and between the first and second axial superlayers. The stereo layer is the similar with the axial layer, but one end plate rotates a few tens of milli radian when the other end plate is fixed. The stereo layer can determine the ϕ information of a track within the limit of rotated angle(stereo angle), while the main purpose of the stereo layer is to provides a high-efficient z-trigger combined with the cathode layers. For the case of axial superlayer and stereo superlayer, each superlayer consists of two to five layers, while the cathode layer consists of one layer of strip.

The signals from each sense wires are amplified by the preamplifiers and send to Shaper/Discriminator/QTC modules. The QTC means a charge(Q)-to-time(T) conversion, which generates a logic-level output, where the leading edge T_{LE} corresponding to the drift time(t_d) and the width(T_W) is proportional to the input pulse height($T_W = a \times Q + b$). This technique is a simple extension of the ordinary TDC/ADC readout scheme, but allows to use only

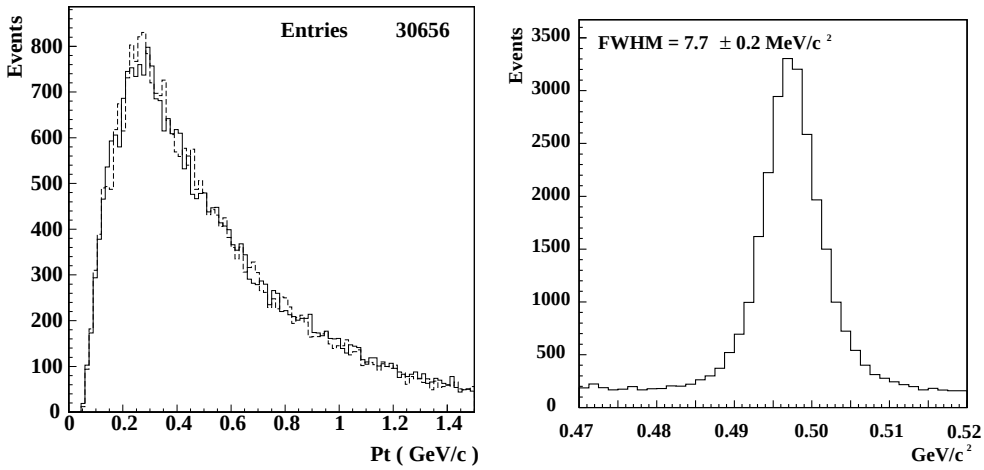

Figure 2.12: The distribution of transverse momenta of the pions for the inclusive $K^0_S \to \pi^+\pi^-$ decays (Left) and their mass distribution (Right)

TDCs to measure both the timing and charge of the signals. The QTC technique is also used to take the data of ECL and other sub-detectors.

In order to operate CDC in the high beam-background environment, we readjusted high voltages and electronics parameters such as the bias voltage of the preamplifiers. These changes reduce cross-talk noise hits caused by the very large signals due to background particles spiraling around sense wires. These changes also reduced the preamplifier's gain and slowed their response times. The calibration constants were recalculated using the beam data. In addition, corrections for the additional magnetic field non-uniformity caused by the accelerator magnet components near the interaction region were introduced into the Kalman fitter using a magnetic field map data measured with these magnets in place. We again obtained 130 μm overall spatial resolution, although the residual distribution has considerable non-Gaussian tails.

We analyzed $e^+e^- \to \mu^+\mu^-$ process, detector as two charged tracks by CDC and identified as muon by the outer detectors, ot extract the p_t reso-

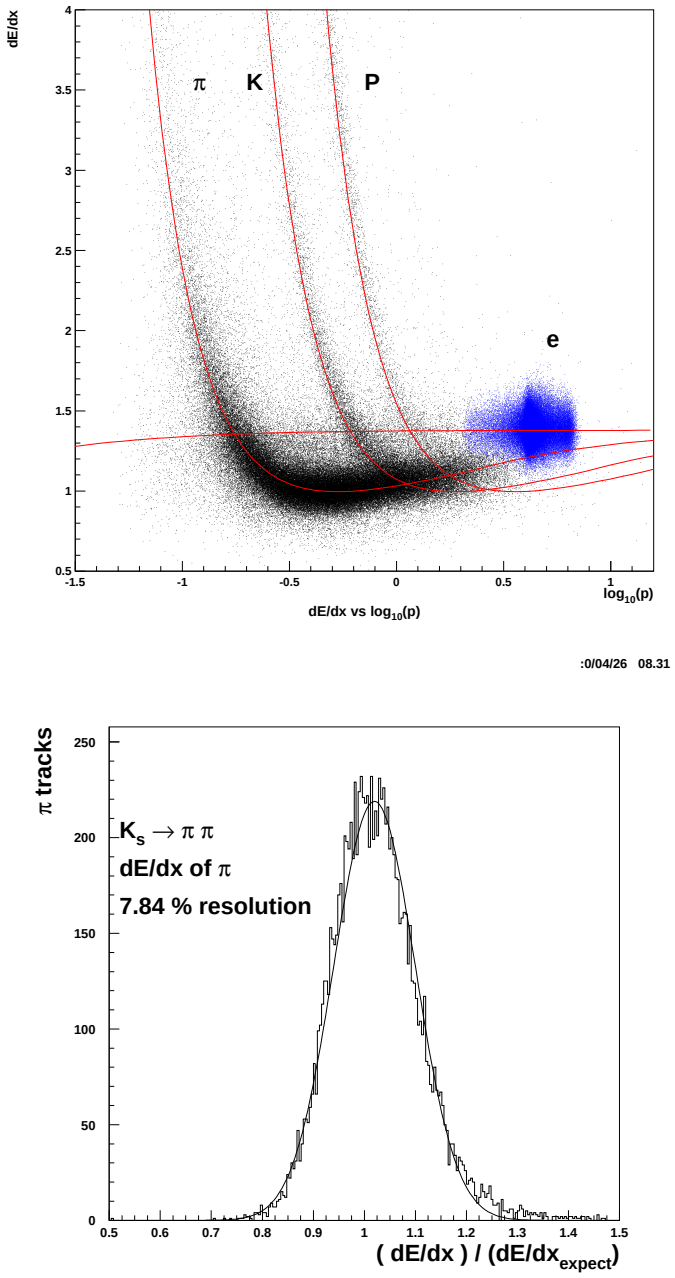

Figure 2.13: Truncated $\langle dE/dx \rangle$ vs. momentum observed in collision data(Top) and the distribution of $\langle dE/dx \rangle / \langle dE/dx \rangle_{\rm exp}$ for pion from K^0_S decays(Bottom)

lution of CDC. We can calculate the p_t resolution using the fact that each muon track has the same momentum in the center of mass system. The p_t resolutioin measured is $1.64 \pm 0.04\%$ in the p_t range from 4 to 5.2 GeV/c, which is imposed by kinematics and the acceptance of the TOF system used for triggering. This result is somewhat worse than the resolution of 1.38% expected from Monte Carlo simulations.

The ϕ dependence of the Δp_t resolution has been checked with $e^+e^- \to \mu^+\mu^-$ events. No significant ϕ-dependent systematic effects were observed. The K^0_S mass was reconstructed from $K^0_S \to \pi^+\pi^-$ decays in hadronic events in order to check the p_t resolution at low momenta. Most of the decay pions have momenta below 1 GeV/c as shown in the left hand figure in Fig. 2.12. The full width half maximum(FWHM) of the distribution is 7.7 MeV/c^2, which is slightly worse than the idealized Monte Carlo proediction 6.9 MeV/c^2. The right hand figure in Fig. 2.12 shows a $\pi^+\pi^-$ invraiant mass distribution.

The truncated-mean method was employed to estimate the most probable energy loss. The largest 20% of measured dE/dx value for each track were discarded and the remaining data were averaged in order to minimize occasional large energy fluctuations in the Landau tail of the dE/dx distribution. The $\langle dE/dx \rangle$ is expected to give 5% resolution. A 2-dimensional scatter plot of $\langle dE/dx \rangle$ versus particle momentum is shown in the left hand figure in Fig.2.13, together with different particle species. Populations of pions, kaons, protons, and electrons can be clearly seen. The normalized $\langle dE/dx \rangle$ distribution for minimum ionizing pions from K^0_S decays is shown in the right hand figure in Fig. 2.13

At present the resolutions obtained from the beam data seem to be slightly worse than those expected from the cosmic ray data and Monte Carlo simulations. Although the present performance level of CDC provides the momentum resolution sufficient for the goals of the Belle experiment, efforts to further improve CDC performance are being made.

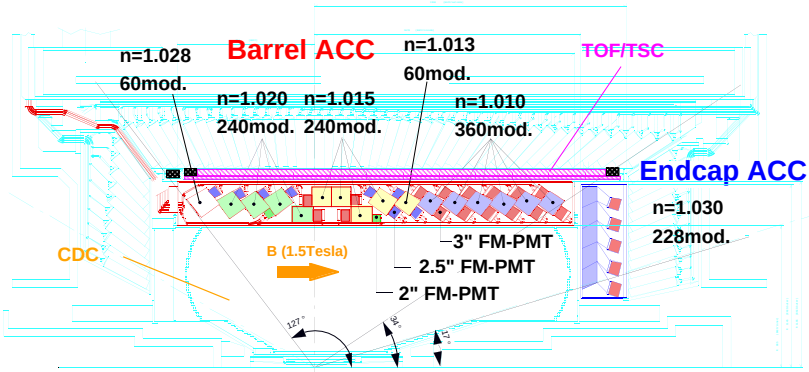

Figure 2.14: ACC arrangement

2.2.4 Aerogel threshold Chrenkov Counters(ACC)

Particle identification, specifically the ability to distinguish between $\pi^{\pm}$ and $K^{\pm}$, plays a key role in the probe of CP violation. An array of silica areogel threshold Cerenkov counters(ACC) has been selected as part of the Belle particle identification system to extend the momentum coverage beyond the reach of particle identification of CDC by using $\langle dE/dx \rangle$.

The configuration of ACC is shown in Fig. 2.14. ACC consists of 960 counter modules segmented into 60 cells in the ϕ direction for the barrel part and 228 modules arranged in 5 concentric layers for the forward endcap part of the detector. In order to obtain good π/K seperation for the whole kinematic range, the refractive indices of aerogels are selected to be between 1.01 and 1.03, depending on their polar angle region.

A typical single ACC module is shown in Fig. 2.15 for (a) the barrel and (b) the endcap ACC. The modules themseleves are composed of silica aerogel (a clloidal form of SiO_2 with more than 95% porosity), a unique material occupynig th refractive-index gap between compressed gases and liquids, and

a) Barrel ACC Module

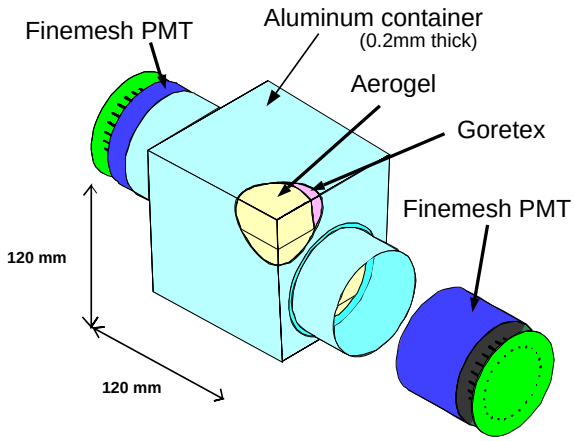

b) Endcap ACC Module

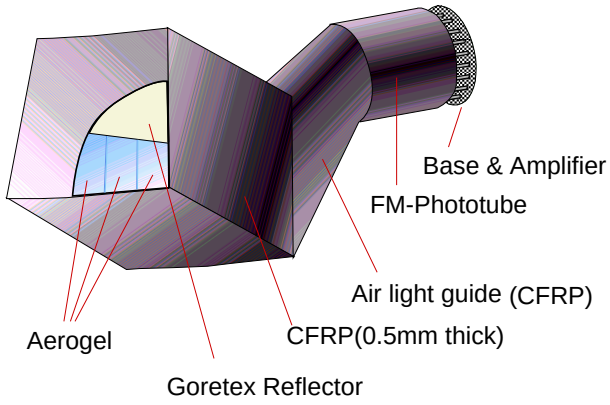

Figure 2.15: ACC module

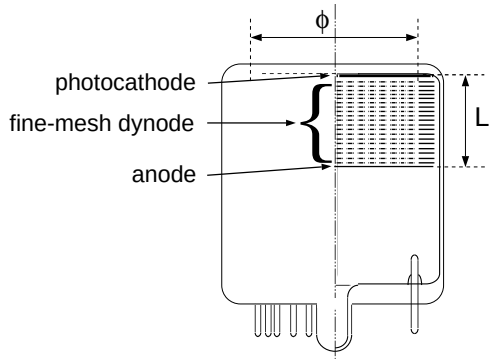

Figure 2.16: Cross sectional view of FM-PMT.

thus providing a Cerenkov light threshold suitable for π/K seperation in the O(1GeV/c) region. Five aerogel tiles are stacked in a thin(0.2 mm thick) aluminum box of approximate dimensions $12 \times 12 \times 12\text{cm}^3$. In order to detect Cerenkov lights effectively, one or two fine mesh-type photomultiplier tubes (FM-PMTs), which are operated in a magnetic field of 1.5 T, are attached directly to the aerogels at the sides of the box.

The performance of prototype ACC modules has been tested using the $\pi-2$ beam line at KEK PS. Typical pulse-height distributions for 3.5 GeV/c pions and protons measured by an aerogels counter, with n = 1.015 and read by two 2.5 inch FM-PMTs, are shown in Fig. 2.16, with and without a magnetic field of 1.5T, respectively. The number of photoelectrons(N_{pe}) for 3.5 GeV/c negative pions is measured to be 20.3. Pions and protons are clearly seperated by more than 3σ.

The initial calibration of the detector was carried out using cosmic rays. Figure 2.17 shows the measured pulse height distribution for the barrel ACC for $e^{\pm}$ tracks in Bhabha events and also $K^{\pm}$ candidates in hadronic events, which are selected by TOP and dE/dx measurements [73]. The figure demonstrates a clear seperation between high energy electrons and below-threshold particles. It also indicates good agreement between the data dn MC simulations [**?**]. A careful calibration for the pulse height of each FM-PMT signal

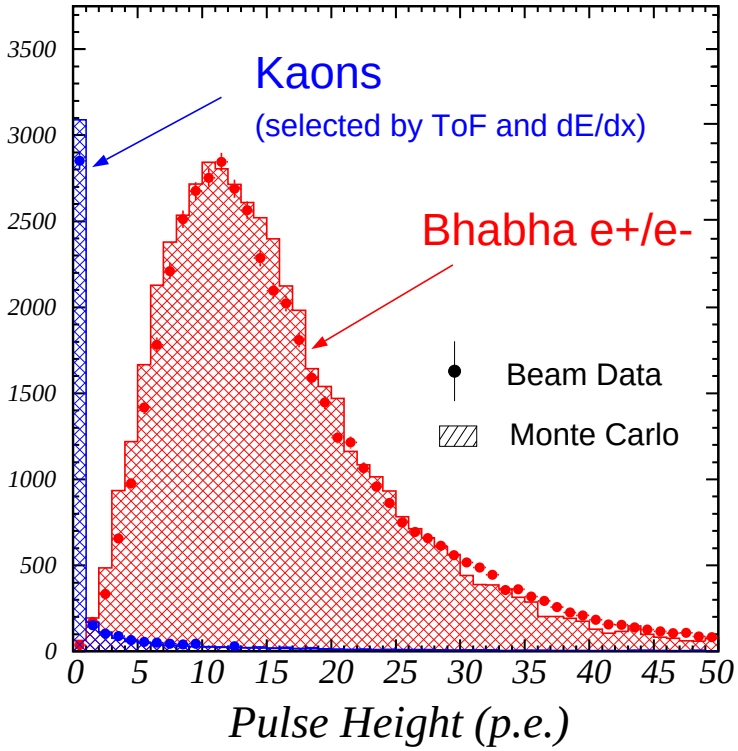

Figure 2.17: Pulse-height distribution in units of photoelectrons observed by barrel ACC for electrons and kaons. Kaon candidates were obtained by dE/dx and TOF measurements. The Monte Carlo expectations are superimposed.

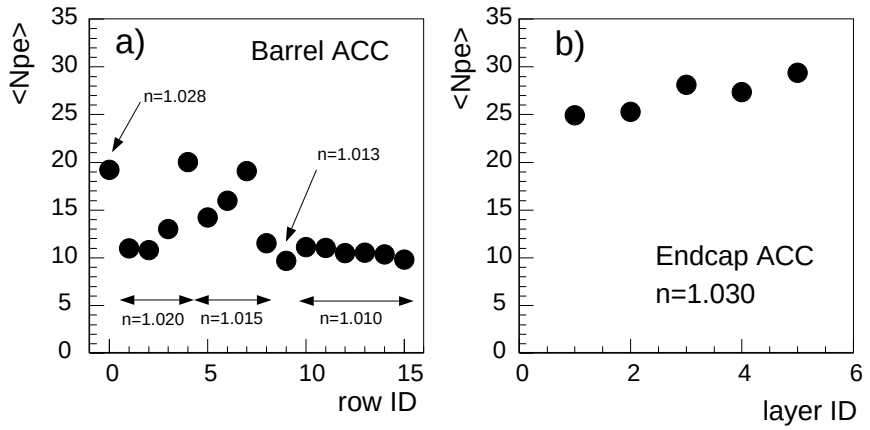

Figure 2.18: Average number of photoelectrons $\langle N_{\rm pe}\rangle$ for (a) each counter row in barrel ACC and (b) each layer in end-cap ACC .

has been performed with μ-pair events. Figures 2.18(a) and (b) shows the average number of photoelectrons $\langle N_{pe}\rangle$ for each counter row in the barrel ACC and each layer of the endcap ACC, respectively. In the barrel ACC each row has on average 60 boxes and the row number is given from left to right in Fig. 2.14. The layer number of the endcap ACC is given from the inner to the outer side. The light yield for the μ tracks depends on the refractive index of aerogel radiators, size and number of FM-PMTs attached on the counter module, and geometry of the counter module box. The light yield ranges from 10 to 20 for the barrel ACC and from 25 to 30 for the endcap ACC, high enough to provide useful π/K seperation.

2.2.5 Time-of-flight Counters(TOF)

A time-of-flight(TOF) detector system using plastic scintillation counters is very powerful for particle identification in e^+e^- collider detectors. For a 1.2 m filght path, the TOF system with 100 ps time resolution is effective for particle momenta below about 1.2 GeV/c, which encompasses 90% of the

particles produced in $\Upsilon(4S)$ decays.

In addition to particle identification, TOF counters provide fast timing signals to the trigger system generating gate signals for ADCs and stop signals for TDCs. To avoid pile-up in the trigger queue, the rate of the TOF trigger signals must be kept below 70 kHz. The gate and stop timing for the CsI calorimeter and CDC sets a time jitter requirement of less than $\pm$ 10 ns. Simulation studies indicate that to keep the fast tirgger rate below 70 kHz in any beam background conditions, the TOF counters should be augmented by thin trigger scintillation counters(TSC)[77, 78].

To achieve the design goal of 100 ps, (1) we used a fast scintillator with an attenuation length longer than 2m, (2) light guides are not used to minimize the time dispersion of scintillation photons propagating in the counter, and (3) the phototubes with large-area photocathodes were used to maximize photon collection.

These consideration led us to a configuration with fine-mesh-dynode photomultiplier tubes (FM-PMT) [75] mounted directly on the TOF and TSC scintillation counters and placed in a magnetic field of 1.5 T.

The TOF system consists of 128 TOF counters and 64 TSC counters, where each counters are made of BC408 plastic scintillator with a thin film wrapping for light confinement. Two trapezoidally shaped TOF counters and one TSC counter, with a 1.5 cm intervening radial gap, form one module. The width of the TOF counter is approximately 6 cm. In total 64 TOF/TSC modules located at a radius of 1.2 m from the interaction point cover a polar angle range from 34° to 120°. The minimum transverse momentum to reach to the TOF counters is about 0.28 GeV/c. The modules are mounted on the inner wall of the barrel ECL container. Each PMT signal is split into two. One is sent to QTC and then to a multihit TDC for charge measurement. The other generates signals corresponding to two different threshold levels: a high level(HL) and a low level(LL), where the threshold levels are in between 0.3$\sim$0.5 Mips for HL and 0.05$\sim$ 0.1 Mips for LL. The LL output provides the

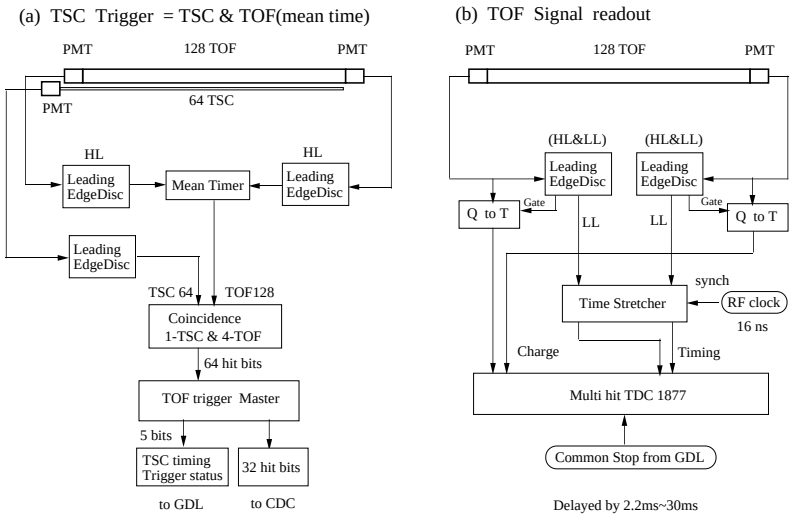

Figure 2.19: Block diagrams of the TOF electronics for (a) trigger and (b) readout.

TOF timing and the HL output provides a trigger signal. The gain of each PMT was adjusted using pulse provided by a laser calibration system, which consists of a N_2-dye laser source(420 nm) and three optical fiber bundles for the TOF forward and backward PMTs and the TSC PMTs. The variation of the PMT gains was 18%(rms). Figures 2.19(a) and (b) show block diagrams of the TOF front-end electronics for (a) event trigger and (b) readout of charge and timing of TOF signals. The gated LL signals from two ends of a counter are mean-timed and coincidenced with the TSC signals to create a fast trigger signal. The nominal coincidence arrangement between one TSC counter and four TOF counters is used to ensure triggers for low-momentum tracks.

For calibation, 150×10^3 of μ pair events were used, which corresponds to an accumulated luminostiy of 250 pb^{-1} [76]. Figure 2.20 shows time resolutions for forward and backward PMTs and for the weighted average time as a function of z. The resolution for the weighted average time is about 100 ps with a small z dependence. This satisfies the design goal, but we expect

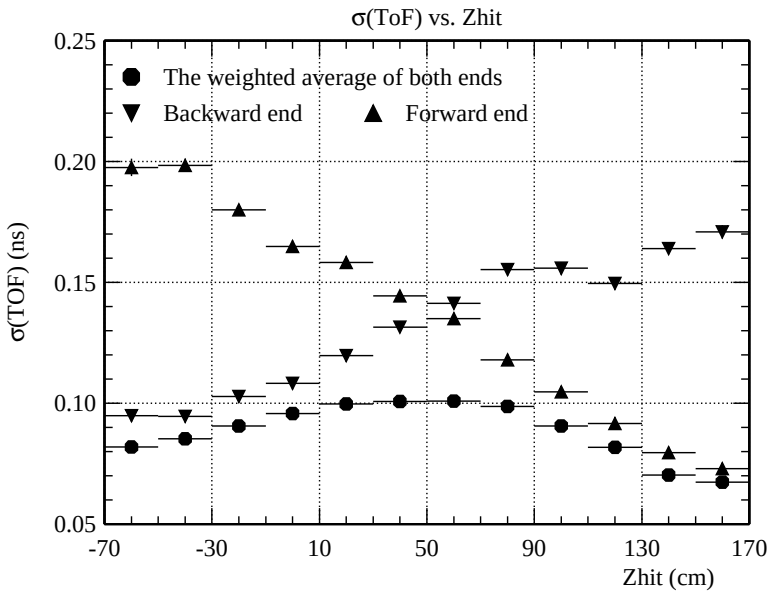

Figure 2.20: Time resolution for μ-pair events.

further improvement.

Figure 2.21 shows the mass distribution for each track in hadron events, calculated using the equation,

$$\text{mass}^2 = \left(\frac{1}{\beta^2} - 1\right) P^2 = \left(\left(\frac{c T_{\text{obs}}^{\text{twc}\,2}}{L_{\text{path}}} - 1\right) P^2\right) \tag{2.4}$$

where β is the parameter proportional to the velocity determined from an analysis of large number of hadronic events, P and L_{path} are the momentum and path length of the particle determined from the CDC track fit assumming the muon mass. Clear peaks corresponding to $\pi^{\pm}$, $K^{\pm}$ and protons are seen. The data points are in good agreement with a Monte Carlo prediction (histogram) obtained by assumming $\sigma_{\text{TOF}} = 100$ps

The descrimination power of $\pi^{\pm}/K^{\pm}$ separation is shown in Fig. 2.22 as a function of momentum. The descrimination power is defined as

$$\sigma_{\pi^{\pm}/K^{\pm}} = \frac{T_{\text{obs}}^{\text{twc}}(K) - T_{\text{obs}}^{\text{twc}}(\pi)}{\sqrt{\sigma_K^2 + \sigma_\pi^2}} \tag{2.5}$$

where σ_K and σ_π are the time resolution for K and π, respectively. This demonstrates clear 2σ separation for particle momenta upto 1.25 GeV/c.

2.2.6 Electromagnetic Calorimeter(ECL)

The main purpose of the electromagnetic calorimeter is the detection of photons with high efficiency and good resolution in terms of energy and position[66]. Since most of these photons are end-products of cascade decays, they have relatively low energies and, thus, good performance below 500 MeV is especially important. Electron identification in Belle relies primarily on a comparision of the charged particle momentum and the energy deposits in the electromagnetic calorimeters. Good energy resolution results in better hadron rejection. High momentum π^0 detection requires the separation of two nearby photon and a precise determination of their opening angle. This

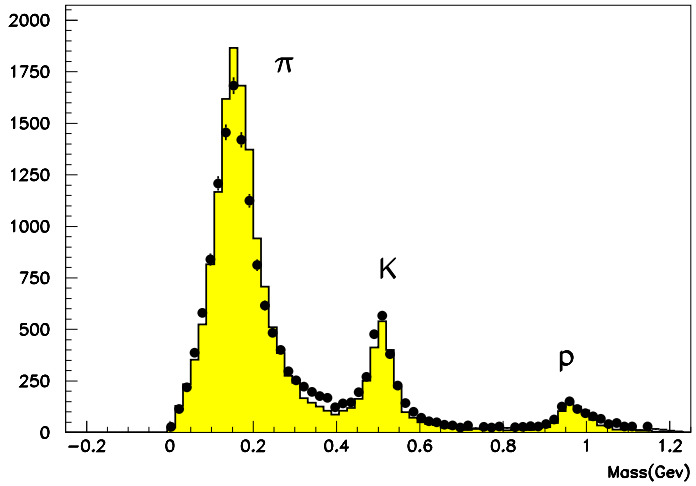

Figure 2.21: Mass distribution from TOF measurements for particle momenta below 1.2 GeV/c.

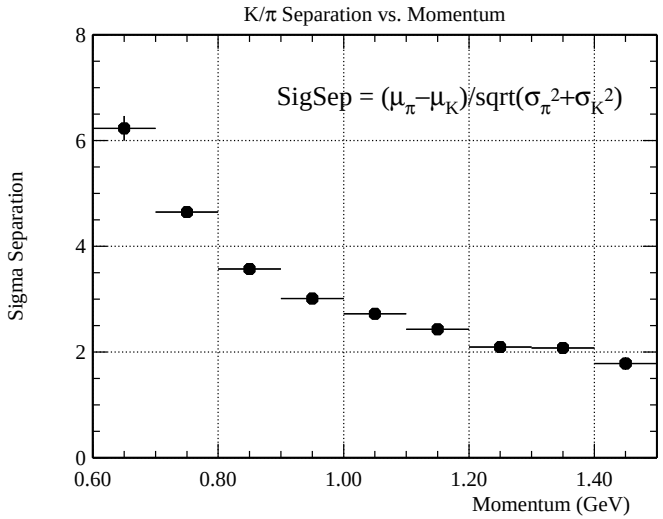

Figure 2.22: $\pi^{\pm}/K^{\pm}$ separation by TOF

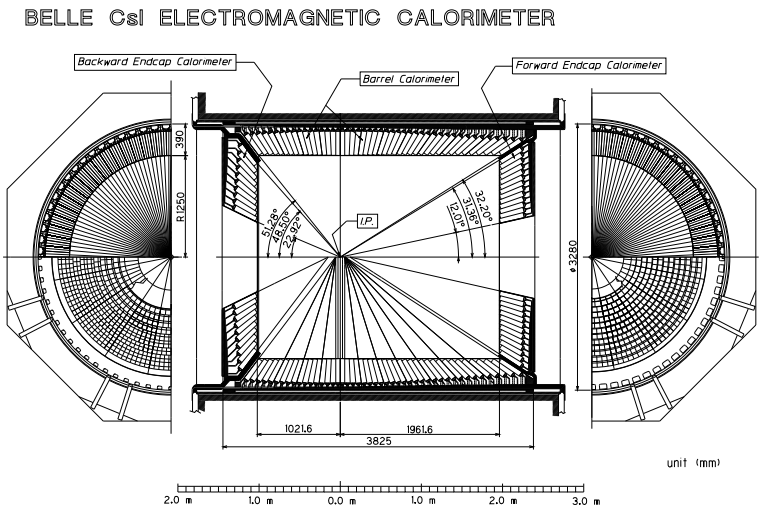

Figure 2.23: ECL configuration

requires a fine-grained segmentation in the calorimeter. The ECL also plays an important role in triggering the τ decay events, since its low track multiplicity make relatively harder to distinguish from background events which has low multiplicity such as Bhabha and di-muon events.

In order to satisfy the above requirements, a highly segmented array of CsI(Tl) crystals with silicon photodiode readout is employed. CsI(Tl) crystals have various nice features such as a large photon yield, weak hygroscopicity, mechanical stability and moderate price. The properties of CsI(Tl) crystal scintillator are summarized in Table 2.3.

The calorimeter covers $17° < \theta < 150°$ in polar angle, which corresponds to 91% of total solid-angle. Small gaps between barrel and endcap crystals provides a pathway for cables and supporting structures for inner detectors. The loss of solid angle associated with these gaps is approximately 3% of the total acceptance. The entire system contains 8736 CsI(Tl) detectors and weighs 43 tons. The size of each CsI(Tl) crystal is determined by the condition that approximately 80% of the total energy deposited by a photon injected at the center of the crystal is contained in that crystal. Crystals with smaller cross-sections would have somewhat improved position resolu-

Density	4.51(g/cm^3)
Decay constant	1300 ns
Peak emission	560 nm
Radiation length	1.85 cm
dE/dx	5.6 MeV/cm
Nuclear interation length	37 cm
Refractive index	1.79
Light yield	∼60000 photons/MeV
Light yield variation	0.3% / °C
Hygroscopicity	slight

Table 2.3: Properties of CsI(Tl) crystal

tion and two-photon separation but at the cost of an increased number of channels and poorer energy resolution. The latter is caused by the increase of gaps and inactive materials between crystals. The transverse dimensions of the crystals vary depending upon their polar angle positions; typical dimension of a crystal being 55 mm × 55 mm (front face) and 65 mm × 65 mm (rear face) for the barrel part. Dimensions of the end-cap crystals have a large variation. The dimensions of the front and rear surfaces vary from 44.5 to 70.8 mm and from 54 to 82 mm, respectively. The 30 cm length (16.2 X_0) is chosen to avoid deterioration of the energy resolution at high energies due to the fluctuations of shower leakages out the rear of the counter. A beam test result indicates that the energy resolution for 25 cm CsI(Tl) counters is $\sim$ 2.5% for electron energies above 1 GeV [79]. The abolute energy calibration has been carried out by using Bhabha and $e^+e^- \to \gamma\gamma$ events. With Bhabha samples, the calibration constant of jth counter g_j can be obtained by minimizing χ^2 defined as

$$\chi^2 = \sum_k^{events} \left(\frac{E_k(\theta) f(\theta) - \Sigma_j g_j E_j}{\sigma} \right)^2 \tag{2.6}$$

where E_k is the expected energy of the Bhabha electrons. This value is known as a function of θ in the asymmetric collider. The function $f(\theta)$ is the correc-

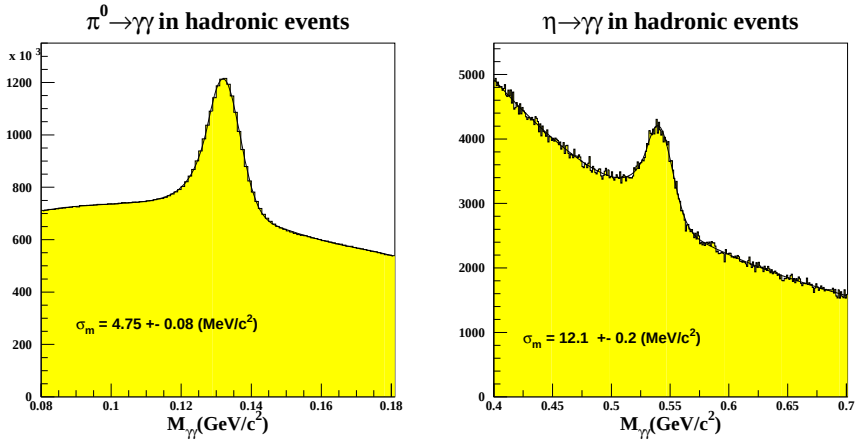

Figure 2.24: Reconstructed invariant mass using two photons for hadronic events in $\pi^0 \to \gamma\gamma$ (left-hand) and in $\eta \to \gamma\gamma$ (right-hand), where each photon energy was greater than 30 MeV in the barrel region.

tion factor due to the shower leakage and the front material effect, which was determined by a MC simulation. This function was introduced in the χ^2 minimization in order to maintain the consistency between real and MC events. The minimization was carried out by taking $\sim 8500 \times 8500$ sparse matrix inversion into account. Approximately 50 events per counter were used for this calibration.

2.2.7 K_L^0 and Muon Detection System(KLM)

The K_L^0 and Muon detector is designed to identify K_L^0 and muon with hight efficiency over a broad momentum region greator than 600 MeV/c[67]. The barrel-shaped region around the beam axis covers the polar angle region from 45° to 125°. KLM consists of alternating layers of charged particle detectors and 4.7 cm-thick iron plates. There are 15 detector layers and 14 iron layers in the octagonal barrel region and 14 detector layers in each of the forward and backward endcaps. The iron plates provide 3.9 interaction

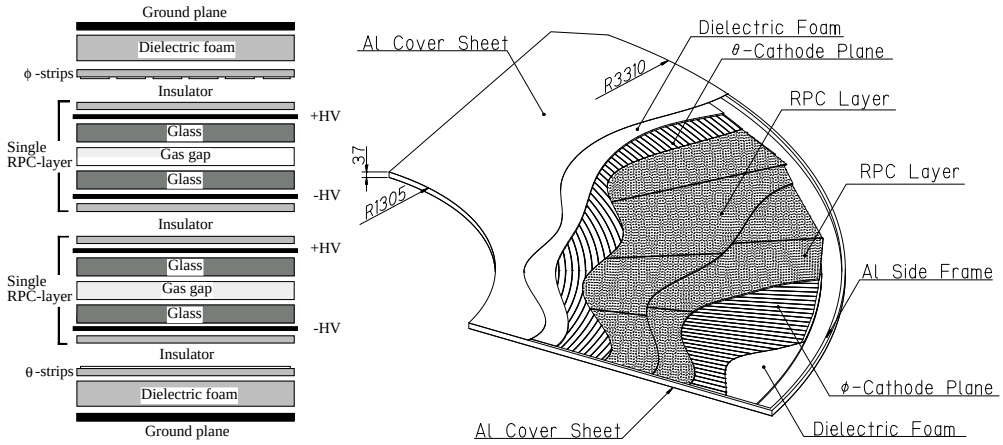

Figure 2.25: The KLM superlayer for barrel(left) and endcap(right) in cross-sectional and cut-away view, respectively.

lengths in total for a particle traveling in the detector. In addition, ECL provides another 0.8 interaction length. If K_L^0 interact inside of the iron or ECL, it produces a shower of ionizing particles. This shower can be located but does not allow a useful measurement of its energy because of large energy fluctuations. The multiple layers of charged particle detectors and iron allow the discrimination between muons and charged hadrons (π, K) based upon their range and transverse scattering. Muon travels much further with smaller deflection on average than hadrons which interect strongly with detector materials.

The charged particles are detected by glass-electrode resistive plate counter (RPC). Figure 2.25 shows the cross section of a super-layer, in which two RPCs are sandwiched between the orthogonal θ and ϕ pickup-strips with the ground planes for signal reference and proper impedance. RPC have two parallel plate electrodes with high bulk regsistivity ($\leq 10^{10}\Omega$ cm) separated by a gas-filled gap. In the streamer mode, an ionizing particle traversing the gap initiates a streamer in the gas that results in a local discharge of the plates. This discharge is limited by the high resistivity of the plates and the

quenching characteristics of the gas. The discharge induces a signal on external pickup strips, which can be used to record the location and the time of the ionization.

Identification of K_L^0 and muon can be done by using the signals from the isolcated clusters of KLM detector and the track location extrapolated by CDC track informations. The isolated clusters are constructed by calculating the center of gravity of the hits which is used to determine the direction of flight from the interaction point. Then the isolated clusters where it is located within 15° to the direction of extrapolated track are excluded and can be identified as muon candidates, otherwise identified as K_L^0.

Cosmic rays were used to measure the detection efficiency and resolution of the super-layers. The momenta of cosmic muons were measured by CDC with the solenoid field of 1.5 T. The required energy for muon to be detected at KLM is at least 500 MeV/c. Some fraction of charged pions and kaons are misidentified as muons. In order to estimate the fake rate, a sample of $K_S^0 \to \pi\pi$ events in e^+e^- collision data is used. Figure 2.26 shows the muon detection efficiency and fake rate versus momentum with a likelihood condition $\mathcal{L}_\mu > 0.66$. When the particle energy is higher than 1.5 GeV/c, the detection efficiency is converging to 90% and the fake rate is decreasing from 5% to 0.

2.2.8 Trigger

In the high luminosity conditions the physics events which we want to observe can be suffered from the large background of Bhabha and other unwanted processes. However, these processes are not fully rejected due to the calibration for luminosity and detector response which is done time to time. Table 2.4 provides the cross section and event rate for each physics process.

Because of the high beam current, beam backgrounds are in high level. Another 100 Hz from beam-related background are expected in the MC sim-

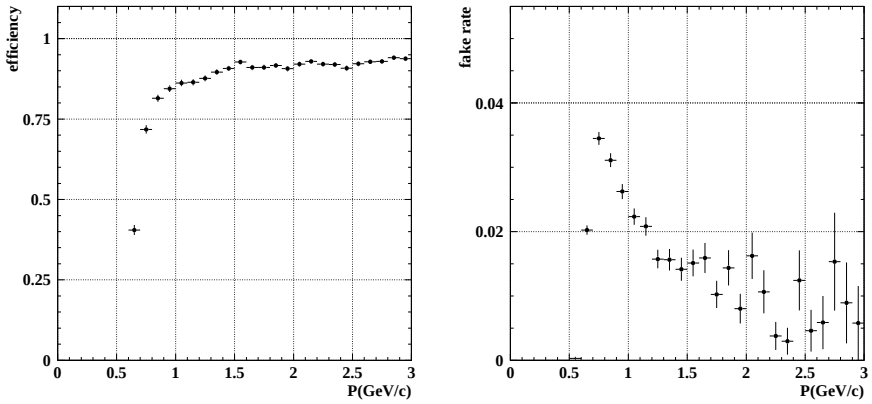

Figure 2.26: Particle Identification performance for muon efficiency(left) and its fake rate(right) using KLM.

Physics process	Cross section(nb)	Rate(Hz)
$\Upsilon(4S) \to B\bar{B}$	1.15	11.5
$e^+e^- \to q\bar{q}$	2.8	28
$e^+e^- \to l^+l^-$	1.6	16
Bhabha ($\theta_{\rm lab} \geq 17^\circ$)	44	4.4
two-photon ($\theta_{\rm lab} \geq 17^\circ$)	~ 15	~ 35
Total	~ 67	~ 96

Table 2.4: Total cross section and trigger rate of the physic processes with $\mathcal{L} = 10^{34}\text{cm}^{-2}\text{sec}^{-1}$ at 10.58 GeV. The rates are prescaled by factor of 1/100 with restricted condition on transvers momenta $|\vec{p}_t| \geq 0.3$ GeV/c.

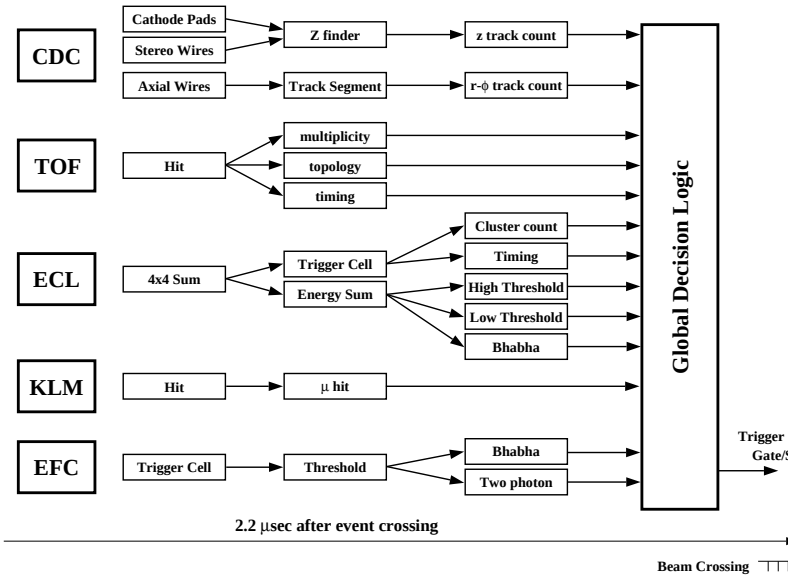

Figure 2.27: Level-1 trigger system scheme

ulations. These backgrounds fully depend on the accelerator condition and are unpredictable. In order to cope with these background, the redundancy of trigger system is quite required. The high luminosity environment also bring the other important issue, the event decision, since the detectors and other relevant electronics have a certain limit of response and data follow rate.

The Belle trigger system[81] consist of the Level-1 hardware trigger and the Level-3, Level-4 are software trigger. Level-1 trigger, so called L1 trigger consists of the many input logics for sub-trigger system and the central decision making logic called as Global Decsion Logic(GDL) as depected in Fig. 2.27 The sub-detector trigger system can be categorized into two: track triggers and energy triggers. The trigger signal from CDC and TOF includes the information for charged particles. The CDC trigger provides $r-\phi$ and $r-z$ informations. On the other hands, The ECL trigger is a set of signals including the total energy deposited and cluster counting of crystal hits. The KLM trigger provides additional information for muons. The EFC trigger are used for tagging two photon events as well as Bhabha events. The

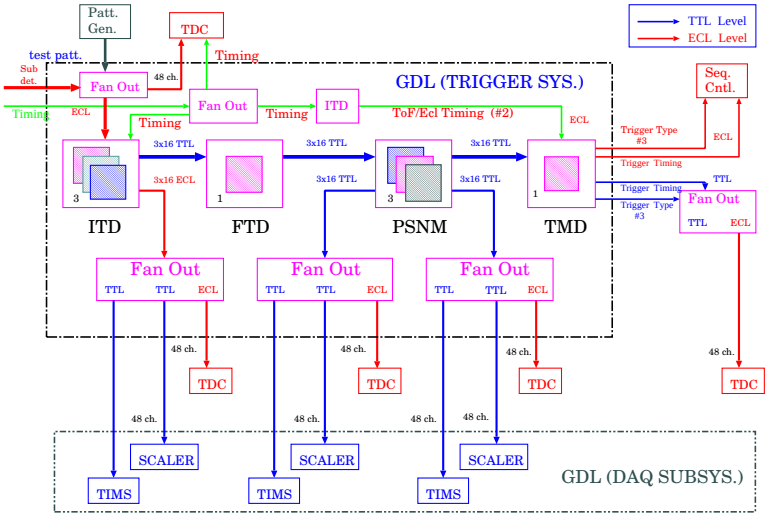

Figure 2.28: A schematic view of Global Decision Logic

sub-detectors process the event signals in parallel and provide the trigger information to GDL which all information is combined and charaterized into a certain type of event. Information from SVD has not been implemented in the grobal trigger system, but the Level-0 trigger signal from the VA1TA of SVD is used in determining the integration of charge of SVD inside the SVD detector.

The configuration of GDL is shown in Fig. 2.28 GDL receives upto 48 trigger signals from sub-detectors and reformulate global correlations among them. It generates more or less than 50 types fo event trigger signals.[I] The required decision time for GDL is 350 ns. The functionality of GDL is shared by several types of modules as shown in Fig. 2.28. Input Trigger Decay(ITD) adjusts the timing of input trigger signals to meet the latency of 1.85μs. Fignal Trigger Decision(FTD) performs the global trigger logic which reformulate the information from sub-detector trigger. Prescale and Mask(PSNM) prescales the high rate input triggers for calibration and monitoring purpose and disables the unused triggers. Timing Decision(TMD) generates the final trigger signal at 2.2 μs latency based on the timing information of the

[I] This is quite depend on the situations.

"timing trigger" from TSC and ECL.

The final output from GDL are categorized as follows:

- Multi-track triggers: These require three or more tracks in CDC $r-\phi$ and at least one track in CDC $z-$trigger. Several types are formed depending on the condition for the number of full tracks, opening angle, TSC/TOF hits, and ECL cluster hits.

- Total energy triggers: These are based on the ECL energy sum triggers and vetoed by ECL Bhabha and cosmic triggers.

- Isolated cluster counting trigger: We require four or more ECL isolated clusters to avoid Bhabha events but still require cosmic veto to reduce the cosmic rate.

- Bhabha trigger: We prescale these triggers depending on the luminosity to keep the rate less than 10 Hz.

- Two-track triggers: These triggers take two or more tracks in CDC $r-\phi$ and at least one in CDC $z-$triggers. In order to reduce the rate, these require CDC opening angle, TSC/TOF hits, and ECL energy or clusters.

- Muon triggers: These require two or more CDC $r-\phi$ tracks and KLM trigger. The track trigger conditions are loose.

- Monitor triggers: These include a random trigger and prescaled triggers with loose conditions for monitoring purpose.

Triggers 1∼3 are intended to catch multi-hadronic events, which provide a redundancy. In a typical running condition, the average trigger rate is about 200 to 300 Hz. According to increase of the beam current and luminosity during several months of runs, we adjusted the trigger condition and prescale values keeping the average trigger rate less or around 400 Hz.

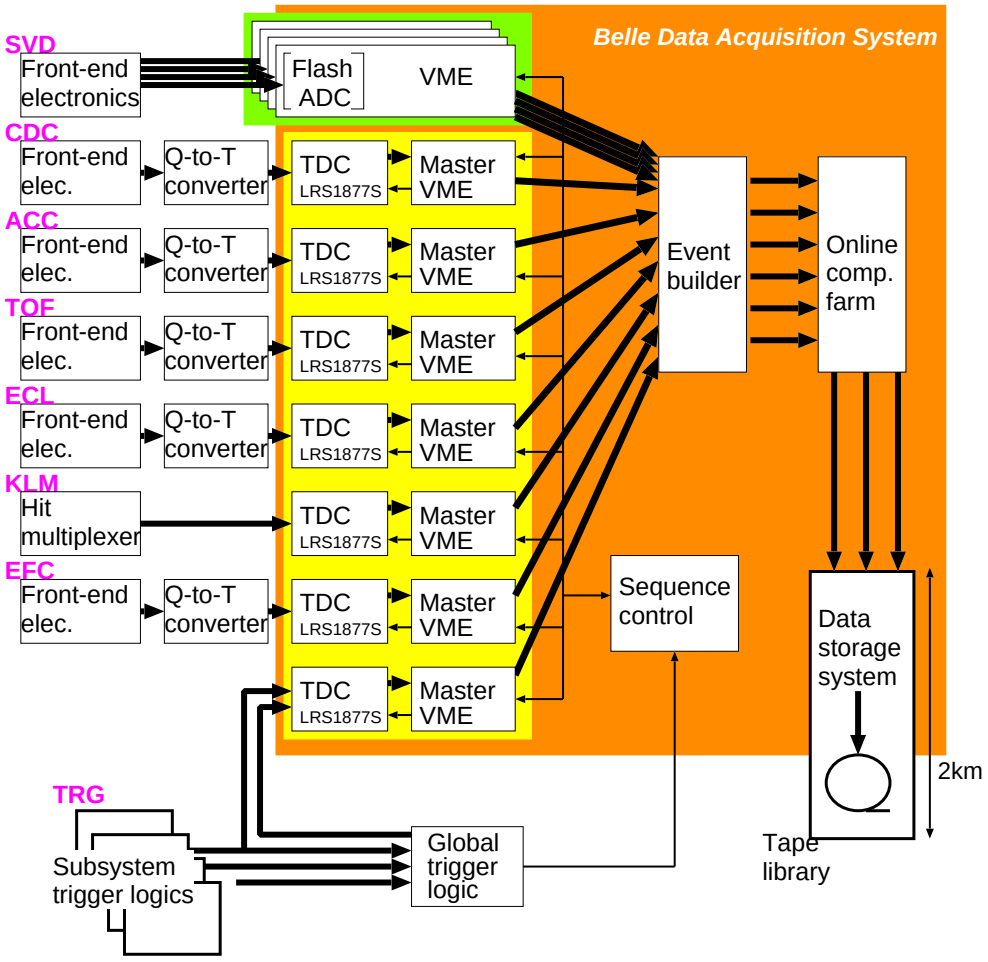

Figure 2.29: Global scheme of the data acquisition system

2.2.9 Data Acquisition System(DAQ)

In order to satisfy the data acquisition operated at 0.5∼1 kHz with at most 10% of dead time fraction, the distributed-parallel system has been devised. The global scheme of the system is shown in Fig. 2.29. The entire system is segmented into 7 subsystems running in parallel, each handling the data from a subdetector. Data from each subsystem are combined into a single event recorded by an event builder that converts “data streams” to a “data river”. The event builder output is transferred to an online computer farm,

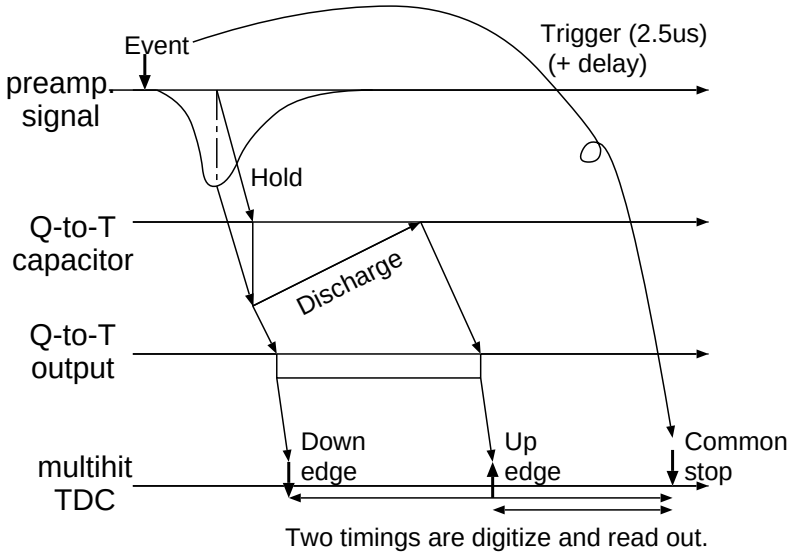

Figure 2.30: A schematic view of Q-to-T and TDC based digitization.

where another level of event filtering is done after fast event reconstruction which is called as "L-4" trigger. The data are then sent to a mass storage system located at the computer[84].

A Q-to-T technique with commom-stop scheme is used to read out the signals from the sub-detectors. Once the event is occured, the charge of signal is stored in a capacitor and discharged with a constant rate. Then the Q-to-T output start producing the negative signal, and end producing the signal when the discharging is complete. The multihit TDC records both edge timing of the signals so the difference of two edge becomes the size of the detector signal. With this technique, we can determine both the signal timing and amplitude. The illustration of Q-to-T technique is well depected in Fig. 2.30. For time digitization, we use a multi-hit FASTBUS TDC module, LeCroy LRS1877s. Up to 16 timing pulses are recorded for 96 channels in a single width module with a sparsification capability. Most of the detectors, CDC, ACC, TOF, ECL and EFC, are read out by using Q-to-T and TDC technique. The KLM strip information is also read out by using the same

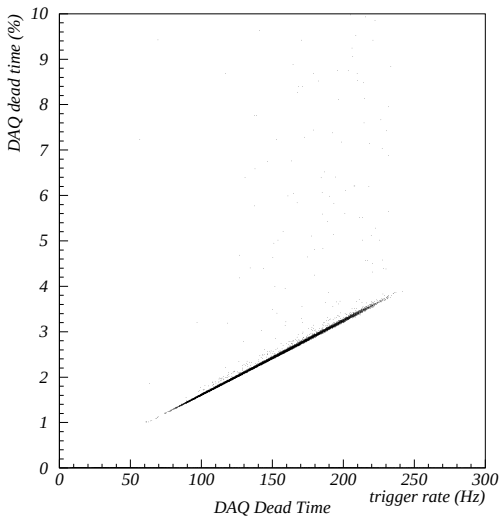

Figure 2.31: DAQ deadtime as a function of trigger rate

type of TDC. A unified FASTBUS TDC readout subsystem was developed, which is applicable to all the detectors except SVD. A FASTBUS processor interface, FPI, developed bus controls these TDC modules, and FPI is controlled by a readout system controller in a master VME crate. Readout software runs on the VxWorks real time operating system on a Motorola MVME5100, which has PowerPC740 and two fast Ethernet interfaces, one of which is used for general purpose control and the other is used for the actual data transmision.

SVD data are read out from 81,920 strip channels, whose occupancy is typically a few percent depending on the beam condition. The charge information is read out by intelligent flash ADC modules with an embedded DSP, which performs data sparsification. A timing signal for a readout sequence is handled by a central sequence controller and TDMs. The sequence controller receives a timing signal from the trigger system and distributes it to TDM located at the VME crate of each detector readout system.

Figure 2.31 shows the total deadtime of the DAQ system as a function of trigger rate measured in real beam runs. The typical trigger rate is about 300

Hz. The deadtime linearly increases as the trigger rate increases and reaches up to 5.5% at 300 Hz which is consistent with the designed value. The overall error rate of the data acquisition flow is measured to be less than 0.05%.

A new DAQ systme is being installed and used to cope with the increasing luminosity and trigger rate. This new data logging system, called COPPER(COmmon Pipelined Platform for Electronics Readout), is based on the PCI bus technology. The mainboard of 9U-VME type consist of four slots for signal digitization modules which are called FINESSE (Front-end INstrumentation Entity for Sub-detector Specific Electronics). By using COPPER system, the readout speed can be increased up to 125 MB/s [85]. Currently, some of the DAQ systems of Belle detector have been migrated to COPPER based system from the old LeCroy TDC system. All the DAQ systems are expected to employ COPPER based DAQ system at Belle-II experiment.

2.2.10 Computing Systems and Softwares

The computing and software system is of great importance to the Belle experiment as very complex data analysis techniques using a large amount of data are required for physics discoveries. A traditional HEP computing model has been adopted by the Belle collaboration. Namely, the Belle collaboration has chosen to use tape library systems with the sequential access method for the input and output of experimental data as the mass storage system [84].

The KEK B computers are schematically shown in Fig. 2.32. This system consists of the three cardinal links; computing network, user network and internal network. The computing network interconnects the servers with the PC farms which are operated as a batch job system controlled by the LSF scheduler. The computing network is also attached to the tape robotic device, where raw data and DST data are saved. The user network links the several work group servers to the storage devices, which consist of file sever and hierarchy mass storage(HSM). The work group servers also connected

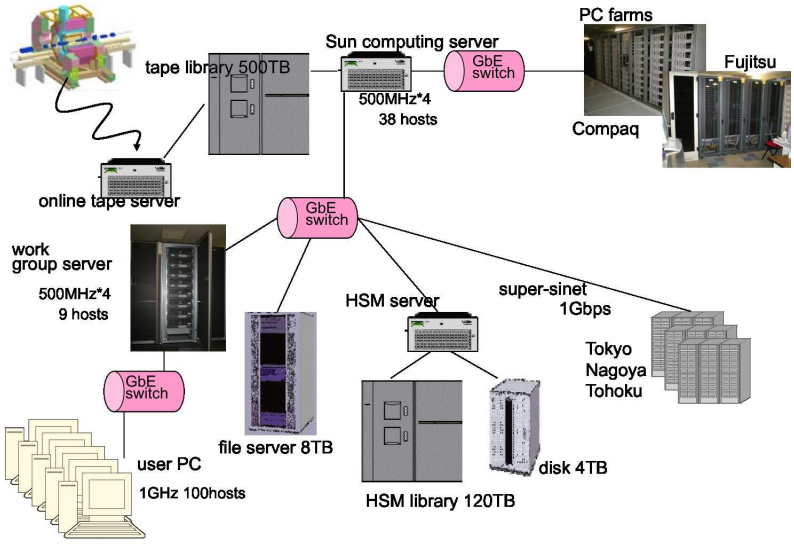

Figure 2.32: Belle computing system. The storage capacities are quite flexiable according to the Belle data accumulation and analysis situiation.

to hundreds of PCs for users. The last network, internal network, links to the other computing resource in major Japanese universities. i.e. Tokyo-U, Nagoya-U and Tohoku-U. Especially, Nagoya university provides important resources for tau physics analysis to users.

The core utility of the Belle analysis is BASF abbrebiation of Belle AnalySis Framework. This is a "home-made" core software developed by the Belle group. In this scheme, each program, written in C++, is compiled as a shared object, and it is treated as a module. When one wants to run a program with this framework, the modules defined in its scripts are dynamically loaded. The data handling is done with the traditional bank system, named as PANTHER, with a zlib compression capability. In this utility, data transfer between different modules is made and data I/ O is manipulated. PANTHER is the only software to handle our data at any stage of the data processing. The event flow scheme is depected in Fig. 2.33. The shared object are loaded dynamically by user's script which assign the location of data, recognized

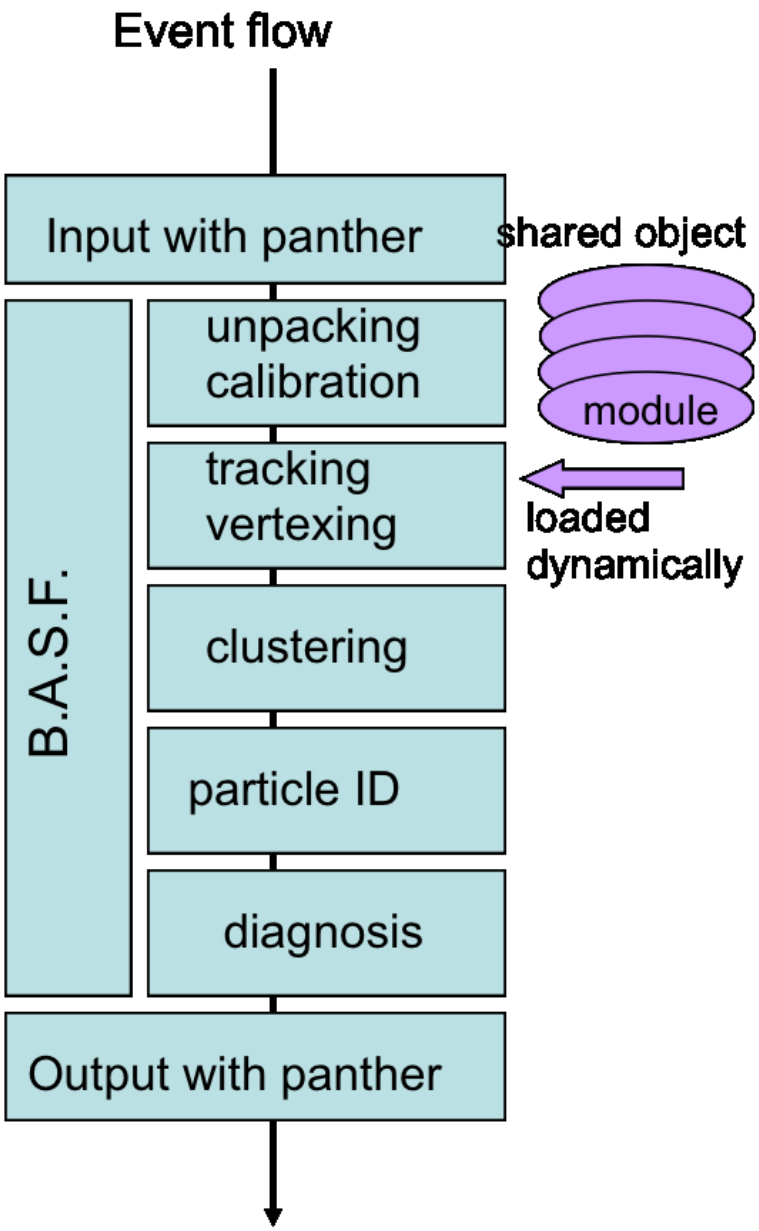

Figure 2.33: The event flow scheme in BASF. The PANTHER is loaded when the BASF is called.

performance Year	1997	2001	2006
Computing Server	~ 100	$\sim 1,250$	$\sim 42,500$
Disk Capacity [TB]	~ 4	~ 9	1,000 (1 PB)
Tape Library Capacity [TB]	160	620	3,500 (3.5 PB)
Work Group Sever [# of hosts]	3 + (9)	11	80 + 16 FS
User Workstation [# of hosts]	25 WS + 68 X	23 WS + 100 PC	128 PC

Table 2.5: The history of the Belle computing system

by PANTHER. After processing data, the result are recorded in a form of PANTHER.

However, the BASF and PANTHER are a part of the "home-made" softwares. The Belle members built a set of libraries which accomodate data analysis as well as the event processing. This is called as "Belle library" that include the useful libraries and source codes for the end-user analysis: various monte carlo event generator, the detector simulator, several fitters and so forth.

As time goes by, however, the computing systems have to be changed into newer systems in order to cope with massive data. In 2006 Belle introduced new computing systems provided and supported by DELL and SONY. Table 2.5 shows the history of the Belle computing system. As the luminosity increase, the necessity of more powerful computing power and storage is inevitable. This system is less expensive and provide reasonable reliability. The system upgrade has continued and ended on 2009, the year before the end of the Belle operation.

2.2.11 Monte Carlo simulation in τ analysis

In the Belle experiment, several physics event generators based on the Monte Carlo techinique are embeded on the home-made libraries, called as "Belle library". The KKMC Monte Carlo event generator [86] is implemented to generate $e^+e^- \to f\bar{f} + n\gamma$ processes, where $f = \mu, \tau, u, d, s, c, b$, so that τ pair are generated with $\sigma_{\tau\tau} = 0.919$ nb of cross-section. In order to pro-

duce the hadronic or leptonic final state decays of τ lepton, TAUOLA event generator package [87] are used. The TAUOLA library provides 22 different τ decay modes within the context of Vector Meson Dominance. All channels are implemented to the best available knowledge, combining theoretical expectation and experimental information. The τ lepton decay is a kind of the charged-current V-A interaction written as

$$g_v\gamma_\mu - g_a\gamma_\mu\gamma_5 \tag{2.7}$$

where the vector (g_v) and axial-vector (g_a) couplings can be changed by user. And the mass of the τ neutrino and all branching fractions can be set by the user. A few details about the decay mode of interest are given below:

- $\tau \to e\bar{\nu}\nu$ and $\tau \to \mu\bar{\nu}\nu$: These are simulated according to the Standard Model matrxi element with full electroweak corrections.[]
- $\tau \to \pi\nu$ and $\tau \to K\nu$: These channels can be modeled by theory with radiative correction.
- $\tau \to \pi\pi\nu$: This decay is modeled by ρ and ρ'.
- $\tau \to 3\pi\nu$: The decay chain $a_1 \to \rho\pi$ and $\rho \to \pi\pi$ can be tested by Kuhn/Santamaria model
- $\tau \to K\pi\nu$: This decays through the $K^*(892)$ resonance.
- Three-meson final states : As described in Sec.1.2, the hadronic current can be described by the form factors: axial-vector current, pseudoscalar current and the Wess-Zumino current can be implemented according to the final state mesons.
- n-Pion channels : Four-pion channels are described by vector current and somtimes Wess-Zumino current. The five or six pion channels are generated by the phase space decay with CVC hypothesis.

For the study of detector effects in the Monte Carlo simulation, the Belle members built a detector simulator, called gsim, based on the GEANT 3 framework written by FORTRAN 77. This detector simulator accomodates several well known mesonic/hadronic decays, i.e. $\pi^0 \to \gamma\gamma$, $K^0_S \to \pi^+\pi^-$, as well as the interactions between the particle and the detctor materials when the particles traverse through the materials. The detector materials and their responses can be controlled and regulated accroding to the detector studies, which is cope with the timely variation of detector response: degradation, aging and so other problems.

Mode	F_1	F_2	F_4	F_5
$\tau^- \to 3\pi\nu_\tau$	$a_1 \to \rho\pi$	$a_1 \to \pi\rho$	$\pi'(1300)$	-
	$\rho \to \pi\pi$	$\rho \to \pi\pi$	-	-
$\tau^- \to K^+K^-\nu_\tau$	$a_1 \to K^*K$	$a_1 \to \pi\rho$	-	$\rho \to K^*K$
	$K^* \to K\pi$	$\rho \to KK$	-	$K^* \to K\pi$
$\tau^- \to K^0\bar{K}^0\pi^-\nu_\tau$	$a_1 \to K^*K$	$a_1 \to \pi\rho$	-	$\rho \to K^*K$
	$K^* \to K\pi$	$\rho \to KK$	-	$K^* \to K\pi$
$\tau^- \to K^-K^0\pi^0\nu_\tau$	-	$a_1 \to \pi\rho$	-	-
	-	$\rho \to KK$	-	-
$\tau^- \to K^-\pi^0\pi^0\nu_\tau$	$K_1 \to K^*\pi$	$a_1 \to \pi\rho$	-	-
	$K^* \to K\pi$	$\rho \to KK$	-	-
$\tau^- \to K^-\pi^+\pi^-\nu_\tau$	$K_1 \to K\rho$	$a_1 \to \pi\rho$	-	$K^* \to \rho K$
	$\rho \to \pi\pi$	$\rho \to KK$	-	$\rho \to \pi\pi$
$\tau^- \to K^0\pi^-\pi^0\nu_\tau$	-	$K_1 \to K\rho$	-	$K^* \to \rho K$
	-	$\rho \to \pi\pi$	-	$\rho \to \pi\pi$
$\tau^- \to \eta\pi^-\pi^0\nu_\tau$	-	-	-	$\rho \to \rho\eta$
	-	-	-	$\rho \to \pi\pi$

Table 2.6: Form factors of the three-meson final states in TAUOLA [88]. F_1 and F_2 axial-vector, F_4 pseudoscalar, and F_5 Wess-Zumino anomaly.

Chapter 3

$\tau^+\tau^-$ event selection

In order to study several τ decays of interest, a sample of $e^+e^- \to \tau^+\tau^-$ events have to be isolated. These are selected by requiring a set of criteria that are established by the studies using Monte Carlo simulations. The event selection procedure is consists of two steps, one is the τ pre-selection, and the other is the application of criteria dedicated to the specific decay channels being studied.

3.1 Pre-selection of τ events

The event selection starts with requirements on the number of charged tracks in an event. Most τ decay processes produce final states that have fewer charged tracks than for continuum processes, because of limited available phase space.

Figure 3.1 shows the number of track distribution for different types of processes, where we can see clear differences between (a) τ events and (d) uds events. Based on these distributions, the number of track are required to be in the range $2 \leq \mathrm{N_{track}} \leq 8$. From the figure it is clean that this requirement does

not discriminate against di-muon events(b) or $\gamma\gamma \to e^+e^-e^+e^-$ processes(c). In order to reject the $e^+e^- \to \mu^+\mu^-$ and Bhabha events, the vector sum of track momenta in the CM frame and the total energy of ECL clusters are limited to $\sum \vec{p}_{CM} < 10$ GeV/c and $\sum E_{ECL} < 10$ GeV/c^2, respectively. For two-track events, large background from Bhabha process still remains due to its high cross section; tighten conditions are required: $\sum \vec{p}_{CM} < 9$ GeV/c and $\sum E_{ECL} < 9$ GeV/c^2. With this cut, most $e^+e^- \to \mu^+\mu^-$ and Bhabha events are rejected while the number of τ pair events is not affected seriously. (See Fig. 3.2)

The 2-γ events produce many tracks with low transverse momentum, $\vec{p}_T$, where the transverse direction is perpendicular to the beam direction(z direction). We can avoid the 2-γ events using the cut on transverse momentum defined as $\vec{p}_T > 0.5$ GeV/c. The τ pair events in which all charged tracks have low-$\vec{p}_T$ are not significant contributors to the for the physics analyse

Surviving two-track events, requriement on the polar angle of the missing momentum are used to reject radiative $\mu\mu$, Bhabha and 2-γ events, where the missing momentum is defined as $\vec{p}_{miss} = (\vec{p}_{init} - \Sigma\vec{p}_{track} - \Sigma\vec{p}_{\gamma})$. In Fig. **??** it can be seen that most of the radiative $\mu\mu$ and Bhabha events have $\vec{p}_{miss}$ directed near the beam pipe direction while for τ pair events, most are in the range $5^\circ < \theta_{miss} < 175^\circ$. The 2-$\gamma$ events tend also to be directed along the initial beam direction.

The reconstructed energy and transverse momentum for 2-γ or beam background events tend to be lower than for τ-pair events. Because of this feature, these background can be rejected by requiring $E_{\rm rec} > 3$ GeV and $\vec{p}_T > 1.0$ GeV/c. Also, we further reduce beam background events, by requiring the event vertex condition, in terms of the radial/longitudinal distance, from the interaction point(IP), $|r| < 0.5$ cm, $|z| < 3$ cm. Figure 3.5 shows four 2-D scatter plots for $E_{\rm rec}$ and maximum $\vec{p}_T$ after the conditions on the number of tracks, maximum $\vec{p}_T$ and θ_{miss} are applied.

In the case of 2 or 4 track events, we require additional conditions since

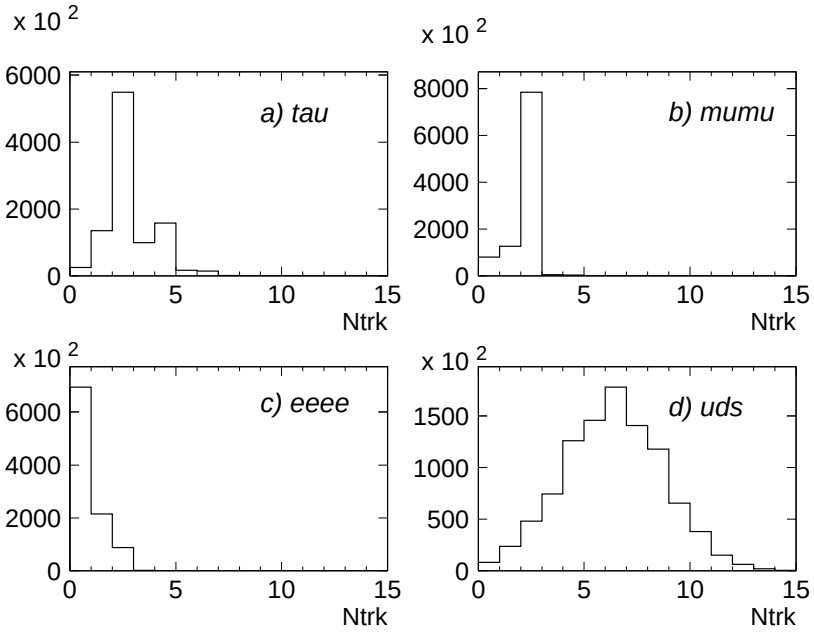

Figure 3.1: Number of detected charged tracks for a) $\tau\tau$ events, b) $\mu\mu$ events, c) 2-γ and d) continuum (uds).

many Bhabha events survive the above conditions. Most of the remaining Bhabha events have more than one missing radiative photons that are lost in the gap of the ECL detector. These (radiative) Bhabha events can be removed by requiring on $E_{\rm tot} < 9$ GeV and the maximum opening angle, $\theta_{\rm Max} < 175^\circ$, where $E_{\rm tot} = E_{\rm rec} + |\vec{P}^{CM}_{miss}|$ and $\theta_{\rm Max}$ is the maximum angle of the two tracks for all combinations. Most of particles produced by surviving Bhabha events are directed toward the end cap region with higher momentum. We reject these events by requiring $N_{\rm barrel} \geq 2$ and $E_{\rm ECL,tracks} < 5.3$ GeV, where $N_{\rm barrel}$ is the number of tracks located at barrel region and $E_{\rm ECL,tracks}$ is the total energy of ECL cluster for the tracks. Figure 3.6 and 3.7 shows two 2-D plots, one for the $E_{\rm tot}$ and $\theta_{\rm Max}$ and the other for $N_{\rm barrel}$ and $E_{\rm ECL,tracks}$.

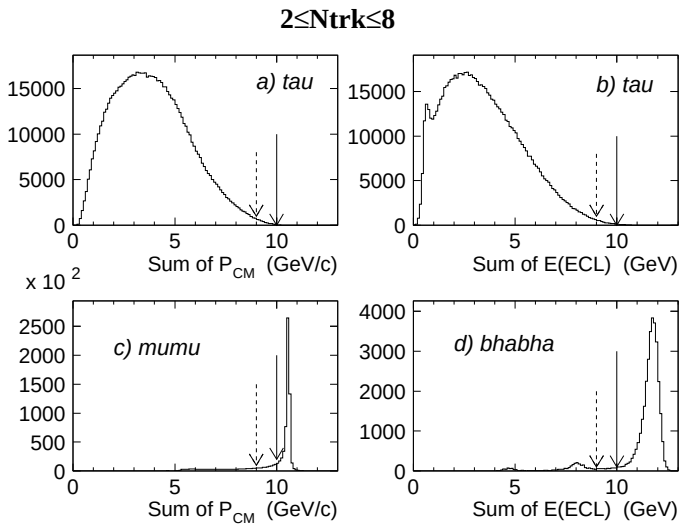

Figure 3.2: Sum of momentum in CM frame for a) τ event and c) $\mu\mu$ event, and sum of energy measured in ECL for b) τ events and d) Bhabha with the number of track condition. The arrows with solid(dashed) line show the condition for (two-tracks) events.

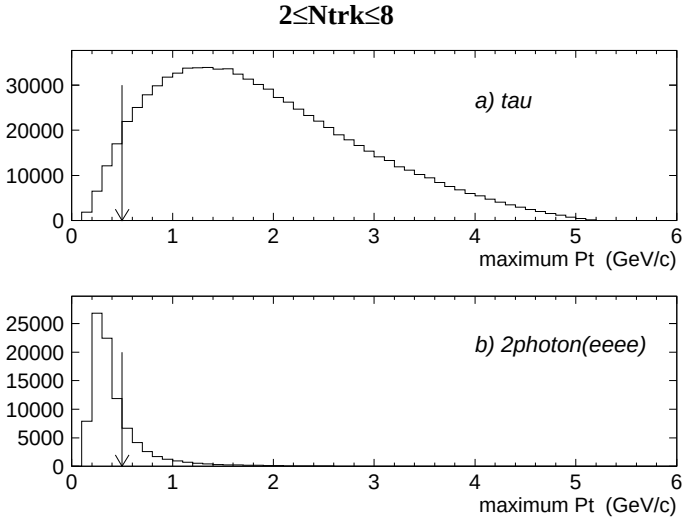

Figure 3.3: Maximum $\vec{p}_T$ among the charged tracks for a) τ events and b) 2-γ

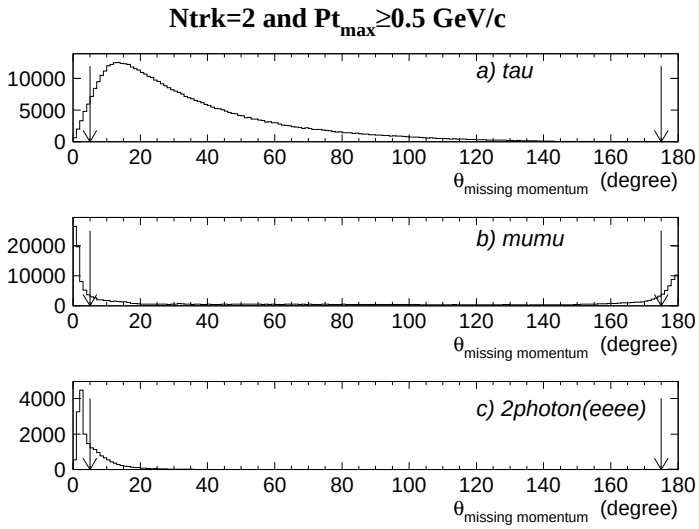

Figure 3.4: Polar angle of missing momentum θ_{miss} for a) τ events, b) $\mu\mu$ events and c) 2-γ events under the condition on $N_{track} = 2$ and $\vec{p}_T \geq 0.5$ GeV/c.

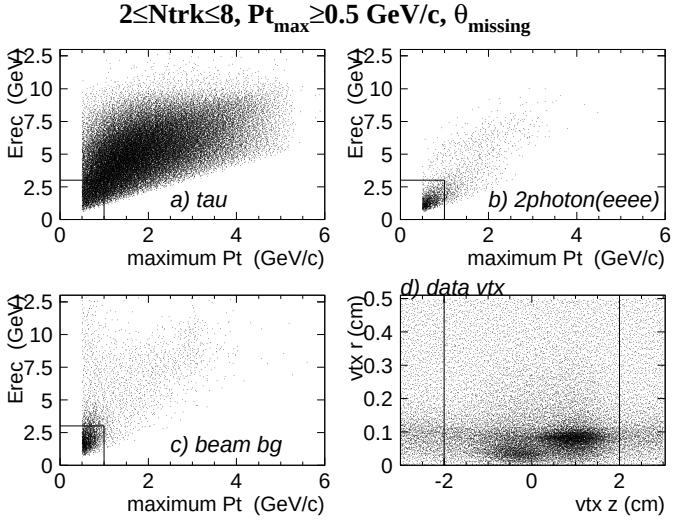

Figure 3.5: 2D plot of $E_{\rm rec}$ and maximum $\vec{p}_t$ for a) τ events, b) 2-γ event and c) beam background event. The beam background events are selected with the event vertex of $|z| > 2$ cm as plotted in d). Lines show the cut condition.

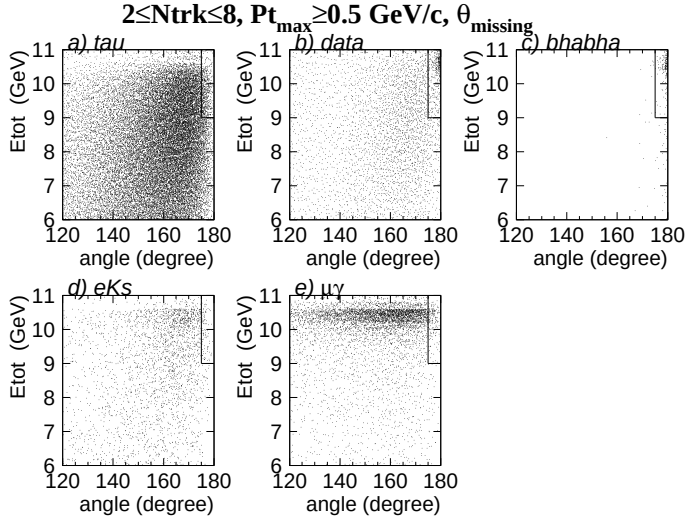

Figure 3.6: $E_{\rm tot}$ and θ_{Max} among the charged tracks for a) τ events, b) data c) Bhabha, d) $\tau \to eK^0_S\nu_\tau$ and e) $\tau \to \mu\gamma\nu_\tau$.

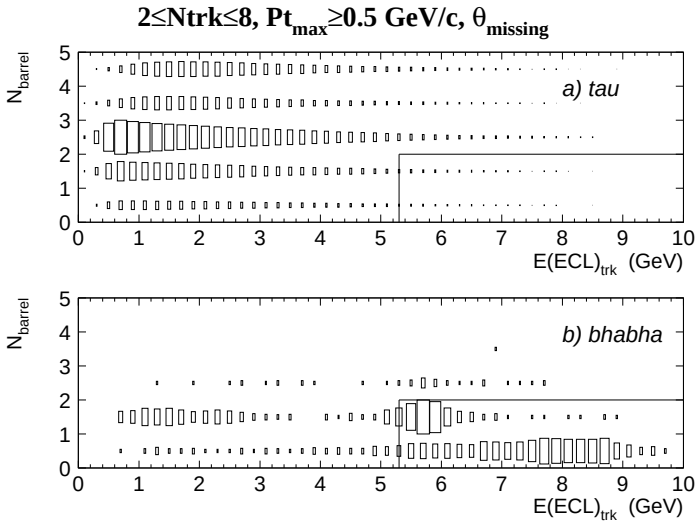

Figure 3.7: Plot of $N_{\rm barrel}$ and $E_{\rm ECL,tracks}$ for a) τ and b) Bhabha events

3.2 Selection of hadronic τ decays

As described in the previous section, the primary τ pair events are prepared for the further event selection. In order to obtain good τ samples, we apply additional conditions on pre-selected data set with respect to the type of event configuration. Our decay modes of interest are 6 channels of exclusive hadronic decays: $K^0_S\pi^-\nu_\tau$, $K^0_SK^-\nu_\tau$, $K^0_S\pi^-\pi^0\nu_\tau$, $K^0_SK^-\nu_\tau, K^0_SK^0_S\pi^-\nu_\tau$ and $K^0_SK^0_S\pi^-\pi^0\nu_\tau$. In order to study six decay modes, it is easy to start selecting the inclusive decay with K^0_S which also provides useful information and constrains the branching fractions for hadronic τ decay. In this study, we applied slightly different selection criteria accroding to the number of K^0_S in their events. For the event involving single K^0_S, we required single lepton track on the tag side. This method reduces several systematic uncertainties due to the tracking and particle identification which are the dominant source of uncertainty. On the other hand, the branching fraction for the event involving more than one K^0_S is expected to be an order of 10^{-4} or 10^{-5} and their signal efficiency is also smaller than other decay modes, so that not only the lepton tagging but also hadron tagging is necessary for the sufficient signal yields. For this reason, we separate the event selection according to the number of involing K^0_S in an event.

Inclusive K^0_S events

Before the event selection of hadronic τ decays, we define good tracks and gammas. The definition of a good track is consists of two parts. The conditions for the first good track are $P_T > 0.1$ GeV/c, |dr| $\leq$ 1cm and |dz| $\leq$ 3cm, where dr and dz are the impact parameter and P_T is the transverse momentum of charged track.

Since K^0_S has a long lifetime, its decay position is away from the IP over 1 cm in the transverse direction. The condition for tracks for K^0_S reconstruction

Symbol	Description and Conditions
$N_{\rm track}$	Number of tracks ≥ 2
$E_{\rm ECL}$	Total energy of ECL clust. < 9 GeV
$\vec{p}_{Missing}$	1 GeV $< \lvert\vec{p}_{miss}\rvert < 7$ GeV
	$30^\circ < \theta_{miss} < 150^\circ$
$\lvert\vec{p}_{\rm thrust}\rvert$	Magnitude of thrust vector > 0.9
$\lvert Q_{sum}\rvert$	Total charge $= 0$
Hemisphere	# of tracks on signal hemisphere ≥ 3
	# of tracks on tag hemisphere $= 1$
Lepton ID	e-ID > 0.9 , μ-ID > 0.9
$N_{K^0_S}$	Number of $K^0_S \geq 1$
N_{π^0}	Number of $\pi^0 \geq 0$
$E^{\rm extra}_\gamma$	Remaing photon energy < 0.2 GeV

Table 3.1: Selection criteria for $\tau^- \to X^- K^0_S(\geq 0\ {\rm n}\gamma)\nu$

have to be rather loosened comparing to the first good track condition. The second good track condition is $P_T > 0.1$ GeV/c with goodKs condition which described in later section. The difference of $|dr|$ distribution depending on the two good track conditions is shown in Fig.3.9. $|dr|$ of non-K^0_S tracks is distributed closely to the interaction point(IP,$|dr| = 0$). On the other hand, $|dr|$ of K^0_S tracks are distributed rather away from the IP. By checking duplication of the tracks which passed through the first or the second condition, we select good tracks.

For good gamma selection, we require different energy condition by its detecting location; $\rm E_{cluster} > 80$ MeV in the barrel region ($34^\circ \leq \theta \leq 128^\circ$) and $\rm E_{cluster} > 100$ MeV in the endcap region ($24^\circ \leq \theta \leq 30.5^\circ$ and $128^\circ \leq \theta \leq 138^\circ$).

After the selection of good tracks and good gammas, we select the event where the number of tracks are $N_{tracks} \geq 2$ (No limits on the number of gammas).

The sum of energies deposited in the ECL clusters is $E_{ECL} < 9$ GeV for

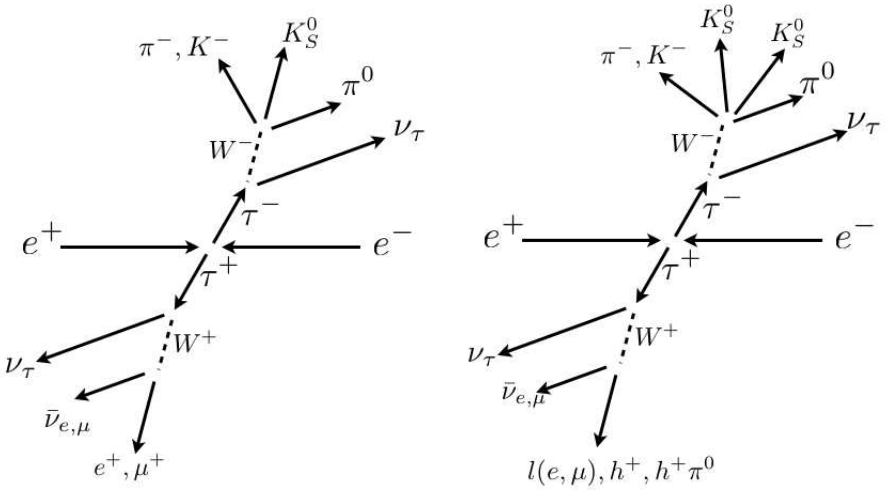

Figure 3.8: A schematic view of a $\tau^- \to K^0_S h^- \pi^0 \nu_\tau$ event (left) and $\tau^- \to K^0_S K^0_S h^- \pi^0 \nu_\tau$ event (right). Typically, a τ event can be subdivided into two hemispheres each containing at least a single track with respect to the thrust vector. The events involving one K^0_S are selected by requiring leptonic decays($\tau^- \to l^- \bar{\nu}_l \nu_\tau$) on tag side. On the other hand, the events involving two K^0_S are selected by requiring hadron decays($\tau^- \to h^-(\pi^0 \nu_\tau)$) as well as leptonic decays on tag side.

the further suppression of some surviving Bhabha events.

The missing mass, $p^2_{miss} = (p_{init} - \Sigma p_{track} - \Sigma p_\gamma)^2$, and its polar angle ($\theta_{miss}$) with respect to the beam direction in the c.m. frame is efficient for reducing two-photon and Bhabha backgrounds, where p is a four momentum, p_{init} is the initial four momentum of the e^+e^- collision in the c.m frame. In the missing mass calculation, all good tracks and gammas are considered. The missing mass condition is 1 GeV $< p_{miss} <$ 7 GeV and $30^\circ < \theta_{miss} < 150^\circ$. Figure 3.10 shows the 2-D distribution for data(top) and MC(bottom). The selection criteria clearly distinguish τ pair events from

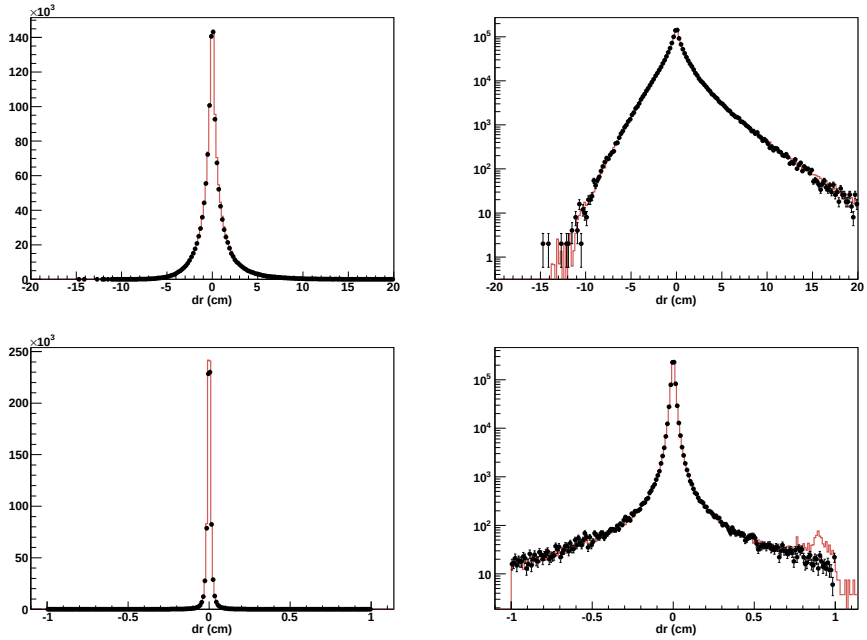

Figure 3.9: dr distribution of K^0_S daughter's tracks in the linear (Top left) and log (Top right) scale; non-K^0_S tracks in linear (Bottom left) and log (Bottom right) scale. The closed circles are data and the red line is MC samples. The cut $|dr| < 1$ cm is applied to non-K^0_S tracks. No $|dr|$ conditions are applied to K^0_S daughter tracks.

two-photon and Bhabha events.

The evaluation of the thrust vector is useful to determine the event shape and the hemisphere of the tracks and gammas. The definition of the thrust vector, $\vec{n}$ which maximizes $(\Sigma_i|\vec{n}\cdot\vec{p_i}|)/(\Sigma_i|\vec{p_i})|$ in the CM frame. The magnitude of the thrust is required to be greater than 0.9, see Fig. 3.11.

In general, most of τ pair events can be subdivided into two hemispheres using the thrust axis in the CM frame. For this mode we require one track for the tag side and any number of tracks for the signal side. This is the so

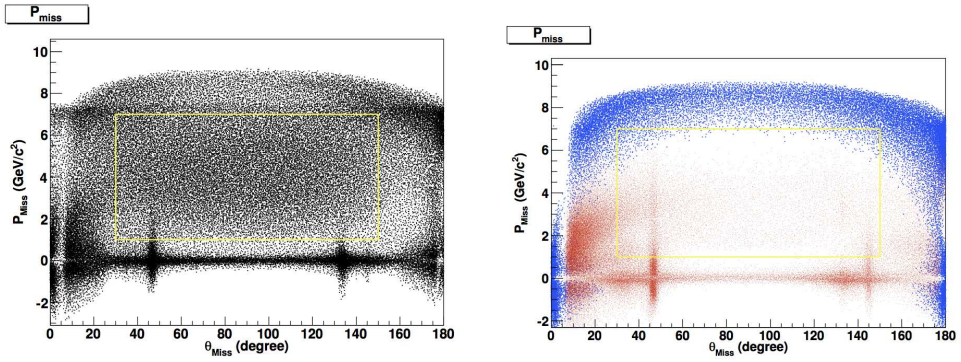

Figure 3.10: 2D distribution of missing momentum and angle. The left figure shows data. In the right figure, the Blue dot histogram shows two-photon events and the red dot histogram Bhabha events. The yellow box is the selection criteria.

called "1-n prong topology" interms of tracks exclusively. The number of good gammas is not taken into account for this topology. We check a sign of the charge of each hemisphere and constrain the charge sum of two hemisphere to be zero.

Since the lepton tagging method is to be applied in this selection, we apply an electron Id or muon Id condition to the track on tag side.

3.2.1 K^0_S selection

For K^0_S candidates, we referred to the table collected a set of vertexes reconstructed by using two tracks with assumption of pion track. Following items are considered to select good K^0_S candidates:

- $|dr| > 0.05$ (cm) : $|dr|$ is the smaller of dr1 and dr2, which are the smallest approach from the IP to the two tracks in the x-y plane;
- $d\phi < 0.3$ (rad) : $d\phi$ is the azimuthal angle between the momentum vector and the decay vertex vector of a Ks candidate;

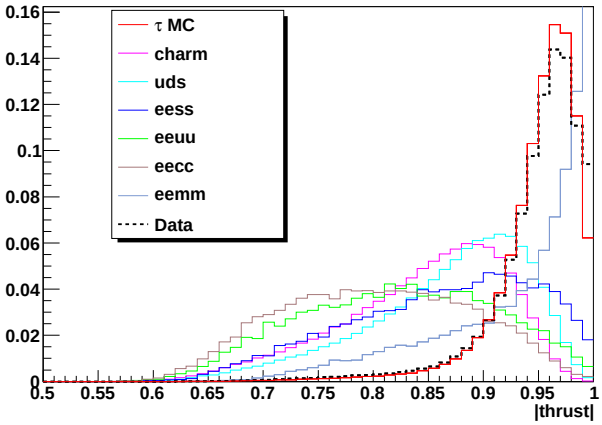

Figure 3.11: The magnitude of the thrust vector for different MC samples and data. Most of τ pair events are gathered over 0.9 in contrast to the continuum events (uds,$c\bar{c}$).

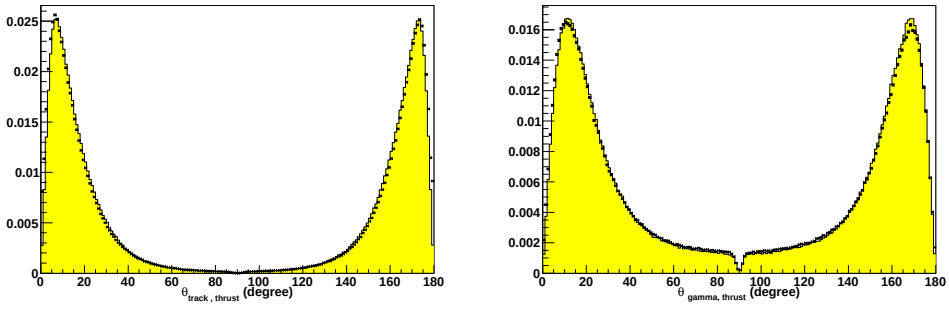

Figure 3.12: The angluar distribution of the momentum between good track(photon) and the thrust vector in the CM frame for τ pair events. The left and right figure are for track and photons, respectively.

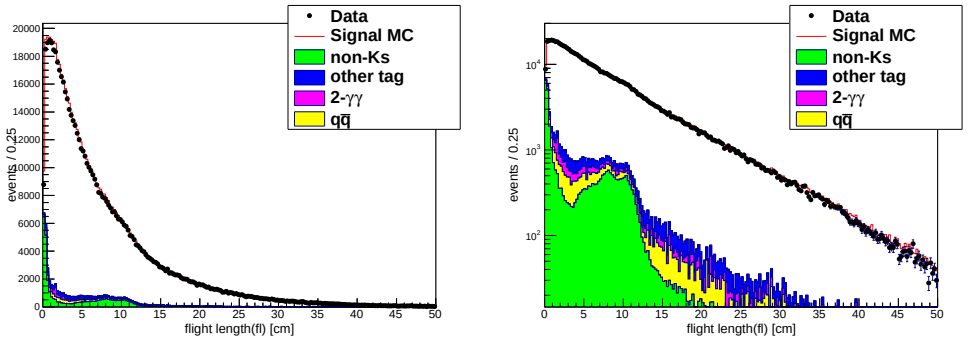

Figure 3.13: The flight length(fl) distribution for K^0_S candidates in the x-y direction.

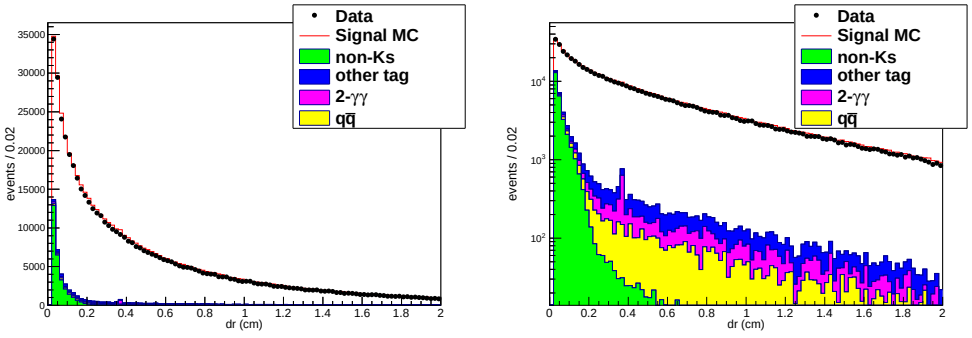

Figure 3.14: The dr distribution for K^0_S candidates. The small peak around 0.4 cm is due to the vertex of $\gamma + N \to e^+e^-$ at the SVD.

- $z_{dist} < 2.4$ (cm) : z_{dist} is the distance between the two daughter tracks at their interception point;
- $fl > 0.08$ (cm) : fl is the flight length of the Ks candidate in the x-y plane.

In order to reduce the background from other background from tau decays, i.e. $\tau \to 3\pi\nu_\tau$, the additional conditions are given as below:

- $2 < fl$ (cm) : See Fig **??**

- $dr > 0.1$ (cm) : See Fig. 3.14
- 0.485 GeV/c^2 $< \mathrm{M}_{\pi\pi} < 0.512$ GeV/c^2 : See Fig. **??**

The K^0_S candidates are contaminated mostly by the $\tau \to 3\pi$ (≥ 0 neutral)ν decay whose the branching fraction is known as $(15.18 \pm 0.08)\%$, which is more than 10 times larger than for K^0_S inclusive decay. In order to purify K^0_S candidates from the three-pion events, its decay length should be greater than 2 cm and $dr > 0.1$ (cm).

3.2.2 π^0 selection

π^0 is reconstructed by two good gammas defined in the previous section. In the reconstruction of π^0, we introduce the normalized $\gamma\gamma$, $S_{\gamma\gamma}$, defined as :

$$S_{\gamma\gamma} \equiv \frac{m_{\gamma\gamma} - m_{\pi^0}}{\sigma_{\gamma\gamma}}. \tag{3.1}$$

where $m_{\gamma\gamma}$ is the invariant mass of two gammas, m_{π^0} is given by the π^0 mass from PDG and $\sigma_{\gamma\gamma}$ is defined

$$\sigma_{\gamma\gamma} = \frac{\sigma_L + \sigma_R}{2}. \tag{3.2}$$

where σ_R and σ_L are the upper and lower side of the resolution, respectively. The resolution depend on the π^0 momentum region and location in the ECL cluster. The nominal resolution is 5$\sim$9 MeV for σ_R and 6$\sim$11 MeV for σ_L. At this stage, π^0 candidates are selected by the cut $-20 < S_{\gamma\gamma} < 20$. Like as K^0_S selection, these π^0 events are conteminated by non-π^0 events, we apply additional conditions later.

3.2.3 Particle Identification

The likelihood of Kaon or pion is calculated with the information from CDC, ACC and TOF. The likelihood ratio of a kaon defined as $\mathcal{L}(K)/(\mathcal{L}(K)+$

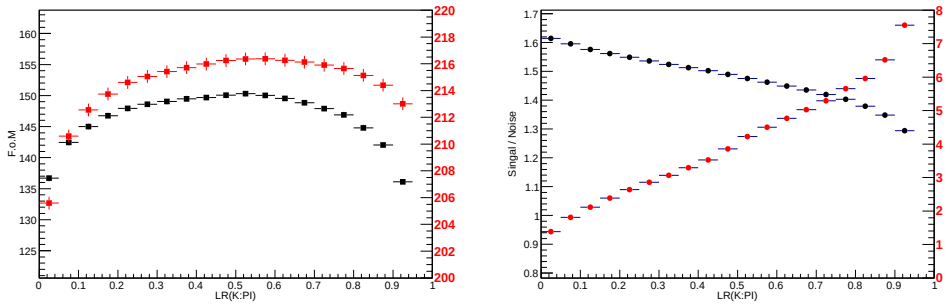

Figure 3.15: The figure of merit and the signal to background ratio for two different decay modes. The black dot is for $\pi K^0_S \pi^0$ and red dot is for $K K^0_S \pi^0$. The background is estimated by using tau generic MC. The selection condition for $\mathcal{L}(K|\pi)$ is determined to be 0.7 according to the signal to background ratio.

$\mathcal{L}(\pi)$) is a good variable to separate kaon and pion tracks. The likelihood ratio depends on the angle and momentum of the track and the PID efficiency changes with a likelihood ratio cut. In order to increase the selection efficiency, the figure of merit (F.O.M) and the signal to background ratio (S/B) are checked by varying the $\mathcal{L}(K)$. The two variables are defined as :

$$\text{F.O.M} = \frac{S}{\sqrt{S+B}} \quad and \quad \text{S/B} = \frac{S}{B} \tag{3.3}$$

where S is the number of reconstructed signal mode events and B is the number of background events. The backgrounds are estimated from generic MC. The contents of the background can be different for the dedicated decay modes. F.O.M for $\tau^- \to \pi^- K^0_S \pi^0 \nu$ and $\tau^- \to K^- K^0_S \pi^0 \nu$ shown in Fig.3.15 seems to be not so sensitive to the PID condition. However the signal to background ratio shows sensitive behavior for the PID condition. In this analysis, we set $\mathcal{L}(K|\pi) > 0.7$ for the kaon Id and $\mathcal{L}(K|\pi) < 0.7$ for the pion ID.

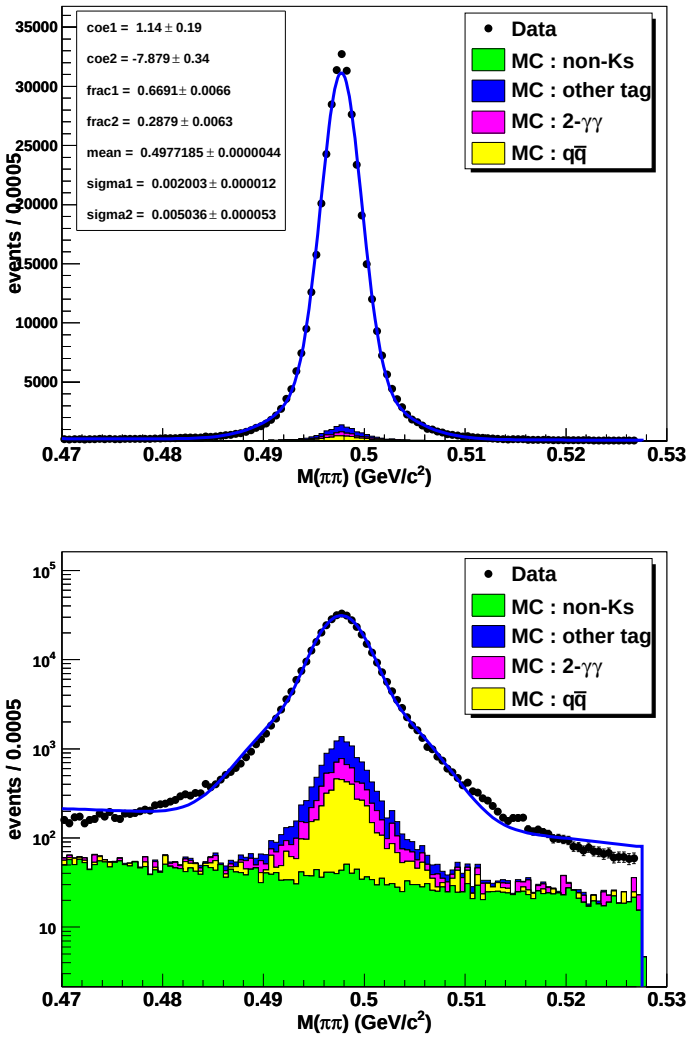

Figure 3.16: The invariant mass distribution of $\pi^+\pi^-$. The histogram was fitted by a double Gaussian with the same mean values and the first-order polynomial for background estimation. The right figure shows a log-scaled one. The color shaded histograms are the BG expectation. All MC histograms are stacked

3.2.4 $\tau^- \to K^0_S$ (particles)$^-\nu_\tau$ events

Before applying the PID condition, we select $\tau^- \to K^0_S$ (particles)$^-\nu_\tau$ events in order to check the consistency to the PDG result. For the event selection, we require one charged track, one K^0_S candidates and any number of good gammas in the signal hemisphere. At this stage π^0 is not reconstructed. The number of good gammas on the tag side is set to $N_{gamma} \leq 1$. Figure 3.16 shows the invariant mass distribution of $\pi^+\pi^-$. We decide that the mass region of $\pm 4\sigma$ ($0.485\ \mathrm{GeV}/c^2 < \mathrm{M}_{\pi\pi} < 0.512\ \mathrm{GeV}/c^2$) is the K^0_S signal and the other side are background. After all cut are applied, 387806 ± 631 signal candidates are selected.

3.2.5 $\tau^- \to \pi^-(K^-)K^0_S\nu_\tau$

These two decay mode can be selected from the $\tau^- \to K^0_S$ (particles)$^-\nu_\tau$ events. We applied PID condition $\mathcal{L}_\pi > 0.3$ for $\pi^- K^0_S$ events and $\mathcal{L}_K > 0.7$ for $K^- K^0_S$ event with π^0 veto condition. In order to suppress the decays with π^0, the highest photon energy is limited to 0.2 GeV for both side. The number of selected events is found to be 157836 ± 397 events for $\pi^- K^0_S$ and 32491 ± 180 events for $K^- K^0_S$.

3.2.6 $\tau^- \to \pi^-(K^-)K^0_S\pi^0\nu_\tau$

After the selection of $\tau^- \to K^0_S$ (particles)$^-\nu_\tau$ events, we required one charged pion(kaon), one K^0_S and one π^0 in the signal hemisphere. To select the π^0 signal, the normalized $\gamma\gamma$ invariant mass is required within $-6 < S_{\gamma\gamma} < 5$. In order to reduce the decay modes having multiple π^0 such as $\pi^- K^0_S \pi^0 \pi^0 \nu$, we require the maximum energy of the extra photon in the signal side to be less than 0.2 GeV. Fig. 3.17 shows the energy distribution of the extra photons normalized to the integrated luminosity. The data (closed circles) agree with the MC (histograms) expectation reasonably, which sup-

port the correct modeling of the extra photons in MC. After requiring these conditions, 35505 ± 188 (10666 ± 103) signal candidates are remained for $\pi^- K^0_S \pi^0 (K^- K^0_S \pi^0)$ event.

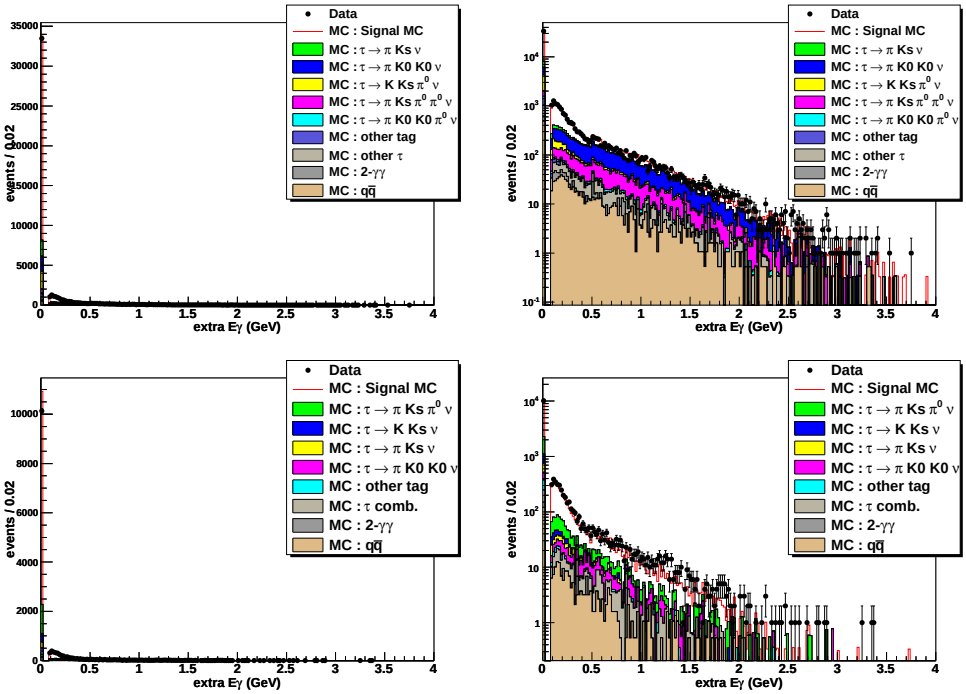

Figure 3.17: The extra highest γ energy distribution for $\tau^- \to \pi^- K^0_S \pi^0 \nu_\tau$ in the linear (Top left) and log (Top right) scale, and for $\tau^- \to K^- K^0_S \pi^0 \nu_\tau$ in the linear (Bottom left) and log (Bottom right) scale. These extra γs remain after π^0 reconstruction. The closed circles represent data and histograms are the MC expectation. Since $E_\gamma > 80$ MeV for the barrel and 100 MeV for the endcap, there is a gap between $E_\gamma = 0$ and $E_\gamma \sim 0.08$. The histograms are accumulated and normalized to the luminosity.

3.2.7 $\tau^- \to \pi^- K^0_S K^0_S(\pi^0)\nu_\tau$

Based on the event selection for $\tau^- K^0_S(\text{particles})^-\nu_\tau$, we required additional conditions for selecting the event having two K^0_S in an event. The number of track is restricted to 6. According to the hemisphere defined by thrust axis, we require 5 tracks on the signal side and 1 track on tag side. Since the branching fraction for these process is expected to be at most an order of 10^{-4}, we require not only leptonic decays but also hadronic decays with a neutral pion on the tag side.

For the reconstruction of two K^0_S, we used 4 tracks among 5 tracks in the signal side. Because of the large multiplicity of these decays with tight condition on K^0_S selection, non-K^0_S backgrounds are expected to be less than $1 \sim 2$ %. In order to increase the total yeild, there is no conditions for flight length, z_{dist} and dr, except for the M($\pi\pi$) mass window : 485 MeV/c^2 < M($\pi\pi$) < 512 MeV/c^2.(See in Fig. 3.18) Fig. 3.19 shows the flight length distribution between data and MC.

In this selection, a π^0 on tag side is reconstructed. The number of π^0 is 1 at most. However, there are many hadronic decays of single track with multiple π^0s. In order to suppress those events, it is necessary to apply the extra γ energy condition to be less than 0.2 GeV on tag-side. And we also require the extra γ energy on signal side, $E^{\text{extra}}_\gamma < 0.3$, in order to suppress possible multiple π^0 backgrounds. Figure 3.2.7 and 3.2.7 shows the distribution of extra γ energy on signal side. The distribution for data(dotted) and MC(shaded) are agreed with each other. Using the hadron and lepton tagging condition, we obtained 6684 ± 82 and 303 ± 17 events for $\pi^- K^0_S K^0_S$ and $\pi^- K^0_S K^0_S \pi^0$ events.

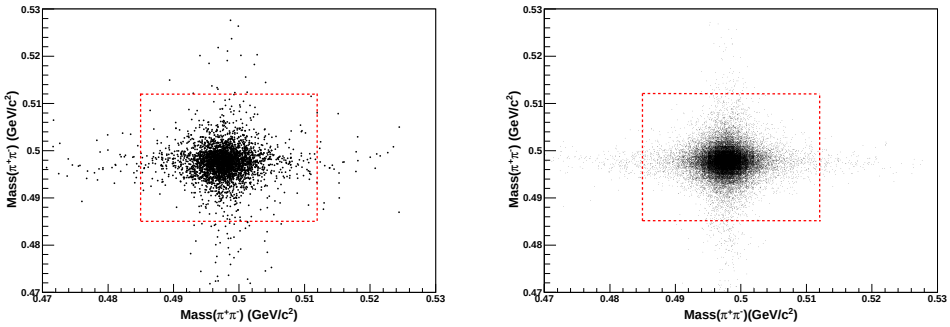

Figure 3.18: The 2-D M($\pi\pi$) distribution. The left-hand and right-hand plots are for data and MC, respectively

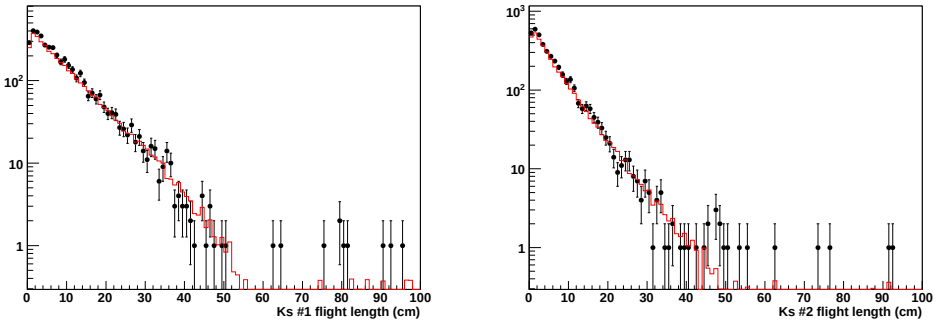

Figure 3.19: The flight length distribution for two K_S^0 in $\pi^- K_S^0 K_S^0$ event.

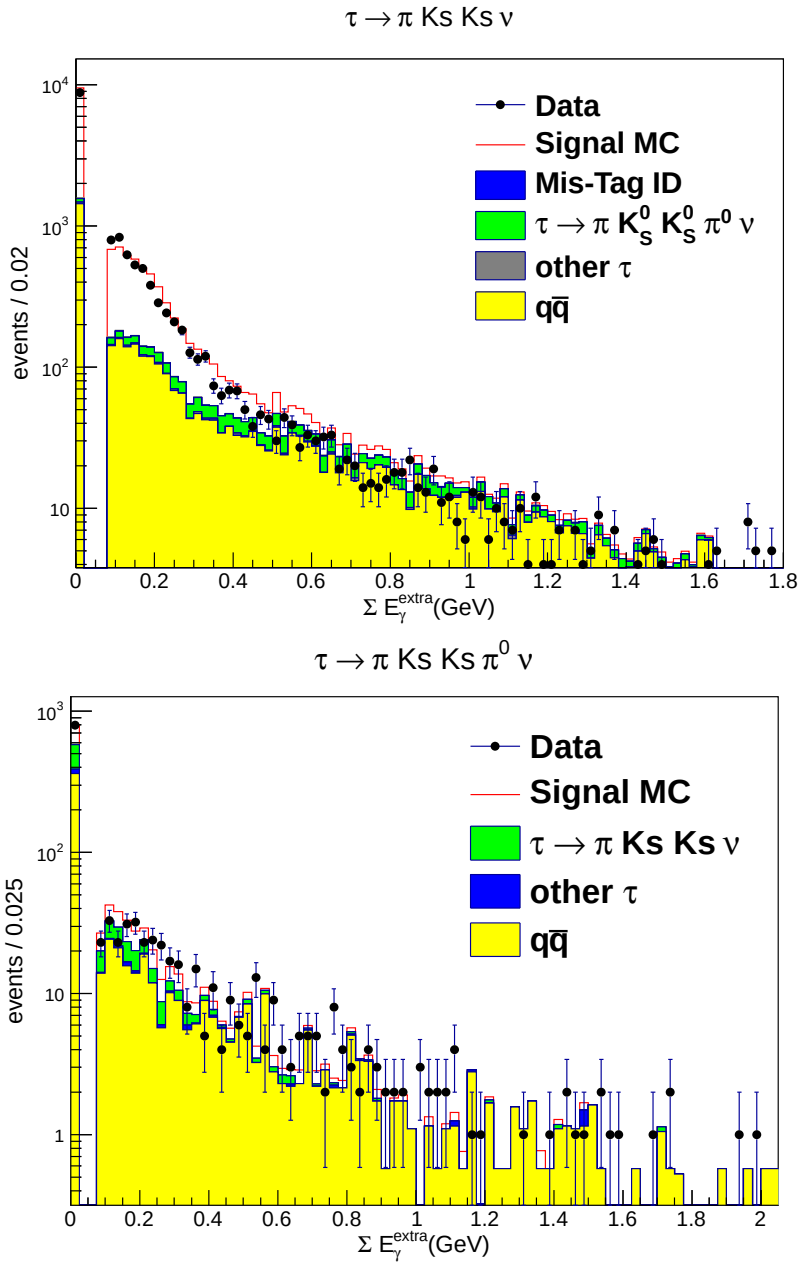

Figure 3.20: The energy distribution of high energy photon in $\pi^- K^0_S K^0_S$ (top) and $\pi^- K^0_S K^0_S \pi^0$ (bottom) event

3.3 Selection of e-μ events

In order to calculate the leptonic branching fraction, it is necessary to estimate the number of e-μ events, $\tau^+\tau^- \to e^+\nu_e\bar{\nu_\tau}\mu^-\bar{\nu_\mu}\nu_\tau$, and its efficiency precisely. For the selection of e-μ pairs events, the number of tracks should be two. As described in previous sections, the same conditions are applied to E_{ECL}, p_{miss}, θ_{miss}, $|thrust|$ and $|Q_{sum}|$. The tracks are subdivided into two hemispheres with respect to the thrust axis. For each track, we require a lepton id condition: EID > 0.9 , MuID > 0.9. The electron and muon tracks should lay in the opposite hemispheres. Finally, in order to reject some of $\tau^- \to h^-(\geq 0\pi^0)\nu$ events, the highest energy of extra γ should be less than 0.2 GeV for each hemisphere. We summarize the selection criteria for e-μ event in Table 3.2

Condition	Description
N_{track}	$N_{track} = 2$
E_{ECL}	Sum of Energy of ECL clusters < 9 GeV
$P_{Missing}$	1 GeV $< \|p_{miss}\| < 7$ GeV
	$30^\circ < \theta_{miss} < 150^\circ$
|Thrust|	|thrust| > 0.9
$\|Q_{sum}\|$	sum of charge $= 0$
Hemisphere	1 track on each side
Lepton ID	EID > 0.9 , MuID > 0.9
e-μ combination	e track | μ track
extra E_γ	Highest extra γ energy < 0.2 GeV

Table 3.2: The selection criteria for e-μ events

The total selected candidates are 7661052 ± 2767. Estimation of the number of e-μ events and the background events has been done using τ generic MC, two-photon, Bhabha, $ee \to \mu\mu$, and $ee \to q\bar{q}$ MC samples. The invariant mass of an e-μ pair is shown in Fig. 3.22.

The total background from e-μ events was estimated to be 4.19% of total candidates. Most of the backgrounds come from 1-prong decays with

Process	Yield	Ratio(%)
$\tau \to \pi\ (\pi^0)\nu$	183876 ± 429	2.40
other τ	14421 ± 120	0.19
2-γ	122782 ± 350	1.60
$q\bar{q}$	169 ± 13	0.002
Total	321248 ± 567	4.19

Table 3.3: The background contents of e-μ pairs

some number of neutral pions, e.g.,$\tau^- \to \pi^-\nu$ and $\tau^- \to \pi^-\pi^0\nu$ decay, which takes 2.4% of total candidates. The non-τ background come from two-photon process $ee \to ee\mu\mu$ which contributes by 1.6% of total candidates. The backgrounds contribute to the e-μ selection are listed in Table **??**. The estimated signal yield is 7339595 ± 2825.

The number of events selected in MC and data are summarized in Table 3.4. The number of selected events is found to be 23653089 ± 4863 after taking the PID correction into account. The PID corrections for electron and muon tracks are 0.9821 ± 0.0201 and 0.9555 ± 0.024, respectively. The efficiency for selection of e-μ pairs is $19.31 \pm 0.03\%$.

For a cross-check, we calculate the product of the branching fractions, i.e., $\mathcal{B}(\tau \to e\bar{\nu}\nu) \times \mathcal{B}(\tau \to \mu\bar{\nu}\nu)$ from Eq. 5.1 using the luminosity,

$$\begin{aligned}\mathcal{B}(\tau \to e\bar{\nu}_e\nu_\tau|\tau \to \mu\bar{\nu}_\mu\nu_\tau) &= \frac{N_{sig}(e\text{-}\mu)}{2 \cdot \epsilon_{e\text{-}\mu} \cdot N_{\tau\bar{\tau}}} = \frac{7339595 \pm 2825}{2 \times 0.1931 \times 616 \times 10^6} \\ &= (3.0876 \pm 0.0012)\% \end{aligned} \tag{3.4}$$

Where $N_{sig}(e\text{-}\mu)$ is the number of e-μ signal events and $\epsilon_{e\text{-}\mu}$ is its efficiency. It should be noticed that $N_{\tau\tau}$ is deduced from our luminosity measurement.

On the other hand, $\mathcal{B}(\tau \to e\bar{\nu}_e\nu_\tau|\tau \to \mu\bar{\nu}_\mu\nu_\tau)$ can be obtained from the PDG averages:

$$\begin{aligned}\mathcal{B}(\tau \to\ e\bar{\nu}_e\nu_\tau|\tau \to \mu\bar{\nu}_\mu\nu_\tau) &= \mathcal{B}(\tau \to e\bar{\nu}_e\nu) \times \mathcal{B}(\tau \to \mu\bar{\nu}_\mu\nu) \\ &= (17.85 \pm 0.05)\% \times (17.36 \pm 0.05)\% \\ &= (3.098 \pm 0.012)\% \end{aligned} \tag{3.5}$$

This shows good consistency between our result and PDG average within a 0.33% difference. $\mathcal{B}(\tau \to e\bar{\nu}_e\nu_\tau|\tau \to \mu\bar{\nu}_\mu\nu_\tau)$ is obtained by normalization to the luminosity, so that Eq. **??** and Eq. **??** will produce a similar result. Notice that $\mathcal{B}(e\bar{\nu}\nu|\mu\bar{\nu}\nu)$ of TAUOLA sample used in this analysis was set to 3.335%. Especially, $\mathcal{B}(\tau \to e\bar{\nu}\nu) = 19.2\%$, which is rather different from the current PDG average, 17.85%. In this analysis, the MC event $\tau \to e\bar{\nu}\nu$ is weighted by 0.929, so that the branching fraction is effectively the same as the PDG average.

Exp	$\epsilon_{e-\mu}$ (%)	N_{data}	N_{BG}	N_{sig}	$\mathcal{B}$(%)
svd1	19.74 ± 0.07	1795456	74824	1720632	3.0775 ± 0.0024
svd2	19.17 ± 0.04	5865596	246633	5618963	3.0919 ± 0.0014
All	19.31 ± 0.03	7661052	321457	7339595	3.0870 ± 0.0012

Table 3.4: The relavant numbers for the branching fraction for e-μ events.

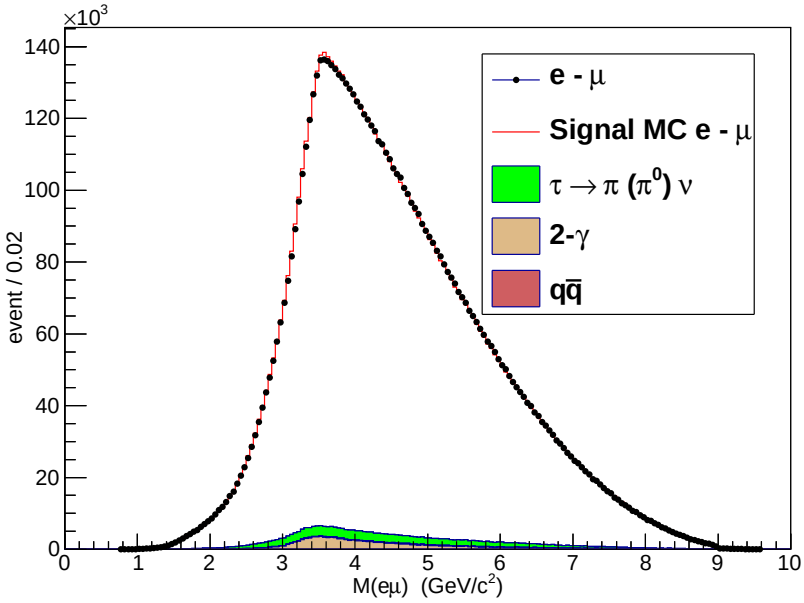

Figure 3.21: The e-μ invarinant mass distribution. The green shaded histogram is τ combinatorial background mostly from $\tau^- \to \pi^-\nu_\tau$ and $\tau^- \to \rho^-\nu_\tau$ decays. All histograms are stacked and normalized to the luminosity.

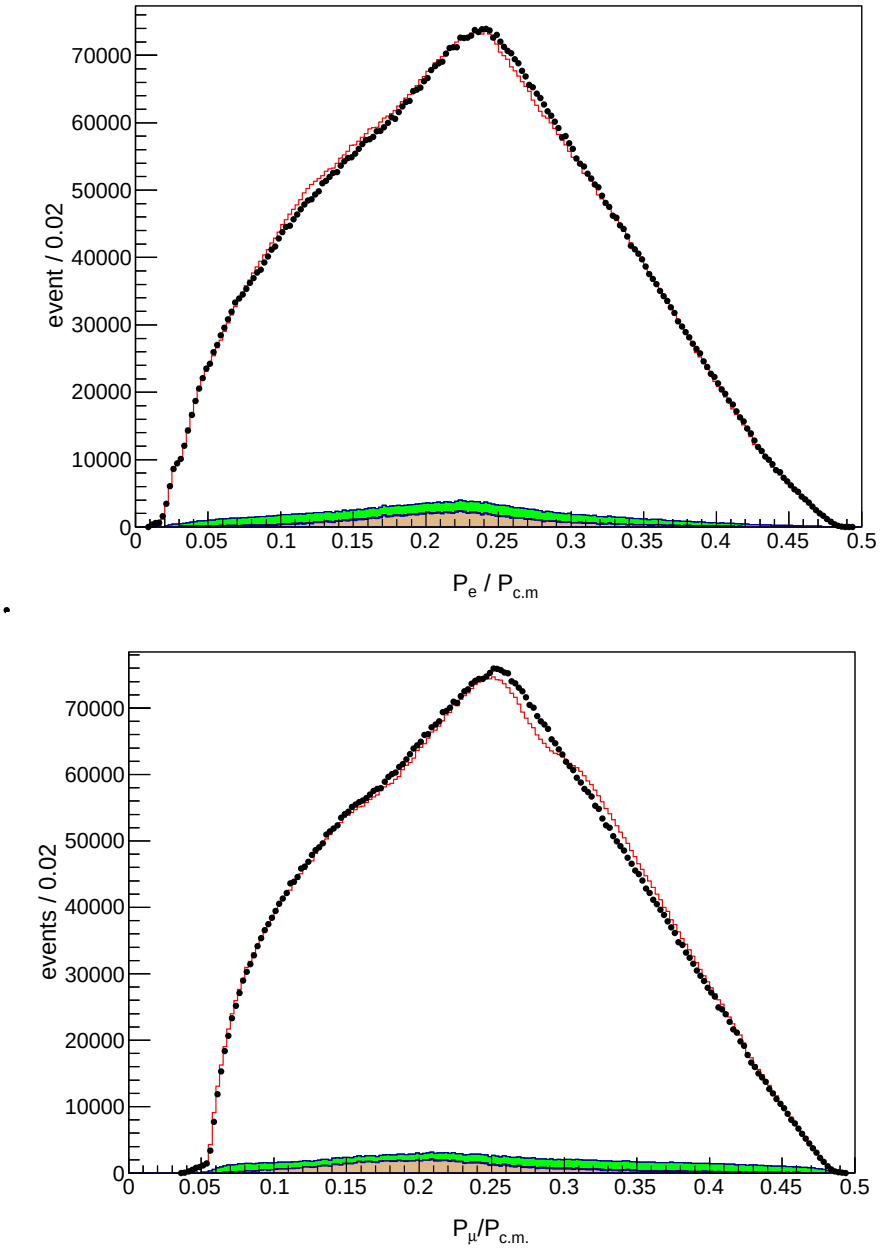

Figure 3.22: The $|\vec{P}|/E_{beam}$ distribution for e(top) and μ(bottom)

Chapter 4

Data analysis

In this chapter, we discuss about the efficiency and background estimation for the branching fraction measurements. The efficiency estimation for each decay modes are studied by using the MC sample.

4.1 Efficiency

We estimate the efficiency for the signal process with MC samples generated by the TAUOLA based KKMC generator. Generally, the signal efficiency ϵ_{signal} can be expressed by :

$$\epsilon_{\text{signal}} = \eta_{\text{det}}\ \eta_{\text{cut}}\ \eta_{\text{trk}}\ \eta_{\text{PID}}\ \eta_{K^0_S}\ \eta_{\pi^0} \tag{4.1}$$

where η_i is the efficiency for each condition i. We start this section with investigating the cut efficiency. We studied the track and PID systematic uncertainty and its correction factors. There may be possible uncertainty exists in the decay models of TAUOLA event generator, so that it should be estimated its effects. Selection efficiency for K^0_S and π^0 reconstruction and its corrections are mentioned at the last section.

4.1.1 The event selection efficiency

The several cuts are given to the event selection. The cut efficiency has been checked by the order of the list in Table 3.1 and K^0_S, π^0 loose selection. (See section 3.2.1,3.2.2) The efficiency for each step are summarized in Table 4.1.

	Efficiency (N_{Passed}/N_{init}) %				
condition	$\pi^- K^0_S$	$K^- K^0_S$	$\pi^- K^0_S \pi^0$	$K^- K^0_S \pi^0$	$q\bar{q}$
Trigger	82.6	83.6	87.9	87.6	100
τ-skim	63.8	68.7	69.1	71.7	66.8
N_{tracks}	63.0	67.8	67.8	70.2	25.9
N_{gamma}	62.3	67.0	62.3	65.0	7.96
E(ecl)	61.9	66.6	61.5	64.3	7.84
P_{miss}	47.7	54.2	51.2	54.7	4.40
$\lvert thrust \rvert$	44.1	50.6	46.8	51.4	1.14
$\lvert Q_{sum} \rvert$	33.4	38.4	31.9	35.5	0.03
hemisphere	19.9	22.3	20.6	22.1	0.02
Lepton ID	16.6	18.3	17.0	17.9	$< 1e^{-4}$
K^0_S selelection	16.4	18.1	16.8	17.7	
π^0 veto	14.8	13.5	-	-	
π^0 selelection	-	-	9.0	7.3	

Table 4.1: The cut efficiency for $\tau^- \to K^0_S(\text{particles})^- \nu_\tau$ events and $q\bar{q}$ background using signal MC. The cut condition for K^0_S , π^0 are loosen for the use of further analysis.

Following are several questions and answers about Table 4.1.

- Why does the efficiency drop so much after the requirement of the hemisphere ?
  It should be noticed that the condition $2 \leq N_{track}$ is applied at the early stage of selection so that many events can survive before the hemisphere

condition is applied. By the way, the hemisphere condition requires the 1-n topology in terms of the number of tracks. The hemisphere condition constrains not only on the location of tracks, but also on their numbers on each side, so that a large efficiency drop can be seen. (affecting about 80% of the tracking efficiency for a track)

- Why is there a small change of the efficiency for lepton ID?
  The lepton ID efficiency performance is almost 90% for a track. Considering the branching fraction for 1-prong decays(80%) and the total leptonic branching fraction (35%) in tau decays, the event loss of about 20% after the lepton ID condition is reasonable as expected.

- Does the hemisphere condition include the lepton ID in the tag-side?
  No. Instead, we require the lepton ID condition for the tag side right after the hemisphere condition.

- Why is the K^0_S selection efficiency so high ?
  Because we require *the second good track condition* at the early stage of event selection.(see **??**)

- Why are the final efficiencies of two modes so different from that of this table ? E.g., in the $\pi K^0_S \pi^0$ mode, 9.0%(this) $\rightarrow$ 2.83%(final) ?
  It should be noticed that we applied loose conditions for K^0_S and π^0 selection in this Table. In addition, we require the extra high energy photon condition for each hemisphere. Then, we applied π^0 SB subtraction for the final selection. For the simple estimation, assuming that the K^0_S, π^0 and SB subtraction efficiencies are 50%, 80% and 80%, respectively, we can deduce the final efficiency for each decay mode approximately.

4.1.2 Corrections for the particle ID

The particle identification(PID) technique is powerful for the identification of flavors of the charged tracks. However, there is always a discrepancy between data and MC simulation, which results in use of any conditions so that the difference due to PID condition should be corrected somehow. The difference has been studied using the decay chain $D^{*+} \to D^0\pi_s^+ \to K^-\pi^+\pi_s^+$ decays. By comparing the efficiency estimated by using data and MC samples, the correction table for each flavor are provided as a function of the momentum and angle in the lab frame. For the selection of exclusive decays, we need only to identify single tracks for each hemisphere. In the middle of the efficiency estimation using MC samples, the track on which PID is applied has to be multiplied by a correction factor in order to get the true efficiency as possible. Usually the difference is small, less than 4%, however, it becomes significant for precise measurements. It is also very important to obtain the true invariant mass spectra. We applied the corrections to the signal MC samples in event-by-event. The corrections used in this analysis are listed in Table 4.2. The efficiency tables provide for two experiment periods, svd1 and svd2.

Data Set	Track	$\pi^- K_S^0$	$\pi^- K_S^0\pi^0$	$K^- K_S^0$	$K^- K_S^0\pi^0$
svd1	e	0.9806 ± 0.0227	0.9805 ± 0.0222	0.9800 ± 0.0232	0.9795 ± 0.0225
	μ	0.9704 ± 0.0249	0.9710 ± 0.0247	0.9681 ± 0.0250	0.9693 ± 0.0248
	π	0.9709 ± 0.0045	0.9719 ± 0.0045	1.0007 ± 0.0086	1.0058 ± 0.0081
svd2	e	0.9811 ± 0.0213	0.9808 ± 0.0208	0.9807 ± 0.0213	0.9814 ± 0.0209
	μ	0.9494 ± 0.0263	0.9500 ± 0.0257	0.9495 ± 0.0266	0.9504 ± 0.0261
	π	0.9712 ± 0.0045	0.9683 ± 0.0044	0.9905 ± 0.0072	0.9981 ± 0.0071

Table 4.2: PID efficiency corrections to the sinal MC smaples of $\pi^- K_S^0$ and $\pi^- K_S^0\pi^0$ according to the data set. The typical error for the correction is $\sim$ 2% for lepton and 0.4$\sim$0.8% for pions.

4.1.3 Correction for K^0_S efficiency

The discrepancy between data and MC for K^0_S reconstruction is corrected by the scale factors obtained from the study of $D^* \to D^0\pi$ and $D^0 \to K^0_S\pi\pi$ decay chain. Using these pure K^0_S data samples, the number of K^0_S is estimated for both data and MC. The correction factor R for the data is

$$R = \frac{S_{data}}{S_{MC}} = (97.89 \pm 0.41)\%. \tag{4.2}$$

and applied to the signal efficiency.

4.1.4 Correction to π^0 efficiency

The difference between data and MC has been estimated from the study of $\tau^- \to \pi^-\pi^0\nu_\tau$ samples. Since the branching fraction for $\tau^- \to \pi^-\pi^0\nu_\tau$ has been measrued for the decades and its central value and uncertainties confirmed by several experiments. The ratio of two branching fractions, one for the event where τ decays into $\pi\pi^0\nu_\tau$ on the one side and the other for the event when τ decays into $\pi\pi^0\nu_\tau$ on both side, can estimate the discrepancy between data and MC. The correction factor R for the π^0 efficiency is

$$R = \frac{\mathcal{B}_{single\ \pi\pi^0}}{\mathcal{B}_{double\ \pi\pi^0}} = (95.7 \pm 2.2)\% \tag{4.3}$$

More details can be found in the Appendix A.

4.1.5 Efficiency dependence on hadronic current

As described in Sec. 1.2, semileptonic τ decays carry the vector or axial-vector current. The decay modes of interest consist of at least two meson in final state and the vector or axial-vector current are expected. However, the properties of hadronic currents involved in semileptonic τ decays are not known well so far. The latest version of TAUOLA event generator adopted rather latest knowlege for the hadronic currents as described in Sec. 2.2.11.

The MC precision does not satisfy to the precision expected by our measurements. So the our estimation of efficiency sufferred by the uncertainty due to the not-well-known-hadronic currents. The uncertainty can be estimated by weighted-bin methods described as follow:

- Generate events using different hadronic decay models and obtain the initial invariant mass distribution(g) for each model. (In this analysis, we adopt TAUOLA and Phase space decay)
- Obtain the mass distribution for accepted events as a function of invariant mass(a^{MC}).
- Extract true(data) invariant mass distribution(h^{data}) by subtracting background distribution.
- Calculate the weight factors bin by bin

$$w_i = \frac{h_i^{data}}{a_i^{MC}} \tag{4.4}$$

  where i is the ith bin of the distribution.

- Apply the weight factors to the generated and accepted distributions.

$$gw_i = g_i w_i, \quad aw_i = a_i w_i \tag{4.5}$$

- Using the weighted mean, calculate the efficiency and check their difference.

We generate about three million of $\pi^- K_S^0 \pi^0$ events and about two million of $K^- K_S^0 \pi^0$ events using TAUOLA and Phase Space model. In order to determine the signal efficiency and to study for the different hadron system, we first correct the MC mass distributions by the weighting method so that they agree with the data. Then the signal efficiency is obtained using TAUOLA and phase space MC events. In this way, we can check the effect of the different angular distribution of the hadronic system on the efficiency.

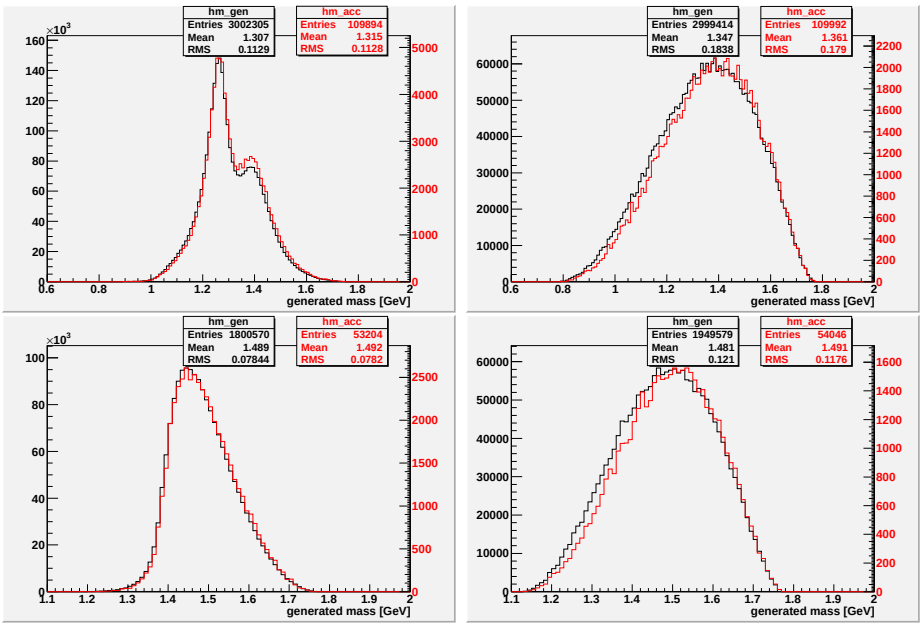

Figure 4.1: The invariant mass distribution of $\tau^- \to \pi^- K^0_S \pi^0 \nu_\tau$ (top) and $\tau^- \to K^- K^0_S \pi^0\ \nu_\tau$ (bottom) at the generator level. The right figure shows the model decay implemented in TAUOLA and the left figure shows the phase-space decay. The black histogram represents initially generated events and red histogram is for accepted events in all figures. The scale of the y axis is given in both sides for each color.

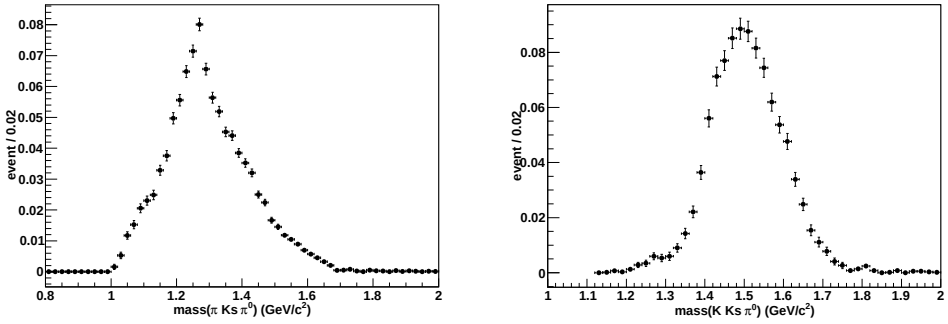

Figure 4.2: The signal distribution of $\tau^- \to \pi^- K^0_S \pi^0 \nu_\tau$ (left-hand) and $\tau^- \to K^- K^0_S \pi^0 \nu_\tau$ (right-hand).

The result is in Table 4.3 and 4.4 for $\tau \to \pi\ Ks\ \pi^0\ \nu$. These results show that the systematic uncertainty due to the MC decay model is:

- $\tau \to \pi\ Ks\ \pi^0\ \nu : (3.48 - 3.47)/3.48 = (0.28 \pm 0.28)\%$
- $\tau \to K\ Ks\ \pi^0\ \nu : (2.92 - 2.82)/2.92 = (3.42 \pm 0.34)\%$

Hence, this result shows the efficiency dependence on the hadron resonance model is just a few percent.

	TAUOLA		Phase space	
	unweighted	weighted	unweighted	weighted
generated	3002305	3000843	2999414	2997954
accepted	1056796 ± 325	104429 ± 323	105728 ± 324	104029 ± 322
efficiency	3.51 ± 0.01 (%)	3.48 ± 0.01 (%)	3.51 ± 0.01 (%)	3.47 ± 0.01 (%)

Table 4.3: Efficiency check for TAUOLA and phase space decay in $\tau^- \to \pi^- K^0_S \pi^0 \nu_\tau$

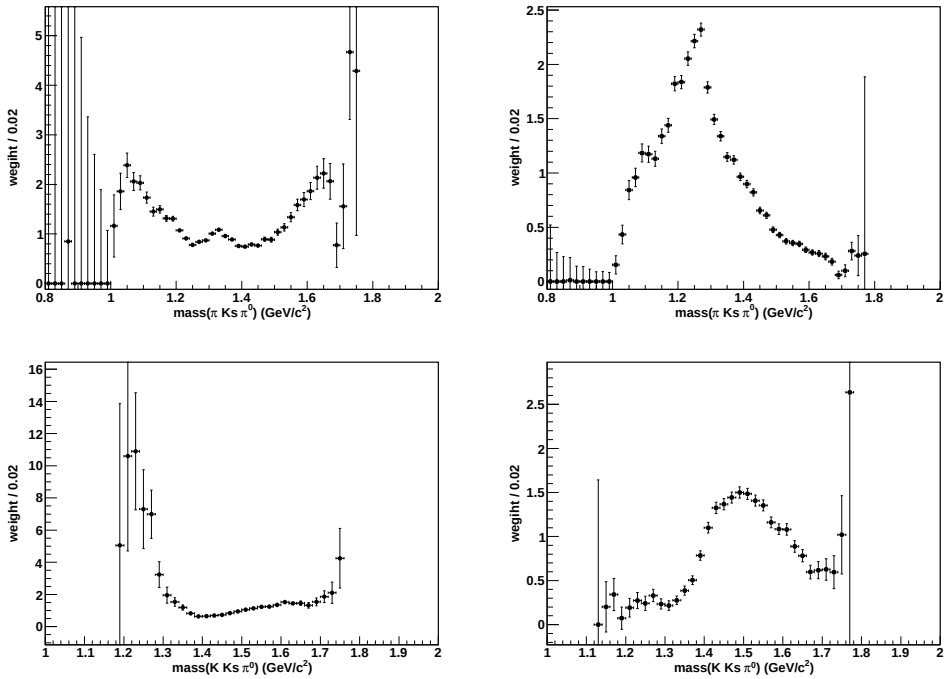

Figure 4.3: The weight factor distributions of $\tau^- \to \pi^- K^0_S \pi^0 \nu_\tau$ (top) and $\tau^- \to K^- K^0_S \pi^0 \nu_\tau$ (bottom) which are obtained by from Eq.4.4. The left figure is for TAUOLA and the right figure is for Phase-space decay. These distributions will be given for the generated / accepted distribution in Fig. 4.1 as a weight factor, individually.

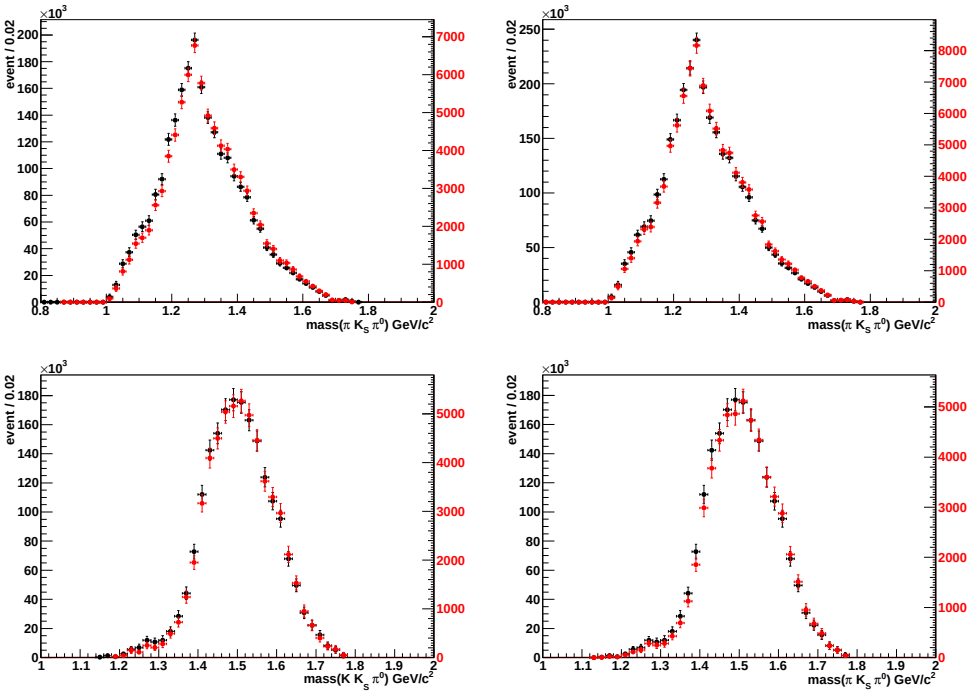

Figure 4.4: The weighted distributions of $\tau^- \to \pi^- K^0_S \pi^0 \nu_\tau$ (top) and $\tau^- \to K^- K^0_S \pi^0 \nu_\tau$ (bottom) which are obtained by using weighting from Fig. 4.3 for Fig. 4.1. The left figure is for TAUOLA and the right one is for Phase-space decay.

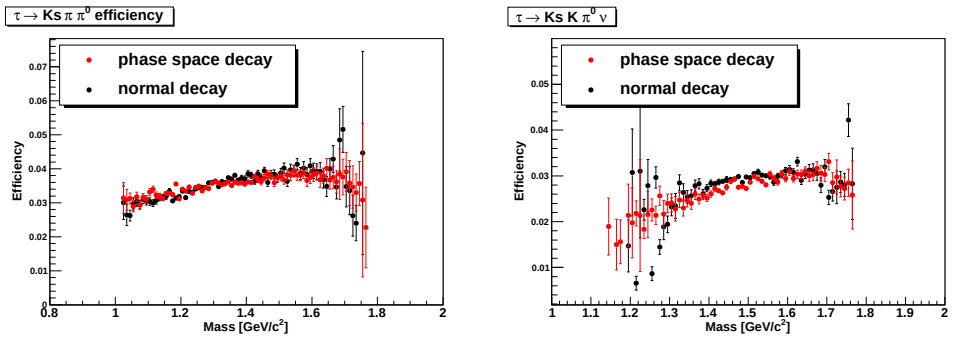

Figure 4.5: Efficiency check for different decay models. The left plot is for $\pi^- K_S^0 \pi^0$ and the right plot is for $K^- K_S^0 \pi^0$. Here normal decay means TAUOLA model.

	TAUOLA		Phase space	
	unweighted	weighted	unweighted	weighted
generated	1800570	1767429	1949579	1915967
accepted	52655 ± 229	51708 ± 227	53675 ± 232	54098 ± 232
efficiency	2.92 ± 0.01 (%)	2.93 ± 0.015 (%)	2.75 ± 0.01 (%)	2.82 ± 0.015 (%)

Table 4.4: Efficiency check for TAUOLA and phase space decay in $\tau^- \to K^- K_S^0 \pi^0 \nu_\tau$

4.1.6 Efficiency of $S_{\gamma\gamma}$ sideband subtraction

Non-π^0 background in the signal candidate can be estimated by counting the number of event in the sideband of $S_{\gamma\gamma}$ distribution with proper scale(See Sec. 4.2.1). However, the number of events in the sideband also include the true signal events, the subtraction using the sideband event cause the signal efficiency drop. Using Eq. 4.7, the relative efficiency only for the sideband subtraction is found to be 82.5%.

4.2 Background estimation

The backgrounds for the inclusive K^0_S decays consist of :

1) non-π^0 background,

2) other τ decays,

3) background in tag-side,

4) continuum ($e^+e^- \to q\bar{q}$)and

5) two-photon processes ($e^+e^- \to e^+e^- f\bar{f}$).

1), 2) and 3) are the background from τ decays and the others are from non-τ decays. The estimation of the τ background uses τ generic MC samples corresponding to 1870 fb^{-1}, about three times larger than the size of accumulated luminosity. τ MC samples are generated from TAUOLA with the user-defined branching ratio table which is different from the current known value. In order to correct the size of the backgrounds, we prepared the scale factors using PDG and TAUOLA values. Table 4.5 shows the recent branching fractions(1st col.)and TAUOLA setting(2nd col.). The scale factors and its errors are given in an order.

The backgrounds in our decay modes of interest are dominated by other τ decays due to the mis-identification of flavors in the particle identification. The decays involving charged kaon have large background from the decay involving pions because of the mis-identification of pion to kaon, which is called as π fake. Using the control samples $D^{*+} \to D^0\pi^+ \to K^+\pi^-\pi^+$, π fake rate is estimated.

Some decay modes involving π^0 in the final states have backgrounds from non-π^0 τ decays: e.g, the selected events for $\tau^- \to \pi^- K^0_S \pi^0 \nu_\tau$ decay have a large background events from $\pi^- K^0_S$ and $K^- K^0_S$. These contribution can be reduced by studying a sideband of $S_{\gamma\gamma}$ distribution.

Process	$\mathcal{B}$ (%)		$\triangle\mathcal{B}/\mathcal{B}_{\rm PDG}$	Scale factor	
	PDG'11	TAUOLA	(%)	$f_{\rm scale}$	$\triangle f_{\rm cor}$
$\pi^- K^0_S \pi^0$	0.195 ± 0.02	0.1864	10.3	1.046	0.108
$K^- K^0_S \pi^0$	0.0785 ± 0.01	0.0754	12.7	1.041	0.132
$\pi^- K^0_S$	0.42 ± 0.02	0.4182	4.8	1.004	0.048
$K^- K^0_S$	0.079 ± 0.08	0.075	10.1	1.051	0.106
$\pi^- K^0_S \pi^0 \pi^0$	0.013± 0.012	0.0127	92.3	1.0236	0.944
$\pi^- K^0 \bar{K}^0$	0.17 ± 0.04	0.1569	23.5	(Not applied)	
$\pi^- K^0 \bar{K}^0 \pi^0$	0.031± 0.023	0.0315	74.1	(Not applied)	
	Belle	TAUOLA	(%)	$f_{\rm cor}$	$\triangle f_{\rm cor}$
$\pi^- K^0 \bar{K}^0$	0.0241±0.0023	0.1569	8.6	0.614	0.053
$\pi^- K^0 \bar{K}^0 \pi^0$	0.0021±0.0003	0.0315	11.9	0.261	0.031

Table 4.5: The table of branching fractions used in the background MC study. The second and thrid column show branching fractions given in PDG'11 and TAUOLA event generator, respectively. The scale factor for the background estimation and its error is in fifth and sixth column.

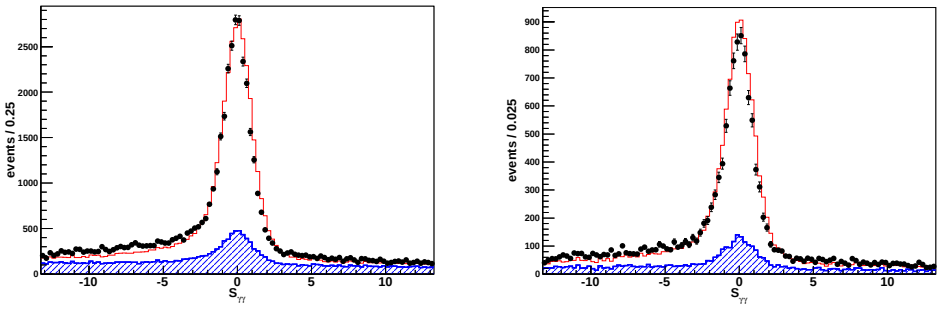

Figure 4.6: $S_{\gamma\gamma}$ distribution of $\tau^- \to \pi^- K^0_S \pi^0 \nu_\tau$ (Left) and $\tau^- \to K^- K^0_S \pi^0 \nu_\tau$(Right). The blue dashed histogram is the expected background and red line histogram is the signal MC expectation.

In the previous studies for $\pi^- K^0 \bar{K}^0$ and $\pi^- K^0 \bar{K}^0 \pi^0$, their branching fractions were badly measured with few events [17]. In this case, we determined the branching fractions which applied to the MC simulation for estimating the background ratios.

For the estimation of non-τ decay backgrounds, we used continuum($q\bar{q}$), two-photon, $B\bar{B}$ and Bhabha MC samples. Usually Bhabha, $B\bar{B}$ and two-photon backgrounds are suppressed effectively in the middle of τ pair selection. $q\bar{q}$ continuum process takes large portion of non-τ background but shows some different behavior over the τ mass thershold. To estimate the contribution from $q\bar{q}$ backgrounds, a binned χ^2 method is used. [I]

4.2.1 Non-π^0 background

For the decay having neutral pions, it is possible to subtract the backgrounds coming from non-π^0 events. Figure 4.6 shows the $S_{\gamma\gamma}$ distribution of $\tau \to \pi^- K^0_S \pi^0 \pi^0 \nu_\tau$ and $\tau \to K^- K^0_S \pi^0 \nu_\tau$ events. The figures show that the

[I] However, the final contribution of these non-τ backgrounds is quite small, less than 2%

distributions in data and MC are consistent.
We select the signal region(SIG) as $-6 < S_{\gamma\gamma} < 5$ and the sideband region(SB) as $-13 < S_{\gamma\gamma} < -8$ and $7 < S_{\gamma\gamma} < 11$. The spurious π^0 contribution in the signal region can be subtracted by

$$N' = N^{SIG} - \frac{11}{9} N^{SB} \tag{4.6}$$

Here N', N^{SIG} and N^{SB} stand for the number of subtracted, signal region and sideband region events, respectively. (Hereafter, the superscript stands for the $S_{\gamma\gamma}$ selection region. The subscript stands for the data type, e.g, data, background(BG)...). Table 4.2.1 shows the number of events of BG for different $S_{\gamma\gamma}$ regions. The non-π^0 background in $\pi^- K^0_S \pi^0 \nu_\tau$ selection is found to be $\pi^- K^0_S \nu_\tau$ events, which is rather reduced by the sideband subtraction. $K^- K^0_S \nu_\tau$ and $\pi^- K^0_S \nu_\tau$ events contributing to $K^- K^0_S \pi^0 \nu_\tau$ event selection as a non-π^0 background are suppressed by the subtraction to 0.01 and 0.03 %, respectively. This means that the sideband subtraction is quite effective for non-π^0 background.

	$\pi^- K^0_S \pi^0$			$K^- K^0_S \pi^0$		
Process	N^{SIG}	N^{SB}	N'	N^{SIG}	N^{SB}	N'
$\pi^- K^0_S \pi^0$	-	-	-	1208 ± 28	154 ± 10	1054 ± 30
$K^- K^0_S \pi^0$	2365 ± 28	298 ± 10	2067 ± 30	-	-	-
$\pi^- K^0 \bar{K}^0$	1459 ± 17	883 ± 22	576 ± 35	161 ± 10	132 ± 6	29 ± 14
$\pi^- K^0_S \pi^0 \pi^0$	655 ± 14	205 ± 8	434 ± 17	-	-	-
$\pi^- K^0 \bar{K}^0 \pi^0$	419 ± 6	117 ± 3	284 ± 7	-	-	-
$\pi^- K^0_S$	2099 ± 26	2085 ± 26	6 ± 37	235 ± 13	239 ± 13	-4 ± 18
$K^- K^0_S$	-	-	-	346 ± 11	348 ± 11	-2 ± 15

Table 4.6: This table shows the number of background events in $S_{\gamma\gamma}$ signal(N^{SIG}) and sideband(N^{SB}) region, and the number of their subtraction(N') for each $\pi^- K^0_S \pi^0$ and $K^- K^0_S \pi^0$ mode.

Figure 4.7 shows the mass distribution of the SB events. The black shaded histogram is the background and the red line histogram is the signal MC.

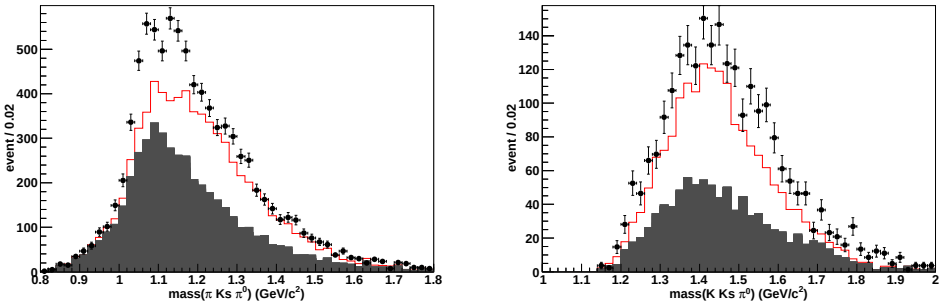

Figure 4.7: The invariant mass distribution of $\tau^- \to \pi^- K^0_S \pi^0 \nu_\tau$(top) and $\tau^- \to K^- K^0_S \pi^0 \nu_\tau$(bottom) event selected in the sideband region. The closed circle with an error bar is for data and the gray shaded histogram is for background. The red lined histogram is for signal MC. All MC histograms are stacked and normalized to the luminosity.

All MC histograms are stacked. The closed circles with error bars is for data. The figures show that SB events include not only the backgrounds but also the signal candidates. However, the current signal MC is not appropriate to estimate the number of signal candidates in SB. *In order to estimate the efficiency correctly, we decided not to use signal MC but to use data themselves.* The number of signal candidates in SB is calculated by $N^{SB}_{sig} = N^{SB}_{data} - N^{SB}_{BG}$ and the number of signal candidates in the signal region is calculated by $N^{SIG}_{sig} = N^{SIG}_{data} - N^{SIG}_{BG}$, so that the efficiency after non-π^0 subtraction is

$$\epsilon' = \epsilon \times \frac{N^{SIG}_{sig} - \frac{11}{9} N^{SB}_{sig}}{N^{SIG}_{sig}} \tag{4.7}$$

Where ϵ' is the efficiency after non-π^0 subtraction and ϵ is the efficiency before non-π^0 subtraction. The efficiency of the subtraction is found to be 82.5% for both decay modes.

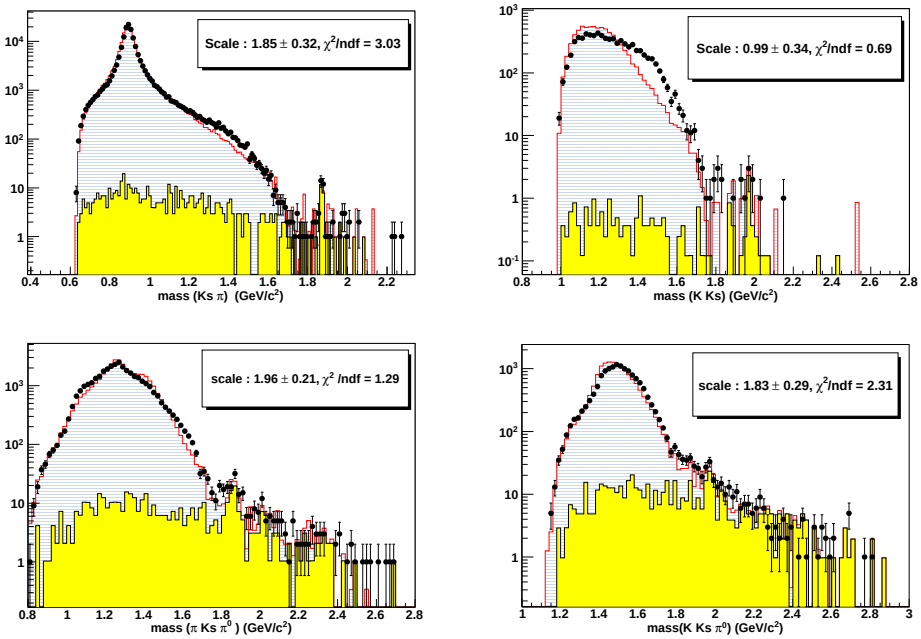

Figure 4.8: Continuum rescaling of two decay channels. From the top to bottom, $\tau \to \pi K^0_S \pi^0 \nu_\tau$, $\tau \to K K^0_S \pi^0 \nu$. The yellow shade histogram is the continuum background (h^{qq}) and blue dashed red lined histogram is non-continuum background (h^{non-qq}). The scale and χ^2/ndf are given in the figure.

4.2.2 Continuum background

The background from non-τ decay is expected to be few percent level than that from τ decays. Among the non-τ backgrounds, continuum backgrounds takes larger portion than other background, e.g. two-photon, BhaBha, $\mu - \mu$, $B\bar{B}$ events. So the study of continuum background is necessary for the precise measurements. Initially, non-τ backgrounds are normalized to the luminosity. It is well known that the low multiplicity event generation for $q\bar{q}$ MC is not perfect, so that the continuum background is usually rescaled assuming that shape of the mass distribution is correct. To estimate the continuum back-

ground, we find the most appropriate scale factor, α, by fitting $q\bar{q}$ histogram to the data above τ mass threshold region with following formula :

$$S(\alpha) = \sum_i (h_i^{data} - (h_i^{non-qq} + \alpha \times h_i^{qq}))^2 \tag{4.8}$$

where i is a mass bin number and the mass bin should be over τ mass threshold ($M_\tau = 1.8$ GeV). h_i^{data} is the data histogram, h_i^{non-qq} is the non-qq background histogram and h_i^{qq} is the qq background histogram to be scaled by α. It should be noticed that data is used in order to find the scale factor. α is found to be 1.96 ± 0.21 (1.83 ± 0.29) for $\pi^- K_S^0 \pi^0 \nu_\tau$ ($K^- K_S^0 \pi^0\ \nu_\tau$). The figure in Fig. 4.8 shows how the mass distribution are well matched to the MC distribution when scale factors are applied for the continuum background.

4.2.3 Background from $\tau^- \to \pi^- K_S^0 K_L^0 \pi^0 \nu_\tau$ decays

The background contribution to $\pi^- K_S^0 \pi^0 \nu_\tau$ estimated by using TAUOLA MC is shown in the left side of Fig. 4.9. As seen from the figure, the estimated background is bigger than data in low mass region ($M < 1.1$ GeV), where the region $\pi^- K^0 \bar{K}^0 \pi^0$ process is dominated. Such an overestimation is due to the ill-determined branching fraction deduced from the $\mathcal{B}(\tau^- \to \pi^- K_S^0 K_L^0 \pi^0 \nu_\tau)$ [15]. In fact, the branching fraction set in MC is $(3.1 \pm 2.3) \times 10^{-4}$ but the measurement for this process had only maden in one of the channels, $\tau \to \pi\ K_S^0 K_L^0 \pi^0 \nu$ ($\mathcal{B} = (3.1 \pm 1.2) \times 10^{-4}$). The error is quite big and brings a question for the branching fraction itself. In order to estimate the branching fraction for $\pi^- K^0 \bar{K}^0 \pi^0$, we select the $\pi^- K_S^0 K_S^0 \pi^0 \nu_\tau$ and $\tau^- \to \pi^- K_S^0 K_S^0 \nu_\tau$. The branching fraction is measured to be $\mathcal{B}(\pi^- K_S^0 K_S^0 \pi^0) = (2.05 \pm 0.24 \pm 0.23) \times 10^{-5}$, which is 1/4 of the value in PDG'11.

(a) The $\mathcal{B}(\pi^- K^0 \bar{K}^0 \pi^0) = (0.0082 \pm 0.0014)\%$ is obtained from the four times of the measured values $\mathcal{B}(\pi^- K_S^0 K_S^0 \pi^0) = (2.05 \pm 0.34) \times 10^{-5}$ ($\triangle\mathcal{B}/\mathcal{B} = 16.6\%$).

(b) The $\mathcal{B}(\pi^- K^0 \bar{K}^0) = (0.096 \pm 0.008)\%$ is obtained from the four times of the measured values $\mathcal{B}(\pi^- K^0_S K^0_S) = (0.024 \pm 0.002)\%$ ($\triangle\mathcal{B}/\mathcal{B} = 9\%$).

Using the result, we rescaled the number of $\pi^- K^0 \bar{K}^0 \pi^0 \nu_\tau$ background and found that the rescaling is quite consistent to the data. (See Fig. 4.9)

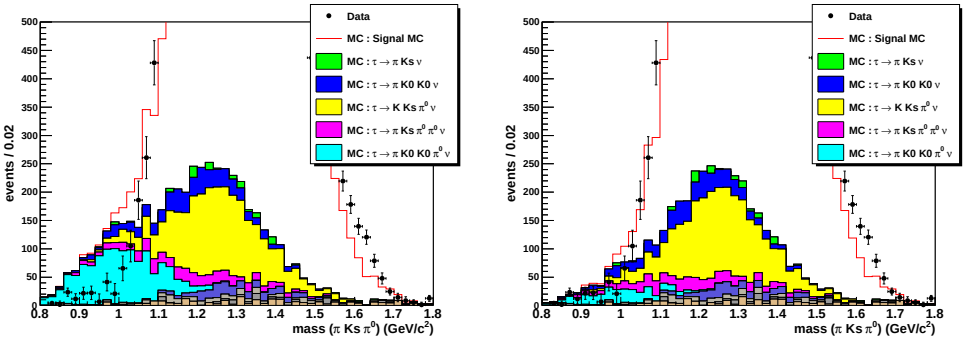

Figure 4.9: A zoom-in-view of the mass spectra for $\pi^- K^0_S \pi^0$ with sideband subtraction. The figure of non-scaled $\pi^- K^0_S K^0_S \pi^0$ distribution is on the left-hand side, and that of scaled $\pi^- K^0_S K^0_S \pi^0$ distribution is on the right-hand side.

4.2.4 Summary of the background

Here we summarize the backgrounds in each τ decay modes of interest.

backgrounds in the inclusive K^0_S events The backgrounds in the inclusive K^0_S events consist of non-K^0_S, other τ, continuum and two-photon events. More details can be found in Table 4.7

backgrounds in $\pi^- K^0_S$ and $K^- K^0_S$ events The total number of background events in $\pi^- K^0_S$ events is found to be 31435 ± 1446, 19.9% of total selected events. The dominant background is from $\tau^- \to \pi^- K^0 \bar{K}^0 \nu$ determined to be 6.32% of the total. The background from the other tag contribution

background	# of events	Ratio(%)
non-K^0_S	1911 ± 27	0.48
other τ	5928 ± 48	1.49
$q\bar{q}$	5671 ± 15	1.43
2-γ	3196 ± 10	0.80
Total	16705 ± 58	4.20

Table 4.7: The background for $\tau^- \to K^0_S(\text{particles})^-\nu_\tau$

is very similar to the other decay mode to around 0.83%. The background contribution from 3 pion decay is found to be 0.04%, reduced by two requirements of K^0_S flight length > 2cm and K^0_S dr > 0.1 cm. In case of continuum background, we rescale the normalization using the method described in section 4.2.2. The scale factor is found to be 1.85 ± 0.32 with $\chi^2/ndf = 3.03$ (See Fig. 4.8).

The total number of background events in $K^-K^0_S$ events is estimated to be 11847±303, 36.5% of all selected events. The dominant background is from $\tau^- \to K^-K^0_S\pi^0\nu$ and $\tau^- \to \pi^-K^0_S\nu$ with 10.99% and 20.53% of total, respectively. Especially, the background having pion tracks, for example, π K^0_S and $\pi K^0_S\pi^0$, is estimated by MC with the PID correction factor of 2.00 ± 0.05. The background from the other tag contribution is around 0.67%. In case of continuum background, we normalized with the method described in section 4.2.2. The scale factor is found to be 0.99 ± 0.34 with $\chi^2/ndf = 0.69$ (See Fig. 4.8). The scale factor seems rather small compared to the other decay modes, because of the small number of events in the mass region over 1.8 GeV. However, the non-τ contribution is less than 2% of the total, so the systematic contribution is expected to be negligible. Table 4.8 summarized the background for $\pi^-K^0_S$ and $K^-K^0_S$ events.

backgrounds in $\pi^-K^0_S\pi^0$ and $K^-K^0_S\pi^0$ events In previous section, we rescaled the number of background for $\pi^-K^0_SK^0_L\pi^0\nu_\tau$ process. However, the

Background	$\pi^- K^0_S$		$K^- K^0_S$	
	# of events	Rate(%)	# of events	Rate(%)
$\pi^- K^0_S \pi^0$	9339 ± 471	5.92	479 ± 27	1.48
$K^- K^0_S \pi^0$	1079 ± 138	0.68	3570± 455	10.99
$\pi^- K^0 \bar{K^0}$	9968 ± 859	6.32	560 ± 50	1.72
$\pi^- K^0_S$	-	-	6672 ± 324	20.53
$K^- K^0_S$	5798 ± 582	3.67	-	-
other τ decay	2745 ± 824	1.74	121 ± 37	0.37
tagging	1274 ± 134	0.84	204 ± 24	0.67
two-photon	905 ± 273	0.57	153 ± 46	0.47
continuum	259 ± 35	0.16	88 ± 12	0.27
Total	31435 ± 1446	19.9	11847 ± 561	36.5

Table 4.8: The background contents in $\pi^- K^0_S$ and $K^- K^0_S$ events.

branching fractions for other τ decay processes used in current MC study are slightly (sometime largely) different from the values in PDG'11. We rescaled the background process from τ decay to PDG'11. Table 4.5 shows the scale factors for the each decay process and its errors. For the process $\pi^- K^0 \bar{K}^0$ and $\pi^- K^0 \bar{K}^0 \pi^0 \nu_\tau$, we measured the branching fractions and used here.

After the background rescaling and sideband subtraction, the backgrounds of $\pi^- K^0_S \pi^0$ and $K^- K^0_S \pi^0$ are estimated as in Table 4.9. The dominant background for $\pi^- K^0_S \pi^0$ is the decay of $K^- K^0_S \pi^0$ with 8.09%. As same as for $\pi^- K^0_S \pi^0$, the dominant background for $K^- K^0_S \pi^0$ is to be $\pi^- K^0_S \pi^0$ with 13.39%. A large number of $\pi^- K^0 \bar{K^0} \nu_\tau$ event are estimated from the MC study, since $\tau^- \to \pi^- K^0_S K_L \nu_\tau$ decays with missing K_L can be selected. The background from tagging (mainly due to $\tau^- \to \pi(\pi^0 \geq 0)\nu$) for $\pi^- K^0_S \pi^0 (K^- K^0_S \pi^0)$ is found to be 0.95% (0.98%). Finally, the total background is estimated to $4153 \pm 153 (1322 \pm 50)$, which is 15.70%(16.14%) of total candidates.

backgrounds in $\pi^- K^0_S K^0_S$ and $\pi^- K^0_S K^0_S \pi^0$ event The total number of background in $\pi^- K^0_S K^0_S$ events is estimated by 1424 ± 111, 21.31% of total.

The most dominant background is from the mis-identified tagging events, which is mostly due to muon fake(A muon identified as a pion) We estimate its number as 914±91, which is 13.67% for the selected events. The secondary background is from the continuum, 4.4%. The contents of background are listed in Table 4.10. It is noticed that the continuum background is well fitted to the data, so there is no another scaling to the continuum background. (See Fig. 5.5)

Background	$\pi^- K^0_S \pi^0$		$K^- K^0_S \pi^0$	
	# of events	Rate(%)	# of events	Rate(%)
$\pi^- K^0_S \pi^0$	-	-	1107 ± 38	13.39
$K^- K^0_S \pi^0$	2152 ± 53	8.09	-	-
$\pi^- K^0 \bar{K^0}$	576 ± 48	2.16	18 ± 13	0.21
$\pi^- K^0_S \pi^0 \pi^0$	445 ± 29	1.67	-	-
$\pi^- K^0 \bar{K^0} \pi^0$	298 ± 23	1.12	-	-
$\pi^- K^0_S$	5 ± 65	0.02	(4) ± 22	(0.06)
$K^- K^0_S$	-	-	(2) ± 27	(0.02)
other τ decay	209 ± 27	0.79	80 ± 13	0.97
tagging	228 ± 17	0.95	69 ± 10	0.98
two-photon	33 ± 14	0.12	22 ± 6	0.26
continuum	207 ± 22	0.78	34 ± 9	0.41
Total	4153 ± 515	15.70	1322 ± 130	16.14

Table 4.9: The background contents in $\pi^- K^0_S \pi^0$ and $K^- K^0_S \pi^0$ events.

Background	$\pi^- K^0_S K^0_S$		$\pi^- K^0_S K^0_S \pi^0$	
	# of events	Rate(%)	# of events	Rate(%)
$\pi^- K^0_S K^0_S$	-	-	91 ± 3	29.9
$\pi^- K^0_S K^0_S \pi^0$	115 ± 13	1.73	-	-
other τ decay	33 ± 4	0.49	3 ± 1	0.96
tagging	914 ± 9	14.4	23 ± 1	7.73
continuum	296 ± 11	4.43	35 ± 4	11.6
Total	1403 ± 20	21.0	152 ± 10	50.2

Table 4.10: The background contents in $\pi^- K^0_S K^0_S(\pi^0)$ events

Chapter 5

Determination of the branching fractions

In this chapter we describe the details of the branching fraction measurement for inclusive K^0_S mode in τ decays and its exclusive decay modes; $\tau^- \to \pi^- K^0_S \nu$, $\tau^- \to K^- K^0_S \nu$, $\tau^- \to K^- K^0_S \pi^0 \nu$, $\tau^- \to \pi^- K^0_S \pi^0 \nu$, $\tau^- \to \pi^- K^0_S K^0_S \nu$ and $\tau^- \to \pi^- K^0_S K^0_S \pi^0 \nu$. Since Belle have already reported the branching fraction for $\mathcal{B}(\tau^- \to \pi^- K^0_S \nu)$) [90], it can be used for a consistency check. The branching fractions for other modes are measured with better precision ever maden. Especially, the decay mode $\tau^- \to \pi^- K^0_S K^0_S \pi^0 \nu$ has not been reported by other experiments.

5.1 Method of branching fraction calculation

There are two methods to obtain the branching fractions of the decay modes of interest. One method is to use luminosity for normalization, a nomial way to determine the branching fraction. The branching fraction for $\tau^- \to X^- \nu_\tau$

can be calculated as :

$$\mathcal{B}(\tau^- \to X^-\nu_\tau) = \frac{N(X^-)}{2 \times N_{\tau\bar{\tau}} \times \mathcal{B}(\tau \to l(h)\bar{\nu}\nu) \times \epsilon(X^-)} \tag{5.1}$$

where $N(X^-)$ is the number of signal events with the any type of tagging method, $\mathcal{B}(\tau \to l(h)\bar{\nu}\nu)$ is a sum of the branching fractions for τ leptonic(hadronic) decay modes. ϵ_{sig} is the efficiency of $\tau \to \mathrm{X}^-\nu_\tau$. The number of τ pairs, $N_{\tau^+\tau^-}$, is easily calculated from :

$$N_{\tau^+\tau^-} = L \times \sigma_{\tau\tau} = 670\ \mathrm{fb}^{-1} \times 0.919\ \mathrm{nb} = 6.16 \times 10^8 \tag{5.2}$$

This method is used to determine $\mathcal{B}(\tau^- \to \pi^- K^0_S K^0_S \nu_\tau)$ and $\mathcal{B}(\tau^- \to \pi^- K^0_S K^0_S \pi^0 \nu_\tau)$, since these two events are selected by hadron tagging as well as lepton tagging.

As the second method, the branching fractions for tau leptonic decays are measured with good precision so that the normalization to the number of τ leptonic events can be used.

$$\mathcal{B}(\tau^- \to X^-\nu_\tau) = \frac{N(X, l_i)}{\epsilon(X, l_i)} \frac{\epsilon(l_i, l_j)}{N(l_i, l_j)} \mathcal{B}(\tau \to l_j \bar{\nu}\nu) \tag{5.3}$$

where $l_i, l_j = e, \mu$ vice versa. $N(X, l_i)$ and $\epsilon(X, l)_i$ are the number and MC efficiency for (X, l_i) event. $N(l_i, l_j)$ and $\epsilon(l_i, l_j)$ are the number and MC efficiency for (l_i, l_j) event. This method can reduce some systematic errors; e.g., the tracking efficiency, the particle identification efficiency and so forth.(See Sec.**??**)

5.2 The branching fraction measurement

5.2.1 For inclusive decay

After the event selection introduced in the section **??**, we selected 397806$\pm$ 631 signal candidates and estimate 16705 $\pm$ 58 events for background via

MC study. We applied PID corrections for the each type of tagging track with respect to the momentum and θ. The correction for K_S^0 reconstruction efficiency is applied, too. The signal efficiency is found to be $(9.66 \pm 0.17)\%$ from MC study. We estimate the background contents and their proportions using generic τ MC. The total background ratio is estimated to be $(4.20 \pm 0.17)\%$. The branching fraction is found to $(0.914 \pm 0.001 \pm 0.028)\%$, consistent to the PDG'11 average for K_S^0 inclusive decay$(0.92 \pm 0.04)\%$ with better precision. The branching fraction is also checked by different normalization using luminosity, giving a value $(0.910 \pm 0.001 \pm 0.046)\%$.

tag	Eff. (%)	N_{data}	N_{bkg}	$\mathcal{B}_l(\times 10^{-3})$	$\mathcal{B}_{\rm lum}(\times 10^{-3})$
e	10.14	211308 ± 460	7583 ± 419	9.18 ± 0.02	9.14 ± 0.02
μ	9.12	186498 ± 432	9122 ± 590	9.13 ± 0.02	9.09 ± 0.02
comb.	9.66	397806 ± 631	16705 ± 881	9.14 ± 0.01	9.10 ± 0.01

Table 5.1: The relevant numbers for $\mathcal{B}(\tau^- \to K_S^0(\text{particles})^-\nu_\tau)$

5.2.2 For the decays with one K_S^0

For $\pi^- K_S^0$

Total selected events is 157836 ± 397. The correction for particle ID and K_S^0 reconstruction efficiency is applied. The signal efficiency is found to be (7.11 ± 0.21) %. The invariant mass distribution is shown in Fig. 5.2.1 with data and background histogram. With this result, the branching fraction is esitmated to $(0.411 \pm 0.001 \pm 0.014)\%$, which is consistent to the previous Belle result [90]. The difference of central value is due to the K_S^0 efficiency correction. The relevant numbers for this calculation are given in Table 5.2.

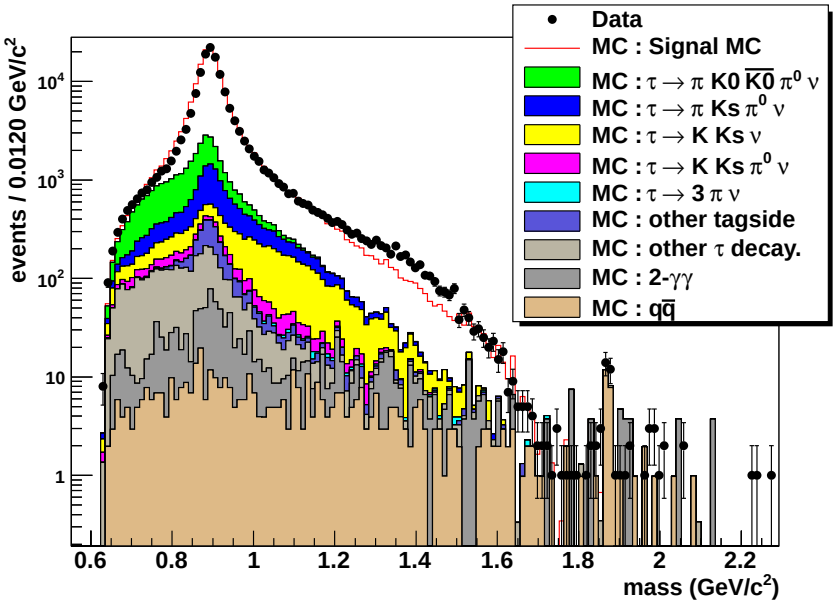

Figure 5.1: The mass spectra for $\pi^- K^0_S$.

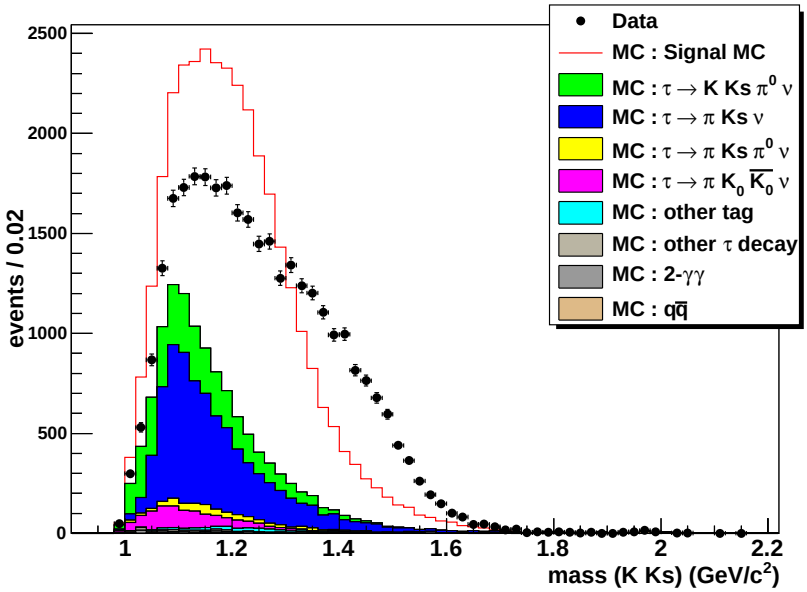

Figure 5.2: The mass spectra for $K^- K^0_S$.

tag	Eff.(%)	N_{Data}	N_{BG}	$\mathcal{B}_l(\times 10^{-3})$	$\mathcal{B}_{\rm lum}(\times 10^{-3})$
e	7.21	81192 ± 285	15880 ± 766	4.14 ± 0.02	4.12 ± 0.02
μ	7.00	76644 ± 277	14685 ± 693	4.09 ± 0.02	4.14 ± 0.02
comb.	7.11	157836 ± 397	31435 ± 1446	4.11 ± 0.01	4.10 ± 0.01

Table 5.2: The relevant numbers for $\mathcal{B}(\tau^- \to \pi^- K^0_S \nu_\tau)$

$K^- K^0_S$

The branching fraction is known to be $(0.079 \pm 0.008)\%$ from PDG [39]. Starting from the event selection of $\tau^- \to K^0_S$ (particles)$^- \nu_\tau$, we apply the particle ID cut and π^0 veto. In order to suppress the decay having a π^0 contribution, the highest photon energy cut is applied as 0.2 GeV. Total selected event is 32491 ± 180. The total number of background events is estimated to be 11847 ± 303, 36.5% of all selected events. We calculate the signal efficiency using signal MC with appropriate corrections on particle ID and K^0_S efficiency. The signal efficiency is found to be 6.72 %. The invariant mass distribution is shown in Fig. 5.1 with data and background histogram. The relevant numbers for this calculation are listed in Table 5.3. With these results, the branching fraction is found to be $(7.19 \pm 0.06 \pm 0.35) \times 10^{-4}$, which is consistent to PDG'11 average with better precision.

tag	Eff.(%)	N_{Data}	N_{BG}	$\mathcal{B}_l(\times 10^{-4})$	$\mathcal{B}_{lum}(\times 10^{-4})$
e	6.88	16936 ± 130	6008 ± 300	7.26 ± 0.09	7.23 ± 0.09
μ	6.54	15765 ± 126	5832 ± 274	7.13 ± 0.09	7.10 ± 0.09
comb.	6.72	32701 ± 181	11840 ± 561	7.19 ± 0.06	7.16 ± 0.06

Table 5.3: The relevant number for $\mathcal{B}(\tau^- \to K^- K^0_S \nu_\tau)$

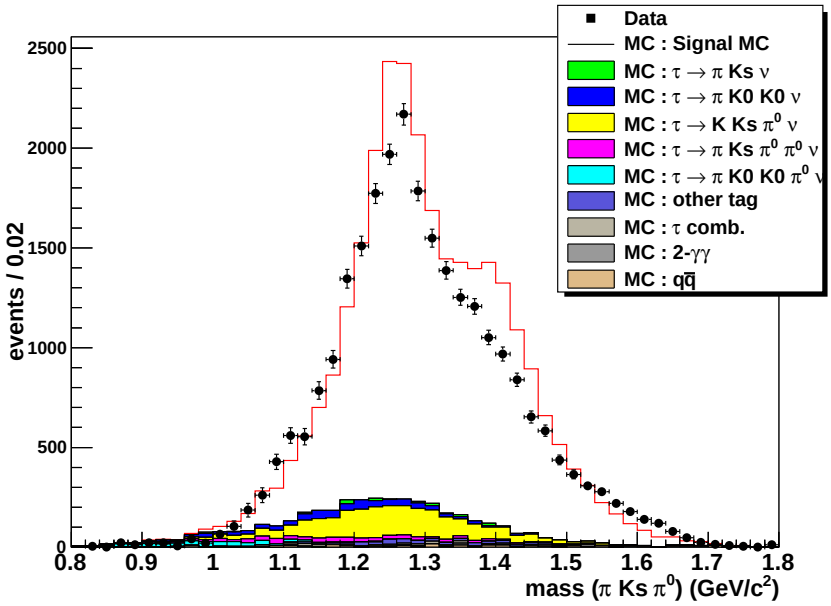

Figure 5.3: The mass spectra for $\pi^- K^0_S \pi^0$.

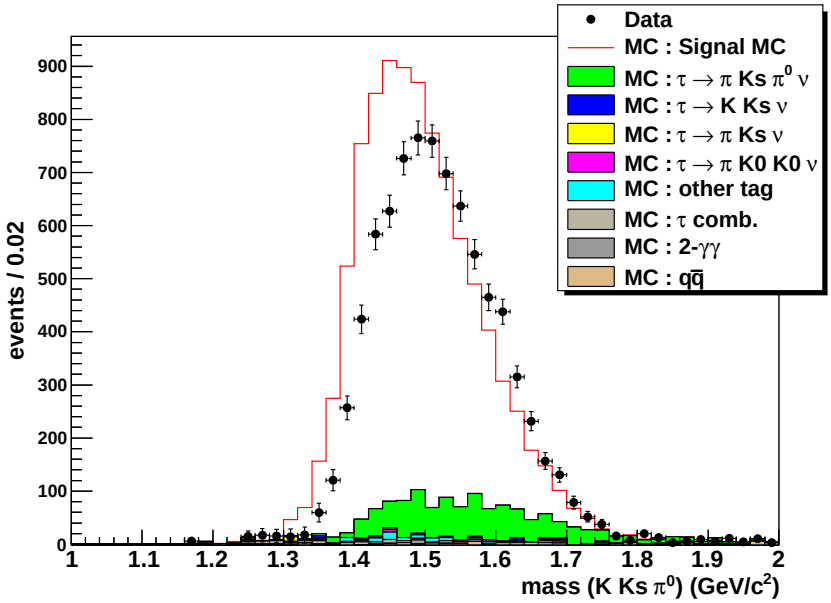

Figure 5.4: The mass spectra for $K^- K^0_S \pi^0$.

$\pi^- K^0_S \pi^0$

The number of selected events is 26605 ± 211 and the background is estimated to 4055 ± 81. The final efficiency is found to be $(2.65 \pm 0.01)\%$ with PID, K^0_S and π^0 corrections. The error is taken into account for the statistical error not only of the signal MC, but also of sideband subtraction. Table 5.2.2 shows the efficiency and the number of data, background and signal events. With this result, the branching fraction is determined to be $(0.196 \pm 0.002)\%$ from Eq. 5.3 and $(0.197 \pm 0.002)\%$ from Eq. 5.1 and both results are consistent with each other. The invariant mass distribution is shown in Fig. 5.2.2

tag	Eff.(%)	N_{data}	N_{BG}	$\mathcal{B}_l(\%)$	$\mathcal{B}_{\rm lum}(\%)$
e	2.69 ± 0.02	13546	1838	0.204 ± 0.003	0.198 ± 0.003
μ	2.65 ± 0.02	13059	2069	0.189 ± 0.003	0.193 ± 0.003
comb.	2.65 ± 0.01	26605	4055	0.197 ± 0.002	0.196 ± 0.002

Table 5.4: The relevant numbers for $\mathcal{B}(\tau^- \to \pi^- K^0_S \pi^0 \nu)$.

$K^- K^0_S \pi^0$

The final number of selected events is 8267 ± 114 and the background is estimated to 1274 ± 50. Table 5.2.2 shows the efficiency and the number of data, background and signal events. The final efficiency is found to be $(2.19 \pm 0.02)\%$. As mentioned previously, the error is taken into account only for the statistical error not only of the signal MC but also of sideband subtraction. With these results, we obtained $\mathcal{B}$ to be $(0.0740 \pm 0.0012)\%$ from Eq. **??** and $(0.0737 \pm 0.0012)\%$ from Eq. 5.1. Two results are agreed within the statistical error. The invariant mass distribution can be found in Fig. 5.3

tag	Eff.(%)	N_{data}	N_{BG}	$\mathcal{B}(\%)$	$\mathcal{B}_{lum}(\%)$
e	2.27 ± 0.02	4297	665	0.0750 ± 0.0017	0.0727 ± 0.0017
μ	2.09 ± 0.02	3970	611	0.0734 ± 0.0017	0.0752 ± 0.0017
comb.	2.19 ± 0.02	8267	1274	0.0740 ± 0.0012	0.0737 ± 0.0012

Table 5.5: The relevant numbers for $\mathcal{B}(\tau^- \to K^- K^0_S \pi^0 \nu_\tau)$

tag	Eff. (%)	N_{data}	N_{BG}	$\mathcal{B}_{\rm lum}(\times 10^{-4})$
lepton	3.58	3972 ± 63	150 ± 31	2.46 ± 0.04
hadron	1.29	2712 ± 52	1293 ± 98	2.38 ± 0.09
combined	2.43	6684 ± 81	1424 ± 111	2.41 ± 0.04

Table 5.6: The relevant numbers for $\mathcal{B}(\tau^- \to \pi^- K^0_S K^0_S \nu_\tau)$

5.2.3 For the decays with two K^0_S

$\pi^- K^0_S K^0_S$

We selected 6684±82 events using the all-tag (lepton + hadron) method. The efficiency is found to be (2.43 ± 0.07) % from the signal MC study. The efficiency seems to be rather low because it is a combined efficiency of hadron and lepton tag use. The hadron tag condition includes not only one track but also one reconstructed π^0, which passes the $-6 < S_{\gamma\gamma} < 5$ condition, which have the combined efficiency decreased. With the numbers in Table 5.6, the branching fraction is obtained by using Eq. 5.1 and the result is in $(2.41 \pm 0.04) \times 10^{-4}$.

$\pi^- K^0_S K^0_S \pi^0$

The branching fraction for this mode has not been measured yet, only the upper limit is set to $\mathcal{B}(\tau^- \to \pi^- K^0_S K^0_S \pi^0 \nu_\tau) < 2.0 \times 10^{-4}$ [39]. However, its counterpart decay, $\tau^- \to \pi^- K^0_S K^0_L \pi^0 \nu_\tau$ has been measured by ALEPH to be $(3.1 \pm 1.2) \times 10^{-4}$ [15]. This branching fraction is determined using the signal efficiency estimated by MC. $\tau^- \to \pi^- K^0 \bar{K}^0 \pi^0 \nu_\tau$ event contributes as

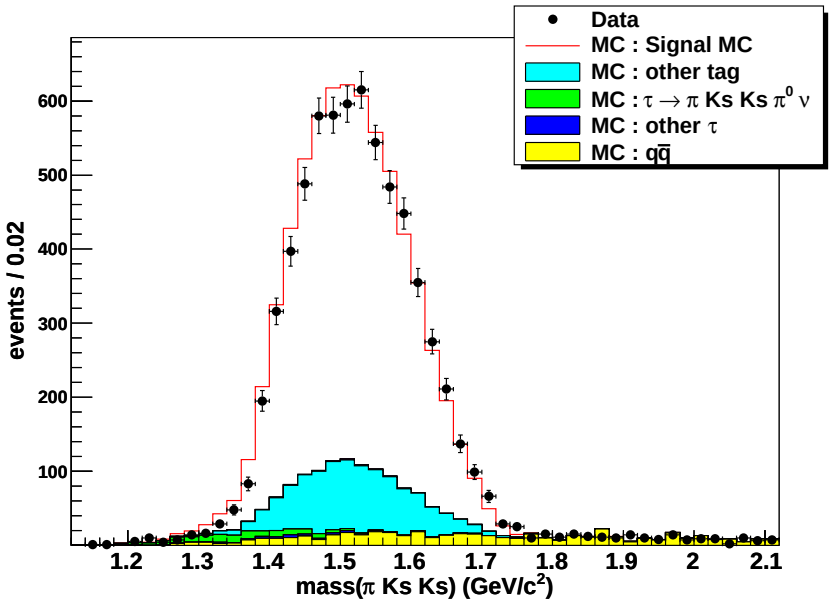

Figure 5.5: The invariant mass of $\tau^- \to \pi^- K^0_S K^0_S \nu_\tau$.

a sizable background to $\tau^- \to \pi^- K^0_S \pi^0 \nu_\tau$ events by missing one $K^0(\bar{K^0})$.

We select 303 ± 17 candidates using combined tagging. The number of backgrounds, mainly due to $\pi^- K^0_S K^0_S \nu$ and continuum, is estimated to be 152 ± 5 in total under the τ mass threshold. The mass distribution for $\tau^- \to \pi^- K^0_S K^0_S \pi^0 \nu_\tau$ with backgrounds is shown at Fig 5.6.

The mass distribution for data is not agreed well with that for MC just above the tau mass threshold, $M(\pi^- K^0_S K^0_S \pi^0) > 1.778$GeV. In order to be sure of our observation, the π^0 mass sideband events are subtracted as depected in 5.6 The subtracted distribution shows a clear excess on the total mass region of less than the tau mass, but, on the other mass region (mass > 1.8 GeV), the distribution is similar to the continuum distribution. Thus, the events laying on the total mass region, $M(\pi^- K^0_S K^0_S \pi^0) < 1.778$, are the signal candidates.

The background is dominated by $\tau^- \to \pi^- K^0_S K^0_S \nu_\tau$ decay, which is measured in this study with better accuracy. In the mass distribution, some of $\tau^- \to \pi^- K^0_S K^0_S \nu$ events can exceed the tau mass threshold due to the additional mass from the π^0 mis-reconstructed by two γ, accidentally. And another dominant background is the continuum. The continuum background is normalized to luminosity and it agrees with data over 1.9 GeV. In the mass range of interest, $1.0 \sim 1.8$ GeV, the number of signal and background events and other values necessary to the branching fraction are summarized in Table 5.7. The branching fraction is found to be $(2.05 \pm 0.23 \pm 0.29) \times 10^{-5}$, which is consistent with the upper limit ($< 2.0 \times 10^{-4}$) given in PDG'11. The results of the lepton and hadron tag are slightly different. However, the uncertainty of the hadron tag is larger than that of the lepton tag and two branching fraction values differ by one statistical error. The details for each tagging are given in Table 5.7

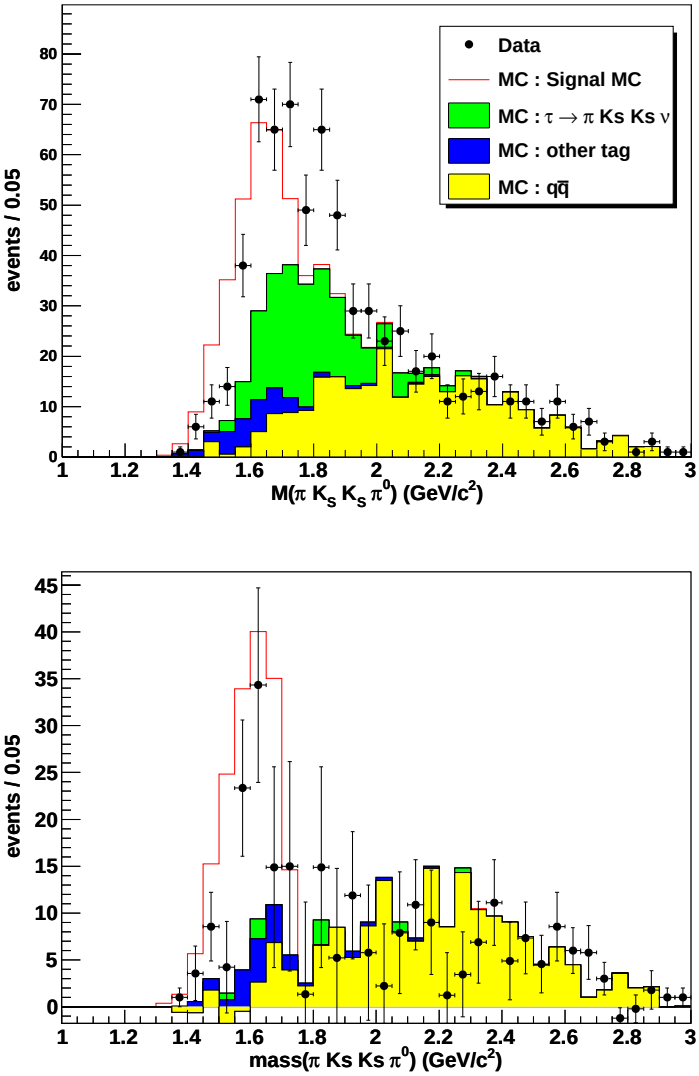

Figure 5.6: The invariant mass distribution of $\tau^- \to \pi^- K^0_S K^0_S \pi^0 \nu_\tau$ without SB subtraction (top) and with SB subtraction (bottom). The yellow shaded histogram is continuum BG and blue shaded one is BG from other tag, e.g., $\tau \to \pi^- n\pi^0 \nu$ where $n \geq 2$. The right figure shows the events in the mass region less than 1.8 GeV

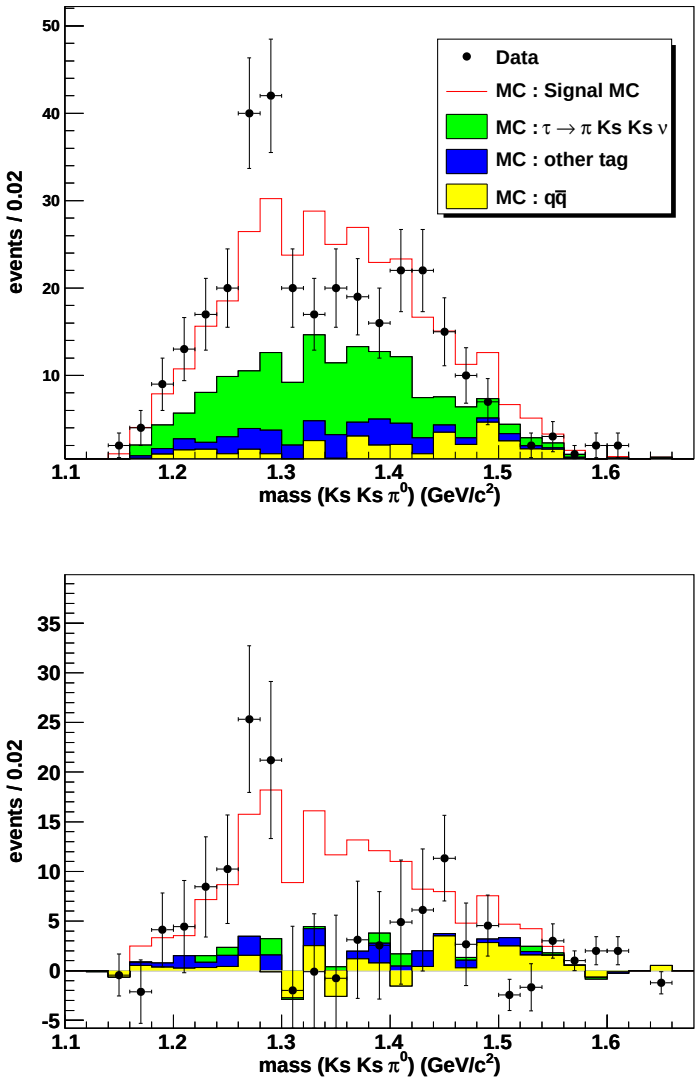

Figure 5.7: The mass distribution of $K^0_S K^0_S \pi^0$ in $\tau^- \to \pi K^0_S K^0_S \pi^0 \nu_\tau$ decay without SB subtraction(top) and with SB subtraction(bottom).

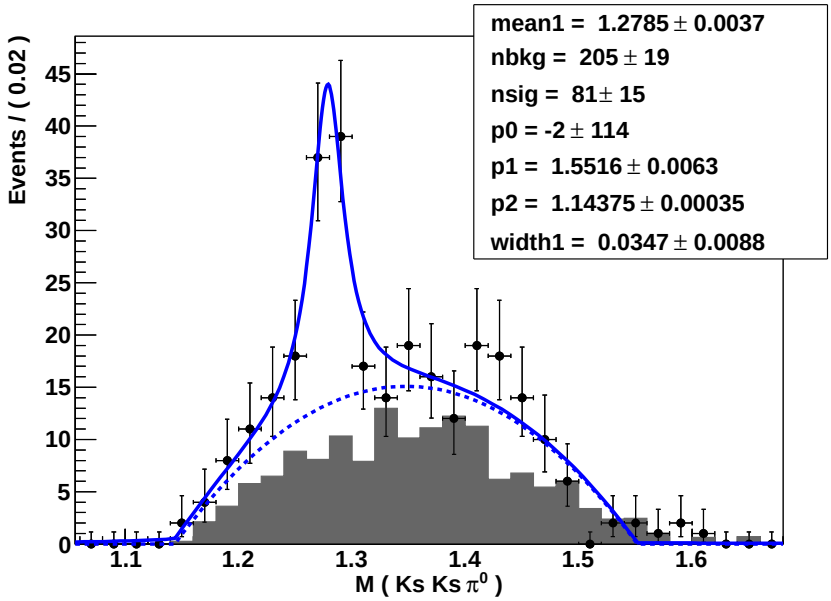

Figure 5.8: The fit result for the invaraint mass of $K^0_S K^0_S \pi^0$ using Briet-Wigner for $f_1(1285)$ and 2nd order polynomial for the background estimation.

tag	Eff. (%)	N_{data}	N_{bkg}	$\mathcal{B}_{\rm lum}(\times 10^{-5})$
lepton	1.19	157 ± 13	63 ± 3	1.80 ± 0.24
hadron	0.45	146 ± 12	94 ± 5	2.49 ± 0.54
combined	0.82	303 ± 17	152 ± 5	2.05 ± 0.23

Table 5.7: The relevant numbers for $\mathcal{B}(\tau^- \to \pi^- K^0_S K^0_S \pi^0 \nu_\tau)$

Reconstruction of $f_1(1285) \to K^0_S K^0_S \pi^0$

The interesting thing in this decay is the sub-mass distribution using $K^0_S K^0_S \pi^0$. In Fig. 5.2.3, it is possible to identify a clear peak around 1.28 GeV for both distributions, one for sideband subtraction and the other for no subtraction. Figure 5.2.3 at bottom shows the result of the fit with a Breit-Wigner function with mass and width floated. The Breit-Wigner with energy independent width is

$$S(m) = \frac{mM\Gamma_0}{(M^2 - m^2)^2 + (m\Gamma_0)^2} \tag{5.4}$$

Where M and Γ_0 are the nominal mass and width, m is the center of mass of 3 hadrons. The shape of the background is assumed to be a 2nd order polynomial whose form is

$$B(m) = p_0(m - p_1)(m - p_2) \tag{5.5}$$

where p_0, p_1 and p_2 are floated in the fit. The resonance is shown clearly at 1.278 ± 0.035 GeV, which can be identified as $f_1(1285)$. The significance is found to be

$$S = \frac{N_{\rm Signal}}{\sqrt{N_{\rm Signal} + N_{\rm Background}}} = \frac{81}{\sqrt{81 + 205}} = 4.8\sigma$$

And total yield of $f_1(1285)$ candidate is found to be 81 ± 15 events when the background is 205 ± 19 events. Using the ratio between the signal yields, we are able to decide the branching fraction for $\tau^- \to f_1(1285)\pi^-\nu_\tau \to \pi^- K^0_S K^0_S \pi^0 \nu_\tau$ and found to be $(1.07 \pm 0.23 \pm 0.16) \times 10^{-5}$

Chapter 6

Systematic uncertainties

The sources of systematic uncertainty for the branching fraction measurements can be categorized into 3 parts:

- Normalization (e-μ events, Luminosity)
- Background estimation
- Signal efficiency

Here we bring again the branching fraction formula introduced in the previous Sec. 5.1:

$$\mathcal{B}(\tau^- \to X^- \nu_\tau) = \frac{N_{dat} - N_{back}}{\epsilon_{sig}} \cdot \frac{\epsilon_{e\text{-}\mu}}{N_{e\text{-}\mu} - B_{e\text{-}\mu}} \cdot \frac{\mathcal{B}_e \mathcal{B}_\mu}{\mathcal{B}_e + \mathcal{B}_\mu}$$

where N_{dat}, N_{back} and ϵ_{sig} are the number of signal candidates, the number of background and the selection efficieincy for the signal, respectively. While $N_{e\text{-}\mu}$, $B_{e\text{-}\mu}$ and $\epsilon_{e\text{-}\mu}$ are the number of e-μ candidates, the number of background in the e-μ sample and the selection efficiency for the e-μ event, respectively. $\mathcal{B}_e$ and $\mathcal{B}_\mu$ are the branching fractions for $\tau^- \to e^- \bar{\nu}_e \nu_\tau$ and $\tau^- \to \mu^- \bar{\nu}_\mu \nu_\tau$. Assuming the no-correlation between the observables, the

total error of the $\mathcal{B}$ can be obtained as:

$$\begin{aligned}\left(\frac{\triangle\mathcal{B}}{\mathcal{B}}\right)^2 &= \left(\frac{\triangle N_{dat}}{N_{dat}-N_{back}}\right)^2+\left(\frac{\triangle N_{back}}{N_{dat}-N_{back}}\right)^2+\left(\frac{\triangle\epsilon_{sig}}{\epsilon_{sig}}\right)^2 \\ &+ \left(\frac{\triangle N_{e\text{-}\mu}}{N_{e\text{-}\mu}-B_{e\text{-}\mu}}\right)^2+\left(\frac{\triangle B_{e\text{-}\mu}}{N_{e\text{-}\mu}-B_{e\text{-}\mu}}\right)^2+\left(\frac{\triangle\epsilon_{e\text{-}\mu}}{\epsilon_{e\text{-}\mu}}\right)^2 \\ &+ \left(\frac{\triangle f}{f}\right)^2\end{aligned} \tag{6.1}$$

where the symbol $\triangle$ indicates the error of that quantity and f is

$$f \equiv \frac{\mathcal{B}_e\mathcal{B}_\mu}{\mathcal{B}_e+\mathcal{B}_\mu}$$

The first term in this equation is treated as a statistical error and other terms are taken into account as systematic errors. The 2nd term in 1st row is the uncertainty from the background estimation and the 3rd term in the same row is the uncertainty of the efficiency. The remaining terms are due to the e-μ normalization. We start our discussion from the uncertainty from e-μ normalization.

6.1 Uncertainty from the normalization

6.1.1 $\triangle\mathcal{B}_e$ and $\triangle\mathcal{B}_\mu$

The error of the last term in Eq. (6.1) is given by

$$\frac{\triangle f}{f} = \sqrt{\left(\frac{\mathcal{B}_\mu}{\mathcal{B}_e}\frac{\triangle\mathcal{B}_e}{\mathcal{B}_e+\mathcal{B}_\mu}\right)^2+\left(\frac{\mathcal{B}_e}{\mathcal{B}_\mu}\frac{\triangle\mathcal{B}_\mu}{\mathcal{B}_e+\mathcal{B}_\mu}\right)^2} \sim \frac{\triangle\mathcal{B}_e}{\sqrt{2}\mathcal{B}_e} \tag{6.2}$$

where the last term assumes $\mathcal{B}_e \sim \mathcal{B}_\mu$ and $\triangle\mathcal{B}_e \sim \triangle\mathcal{B}_\mu$. Taking the PDG2011 values for $\mathcal{B}_e = 0.1785 \pm 0.0005$ and $\mathcal{B}_\mu = 0.1736 \pm 0.0005$, f and $\triangle f/f$ are

$$f = \frac{\mathcal{B}_e\mathcal{B}_\mu}{\mathcal{B}_e+\mathcal{B}_\mu} = 0.0880 \tag{6.3}$$

$$\frac{\triangle f}{f} = 0.15\% \tag{6.4}$$

6.1.2 $\triangle\epsilon_{e\text{-}\mu}$ contribution

Using the numbers given in Sec 3.3 , we obtain

$$\begin{aligned}\epsilon_{e\text{-}\mu} &= \frac{N_{obs}}{N_{gen}}\eta_e\eta_\mu \\ &= \frac{23,653,089}{114,941,289} \times (0.9821 \pm 0.0201) \times (0.9555 \pm 0.024) = 19.31\% \end{aligned} \quad (6.5)$$

where η_e and η_μ are PID correction factors for electron and muon, respectively. The error of $\epsilon_{e\text{-}\mu}$ is

$$\begin{aligned}\frac{\triangle\epsilon_{e\text{-}\mu}}{\epsilon_{e\text{-}\mu}} &= \sqrt{\left(\frac{\triangle N_{obs}}{N_{obs}}\right)^2 + \left(\frac{\triangle\eta_e}{\eta_e}\right)^2 + \left(\frac{\triangle\eta_\mu}{\eta_\mu}\right)^2} \\ &= \sqrt{\left(\frac{1}{\sqrt{23,653,089}}\right)^2 + \left(\frac{0.020}{0.9821}\right)^2 + \left(\frac{0.024}{0.9555}\right)^2} \\ &= \sqrt{(0.0002)^2 + (0.0205)^2 + (0.0252)^2} = 3.2\% \end{aligned} \quad (6.6)$$

Then

$$\epsilon_{e\text{-}\mu} = 19.31 \pm 0.62\%$$

The error of PID correction factors are dominated in $\triangle\epsilon_{e\text{-}\mu}$. We, however, should remember that the lepton-ID is also required in the tag-side of the signal events, therefore there is a correction factor of lepton ID in ϵ_{sig} as $\epsilon_{sig} \propto \eta_e^{ID} + \eta_\mu^{ID}$. Since the net effect of the lepton ID correction proportional to :

$$f_{LID} \equiv \eta_e\eta_\mu/(\eta_e + \eta_\mu)/2$$

, the actual error coming from $\triangle\eta_e$ and $\triangle\eta_e$ is

$$\begin{aligned}\left(\frac{\triangle f_{LID}}{f_{LID}}\right) &= \sqrt{\left(\frac{\eta_\mu}{\eta_e}\frac{\triangle\eta_e}{\eta_e+\eta_\mu}\right)^2 + \left(\frac{\eta_e}{\eta_\mu}\frac{\triangle\eta_\mu}{\eta_e+\eta\mu}\right)^2} \sim \frac{\triangle\eta_\mu}{\sqrt{2}\eta_\mu} \\ &= \frac{0.024}{\sqrt{2}\times 0.9523} = 1.63\%, \end{aligned} \quad (6.7)$$

where the number in the parenthesis is the one obtained from the approximate formula given in the last line in Eq. 6.5. The difference between Eq. 6.6 and Eq. 6.7 explains the merit of use of the e-μ events for the normalization.

Process	N_{obs}	Scale	N_{obs}(corr.)	BG(R) (%)	$\triangle R$ (%)
e-μ pair	7661052				
$\tau^- \to \pi^-\pi^0\nu_\tau$	183876	1.032	189827	2.4778	0.0087
other τ decays	14,421	1.0	14,421	0.1882	0.0188
2 photon	122782	1.0	122,782	0.0160	0.0160
$q\bar{q}$	169	1.0	169	0.0022	0.0022
sum	321248± 567		327199	2.6843	0.0270

Table 6.1: Summary of signal and background for e-μ events.

6.1.3 $\triangle N_{e\text{-}\mu}$ and $\triangle B_{e\text{-}\mu}$

According to Table 3.3 and 3.4, we summarized the number of e-μ events and their background in the 2nd column in Table 6.1. The 3rd column is the scale factors. For $\tau^- \to \pi^-\pi^0\nu_\tau$, the $\mathcal{B}$ in PDG2011 is $\mathcal{B}(\pi^-\pi^0\nu_\tau)_{PDG} = (25.51 \pm 0.09)\%$, while the value used in TAUOLA is $\mathcal{B}(\pi^-\pi^0\nu_\tau)_{PDG} = 24.71$. In order to use the PDG2011 values as a default, a scale factor of $\mathcal{B}_{PDG}/\mathcal{B}_{TAUOLA} = 1.0324 \pm 0.0036$ is taken into account, where the error comes from the error of $\mathcal{B}$ in PDG.

The 4th column is the corrected number of background. The 5th and 6th column is the fraction of the background contained in the observed number of $e-\mu$ events, i.e. $R_i \equiv N^i_{\rm obs}({\rm cor})/N_{e\text{-}\mu}$ and their errors $\triangle R_i$. The fraction of the background in e-μ events is

$$R = (2.684 \pm 0.027)\%$$

In the error of R, we were taking into account the error of $\mathcal{B}$ ($\triangle\mathcal{B}/\mathcal{B} = 0.35\%$) in PDG'11 for $\pi^-\pi^0$, and we assumed 10 % error for "other τ decays" and 100% error for the two-photon and the $q\bar{q}$ processes. Rather conservative error is assumed for two-photon and $q\bar{q}$ but their contribution is very small. From this table, the systematic errors coming from $\triangle N_{e\text{-}\mu}$ and $\triangle B_{e\text{-}\mu}$ are found to be 0.038% and 0.027%, respectively.

6.1.4 Luminosity

Since we are measuring the branching fraction from the ratio to the e-μ events, the luminosity is only used for the estimation of the background. In general at Belle experiment, Belle luminosity measurement has 1.4% uncertainty. However, the backgrounds ratio for each decay channels is $\sim 20\%$ level so the contribution is about $\sim 0.3\%$. On the other hands, the uncertainty from the luminosity 1.4% should be taken into account for the decay channel $\pi^- K^0_S K^0_S$ and $\pi^- K^0_S K^0_S \pi^0$.

6.2 Uncertainty from background estimation

The background uncertainty for $\pi^- K^0_S \pi^0$ and $K^- K^0_S \pi^0$ are summarized in Table 6.2 respectively. The second and third column is the error of the background coming from the MC statistic and the error of branching fraction. We use the errors of our measurements for $\pi^- K^0_S K^0_S$ and $\pi^- K^0_S K^0_S \pi^0$, and the values in PDG for other modes. For the background estimation, we use the luminosity for normalization. The error of luminosity (1.4%) is much smaller than the errors in $\mathcal{B}$, is then ignored in this calculation. The forth column is for the background fraction $r^i_{back} \equiv N^i_{back}/N_{dat}$ for ith mode. The error of r_{back} include both MC statistic and the $\triangle\mathcal{B}$. Taking the summation of the all background, the net background faction becomes

$$r_{back} = (15.7 \pm 1.94)\%$$

for $\pi^- K^0_S \pi^0$ decay and

$$r_{back} = (16.1 \pm 1.57)\%$$

for $K^- K^0_S \pi^0$ decay. The error of this contribution, however, can be reduced later by using the result from our measurement.

The systematic errors from the τ related background and $q\bar{q}$ contributions are as follows (for $\pi^- K^0_S \pi^0$)

Process	$\pi^- K^0_S \pi^0$			$K^- K^0_S \pi^0$		
	$\triangle N_{BG}$		background frac.	$\triangle N_{BG}$		background frac.
	(stat.)	$\triangle\mathcal{B}(syst.)$	$(r_{back} \pm \triangle r_{back})(\%)$	(stat.)	$\triangle\mathcal{B}(syst.)$	$(r_{back} \pm \triangle r_{back})(\%)$
$\pi^- K^0_S \pi^0$	-	-	-	38	114	13.39 ± 1.45
$K^- K^0_S \pi^0$	53	273	8.09 ± 1.05	-	-	-
$\pi^- K^0 \bar{K}^0$	48	50	2.16 ± 0.26	13	2	0.21 ± 0.16
$\pi^- K^0_S$	65	0	0.02 ± 0.24	22	0	0.06 ± 0.26
$K^- K^0_S$	-	-	-	27	0	0.02 ± 0.33
$\pi^- K^0_S \pi^0 \pi^0$	29	411	1.67 ± 1.55	-	-	-
$\pi^- K^0 \bar{K}^0 \pi^0$	23	35	1.12 ± 0.16	-	-	-
others	27	63	0.79 ± 0.26	13	24	0.97 ± 0.33
BG in tag-side	17	25	0.95 ± 0.11	10	8	0.98 ± 0.16
$q\bar{q}$	22	25	0.78 ± 0.12	9	5	0.41 ± 0.13
two-photon	14	10	0.12 ± 0.07	6	6	0.26 ± 0.10
Sum (quadratic)	515		15.7 ± 1.94	130		16.1 ± 1.57

Table 6.2: Summary of the sources of background uncertainties for $\pi^- K^0_S \pi^0$ and $K^- K^0_S \pi^0$.

$$\frac{\triangle N_{back,\tau}}{N_{dat} - N_{back}} = \triangle r_{back}(1 - r_{back}) = 1.94\%/(1 - 0.157) = 2.29\%$$
$$\frac{\triangle N_{back,q\bar{q}}}{N_{dat} - N_{back}} = \triangle r_{back}(1 - r_{back}) = 0.12\%/(1 - 0.157) = 0.14\% \qquad (6.8)$$

In the same way, same kind of contributions for $K^- K^0_S \pi^0$ are 1.87% for tau only and 0.15% for $q\bar{q}$ background.

6.3 Uncertainty from efficiencies

The signal efficiency consists from the several factors such as 1) tracking efficiency, 2) particle ID efficiency 3) K^0_S efficiency, 4)π^0 efficiency, 5)Trigger efficiency and 6) γ veto etc. Another item to be studied is the efficiency dependency on hadron model, which already shown at Section 4.1.5

6.3.1 Tracking efficiency

The uncertainty of the tracking efficiency can be iestimated by the code probided by the Belle tracking group. For the normal track greater than $\sim>$ 200 MeV, the uncertainty is 1% (0.35%) for the case-A and case-B data, respectively. Since we measure the $\mathcal{B}$ using the ratio to the numebr of $e-\mu$ events, i..e , there is 4 track in the signal and 2 tracks iin the $e-\mu$ events, a total 2% (0.7%) uncertaity is assined for case-A (case-B) data.

6.3.2 Charged pion/Kaon ID efficiency

A correction tables for charged pion and Kaon ID efficnecy is provided by PID group. Using this table, the uncertaity of the poin ID is 0.4% and that of the Kaon ID is 0.8 %.

6.3.3 K^0_S efficiency

A systematic stusdy of the K^0_S efficiency is carried out using the K^0_S sample in the decay chain $D^* \to \pi_s D^0, D^0 \to K^0_S \pi^+\pi^-$, where the number K^0_S yield between very loose selection and the sample selected with a routine `goodKs`. In the loose selection, the K^0_S signal is selected only by an invariant mass without using any V^0 and PID of the tracks. The conclusion for the ratio between data and MC yield is

$$R = S_{data}/S_{MC} = (98.2 \pm 0.4 \pm 0.60)\% \tag{6.9}$$

$$\triangle R = \sqrt{0.4^2 + 0.60^2} = 0.72\% \tag{6.10}$$

This is a factor to be applied to the efficiency determined by the current MC.

The uncertainty mainly due to the track finding efficiency(1.01%) and Ks reconstruction efficiency(1.27%). For the estimation of K^0_S efficiency uncertainty, we studied yhe condition for K^0_S flight length, mass, z_{dist} and dr variables. For the K^0_S systematics study, we applied the particular condition

and identify the difference of two cases. The list of uncertainty is tabulated in 6.3. These uncertainties are summed in quadrature.

variable	$K^0_S fl$	K^0_S mass	K^0_S z_{dist}	K^0_S dr	total
changes	0.27 %	0.85 %	0.6%	0.2%	1.1%

Table 6.3: The additional systematics for K^0_S selection efficiency

However, we applied the additional conditions for K^0_S selection, so that the uncertainty coming from such condition should be estimated. The conditions we used are 1) K^0_S flight length, 2) K^0_S invariant mass, 3) K^0_{Szdist} and 4) K^0_{Sdr}. We evaluate the change of $\mathcal{B}$ using the inclusive process $\tau^- \to K^0_S$ (particles)$^-\nu$ by rejecting an particular condition. The uncertainty from additional condition is found to be 1.14%, so that the net uncertainty for K^0_S selection is

$$\triangle R = \sqrt{0.72^2 + 1.14^2} = 1.35\%$$

6.3.4 π^0 efficiency

The calibration of the π^0 is obtained from the ratio of $\mathcal{B}(\tau \to \pi^-\pi^0\nu_\tau)$, described in Appendix A. The result is

$$R = S_{data}/S_{MC} = (95.7 \pm 1.5)\% \tag{6.11}$$

The uncertainty from π^0 efficiency is 1.55 %.

6.3.5 Dependency on hadron model

The efficiency dependence on hadron model has been studied at Section 4.1.5. The uncertainty is found to be 0.28 (3.42%) for $\pi^- K^0_S \pi^0$ ($K^- K^0_S \pi^0$) mode.

Error Source	$\triangle\mathcal{B}/\mathcal{B}$ (%)		
	$K^0_S(\text{particles})^-$	$\pi^- K^0_S$	$K^- K^0_S$
• Efficiency			
Tracking	2.10	2.10	2.10
Particle ID	1.72	1.79	1.80
K^0_S reconstruction	1.27	1.27	1.27
• Background			
τ other decays, $\triangle\mathcal{B}$	0.16	1.14	2.72
Continuum $q\bar{q}$	0.45	0.22	0.23
• Normalization			
$\mathcal{B}_e$,$\mathcal{B}_\mu$	0.15	0.15	0.15
Background in e-μ cand.	0.03	0.03	0.03
e-μ stat.	0.04	0.04	0.04
• Event Selection			
γ veto	-	0.02	1.8
Total	3.07	3.27	4.85

Table 6.4: Summary of the systematic errors for inclusive decays, $\pi^- K^0_S$, and $K^- K^0_S$

6.3.6 Trigger efficiency

The trigger efficiency for the final selected sample is very close to 100%, so the error is negligible.

6.3.7 Effect from γ veto

In the standard selection, the events are rejected if the extra photon has an energy greater than 200 MeV in order to reject the multi π^0 decay mode. The energy distribution of the extra-photon given in Fig.9 for the sample before the cut shows a good agreement between data and MC. We changed the extra photon energy from 0.2 GeV to 1 GeV and check the effect as to $\triangle\mathcal{B}/\mathcal{B} = 1.2\%$ (1.5%) for $\pi^- K^0_S \pi^0$ ($K^- K^0_S \pi^0$)

6.4 Summary of systematic uncertainty

For the estimation of systematic uncertainty, we considered following items : 1) Efficiency 2) Background estimation 3) Normalization. Each item consist of several sources.

For $\pi^- K^0_S$ and $K^- K^0_S$ The uncertainty for signal efficiency is found to be 3.0% which consist of track finding (2.1%), particle ID (1.72%) and K^0_S reconstruction (1.27%). Especially for the K^0_S systematic uncertainty, we studied for additional cut systematics. For the estimation of uncertainty for background, we regard the uncertainty from τ decay branching fractions to be 10% and the normalization for continuum background to be 30% so that the uncertainty for τ and non-τ background are found to be 0.16% and 0.45%, respectively. And the total uncertainty for the background estimation is found to be 0.48%. The uncertainty for the normalization is discussed in the previous section and given to be 0.45%. The total systematic uncertainty is found to be 3.07% for lepton tagging method. The list of systematic uncertainty is given in Table 6.4

For $\pi^- K^0_S \pi^0$ and $K^- K^0_S \pi^0$ The source and the size of systematic uncertainties are summarized in Table 6.5 The uncertainty has been found on tracking(2.10%), particle ID(1.8%), reconstruction of K^0_S(1.35%) and π^0(1.55%), the background estimation(2.3%), normalization(0.15%) and the decay mode (0.28%) for $\pi^- K^0_S \pi^0$ events. For $K^- K^0_S \pi^0$ event, most of uncertainties have identical/similar value except for the hadronic decay mode(3.42%) and the background estimation(1.87%). The total uncertainty for $\pi^- K^0_S \pi^0$ and $K^- K^0_S \pi^0$ are 4.24% and 5.36%, respectively.

For $\pi^- K^0_S K^0_S$ and $\pi^- K^0_S K^0_S \pi^0$ We estimate the systematic uncertainty for several items, and some of which are already presented in the previous section. The uncertainty for signal efficiency is found to be 7.47% which is consist

Error Source	$\triangle\mathcal{B}/\mathcal{B}$ (%)	
	$\pi^- K^0_S \pi^0$	$K^- K^0_S \pi^0$
• Efficiency		
Tracking	2.10	2.10
Electron/muon ID	1.63	1.63
Charged pion/Kaon ID	0.40	0.40
Ks reconstruction	1.35	1.35
π^0 reconstruction	1.55	1.55
Hadron decay model	0.28	3.42
• Background		
τ other decays, $\triangle\mathcal{B}$	2.29	1.87
Continuum $q\bar{q}$	0.14	0.15
•Normalization		
$\mathcal{B}_e$,$\mathcal{B}_\mu$	0.15	0.15
Background in e-μ cand.	0.03	0.03
$e-\mu$ stat.	0.04	0.04
•Event Selection		
γ veto	1.2	1.5
Total	4.24	5.36

Table 6.5: Summary of the systematic errors for $\pi^- K^0_S \pi^0$ and $K^- K^0_S \pi^0$

Error Source	$\triangle\mathcal{B}/\mathcal{B}$ (%)	
	$\pi^- K^0_S K^0_S$	$\pi^- K^0_S K^0_S \pi^0$
• Efficiency		
Tracking	6.20	6.20
Particle ID	2.24	2.23
K^0_S reconstruction	1.80	1.80
π^0 reconstruction	-	1.57
• Background		
τ other decays, $\triangle\mathcal{B}$	1.99	6.6
Continuum $q\bar{q}$	0.98	3.8
• Normalization		
Luminosity	1.3	1.3
$\triangle\sigma_{\tau\tau}$	0.33	0.33
• Event Selection		
γ veto	5.86	5.33
Total	9.35	14.5

Table 6.6: Summary of the systematic errors for $\pi^- K^0_S K^0_S$ and $\pi^- K^0_S K^0_S \pi^0$

of track finding(6.2%), particle ID (2.24%), K^0_S reconstruction(1.8%) and π^0 reconstruction(1.57%). For the uncertainty from background, we regard the uncertainty from τ decay branching fractions to be 10%, because the major τ background is $\pi^- K^0_S K^0_S$ whose $\mathcal{B}$ is measured with 10% error in our measurement. As the continuum distribution is well matched to the data in the mass region over 2 GeV, the uncertainty from the continuum background is expected to be 10% at most. The total uncertainty from $\pi^- K^0_S K^0_S$ and continuum background are found to be 6.6% and 3.8%, respectively, and the total uncertainty for the background estimation is found to be 7.4%. The uncertainty for the normalization is a sum of the error of the luminosity ($\triangle\mathcal{L} = 1.3\%$) and the τ cross-section ($\triangle\sigma_{\tau\tau} = 0.33\%$). The total systematic uncertainty is found to be 14.5% for all-tag method. The list of systematic uncertainty is given in Table 6.6

Chapter 7

Conclusions

The CKM matrix element, $|V_{us}|$, can be determined from hadronic τ lepton decays and, independently, from semi-leptonic kaon decays. The latest fit results from HFAG-TAU report that $|V_{us}|$ obtained from hadronic τ decays is not consistent with that obtained from the CKM unitarity constraint. In order to confirm the unitarity of CKM matrix elements, it is necessary to measure the branching fractions for hadronic τ decays to strangeness = 1 final state with better precision. The Belle experiment is now in a good situation to contribute to tests of CKM unitarity with high precision.

We have measured the branching fractions for inclusive K^0_S mode in τ decays for six exclusive modes: $\pi^- K^0_S \nu_\tau$, $K^- K^0_S \nu_\tau$, $K^- K^0_S \pi^0 \nu_\tau$ and $\pi^- K^0_S \pi^0 \nu_\tau$, $\pi^- K^0_S K^0_S \nu$ and $\pi^- K^0_S K^0_S \pi^0 \nu_\tau$. These events are selected using different tagging methods that depend on the size of the expected branching fractions; if the branching fraction is larger than the order of 10^{-4}, these are enough events selected with only lepton tags, otherwise the events are tagged by any 1-prong decay.

For the precision measurements, we studied the efficiencies and their corrections using the data and MC samples. Discrepencies and fake rates associated with particle identification are corrected by using factors deduced from

$D^{*+} \to D^0\pi^+$ and $D^0 \to K^-\pi^+$ samples. We also use results from extensive studies of K^0_S and π^0 efficiencies using $D^0 \to K^0_S\pi^+\pi^-$ and $\tau^- \to \pi^-\pi^0\nu_\tau$ samples, respectively.

The backgrounds are also studied throughly by comparing the MC samples generated by TAUOLA with the branching fraction tables containing nominal numbers from the Particle Data Group. However, the branching fractions listed by the PDG are found to give a poor description of some τ decays to multiple hadron final states; the background from $\tau^- \to \pi^- K^0_S K^0_S \pi^0 \nu_\tau$ decay make it difficult to estimate background in the low mass region of $\tau^- \to \pi^- K^0_S \pi^0 \nu_\tau$. In addition, the MC-determined continuum event contribution to non-tau backgrounds does not describe the background for τ decays into small number of hadrons very well. These problems are resolved by applying several corrections to the MC samples that are derived from our measurements. For background estimates for the decays involving π^0s, we use the mass sideband of π^0 and subtract the background successfully.

The systematic uncertainties crucial to our branching fractions measurements; those have been checked for the efficiency, backgrounds and the normalization methods, the two decay modes, $\tau^- \to \pi^- K^0_S \pi^0 \nu_\tau$ and $\tau^- \to K^- K^0_S \pi^0 \nu_\tau$,may suffer from the efficiency estimate deficiencies due to a discrepancy of the invarint mass distributions. The efficiency weighted invariant mass distribution does not show any discrepancy between the TAUOLA and Phase space decay models.

According to these studies, we determine the branching fractions with systematic uncertainties summarized in Table 7. Figure 7.1 shows a comparision between our measurements and other experimental results. Our measurements are consistent to the averages but with substantially precision improved analysis. The branching fraction for $\tau^- \to \pi^- K^0_S \nu_\tau$ was measured in an independent Belle analysis [90] to be $\mathcal{B}(\tau^- \to \pi^- K^0_S \nu_\tau) = (4.03 \pm 0.02 \pm 0.13) \times 10^{-3}$, which is consistent with this work. We also provide the branching fractions for inclusive K^0_S decays that provide constraints on

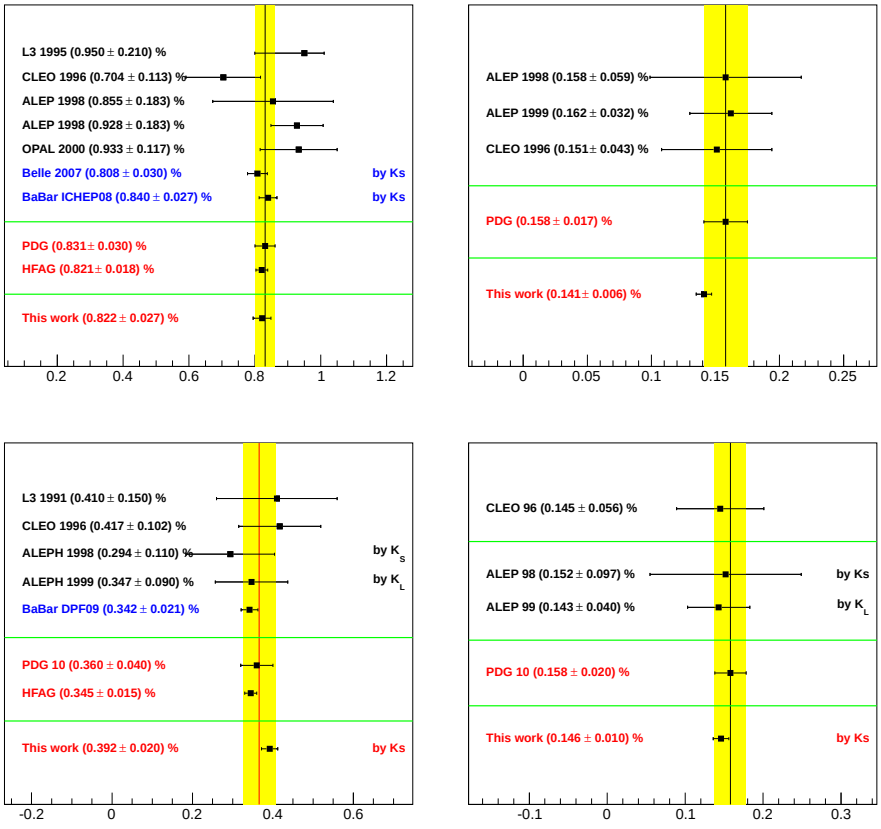

Figure 7.1: Comparision of the branching fractions measured here with previous results.

the predictions for other unmeasrued mode involving a K^0_S: $\pi^- K^0_S 2\pi^0 \nu_\tau$ and $K^0_S h^- h^+ h^- \nu_\tau$ We observe the $\tau^- \to \pi^- K^0_S K^0_S \pi^0 \nu_\tau$ decay for the first time and find a 4.8σ peak in the $K^0_S K^0_S \pi^0$ mass distributions consistent with coming from the $f_1(1285)$, which is the first observation of $\tau^- \to \pi^- f_1(1285)\nu_\tau$ in this channel. The branching fraction for the decay chain $\tau^- \to f_1(1285)\pi^- \nu_\tau$ and $f_1(1285) \to K^0_S K^0_S \pi^0$ is $(1.07 \pm 0.23 \pm 0.16) \times 10^{-5}$

Decay mode	$\mathcal{B}$ ($\times 10^{-3}$)	$\mathcal{B}_{lum}$ ($\times 10^{-3}$)
K^0_S (particles)$^-\nu$	$9.14 \pm 0.01 \pm 0.28$	$9.10 \pm 0.01 \pm 0.46$
$\pi^- K^0_S \nu$	$4.11 \pm 0.01 \pm 0.13$	$4.09 \pm 0.01 \pm 0.20$
$K^- K^0_S \nu$	$0.72 \pm 0.01 \pm 0.03$	$0.70 \pm 0.01 \pm 0.04$
$\pi^- K^0_S \pi^0 \nu$	$1.96 \pm 0.02 \pm 0.08$	$1.95 \pm 0.02 \pm 0.11$
$K^- K^0_S \pi^0 \nu$	$0.73 \pm 0.01 \pm 0.04$	$0.73 \pm 0.01 \pm 0.05$
	$\mathcal{B}$ ($\times 10^{-4}$)	$\mathcal{B}_{lum}$ ($\times 10^{-4}$)
$\pi^- K^0_S K^0_S \nu$	N/A	$2.41 \pm 0.04 \pm 0.23$
$\pi^- K^0_S K^0_S \pi^0 \nu$	N/A	$0.205 \pm 0.023 \pm 0.029$

Table 7.1: The measured branching fraction results. $\mathcal{B}$ is normalized to N(e-μ) and $\mathcal{B}_{lum}$ is normalized to the luminosity.

Bibliography

[1] J. Erler, Rev. Mex. Fis **50**, 200 (2004)

[2] E. Follana, C. T. H. Davies, G. P. Lepage and J. Shingemitsu, Phys. Rev. Lett. **100**, 062002 (2008)

[3] M. A. Shifman, A. L. Vainshtein, and V. I. Zakharov, Nucl. Phys. B **147**, 385 (1979a)

[4] E. Braaten, C. S. Li, Phys. Rev. D **41**, 3888 (1990)

[5] E. Braaten, S. Narison, and A. Pich, Nucl. Phys. B **373**, 581 (1992)

[6] K. G. Chetyrkin, and A. Kwiatkowski, Z. Phys. C **59**, 525 (1993)

[7] G. Abbiendi *et al.*, (OPAL Collaboration) Phys. Lett. B **447**, 134 (1999)

[8] G. Abbiendi *et al.*, (OPAL Collaboration) Phys. Lett. B **551**, 35 (2003)

[9] P. Abreu *et al.*, (DELPHI Collaboration) Eur. Phys. J. C **10**, 201 (1999)

[10] M. Acciarri *et al.*, (L3 Collaboration) Phys. Lett. B **507**, 47 (2001)

[11] A. Anastassov *et al.*, (CLEO Collaboration) Phys. Rev. D **55**, 2559 (1997)

[12] S. Schael *et al.*, (The ALEPH Collaboration) Phys. Rep. **421**, 191 (2005)

[13] R. Barate *et al.*, (The ALEPH Collaboration) Z. Phys. C **74**, 263 (1997a)

[14] R. Barate *et al.*, (The ALEPH Collaboration) Z. Phys. C **76**, 15 (1997b)

[15] R. Barate *et al.*, (The ALEPH Collaboration) Eur. Phys. J. C **1**, 65 (1998a)

[16] R. Barate *et al.*, (The ALEPH Collaboration) Eur. Phys. J. C **4**, 29 (1998b)

[17] R. Barate *et al.*, (The ALEPH Collaboration) Eur. Phys. J. C **4**, 409 (1998c)

[18] R. Barate *et al.*, (The ALEPH Collaboration) Eur. Phys. J. C **10**, 1 (1999a)

[19] R. Barate *et al.*, (The ALEPH Collaboration) Eur. Phys. J. C **11**, 599 (1999b)

[20] Y. S. Tsai, Phys. Rev. D **4**, 2821 (1971), erratum, Phys. Rev. D **13**, 771 (1976)

[21] R. P. Feynman and M. Gell-Mann, Phys. Rev. **109**, 193 (1958)

[22] R. Fischer, J. Wess, Z. Phys. C **3**, 313 (1980)

[23] J. H. Kuhn, A. Santamaria, Z. Phys. C **48**, 445 (1990)

[24] R. Decker, E. Mirkes, R. Sauer, Z. Was, Z. Phys. C **58**, 445 (1993)

[25] Markus Finkemeier, Erwin Mirkes, 69 **243**, 1996 (

[26] KUHN1992 J. H. Kuhn, E. Mirkes, Z. Phys. C **56**, 661 (1992)

[27] S. I. Eidelman and V. N. Ivanchenko, Phys. Lett. B **257**, 437 (1991)

[28] J. Wess, B. Zumino, Phys. Lett. B **37**, 95 (1971)

[29] E. Witten, Nucl. Phys. B **223**, 422 (1983)

[30] G. Kramer, W. F. Palmer, S. Pinsky, Phys. Rev. D **30**, 89 (1984)

[31] G. Kramer, W. F. Palmer, Z. Phys. C **25**, 195 (1984)

[32] S. L. Glashow, Nucl. Phys. **22**, 279 (1961) A. Salam Phys. Rev. **127**, 331 (1962) S. Weinberg Phys. Rev. Lett. **19**, 1264 (1967)

[33] N. Cabibbo, Phys. Rev. Lett. **10**, 531 (1963)

[34] M. Kobayashi and T. Maskawa, Prog. Theor. Phys. **49**, 652 (1973)

[35] L. Wolfenstein, Phys. Rev. Lett. **51**, 1945 (1983)

[36] J. C. Hardy and I. S. Towner, Phys. Rev. C **70**, 05502 (2009)

[37] D. Asner *et al.*, "Averages of b-hadron, c-hadron, and tau-lepton Properties", [arXiv:1010.1589v3]

[38] H. Baer and R. N. Cahn, "Cross-section fromulae for specific processes", Phys. Rev. D **86**, 010001 (2012)

[39] J. Beringer *et al.*, (Particle Data Group), Phys. Rev. D **86**, 010001 (2012)

[40] E. Blucher and W. J. Marciano, "Vud, Vus, the Cabibbo Angle and CKM Unitarity," J. Phys. G **37**, 075021 (2010)

[41] M. Antonelli *et al.*, [The FlaviaNet Kaon Working Group], arXiv:0801.1817; see also http://www.lnf.infn.it/wg/vus.

[42] N. Cabibbo *et al.*, Ann. Rev. Nucl. and Part. Sci. 53, 39 (2003) [hep-ph/0307298]

[43] R. Kowalewski and T. Mannel, "Determination of Vcb and Vub," J. Phys. G **37**, 075021 (2010)

[44] L. Widhalm *et al.*, Phys. Rev. Lett. **100**, 241801 (2008)

[45] J. P. Alexander *et al.*, Phys. Rev. D **79**, 052001 (2009)

[46] B. Aubert *et al.*, Phys. Rev. Lett. **98**, 141801 (2007)

[47] P. U. E. Onyisi *et al.*, Phys. Rev. D **79**, 052002 (2009)

[48] V. M. Abazov *et al.*, Phys. Rev. Lett. **103**, 092001 (2009) [arXiv:0903.0850]

[49] T. Aaltonen *et al.*, (CDF Collab.), Phys. Rev. Lett. **103**, 092002 (2009) [arXiv:0903.0885] T. Aaltonen *et al.*, (CDF Collab.), [arXiv:1001.4577]

[50] T. E. Coan, *et al.*, Phys. Rev. Lett. **92**, 232001 (2004)

[51] D. M. Asner *et al.*, Phys. Rev. D **62**, 072006 (2000)

[52] E. Gamiz, M .Jamin, A. Pich, J. Prades and F. Schwab Phys. Rev. Lett. **94**, 011803 (2005)

[53] E. Gamiz, M .Jamin, A. Pich, J. Prades and F. Schwab Nucl. Phys. B. Proc. Suppl. **169**, 85 (2007)

[54] Y. Miyazaki *et al.*, Submitted to Physics Letters B, arXiv:1206.5595

[55] Y. Miyazaki *et al.*, Phys. Lett. B **699**, 251 (2011)

[56] M. Bischofberger *et al.*, Phys. Rev. Lett. **107**, 131801 (2011)

[57] Y. Miyazaki *et al.*, Phys. Lett. B **692**, 4 (2010)

[58] S. W. Herb *et al.*, Phys. Rev. Lett. **39**, 252 (1977)

[59] A. B. Carter and A. I. Sanda, Phys. Rev. Lett. **45**, 952 (1980)

[60] A. B. Carter and A. I. Sanda, Phys. Rev. D **23**, 1567 (1981)

[61] I. I. Bigi and A. I. Sanda, Nucl. Phys. B **193**, 85 (1981)

[62] T. E. Browder and K. Honscheid, Prog. Part. Nucl. Phys. **35**, 81 (1995)

[63] Accelerator Design of the KEK B-Factory, KEK Report, 90-24 (1991)

[64] KEK Report 95-18, (1995)

[65] Y. Funakoshi *et al.*, Proceedings of EPAC 2004, Lucerne, Switzerland.

[66] H. Sagawa *et al.*, Nucl. Instrum. Meth. A **453**, 259 (2000)

[67] A. Abashian *et al.*, (The Belle Collaboration) Nucl. Instrum. Meth. A **491**, 69 (2002)

[68] M. Hazumi *et al.*, (The Belle Collaboration) Nucl. Instrum. Meth. A **379**, 390 (1996)

[69] G. Alimonti *et al.*, (The Belle Collaboration) Nucl. Instrum. Meth. A **453**, 71 (2000)

[70] R. Abe *et al.*, (The Belle Collaboration) Nucl. Instrum. Meth. A **535**, 379 (2004)

[71] S. Uno *et al.*, (The Belle Collaboration) Nucl. Instrum. Meth. A **379**, 421 (1996)

[72] H. Hirano, *et al.*, (The Belle Collaboration) Nucl. Instrum. Meth. A **455**, 294 (2000)

[73] T. Iijima, *et al.*, (The Belle Collaboration) Nucl. Instrum. Meth. A **453**, 321 (2000)

[74] R. Suda, *et al.*, (The Belle Collaboration) Nucl. Instrum. Meth. A **406**, 213 (1998)

[75] H. Kichimi, *et al.*, Nucl. Instrum. Meth. A **325**, 451 (1993)

[76] H. Kichimi, *et al.*, (The Belle Collaboration) Nucl. Instrum. Meth. A **453**, 315 (2000)

[77] Belle Technical Design Report, KEK Report, 95-1 (1995)

[78] KEKB B-Factory Design Report, KEK Report, 95-7 (1995)

[79] Y. Ohshima, *et al.*, Nucl. Instrum. Meth. A **380**, 517 (1996)

[80] B. G. Cheon *et al.*, (The Belle Collaboration) Nucl. Instrum. Meth. A **494**, 548 (2002)

[81] Y. Ushiroda *et al.*, (The Belle Collaboration) Nucl. Instrum. Meth. A **438**, 460 (1999)

[82] M. Z. Wang *et al.*, (The Belle Collaboration) Nucl. Instrum. Meth. A **455**, 319 (2000)

[83] I.Adachi, R.Itoh, N.Katayama, T.Tsukamoto, T.Hibino, M.Yokoyama, L.Hinz and F.Ronga, Talk from the 2003 Computing in High Energy and Nuclear Physics (CHEP03), La Jolla, Ca, USA, March 2003; arXiv:hep-ex/0306120

[84] I. Adachi *et al.*, Nucl. Instrum. Meth. A **534**, 53 (2004)

[85] T. Higuchi *et al.*, Talk from the 2003 Computing in High Energy and Nuclear Physics (CHEP03), La Jolla, Ca, USA, March 2003; arXiv:hep-ex/0305088

[86] S. Jadach, B. F. L. Ward and Z. Was, Comp. Phys. Commun. **130**, 260 (2000)

[87] S. Jadach, J. H. Kuhn and Z. Was, Comp. Phys. Commun. **64**, 275 (1991)

[88] S. Jadach, J. H. Kuhn, R. Decker and Z. Was, Comp. Phys. Commun. **76**, 361 (1993)

[89] S. Banerjee, B. Pietrzyk, J. M. Roney and Z. Was, Phys. Rev. D **77**, 054012 (2008)

[90] D. Epifanov *et al.*, (Belle Collaboration), Phys. Lett. B **654**, 65 (2007)

Appendix A

π^0 efficiency study using $\tau^- \to \pi^-\pi^0\nu_\tau$

A.1 Introduction

In many process involving π^0, the estimation of the difference between data and MC bring a great or sometimes a serious issue on the analysis. Usually the difference is a level of 5% sometimes even more 10% depending on their analysis mode. π^0 efficiency can be studied by using some dedicated decay channels($\eta \to 3\pi^0$, $\eta \to \gamma\gamma$). In this study we used $\tau^- \to \pi^-\pi^0\nu_\tau$, because in this process, π^0 can be obtained with very clean and high statistics. Furthermore, the branching ratio for this channel is well known with good precision ($\delta B/B = 0.3\%$), so that it can be used to estimate the deviation between MC and data for π^0 efficiency, which is our goal.

The method of obtaining the π^0 efficiency correction start from measuring the branching ratio with reasonable precision. The branching ratio formula we used is :

$$\mathcal{B}(\tau \to \text{sig}) = \frac{N_{\text{sig}}}{\epsilon_{\text{sig}}} \frac{\epsilon_{e\text{-}\mu}}{N_{e\text{-}\mu}} \frac{\mathcal{B}(\tau \to e\bar{\nu}\nu)\mathcal{B}(\tau \to \mu\bar{\nu}\nu)}{\mathcal{B}(\tau \to l\bar{\nu}\nu)} \tag{A.1}$$

where $\epsilon_{e\text{-}\mu}$ and ϵ_{sig} are the efficiency of selection of e-μ pairs and our signal events, and $N_{e\text{-}\mu}$ and N_{sig} are the number of events for e-μ pairs and signal

events, respectively. This e-μ normalization method can reduce some systematic errors, e.g., the tracking efficiency, the particle identification efficiency, and so forth.

Before introducing the method, we want to define the kind of event with respect to the configuration as follows:

- *single* $\pi^-\pi^0$: an event consist of $\tau^- \to \pi^-\pi^0\nu_\tau$ and $\tau^+ \to l^+\bar{\nu}\nu$ or C.C
- *double* $\pi^-\pi^0$: an event consist of $\tau^- \to \pi^-\pi^0\nu_\tau$ and $\tau^+ \to \pi^+\pi^0\nu_\tau$ or C.C

Our goal is to obtain the Data/MC ratio for π^0 efficiency which is supposed to be used as a correction factor, R, for individual analysis. For *single* $\pi^-\pi^0$ events, the number of selected events can be expressed as follows :

$$N^{data}(\pi\pi^0|\ l\ ) = 2\ N^{data}_{\tau\tau}\ \epsilon^{tr}_{\pi^0}\ \epsilon^{other}\ \mathcal{B}_l\mathcal{B}_{\pi\pi^0} \tag{A.2}$$

where $\epsilon^{tr}_{\pi^0}$ is the π^0 efficiency for true which is one of our matter of concern. ϵ^{other} is the efficiency that excluding π^0 efficiency. $\mathcal{B}_l$ and $\mathcal{B}_{\pi\pi^0}$ stand for the branching fraction for leptonic and $\pi^-\pi^0$ decay of τ. $N^{data}_{\tau\tau}$ is the number of τ pairs which is measured in this analysis by using e-μ events.

$$N^{data}_{\tau\tau} = \frac{N(e|\mu)}{\epsilon_{e,\mu}\ \mathcal{B}_e\ \mathcal{B}_\mu} \tag{A.3}$$

where $N(e|\mu)$ is the number of event which one τ goes to electron decay and the other τ decays into muon. The number of *single* $\pi^-\pi^0$ events for MC can be written as follow :

$$N^{MC,obs}(\pi\pi^0|\ l\ ) = \epsilon^{MC}_{\pi^0}\ \epsilon^{other}\ N^{MC,gen}(\pi\pi^0|\ l\ ) \tag{A.4}$$

Using two align, A.2 and A.4, we can obtain

$$N^{data}(\pi\pi^0|\ l\ ) = \frac{\epsilon^{tr}_{\pi^0}}{\epsilon^{MC}_{\pi^0}} 2\ N^{data}_{\tau\tau}\ \epsilon_{TOT}\ \mathcal{B}_l\mathcal{B}_{\pi\pi^0} \tag{A.5}$$

where,

$$\epsilon_{TOT} = \frac{N^{MC,obs}(\pi\pi^0|\ l\ )}{N^{MC,gen}(\pi\pi^0|\ l\ )}$$

ϵ_{TOT} means the signal MC efficiency without π^0 efficiency. From the Eq.A.5, one can obtain R_{single} as :

$$R_{single} = \frac{\epsilon^{true}_{\pi^0}}{\epsilon^{MC}_{\pi^0}} = \frac{N^{data}(\pi\pi^0|\ l\ )}{2\ N^{data}_{\tau\tau}\ \mathcal{B}_l\ \epsilon_{TOT}\ \mathcal{B}_{\pi\pi^0}} = \frac{\mathcal{B}_{single}}{\mathcal{B}_{\pi\pi^0}} \tag{A.6}$$

where,

$$\mathcal{B}_{single} = \frac{N^{data}(\pi\pi^0|\ l\ )}{2\ N^{data}_{\tau\tau}\ \mathcal{B}_l\ \epsilon_{TOT}} \tag{A.7}$$

In case of *double* $\pi^-\pi^0$ events, the number of selected events can be written as follow :

$$N^{data}(\pi\pi^0|\pi\pi^0) = N^{data}_{\tau\tau}\ (\epsilon^{tr}_{\pi^0})^2\ \epsilon^{other}\ (\mathcal{B}_{\pi\pi^0})^2 \tag{A.8}$$

As same as Eq.A.4, one can be express the $N^{obs}(\pi\pi^0|\pi\pi^0)$ for MC as :

$$N^{MC,obs}(\pi\pi^0|\pi\pi^0) = (\epsilon^{MC}_{\pi^0})^2\ \epsilon^{other}\ N^{MC,gen}(\pi\pi^0|\pi\pi^0) \tag{A.9}$$

Using the Eq.A.8 and A.9 to eliminate ϵ^{other}, then one can obtain,

$$N^{data}(\pi\pi^0|\pi\pi^0) = \left(\frac{\epsilon^{true}_{\pi^0}}{\epsilon^{MC}_{\pi^0}}\right)^2\ \epsilon^{TOT} N^{data}_{\tau\tau}\ (\mathcal{B}_{\pi\pi^0})^2 \tag{A.10}$$

where,

$$\epsilon_{TOT} = \frac{N^{MC,obs}(\pi\pi^0|\pi\pi^0)}{N^{MC,gen}(\pi\pi^0|\pi\pi^0)}$$

which is the signal MC efficiency except for π^0 efficiency. Then one can find the square of efficiency ratio, which is defined as R_{double} :

$$R_{double} = \left(\frac{\epsilon^{true}_{\pi^0}}{\epsilon^{MC}_{\pi^0}}\right)^2 = \frac{N^{data}(\pi\pi^0|\pi\pi^0)}{N^{data}_{\tau\tau}\ \epsilon_{TOT}\ (\mathcal{B}_{\pi\pi^0})^2} = \frac{\mathcal{B}_{double}}{(\mathcal{B}_{\pi\pi^0})^2} \tag{A.11}$$

where,

$$\mathcal{B}_{double} = \frac{N^{data}(\pi\pi^0|\pi\pi^0)}{N^{data}_{\tau\tau}\ \epsilon_{TOT}} \tag{A.12}$$

Thus, if we get a square root of R_{double} then $R_{single} = \sqrt{R_{double}}$ shoud be followed. However, this value is still dependent on PDG value. Using R_{single} and R_{double}, we can obtain $R_{genuine}$ which is independent to the PDG value.

$$R_{genuine} = \frac{R_{double}}{R_{single}} = \frac{\epsilon^{true}_{\pi^0}}{\epsilon^{MC}_{\pi^0}} = \frac{N(\pi\pi^0|l)}{N(\pi\pi^0|\pi\pi^0)}\ \frac{\epsilon_{TOT}(\pi\pi^0|\pi\pi^0)}{\epsilon_{TOT}(\pi\pi^0|l)}\ \frac{\mathcal{B}_{\pi\pi^0}}{2\ \mathcal{B}_l} \tag{A.13}$$

The detailed descriptions for the selection of e-μ events and its branching ratio are presented in Sec. 3.3

A.2 Event selection

A.2.1 Data sample

In this analysis we used 669 fb^{-1} of data.

A.2.2 Selection Criteria

The primary selection of τ pair events is described in Sec. 3.1. To obtain good τ samples the events have to be purified, we applied additional condition on the data as described in Table A.1.

Before the event selection, we define good tracks and gammas. The definition of a good track is the one satisfied the conditions: $P_T > 0.1$ GeV/c , |dr| $\leq$ 1cm and |dz| $\leq$ 3cm, where dr and dz are the impact parameter and P_T is the track transverse momentum. We require two such tracks. For the good gamma, $E_{cluster} > 80$ MeV in the barrel region ($34° \leq \theta \leq 128°$) and $E_{cluster} > 100$ MeV in the endcap region ($24° \leq \theta \leq 30.5$ ° and $128° \leq \theta \leq$ 138 °).

Condition	Description
$N_{track} = 2$	Number of tracks
$E_{ECL} < 9$ GeV	Sum of Energy of ECL clusters
1 GeV $< \lvert p_{miss}\rvert < 7$ GeV	Missing energy
$30^\circ < \theta_{miss} < 150^\circ$	Missing angle
$\lvert\text{thrust}\rvert > 0.9$	Magnitude of thrust
$\lvert Q_{sum}\rvert = 0$	sum of charge
1 track on each side	Hemisphere
EID > 0.9 , MuID > 0.9	Lepton ID on tag side
$\pi\lvert K$ ID > 0.3	Particle ID on signal side
$E_\gamma^{extra} < 0.2$ GeV	The highest energy of extra γ

Table A.1: $\tau^- \to \pi^-\pi^0\nu_\tau$ event selection criteria

The sum of energies deposited in the ECL clusters is $E_{ECL} < 9$ GeV which suppresses some Bhabha events.

The missing momentum, $p^2_{miss} = (p_{init} - \Sigma p_{track} - \Sigma p_\gamma)^2$, and its polar angle ($\theta_{miss}$) with respect to the beam direction in the CM frame is an efficient variable for the rejection of two-photon and Bhabha backgrounds, where p is a 4-momentum, p_{init} is the initial energy of the e^+e^- collision in the CM frame. In the missing momentum calculation, all good tracks and gammas are included. The missing momentum condition is 1 GeV $< p_{miss} < 7$ GeV and $30^\circ < \theta_{miss} < 150^\circ$. τ pair events can be divided into two hemispheres using the thrust axis in the CM frame. For this mode we require one track for the tag side and one track for the signal side. We check a sign of the charge of each hemisphere and constrain a sum of the two charges to zero.

Since the lepton tagging method is to be applied, PID condition should be given to both tracks, one for lepton and the other for pion. We set 0.9 as a minimum for electron or muon ID and 0.3 for pion ID ($\mathcal{L}(\pi|K) > 0.3$). In case of *double* $\pi\pi^0$ event, we given the same pion ID condition on both side.

The π^0 is reconstructed by two gamma whose energy is over 0.08 GeV (0.1 GeV) for Barrel (Endcap). The mass of two gamma can be re-normalized

	N_{data}	N_{BG}	Eff(%)
svd1(caseA)	4389873	641869	15.09
svd2(caseA)	14284918	2116510	14.56
svd2(caseB)	4917431	718726	14.88

Table A.2: The number of *single* $\pi\pi^0$ events for data (1st column) and background(2nd column). The 3rd column shows the estimated efficiency using signal MC with given correction for π and leptonic track

by the resolution of itself, depending on the size of the momentum, which is defined as $S_{\gamma\gamma}$. After π^0 reconstruction, we restrict the number of remaining γ ($N_\gamma < 2$) and its energy $E_\gamma < 0.2GeV$ for each hemisphere to suppress other background processes of multiple π^0.

A.2.3 The general features of $\tau^- \to \pi\pi^0\nu_\tau$ candidates

The total number of $\pi\pi^0$ candidates are in Table A.2. For the efficiency estimation using signal MC, we applied PID corrections given by PID group with respect to the momentum and angle event by event basis. The background ratio is found to be around $14.6 \sim 14.8$ % of total selected events, most of them are coming from τ decays, especially due to the process $\tau^- \to \pi^-\pi^0\pi^0\nu_\tau$. The contribution from non-τ decays are less than 1% in total(See Table.A.3). We provide several figures for the invariant mass of $\pi\pi^0$, π^0 momentum and angular distribution and $S_{\gamma\gamma}$ (See Figure A.1,A.2 and A.3). The distribution for each given variables for Data and MC are very well matched to each other.

BG channel	svd1-A (%)	svd2-A (%)	svd2-B (%)
$\pi^-\pi^0\pi^0$	8.92	8.84	8.54
$K^-\pi^0$	0.26	0.27	0.27
π^-	1.03	1.18	1.34
wrong-tagged	1.84	1.85	1.90
other τ	1.68	1.75	1.67
2-γ	0.86	0.89	0.87
qq	0.02	0.02	0.02
Total	14.62	14.81	14.61

Table A.3: The ratio of background for *single* $\pi\pi^0$ events

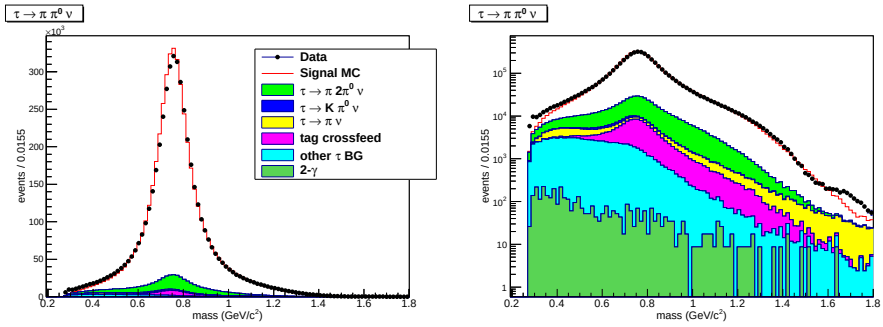

Figure A.1: The mass distribution of $\tau^- \to \pi\pi^0\nu_\tau$ with linear (log) scaled. The dotted histogram is real data and the red lined histogram is the signal MC. Other color shaded histograms are backgrounds estimated by MC. The background and signal MC histograms are accumulated and scaled by luminosity. Most of backgrounds are fed down from τ events, so the proportions of the non-τ backgrounds (2-γ or qq) in selected events are very negligible.

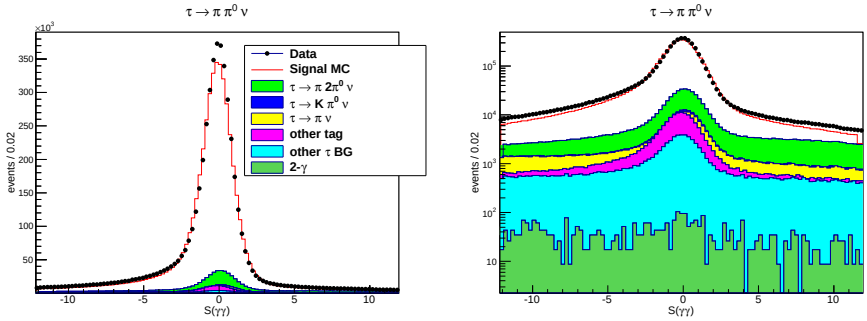

Figure A.2: S($\gamma\gamma$) distribution of $\tau^- \to \pi\pi^0\nu_\tau$ with linear (log) scaled. The dotted histogram is real data and the red lined histogram is the signal MC. Other color shaded histograms are backgrounds estimated by MC. The background and signal MC histograms are accumulated and scaled by luminosity.

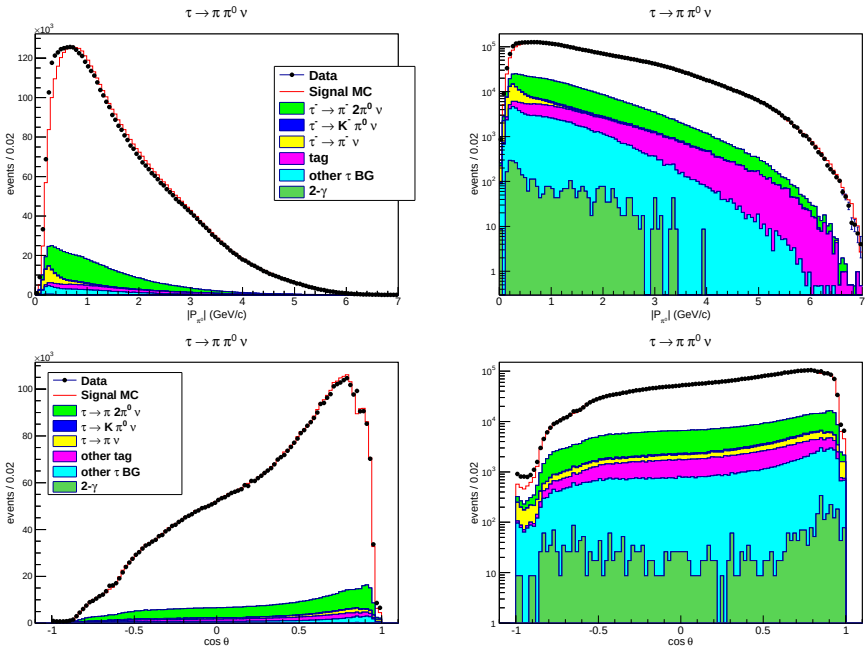

Figure A.3: The π^0 momentum ($\cos\theta$) distribution of $\tau^- \to \pi\pi^0\nu_\tau$ with linear (log) scaled. The dotted histogram is real data and the red lined histogram is the signal MC. Other color shaded histograms are backgrounds estimated by MC. The background and signal MC histograms are accumulated and scaled by luminosity.

A.3 Branching ratios and Efficiency corrections

A.3.1 For *single* $\pi\pi^0$ event

We followed two different estimation method for the number of π^0s. The first one is a fit method using logarithmic gaussian distribution defined by below:

$$dW = \exp\left(-\frac{\ln^2(1-\eta(E-E_p)/\sigma)}{2\sigma_0^2} - \frac{\sigma_0^2}{2}\right)\frac{\eta dE}{\sqrt{2\pi}\sigma\sigma_0} \tag{A.14}$$

where E_p is a parameter for peak position, η is an asymmetry parameter and other parameters will be given later. Using the logarithmic gaussian as signal model($\mathcal{S}$) and linear function as background model($\mathcal{B}$), we can construct a probability distribution function(PDF) :

$$\mathcal{F} = \mathcal{N}[f\mathcal{S} + (1-f)\mathcal{B}] \tag{A.15}$$

where f is relative ratio of $\mathcal{S}$ and $\mathcal{B}$.

The second method is the subtracting the number of $S_{\gamma\gamma}$ signal region by the number of $S_{\gamma\gamma}$ sideband region, where the signal region is defined as $-6 < S_{\gamma\gamma} < 5$ and the sideband region is defined as $-11 < S_{\gamma\gamma} < -8$ or $8 < S_{\gamma\gamma} < 11$. The number of true π^0 in signal region is calculated by following formula:

$$N_{\pi^0}(\text{true}) = \frac{11}{6}(N_{\pi^0}(\text{sig}) - N_{\pi^0}(\text{side})) \tag{A.16}$$

where $N_{\pi^0}(\text{sig})(N_{\pi^0}(\text{side}))$is the number of π^0 in signal (background) region.

The π^0 counting procedure is as follows:

- 1. Subtract all background histograms from the data histogram.

- 2. Do fit / subtraction to obtain the true number of π^0s
- 3. Do 2 again for signal MC data set in order to obtain the MC efficiency

The number of true π^0 , the efficiency and $\mathcal{B}$ are given in Table A.4.

Fit	N_{sig}	$\epsilon(\%)$	$\mathcal{B}(\%)$	Corr(Data/MC)
svd1(caseA)	3387071	13.85	24.68	0.967
svd2(caseA)	10986148	13.41	24.59	0.964
svd2(caseB)	3756191	13.62	24.30	0.952

Sideband	N_{sig}	$\epsilon(\%)$	$\mathcal{B}(\%)$	Corr(Data/MC)
svd1(caseA)	3222346	13.37	24.36	0.954
svd2(caseA)	10451599	12.94	24.25	0.951
svd2(caseB)	3572494	13.13	23.97	0.939

Table A.4: The number of true π^0 (2nd column), the efficiency (3rd), $\mathcal{B}$ (4th) and the correction factor between Data and MC (5th) with respect to the type of data set. In the 3rd column, the efficiency is estimated by signal MC with given correction for a π and a leptonic track

A.3.2 For *double* $\pi\pi^0$ event

As introdueced in Sec. A.1, *double* $\pi\pi^0$ event gives the other way to confirm R_{single} and to obtain the $R_{genuine}$ which is exclusive to our data. We used svd2(caseB) data only in this study.

The *double* $\pi\pi^0$ event has identical decay mode to each hemisphere except for the sign of charge, and there should be no correlation, so the number of π^0 can be estimated for each side independently. The number of π^0 for each hemisphere is estimated by fitting PDF to the $S_{\gamma\gamma}$ distribution and obtained the number of signal $N_{\rm sig}(\pm)$ and the number of background $N_{\rm BG}(\pm)$, where the sign represent the sign of each hemisphere. e.g. if π^0 is selected in which

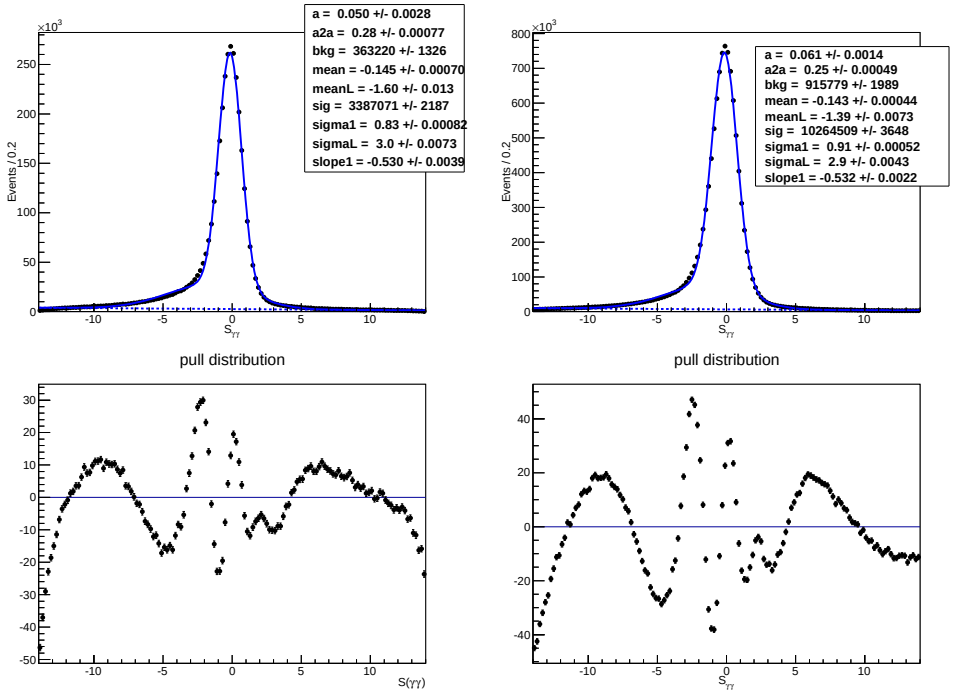

Figure A.4: A fit result of $S_{\gamma\gamma}$ distribution for svd1(caseA) data using logarithmic gaussian with linear background assumption. The left plot is for Data and the right one is for MC. The figures in bottom shows the pull distribution of upper plots with arbitrary unit at y axis.

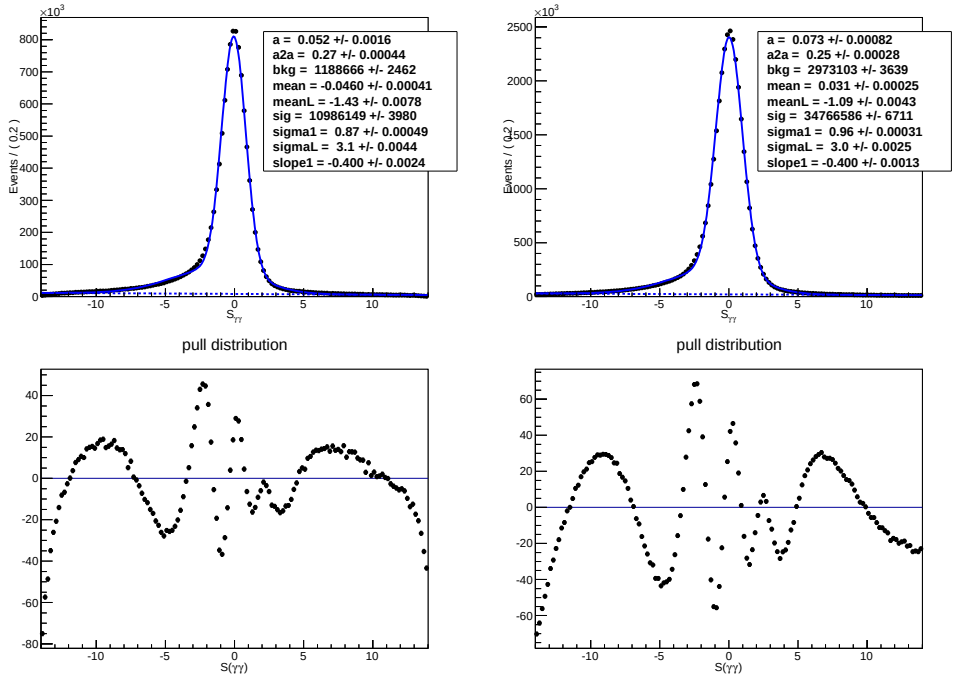

Figure A.5: A fit result of $S_{\gamma\gamma}$ distribution for svd2(caseA) data using logarithmic gaussian with linear background assumption. The left plot is for Data and the right one is for MC. The figures in bottom shows the pull distribution of upper plots with arbitrary unit at y axis.

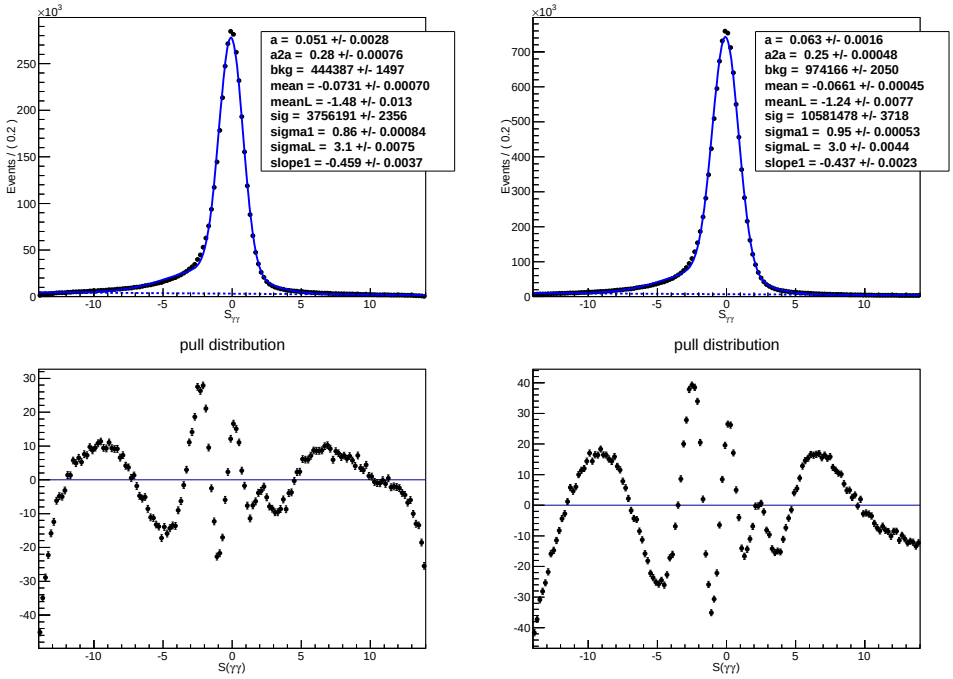

Figure A.6: A fit result of $S_{\gamma\gamma}$ distribution for svd2(caseB) data using logarithmic gaussian with linear background assumption. The left plot is for Data and the right one is for MC. The figures in bottom shows the pull distribution of upper plots with arbitrary unit at y axis.

τ^+ decays, then $N_{\rm sig}(+)$ and $N_{\rm BG}(+)$ are obtained by the fit.
It should be noticed that the number of π^0 so far is only estimated on one side of hemisphere. In order to estimated "true" number of *double* $\pi\pi^0$ event, we should "correct" this number of π^0 with some values. This correction can be obtained using $N_{\rm sig}$ and $N_{\rm BG}$ from opposite side hemisphere.

$$\epsilon_{\rm fit}(\pm) = \frac{N_{\rm sig}(\pm)}{N_{\rm sig}(\pm) + N_{\rm BG}(\pm)} \tag{A.17}$$

where $\epsilon_{\rm fit}(\pm)$ is the correction for the number of π^0 in the fit for each sign of hemisphere. This can be regarded as a relative "efficiency" by the fit exclusively.
Fig.A.6 shows the fit result for the each charged hemispheres for Data and signal MC. The number of π^0 for τ^+ hemisphere($N_{sig}(+)$) is found to be 829502 $\pm$ 1123 and the number of π^0 for τ^- hemisphere($N_{sig}(-)$) is found to be 827337 $\pm$ 1118. (The value for background can be found in the Table A.5) Once the number of π^0 in one side is obtained, the true number of *double* $\pi\pi^0$ can be calculated by multiplying ϵ_{fit} of the opposite side to $N_{\rm sig}$ and efficiency.

$$N_{\rm sig}^{true}(\pm) = N_{\rm sig}(\pm) \times \epsilon_{\rm fit}(\mp) \quad , \quad \epsilon^{true}(\pm) = \epsilon(\pm) \times \epsilon_{\rm fit}(\mp) \tag{A.18}$$

where $N_{\rm sig}^{true}(\pm)$ represents the number of "true" *double* $\pi\pi^0$ event, $\epsilon^{true}(\pm)$ is the efficiency for the one charged hemisphere. *let me remind you that to obtain* $N_{\rm sig}^{true}(\pm)$ *we calculated it using a set of real data but to obtain* ϵ *we used signal MC except for the* $\epsilon_{fit}(\mp)$. $\epsilon_{fit}(\mp)$ *is a kind of correction to get the number of true double* $\pi\pi^0$ *events by considering two* π^0 *in different hemisphere at the same time.* The relevant numbers to this calculation are shown at Table A.5.

The $\mathcal{B}_{double}$ we measured is (5.94 $\pm$ 0.01) % ((5.96 $\pm$ 0.01)%) for $\tau^-(\tau^+)$ hemisphere, so R_{double} is found to be 0.912 $\pm$ 0.008 (0.915 $\pm$ 0.008). Using

	τ^- hemi.	τ^+ hemi.
$N_{\rm sig}$	827337 ± 1118	829502 ± 1123
$N_{\rm BG}$	116277 ± 734	114205 ± 738
$\epsilon(\%)$	8.748 ± 0.006	8.741 ± 0.006
$\epsilon_{fit}^{data}(\%)$	87.67 ± 0.004	86.89 ± 0.004
$\epsilon_{fit}^{MC}(\%)$	90.47 ± 0.002	90.39 ± 0.002
$\mathcal{B}(\%)$	5.94 ± 0.01	5.96 ± 0.01
Corr(Data/MC)	0.912 ± 0.008	0.915 ± 0.008

Table A.5: The relevant numbers for *double* $\pi\pi^0$ events for each sign of hemisphere. ϵ is the selection efficiency of *double*$\pi\pi^0$ event regardless of fit efficiency. N_{sig} is the number of signal event in the fit for τ^+ and τ^-. If the $N_{\rm sig}$ is obtained using $S_{\gamma\gamma}$ distribution where the τ^+ reside, it is equal to $N_{\rm sig}(+)$ vice versa. ϵ_{fit}^{i} is the correction factor for the efficiency(ϵ) and i is a type of data set (Data, MC). The use of ϵ_{fit}^{i} can be found in Eq.(A.18)

the formula in Eq.A.13, we found the correction is

$$R_g = \frac{R_{double}}{R_{single}} = \frac{0.912 \pm 0.008}{0.953 \pm 0.001} = 0.957 \pm 0.008 \qquad \text{(A.19)}$$

where the error is statistical only. The result is consistent to that of *single* $\pi\pi^0$ event.

In Eq.A.11, the square root of R_{double} shoud be same as to R_{single}. This we define R'_{single}, then

$$R'_{single} = 0.955 \pm 0.004 \quad (0.956 \pm 0.004) \qquad \text{(A.20)}$$

This is also consistent to the result of *single* $\pi\pi^0$ event.

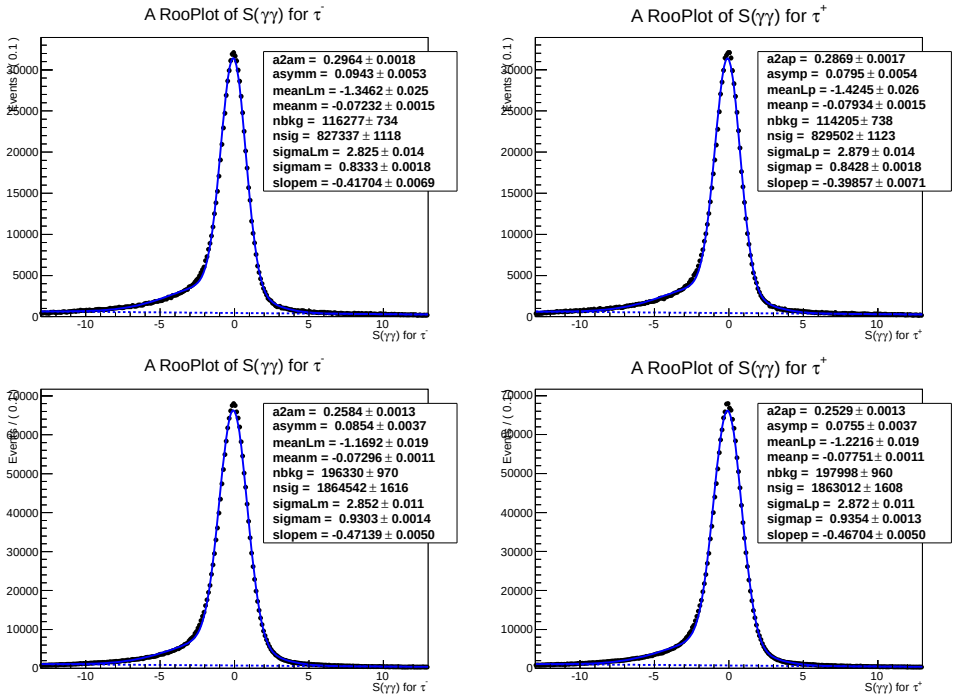

Figure A.7: A fit result of $S_{\gamma\gamma}$ distribution for svd2(caseB) data using logarithmic gaussian with linear background assumption. The top plots are for Data and the bottom one are for MC. The left plot is the result of τ^+ hemisphere and the right one is that of τ^- hemisphere.

A.4 Systematic Uncertainty

In this study we have to consider several sources that give systematic uncertainty to the branching ratios. The track finding efficiency is usually 1% for a charged track for caseA data (0.4% for caseB data). In case of e-μ normalization, 2 track event (*single* $\pi\pi^0$) is divided by 2 track event (e-μ) so the track finding uncertainty can be negligible. For the case of *double* $\pi\pi^0$ event, because we normalized to the luminosity using caseB data, 1.4% of error should be taken into account. The lepton ID systematics is found to be 1.95% (1.35%) and π ID systematics is found to be 0.51%(0.93%). The uncertainty from trigger efficiency and γ veto efficiency was studied by using same decay channel in which the values are 0.05% and 0.14%, respectively. The uncertainty for background estimation can be done by varying the background ratio within the error in PDG. For example, the dominant background in $\pi\pi^0$ event is to be $\tau^- \to \pi^-\pi^0\pi^0\nu_\tau$ mode and its uncertainty is given to 1.1%. The uncertainty from counting the number of true π^0 is found to be about 1.4% which is obtained from the difference between two counting methods (Fit / Sideband). In case of *double* $\pi\pi^0$ event, this uncertainty should be counted once more, $\sqrt{1.4^2 + 1.4^2} = 1.98$. Especially for *double* $\pi\pi^0$ event, because the number of event is normalized to the luminosity, we take the uncertainty due to luminosity and cross section into account, instead of $\mathcal{B}e$, $\mathcal{B}\mu$ and BG of e-μ. So far we included the track finding and PID systematic into the uncertainty estimation. For users, however, most of analysis takes already such uncertainties into account, we recommend to omit such systematics as a pure π^0 systematic(Total(PID excl.) in Table A.6) which provide sources of uncertainty for all data set we used.

The systematic uncertainty for several R is rather straightforward, e.g. svd2 caseB set :

$$\Delta R = \frac{1}{0.9519}\sqrt{(\frac{0.0053}{0.2430})^2 + (\frac{0.09}{25.51})^2} = \frac{0.021}{0.9519} = 2.20(\%) \qquad \text{(A.21)}$$

However, if user want to omit PID systematics which is already applied on

source	svd1-A (%)	svd2-A (%)	svd2-B (%)	*double* $\pi\pi^0$ (%)
Track finding	-	-	-	1.4
LID	1.95	1.95	1.35	-
πID	0.51	0.51	0.93	1.31
Trigger	0.05	0.05	0.05	0.05
γ veto	0.14	0.14	0.14	0.14
Background	0.19	0.19	0.19	0.19
$\mathcal{B}e$, $\mathcal{B}\mu$	0.15	0.15	0.15	-
BG of e-μ	0.43	0.43	0.43	-
Luminosity	-	-	-	1.4
$\sigma_{\tau^+\tau^-}$	-	-	-	0.3
Fit / Sideband	1.34	1.41	1.37	1.98
Total	2.47	2.54	2.19	3.11
Total(PID excl.)	1.44	1.50	1.45	2.46

Table A.6: The source list of systematic uncertainty for caseA and caseB data. Total(PID excl.) is the systematics exclude the uncertainty by tracking and PID.

your systematic study, then

$$\Delta R = \frac{1}{0.9519}\sqrt{(\frac{0.0035}{0.2430})^2 + (\frac{0.09}{25.51})^2} = \frac{0.0148}{0.9519} = 1.57(\%) \qquad \text{(A.22)}$$

$\mathcal{B}(\tau^- \to \pi\pi^0\nu_\tau)$ for each experiment number can be used to check the stability in time. The result is shown at Fig.A.8. $\mathcal{B}_{single}$ in this study(blue dot with errorbar) is oscillating within $\pm 1.5\%$ from the central value(red dashed).

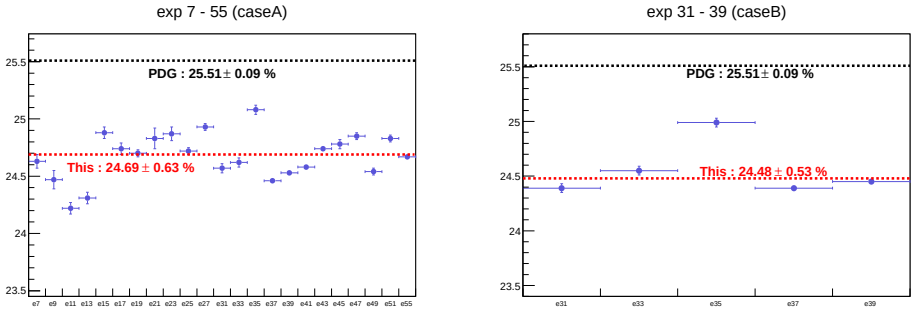

Figure A.8: $\mathcal{B}(\tau^- \to \pi\pi^0\nu_\tau)$ with respect to time(experimental number). The left one is for caseA data and the right one is for caseB data. $\mathcal{B}_{single}$ in this study(blue dot with errorbar) is oscillating within $\pm 1.5\%$ from the central value(red dashed). The branching ratio measurements are stable in time.

A.5 Summary

Using $\tau^- \to \pi\pi^0\nu_\tau$ channel, we studied the π^0 efficiency and obtained R_{single} and $R_{genuine}$. R_{single} is found to be 0.967 ± 0.024 for SVD1 data and 0.953 ± 0.021 for SVD2 data. We also obtained $R_{genuine}$, which is independent to PDG, by using *double* $\pi\pi^0$ events, which is found to be 0.957 ± 0.022 (SVD2), so the result is consistent with that of *single* $\pi\pi^0$ result. The momentum dependence of π^0 efficiency has been studied for different momentum region (12 regions). In Table A.7 the measured branching ratio and correction factors are listed for 12 momentum regions. For users, $R_{genuine}$(or R_{single}) can be used not only for as an overall corrections for π^0 efficiency but also for as a systematic uncertainty by taking (1- Corr), e.g. $1 - 0.957 = 4.3\%$. If users want to use this corrections to their analysis, we recommend to use the correction that PID systematics excluded given in Sec. A.4 when users already include PID systematics in their analysis.

	Fit		Sideband	
data set	$\mathcal{B}(\%)$	Corr(Data/MC)	$\mathcal{B}(\%)$	Corr(Data/MC)
SVD1-A	24.68 ± 0.61	0.967 ± 0.024	24.36 ± 0.60	0.954 ± 0.023
SVD2-A	24.59 ± 0.62	0.964 ± 0.025	24.25 ± 0.61	0.951 ± 0.024
SVD2-B	24.30 ± 0.52	0.952 ± 0.021	23.97 ± 0.53	0.939 ± 0.020

Table A.7: $\mathcal{B}_{single}$ and R_{single} for relevant set of data. Because in this analysis we used PID condition for π and leptons, the errors are rather larger than nominal error of $\mathcal{B}$ given in PDG (0.3% = 0.09).

국문초록

약한 상호작용을 통하여 강입자로 붕괴할 수 있는 유일한 경입자인 타우 입자의 붕괴 현상은 표준 모형에서 중요한 파라메타들 즉, $|V_{us}|$(u 쿼크와 d 쿼크의 섞임정도), m_s(s 쿼크의 질량) 및 α_s(강한 상호작용의 크기)등을 측정함에 있어서 좋은 연구소재가 된다.

이 중 $|V_{us}|$ 의 측정과 직접적으로 연관이 있는 타우 입자의 $K^{\pm}, K^0$ 중간자 및 강입자들로 붕괴하는 현상은 타우 입자 개수의 부족으로 지난 십수년간 제대로 연구되지 않았다. Belle 실험 그룹은 일본 고에너지 가속기 연구소에 위치한 KEK-B 가속기와 Belle 검출기를 사용하여 6.15×10^8 개의 타우 입자 쌍을 생성 및 측정하였고, 이는 타우 입자를 연구함에 있어서 가장 좋은 환경을 제공한다.

본 논문은 Belle 실험을 통해 생성된 타우 입자가 K^0_S 을 포함한 다른 중간자로 붕괴하는 채널들의 갈래비(branching fraction)를 측정한 결과를 보고한다. 비대칭 에너지로 전자와 양전자를 충돌시키는 KEK-B 가속기와 B 중간자 연구에 특화된 Belle 검출기를 이용하여 669 fb^{-1} 의 데이터를 축적하였고, 이를 이용하여 타우 입자의 붕괴 갈래비를 계산한 결과는 다음과 같다.

먼저 타우 입자가 K^0_S을 포함한 강입자로 붕괴하는 채널의 총 비율을 $\mathcal{B}(\tau^- \to K^0_S\ X^-\nu_\tau) = (0.910 \pm 0.001 \pm 0.046)\%$, 이며 X^-는 임의의 강입자들의 조합이다. 하나의 K^0_S 과 다른 강입자로 붕괴하는 채널에 대하여

각각,

$$\mathcal{B}(\tau^- \to \pi^- K_S^0 \nu_\tau) = (4.10 \pm 0.01 \pm 0.21) \times 10^{-3}$$
$$\mathcal{B}(\tau^- \to K^- K_S^0 \nu_\tau) = (7.09 \pm 0.06 \pm 0.41) \times 10^{-4}$$
$$\mathcal{B}(\tau^- \to \pi^- K_S^0 \pi^0 \nu_\tau) = (1.95 \pm 0.02 \pm 0.11) \times 10^{-3}$$
$$\mathcal{B}(\tau^- \to K^- K_S^0 \pi^0 \nu_\tau) = (7.31 \pm 0.12 \pm 0.49) \times 10^{-4}$$

이며, 두개의 K_S^0와 다른 강입자로 붕괴하는 채널에 대하여 각각,

$$\mathcal{B}(\tau^- \to \pi^- K_S^0 K_S^0 \nu_\tau) = (2.41 \pm 0.04 \pm 0.26) \times 10^{-4}$$
$$\mathcal{B}(\tau^- \to \pi^- K_S^0 K_S^0 \pi^0 \nu_\tau) = (2.06 \pm 0.23 \pm 0.24) \times 10^{-5}$$

이다. 여기서 타우 입자가 $\pi^- K_S^0 K_S^0 \pi^0 \nu_\tau$ 로 붕괴하는 채널에 대한 갈래비는 세계 최초로 측정한 결과이다. 또한 이 붕괴 모드 안에서 $f_1(1285)$ 중간자에서 오는 비율을 측정함에 대하여 최초로 보고한다. 이 결과들은 국제 평균값과 근사적으로 일치하며 가장 정밀한 측정값을 보여주며, 이를 통하여 $|V_{us}|$ 의 측정을 보다 정확하게 할 것을 기대한다.

주요어: 타우 경입자, Belle 실험, 경입자 붕괴, Vus
학번: **2007-30779**

감사의 글

녹음이 짙은 한여름에 차지도 덥지도 않은 관악의 산바람을 맞으면서 제 인생의 중요한 순간들에 대해서 생각해보면 지금 이 순간 만큼 기대가 되고 떨리는 순간은 없을 것입니다. 인류가 만들어낸 학문 중에서 가장 으뜸이라 여겨지는 물리학에서 박사학위를 수여 받는 영광을 얻기까지 많은 분들의 도움과 기도와 격려가 숨어 있었음을 부인하지 않을 수 없습니다. 캔버스에 녹아든 음영처럼 보이듯 말듯 저에게 이 길을 갈 수 있도록 등을 밀어주신 분들의 수고에 대하여 얼마 되지 않는 저의 부족한 필력으로 지면을 체운다는 것은 어불성설임을 잘 알고 있습니다. 다만, 그 분들의 이름만이라도 이 곳에 남기는 것이 지금 논문을 마무리 짓는 이 순간 제가 할 수 있는 최소한의 정성이라고 마음 깊이 생각합니다.

제가 아직 아무것도 모르던 학부 과정때 연구실에 들어와 물리학을 공부할 수 있도록 물심양면으로 도움을 주신 김선기 교수님께 마음 속 깊이 감사를 드립니다. 또한 갑작스레 지도교수가 되셨음에도 짧은 기간동안 박사학위를 무사히 받도록 도와주신 최선호 교수님께도 감사드립니다. 제 연구에 관심을 가져주시고 마지막까지 저의 짧은 영어와 씨름을 해주신 스티브 라스 올슨 교수님께도 감사드립니다. 바쁘신 일정 가운데서도 친히 논문 심사를 맡아주신 방형찬 교수님, 김영덕 교수님, 그리고 김형도 교수님께 감사드립니다.

이글을 읽지 못하겠지만 무엇보다도 이 연구결과를 내기 위해서 연구의 시작부터 끝까지 아낌없는 조언과 적극적인 관심과 도움을 주셨던 히사키 하야시 나라대학 교수님께 진심으로 감사를 드립니다. 또한 같은 타우 분석 그룹의 하야사카 상에게도 감사를 전하고 싶습니다. 고령임에도 불구하고 변함없이 저의 연구에 관심을 가져주신 지미 맥노튼 교수님에게도 감사를 드립니다. 일본에서 벨 검출기를 이해하고 공부하는 것에 대해서 많은 도움을 주신 천병구 교수님과 이와사키 교수님 그리고 알렉산더 쿠즈민 교수님에게 감사를 드리고 싶습니다. 천병구 교수님은 적극적으로 도움을 주시려고 하여 많은 위로가 되었습니다. 이와사키 교수님 역시 저를 돕기 위해서 애를 많이 써주셨습니다.

제가 멋모르고 실험실에 들어와 시작한 KIMS 실험에서 알게된 김홍주 교수님, 이직 교수님, 명성숙 박사님, 김상열 박사님, 곽정원 박사님, 이상은 박사님, 양혜영 박사님, 이제는 교수님이 된 현수형, 제가 자주 괴롭힌 승천형, 미국에 계신 명재형, 잘생긴 상준형, 같이 논문을 쓰고 고생한 정훈형과 주희 누나 모두에게 감사를 전하고 싶습니다. 특히 제가 Belle에서 결과를 내고 졸업하는데 명재형의 도움이 컸습니다. 승천형은 연구실 생활 처음 시작할때부터 지금까지 많은 힘이 되었습니다. 그리고 WCU 그룹으로 알게 된 리진 교수님, 슈롱 박사님에게도 고맙다고 전하고 싶습니다. 그리고 재금누나, 제가 좀 미안한 은별이, 항상 밝아보였던 일수, 경원 누나, 귀찮은 봉호, 정환, 정훈, 건보, 다른 실험실이지만 항상 잘 어울렸던 성배, 고생만하는 창우, 그리고 최선호 교수님 밑에서 수학하는 혜구형, 유민, 정석이에게 좋은 결과 내고 항상 행운이 따르길 기도합니다. 항상 옆에서 잔소리를 들려주셨던 경희 누나, 지금 비서일로 수고하시는 혜정씨와 고운씨에게도 좋은 일이 가득하길 바랍니다.

일본에서 생활은 정말 외로운 순간들의 연속이었습니다. 그 와중에도 몇 안되지만 함께 하던 분들이 계서서 위로가 되었습니다. 늘 커피를 사주어 지금의 뱃살을 만들어 준 정현형, 심심하면 같이 자전거를 탔었던 현청형, 츠쿠바홀 2층에서 묵묵히 일하던 효정 누나에게 감사드립니다. 가끔 내가 찾아가 귀찮게 굴었던 운노 상에게도 감사를 드립니다. 같은 Belle 실험 한국그룹의 권영준 교수님과 초롱, 재익, 지금은 나고야에서 수학하고 있는 옥수, 고려대의 원은일 교수님 및 수형씨, 한양대의 인수, 성현, 경북대의 영임, 민정 외 다른 분들은 이 실험이 끝날 무렵에 들어와서 아무도 없는 텅 빈 공간에서 밤낮 혼자서 일을 해야했던 저에게 가끔식 고국에서 찾아왔던 이 분들은 부럽기도 하고 한편으로는 힘이 되기도 하였습니다.

일본 교회에서의 시간은 저에게 큰 활력이 되었습니다. 일본에서 목회를 하시면서 주의 일을 하느라 수고 많으셨던 츠쿠바 희망교회의 박권철 목사님과 사모님, 같이 모여서 즐거운 시간을 나눴던 은하, 예진, 승엽, 지금은 한국에 계신 윤표형, 그리고 이름을 기억 못하는 성도님들에게 많은 신세를 지었습니다. 그곳에서의 기억은 정말 잊지 못할 것입니다.

제가 처음 서울에 올라와서 학업을 시작할때 옆에서 많은 분들이 도와

주셨습니다. 처음 서울 생활을 시작했을때 도와주신 진희 아주머니와 아저씨께 감사드립니다. 당시 생활의 어려움으로 겉으로 드러내지 않았지만 마음속으로 해매었던 적도 많았습니다. 그런 저에게 최효석 목사님과 유인희 사모님의 도움이 무척컸습니다. 신앙적인 부분뿐만 아니라 다른 모든 일들까지 관심있게 봐주시고 돌봐주셔서 감사를 드립니다. 무지개 언약교회에서 알게된 은희, 정희, 유나 누님 세분들, 서글서글한 희남형, 말없는 영빈형, 별로 안 친한 광근형에게 앞으로 좋은 일들이 생기길 바랍니다. 초등학교때부터 봤던 영곤, 정호, 은영, 수정, 효정, 수지, 승연, 혜영, 일수, 성민 외 다른 아이들 전부 이제 곧 대학생이 되거나 이미 되었는데, 부디 좋은 경험 많이하고 열심히 살길 기도합니다.

같은 대학 동기인 비상 구반의 친구들과 선후배들에게 감사를 드리고 싶습니다. 제가 반 활동에 적극적이지 않아서 겉에서 맴돌아도 끈끈한 정으로 뭉쳐진 곳에 속하여 어긋나지 않게 대학생활을 마칠 수 있었습니다. 종립, 정윤, 원재, 현교, 경배, 하나, 수연, 정호, 인하, 선미, 규헌, 태연, 정현, 재극, 형준, 대영, 같이 물리학수업을 들었던 우영형과 철호형, 항상 긍정적인 재홍형, 석호형, 선배든 후배든 엄청난 인맥을 자랑하는 경준형 그리고 다 쓰지 못하지만 선배들과 후배들에게 고맙다는 말을 전하고 싶습니다.

무엇보다도 곁에서 누구보다 말로 다 할 수 없는 고생을 하신 부모님께 정말 마음 깊이 감사를 드립니다. 정말 아들의 가는 길을 누구보다도 걱정하며 고생하시고 뒤에서 눈물을 흘리신 것 알면서도 모르는채 뒤로 흘렸던 적이 많았습니다. 정말로 감사하고 사랑하고 존경합니다. 항상 나의 밑이었는 줄 알았는데 어느 새 나보다 더 많은 세상과 경험을 하고 조언을 해주는 사랑하는 동생 희에게 주님의 축복이 항상 함께하길 바랍니다. 박사과정을 하면서 결코 짧지 않은 시간동안 옆에서 늘 같이 마음 고생을 하며 지낸 사랑하는 준희에게도 마음 속 깊이 수고 많았고 고맙다고 전하고 싶습니다.

그리고 끝으로 이 좋은 세상에서 많은 것을 가지게 해주신 나의 주님께 감사를 드립니다.

2012년 7월, 류수